

THE DYNAMICS OF INHOMOGENEOUS COSMOLOGIES

by

Woei Chet Lim

A thesis
presented to the University of Waterloo
in fulfilment of the
thesis requirement for the degree of
Doctor of Philosophy
in
Applied Mathematics

Waterloo, Ontario, Canada, 2004

© Woei Chet Lim 2004

I hereby declare that I am the sole author of this thesis. This is a true copy of the thesis, including any required final revisions, as accepted by my examiners.

I understand that my thesis may be electronically available to the public.

Abstract

In this thesis we investigate cosmological models more general than the isotropic and homogeneous Friedmann-Lemaître models. We focus on cosmologies with one spatial degree of freedom, whose matter content consists of a perfect fluid and the cosmological constant. We formulate the Einstein field equations as a system of quasilinear first order partial differential equations, using scale-invariant variables.

The primary goal is to study the dynamics in the two asymptotic regimes, i.e. near the initial singularity and at late times. We highlight the role of spatially homogeneous dynamics as the background dynamics, and analyze the inhomogeneous aspect of the dynamics. We perform a variety of numerical simulations to support our analysis and to explore new phenomena.

Acknowledgements

First of all, I want to thank my supervisor and mentor, John Wainwright, for his guidance over the course of my study (both Master's and doctorate). You are always enthusiastic and ready to help. I will do my best to become an exemplary scholar and teacher like you.

Special thanks go to my collaborators Claes Uggla, Henk van Elst, Lars Andersson, Marsha Weaver and Ulf Nilsson, with whom I have had many enlightening discussions on cosmology. The timely G_2 project by Henk, Claes and John provided a bountiful field for this thesis.

I am grateful to Conrad Hewitt, Barry Collins and Ray McLenaghan for their helpful feedback on the thesis proposal.

I would like to acknowledge Alan Rendall, Achim Kempf and David Siegel for discussions on various analytical aspects of cosmology and differential equations. On the numerical aspects, I want to thank Lars Andersson and Mattias Sandberg for their **CLAWPACK** codes for the vacuum OT G_2 models, which helped me begin the captivating numerical project in this thesis. Marsha's timely visit also helped speed up the project. The brane cosmology project with Alan Coley and Yanjing He helped to sharpen my skills in doing numerical simulations. I would also like to acknowledge Matt Chop-tuik, David Garfinkle, Nathalie Lanson and Serge D'Alessio for discussions on numerical simulations.

I have received all of my tertiary education at the University of Waterloo, and I would like to take this opportunity to thank all the faculty members here who have taught me mathematics, physics and computer science.

Lastly, I dedicate this thesis to my parents in Malaysia, who have provided me with the best education they can afford.

Contents

1	Introduction	1
1.1	Background in cosmology	1
1.2	Cosmological Hierarchy	4
1.3	Goals	8
1.4	Overview	10
I	Dynamics of G_2 and SH cosmologies	12
2	The orthonormal frame formalism	13
2.1	1+3 decomposition	13
2.2	1+1+2 decomposition for G_2 cosmologies	19
2.3	Scale-invariant variables	23
3	The G_2 and SH hierarchies	29
3.1	The G_2 hierarchy	29
3.2	G_2 -compatible SH cosmologies	33
4	SH dynamics	40
4.1	The standard Mixmaster dynamics	40
4.2	The G_2 -compatible SH evolution equations	46
4.3	Generalized Mixmaster dynamics	51
4.4	Non-Mixmaster dynamics	65
4.5	Future asymptotics	68
5	The state space for G_2 cosmologies	73
5.1	The evolution equations	73
5.2	Invariant subsets of the β -normalized state space	80

5.3	Asymptotic silence	85
6	Explicit G_2 cosmologies	91
6.1	An explicit solution with “steps”	91
6.2	An explicit solution with “spikes”	96
6.3	Spiky and step-like structures	104
7	Dynamics in the past asymptotic regime	106
7.1	Background dynamics: role of algebraic terms	107
7.2	Effects of spatial inhomogeneity I: role of saddles	109
7.3	Effects of spatial inhomogeneity II: role of spatial derivative terms	115
II	Numerical exploration of G_2 cosmologies	117
8	Equations for numerical simulations	118
8.1	Specifying the initial conditions	119
8.2	Is the system hyperbolic?	123
8.3	Accuracy of numerical schemes	124
8.4	Unsatisfactory aspects of the numerical simulations	131
9	Numerical simulations	133
9.1	Asymptotic silence	134
9.2	Background dynamics	134
9.2.1	Local Mixmaster dynamics	134
9.2.2	Spatial variation in the background dynamics	139
9.2.3	Multiple transitions	141
9.3	Effects of spatial inhomogeneity I: role of saddles	143
9.3.1	Step-like structures	143
9.3.2	Spiky structures	148
9.4	Effects of spatial inhomogeneity II: role of spatial derivative terms	151
9.4.1	Spike transitions	151
9.4.2	Shock waves	157
9.5	Future asymptotics	161
9.6	Close-to-FL epoch	163
10	Conclusion	172
A	G_2 action	175

B	Rotation formulae	180
C	Asymptotic expansions at spike points	182
D	Equations for numerical simulations	185
	Bibliography	188

List of Tables

1.1	Classification of Bianchi cosmologies.	7
3.1	Perfect fluid hierarchy in the presence of a G_2 group.	33
3.2	G_2 -compatible SH cosmologies.	33
4.1	The Hubble-normalized variables for the G_2 -compatible SH cosmologies with $\Lambda = 0$ and g	
4.2	The Hubble-normalized variables for the G_2 -compatible SH cosmologies with $\Lambda = 0$ and G	
4.3	The Hubble-normalized variables for the G_2 -compatible SH cosmologies with $\Lambda = 0$ and d	
4.4	The Hubble-normalized variables for the G_2 -compatible SH cosmologies with $\Lambda = 0$ and c	
4.5	Previous work on G_2 -compatible SH cosmologies with tilt and $\Lambda = 0$. 72	
5.1	The β -normalized variables for G_2 cosmologies.	81
8.1	The rate of convergence of numerical methods: errors relative to the solution on 4096 grid	
8.2	The accuracy of numerical methods: errors in the simulated Σ_\times for the WM solution as n	
8.3	The accuracy of numerical methods: errors in the simulated Σ_- for the transformed WM	
9.1	Predicted and actual growth rates of the triggers	139
9.2	Predicted and actual growth rates at $t = 10$	163

List of Figures

3.1	Classification of G_2 cosmologies.	32
3.2	Action of the G_2 group and the tilt degrees of freedom.	34
3.3	SH cosmologies with generic G_2 action.	35
3.4	SH cosmologies with OT G_2 action.	38
3.5	a) SH cosmologies whose G_2 admits one HO KVF. b) SH cosmologies with diagonal G_2 a	
4.1	a) The Kasner circle and its six-fold symmetry. b) The triggers N_{11} , N_{22} and N_{33} and the	
4.2	The curvature transition set and the arc of instability (into the past) of the trigger N_{11} .	
4.3	The frame transition sets corresponding to the triggers Σ_\times and Σ_2 , respectively.	55
4.4	The unstable Kasner arcs and their triggers.	55
4.5	The tilt transition for v_1	60
4.6	The unstable arcs on \mathcal{K} and $\mathcal{K}_{\pm 1}$ and their triggers.	61
4.7	SH cosmologies with generic G_2 action (more detailed).	64
5.1	The Kasner parabola in the β -normalized state space.	83
6.1	The LRS Bianchi I state space ($\Lambda > 0$), and an LRS dust solution as an “inhomogenized”	
6.2	The two N_-^H transition orbits shadowed by the transformed WM solution.	102
6.3	Snapshots of the variables $\tilde{\Sigma}_-$ and \tilde{N}_- for $f(\bullet) = \cos(\bullet)$	103
6.4	Formation of spiky and step-like structures.	105
7.1	The tilt variable v can develop step-like structures into the past.	110
7.2	The triggers N_- and Σ_\times can develop spikes into the past.	112
9.1	Exponential decay of $(E_1^1)^H$ and r as $t \rightarrow -\infty$ and as $t \rightarrow \infty$.	135
9.2	Exponential decay of Ω^H and Ω_Λ^H as $t \rightarrow -\infty$	136
9.3	Typical evolution along a fixed timeline, showing the transition orbits.	137
9.4	Typical evolution along a fixed timeline.	138
9.5	Snapshots of triggers Σ_\times^H and N_-^H , showing pulses apparently travelling at superluminal s	
9.6	Multiple transitions.	142

9.7	Snapshots of Σ_+^H and v in a diagonal G_2 cosmology, showing step-like structures in v .	144
9.8	Snapshot of the variables $(\Sigma_+^H, \Sigma_-^H, v)$ in a diagonal G_2 cosmology at $t = -4$.	145
9.9	Snapshot of the variables $(\Sigma_+^H, \Sigma_-^H, v)$ in a diagonal G_2 cosmology at $t = -5$.	146
9.10	Snapshot of the variables $(\Sigma_+^H, \Sigma_-^H, v)$ in a diagonal G_2 cosmology at $t = -10$.	147
9.11	Snapshots of Σ_- and the trigger N_- .	149
9.12	Snapshots of the variables $(\Sigma_+^H, \Sigma_-^H, N_-^H)$ in the $(\Sigma_+^H, \Sigma_-^H, N_-^H)$ space. Each dot represents	
9.13	The orbit of an N_- spike transition along x_{spike} , from $t = -2.2$ to $t = -3.3$, projected onto	
9.14	An N_- spike transition.	153
9.15	Influence of $\partial_1 N_-$ on $\partial_t \Sigma_\times$.	154
9.16	Influence of $\partial_1 \Sigma_\times$ on $\partial_t N_-$.	155
9.17	Shock wave in v into the past.	158
9.18	Shock wave in v into the future.	159
9.19	Snapshot showing shock waves or non-differentiability.	160
9.20	Snapshots of v for three solutions with $\gamma = 1.2, \frac{4}{3}$ and 1.5 , showing the asymptotic signature	
9.21	Evolution along a fixed timeline – from the past asymptote to the future asymptote.	165
9.22	Evolution along a fixed timeline – details of the close-to-FL epoch.	167
9.23	Evolution of the Weyl scalars along a fixed timeline.	169
9.24	Snapshot of the initial condition at $t = 0$, showing a small Σ_+ .	170
9.25	Snapshot at $t = 3.48$, showing the wavelengths in the different modes.	171

Chapter 1

Introduction

1.1 Background in cosmology

The goal of relativistic cosmology is to describe the structure of the observable universe on a sufficiently large scale, and to explain its origins, using Einstein's General Theory of Relativity.

The most fundamental cosmological observation is that light from distant galaxies is redshifted (this was discovered by Hubble in the 1920s). The standard interpretation of the redshifts is that the universe is expanding. The second fundamental observation is that the universe is filled with radiation (as discovered by Penzias & Wilson in 1965), which has a blackbody spectrum to a very high accuracy, corresponding to a present temperature of about 3 K. The standard interpretation is that this radiation, called the cosmic microwave background (CMB), was emitted when the universe was denser and hotter, and has travelled freely to us ever since. A third observation, that provides information about the physics of the universe at early times, concerns the overall abundance of helium in the universe (see Peebles 1993 [60, pages 143–4] and Hoyle & Tayler 1964 [39]). The constant abundance of helium in stars and intergalactic matter ($\approx 25\%$ by mass) over time suggests that helium was formed during a very early epoch when the universe was very hot. These three observations form the physical basis for the so-called hot big-bang theory of the universe, which can be summarized in the following history of the universe.

The history begins at the so-called Planck time (see, for example, Coles & Lucchin 1995 [17, page 111]), the time after which classical general rela-

tivity may be assumed to be valid. The corresponding Planck temperature is approximately 10^{32} K. At such a high temperature, photons have enough energy to produce matter and anti-matter in collisions. When the temperature fell to the order of 10^9 K, collisions of photons could no longer produce even the lightest known particles and antiparticles (electrons and positrons), and the radiation-dominated epoch began (i.e. most of the energy was in the form of radiation). Slight asymmetries between matter and anti-matter resulted in all anti-matter being annihilated by matter, and the remaining matter consisted of protons, neutrons, electrons, photons and neutrinos. It was also cool enough at this temperature for most neutrons to be rapidly tied to form helium nuclei in a process called nucleosynthesis (see, for example, Weinberg 1977 [83, page 110]). Radiation was “coupled” to matter in the sense that photons were frequently scattered by electrons and nuclei through Compton scattering, and matter was kept ionized. As the universe expanded and cooled, radiation lost energy faster than matter did, with the result that eventually the universe became matter-dominated. When the temperature dropped to about 3000 K, photons no longer had enough energy to constantly ionize matter. In other words, the free electrons became bound to nuclei, with the result that the photons could travel freely. One says that the photons have decoupled from the matter. These photons form the CMB radiation, which is detected at the present time. The CMB thus provides a snapshot of the universe at a temperature of about 3000 K, but it is also affected by the geometry of spacetime as it travels towards us.

Within this framework, the formation of galaxies occurs due to the growth of density fluctuations under the influence of gravity. The key point is that random fluctuations in the matter density do not grow rapidly enough to form galaxies (see, for example, Peebles 1993 [60, page 619]). Hence one has to postulate the existence of a suitable spectrum of density fluctuations at very early times. The most popular, but not universally accepted, explanation of the origin of density fluctuations is the theory of inflation in the early universe, first proposed by Guth 1981 [29]. During the inflationary epoch, which is postulated to have occurred shortly after the Planck time, the universe underwent exponential expansion, and quantum fluctuations were hugely magnified to create a spectrum of density fluctuations, which were sufficiently large to form galaxies, but not so large as to produce too many black holes (see also Peacock 1999 [59, Chapter 11]).

Over the past 20 years, as cosmological observations have become more extensive and more accurate, an increasingly complicated picture of the uni-

verse has emerged. Redshift surveys (e.g. the Sloan Digital Sky Survey [65], the Las Campanas Redshift Survey [49]) show that galaxies are not distributed uniformly, but form clusters which in turn are grouped into huge structures on a scale of 100 Mpc^1 , e.g. the Great Attractor (probably a supercluster, with galaxy cluster Abell 3627 near its centre), which is attracting several other clusters, including the Local Group. These observations are being used to determine the power spectrum of the distribution of galaxies (see Strauss 2004 [68], Tegmark *et al.* 2004 [69]) and to compare it with the CMB power spectrum (see Hu & White 2004 [40]). Until recently, it was widely believed that the rate of expansion of the universe is slowing down. This belief was challenged when the recent observations of type Ia supernovae suggested an accelerating expansion (see, for example, Riess & Turner 2004 [63] and Turner & Riess 2002 [71]). This observation, when combined with the observations of the power spectrum of the CMB temperature, restricts the total density parameter² Ω to have a value close to 1 (see, for example, Spergel *et al.* 2003 [66]). However visible matter contributes a value of approximately 0.005 to Ω , and non-luminous baryonic matter contributes a value of approximately 0.035 [58]. This dramatic conclusion suggests that the matter-energy content of the universe is dominated by yet unidentified non-baryonic dark matter and/or energy, indicating that our understanding of the physical universe is still quite incomplete.

The simplest mathematical models within the framework of classical general relativity that describe an expanding universe are the Friedmann-Lemaître (FL) models³, which are spatially homogeneous and isotropic (see Ellis 1989 [22] for a discussion of the historical development). An important question is this: Do cosmological observations support the assumption of isotropy and homogeneity on a sufficiently large scale? In view of the innate limitations in making cosmological observations (we can observe only from one point in space and one instant in time on a cosmological scale), and the difficulties in interpreting the observations, the answer is not clear-cut. It is thus desirable to investigate the dynamics of cosmological models more general than the FL models, and to determine what restrictions observations impose on them. This general area of investigation forms the basis of this thesis.

¹1 parsec is about 3 lightyears; the size of a typical galaxy is 1 Mpc and of a typical cluster is 10 Mpc.

²The density parameter is defined in Section 1.2.

³These models are introduced in Section 1.2.

1.2 Cosmological Hierarchy

In this section, we define cosmological models and classify them according to their symmetries.

Cosmological models

A *cosmological model* $(\mathcal{M}, \mathbf{g}, \mathbf{u})$ is determined by a Lorentzian metric \mathbf{g} defined on a manifold \mathcal{M} , and a family of fundamental observers, whose congruence of world-lines is represented by the unit timelike vector field \mathbf{u} , which we often identify with the matter 4-velocity. The dynamics of the model is governed by the Einstein field equations (EFEs)

$$G_{ab} = T_{ab},^4 \quad (1.1)$$

with suitable matter content.

The matter content is assumed to be a perfect fluid with energy density $\mu > 0$, pressure p and (unit timelike) fluid 4-vector \mathbf{u} :

$$T_{ab} = \mu u_a u_b + p(g_{ab} + u_a u_b). \quad (1.2)$$

We assume that the equation of state of the perfect fluid is of the form $p = (\gamma - 1)\mu$, where $1 \leq \gamma < 2$ is constant. The cases $\gamma = 1$ (dust) and $\gamma = \frac{4}{3}$ (radiation) are of primary physical interest. The cosmological constant Λ in the EFEs can be treated as a perfect fluid with $\mu = \Lambda$ and $p = -\Lambda$. A more formal introduction will be presented in the next chapter.

It is helpful to classify cosmological solutions of the EFEs using the dimension of orbits of the symmetry group admitted by the metric. This classification scheme forms a hierarchy of cosmological models of increasing complexity, starting with the FL models:

- 1) Friedmann-Lemaître (FL) cosmologies (G_6)
- 2) Spatially homogeneous (SH) cosmologies (G_3)
- 3) G_2 cosmologies

⁴We use geometrized units throughout, i.e. $c = 1$ and $8\pi G = 1$, where c is the speed of light in vacuum and G is the gravitational constant.

4) generic cosmologies (G_0)

An FL cosmology admits a local 6-parameter group G_6 of isometries acting on spacelike 3-surfaces. i.e. it has 6 independent Killing vector fields (KVF's) whose orbits form spacelike 3-surfaces. An SH cosmology is either a Bianchi cosmology, which admits a local 3-parameter group G_3 of isometries acting simply transitively on spacelike 3-surfaces, or a Kantowski-Sachs cosmology, which admits a group G_4 of isometries acting on spacelike 3-surfaces but does not admit a simply transitive G_3 subgroup. A G_2 cosmology admits a local two-parameter Abelian group of isometries with spacelike orbits, permitting one degree of freedom as regards inhomogeneity. From the viewpoint of analysis, the equations for G_3 cosmologies are ordinary differential equations (ODEs), those for G_2 cosmologies are 1+1 partial differential equations (PDEs), and those for G_0 cosmologies are 1+3 PDEs.

Friedmann-Lemaître cosmologies

As mentioned in the introduction, FL models are spatially homogeneous and isotropic. In physical terms, “spatially homogeneous” means “the same at every point at any given instant of time”, while “isotropic” means “the same in every spatial direction”. Mathematically, the requirements of spatial homogeneity and isotropy imply that the line element admits the maximal group G_6 of isometries acting on spacelike 3-surfaces. With an appropriate choice of time coordinate, the line element can be written as ⁵

$$ds^2 = -dt^2 + l(t)^2 \tilde{g}_{\alpha\beta} dx^\alpha dx^\beta, \quad (1.3)$$

where $\tilde{g}_{\alpha\beta} dx^\alpha dx^\beta$ is the metric of a (spacelike) 3-surface with constant curvature (see, for example, Weinberg 1972 [82, Section 13.5]). The function $l(t)$ is called the *length scale* of the model.

The two most important quantities describing an FL model are the Hubble scalar H , where $H = \dot{l}/l$, and the total⁶ density parameter, defined by

$$\Omega = \frac{\mu}{3H^2}. \quad (1.4)$$

⁵Latin indices run from 0 to 3; Greek indices from 1 to 3; capital Latin indices run from 2 to 3.

⁶In general, μ is a sum of terms, for example matter, radiation and the energy density due to a cosmological constant.

FL models are further separated into three types according to the curvature of the spacelike 3-surfaces $t = \text{const.}$, which is completely determined by Ω :

$$\begin{aligned} \text{Open FL: negative curvature,} & \quad \Omega < 1 \\ \text{Flat FL: zero curvature,} & \quad \Omega = 1 \\ \text{Closed FL: positive curvature,} & \quad \Omega > 1 \end{aligned}$$

We want to be able to determine whether a given cosmological model is exactly FL or close to FL. For this purpose it is necessary to introduce physical quantities called the *kinematical quantities* (see, for example, Wainwright & Ellis 1997 (WE) [77, page 18], and Ellis 1971 [21, page 111]). For a unit timelike vector \mathbf{u} , one can decompose the covariant derivative $u_{a;b}$ of the corresponding 1-form into its irreducible parts – the kinematical quantities σ_{ab} , ω_{ab} , Θ and \dot{u}_a . The scalar Θ is the rate of expansion scalar and \dot{u}_a is the acceleration vector. The tensor σ_{ab} is the rate of shear tensor and ω_{ab} is the rate of vorticity tensor. If the vorticity is zero, we say that \mathbf{u} is irrotational. Because we are working in a cosmological context we shall usually replace Θ by the Hubble scalar H defined earlier, which is related to Θ according to $H = \frac{1}{3}\Theta$. The following theorem characterizes the FL models using the kinematical quantities (see, for example, Krasiński 1997 [44, page 11]):

Theorem 1

A solution of the EFEs with perfect fluid matter content is an FL model if and only if

$$\sigma_{ab} = 0 = \omega_{ab} = \dot{u}_a. \quad (1.5)$$

The FL models can also be characterized using the *Weyl conformal curvature tensor* C_{abcd} , which is interpreted as describing the free gravitational field. The Weyl tensor can be decomposed into its electric part E_{ab} and magnetic part H_{ab} relative to \mathbf{u} . The following theorem characterizes the FL models using E_{ab} and H_{ab} (see, for example, Wainwright 1996 [76, Section 4.1]):

Theorem 2

A solution of the EFEs with perfect fluid matter content and equation of state $p = p(\mu)$ is an FL model if and only if

$$E_{ab} = 0 = H_{ab}. \quad (1.6)$$

Spatially homogeneous cosmologies

Spatially homogeneous cosmologies with an isometry group G_3 acting on spacelike 3-surfaces, the so-called Bianchi cosmologies, are classified according to the structure of the G_3 group, as given in Table 1.1.⁷

Table 1.1: Classification of Bianchi cosmologies.

Group type		Eigenvalues		
Class A	Class B	of $n_{\alpha\beta}$		
IX		+	+	+
VIII		+	+	−
VII ₀	VII _h	+	+	0
VI ₀	VI _h	+	−	0
II	IV	+	0	0
I	V	0	0	0

Bianchi cosmologies comprise two classes,

- i) the *non-tilted* models in which the 4-velocity vector \mathbf{u} is always orthogonal to the spacelike G_3 orbits, were first studied in detail by Ellis & MacCallum 1969 [23].
- ii) the *tilted* models in which \mathbf{u} is never orthogonal to the spacelike G_3 orbits, were first studied by King & Ellis 1973 [43].

The dynamics of non-tilted Bianchi cosmologies have been analyzed in detail (see WE, Hewitt *et al.* 2003 [36] and Horwood *et al.* 2003 [38]). Much less is known about the dynamics of tilted Bianchi cosmologies and work is currently in progress.⁸ Indeed in this thesis we provide a formulation of the EFEs for analyzing the asymptotic and intermediate dynamics of the so-called G_2 -compatible Bianchi cosmologies.

There exist G_3 subgroups within the G_6 isometry group of FL cosmologies. Thus FL cosmologies appear as special cases of SH cosmologies – open FL as

⁷The symmetric matrix $n_{\alpha\beta}$ in Table 1.1 is defined in equation (2.3).

⁸See Hervik 2004 [32] and Hervik & Coley 2004 [33].

Bianchi V and VII_h , flat FL as Bianchi I and VII_0 , and closed FL as Bianchi IX (see WE, page 37). Notice that open and flat FL cosmologies appear as more than one type of Bianchi cosmology. These are instances of *multiple representation* of special models in a more general class of models.

Spatially inhomogeneous cosmologies

The simplest spatially inhomogeneous cosmologies are the G_2 cosmologies, which admit one spatial degree of freedom. These models, which form the main focus of this thesis, will be classified in Chapter 3. We do not consider generic spatially inhomogeneous cosmologies, i.e. the so-called G_0 cosmologies, in this thesis. We refer to Ugglá *et al.* 2003 [72] and Lim *et al.* 2004 [48] for a general framework for analyzing these models.

1.3 Goals

We now discuss three physically important goals of the study of cosmological models more general than FL.

P1. Describe the asymptotic dynamics at early times.

Assuming that the universe is expanding from an initial singularity, the phrase “dynamics at early times” refers to the dynamics in the asymptotic regime associated with the initial singularity, characterized by $l \rightarrow 0$, where l is the overall length scale. Classical general relativity breaks down at the singularity, and should be replaced by a theory of quantum gravity there. The time after which classical general relativity is valid is called the Planck time. Thus in physical terms the phrase “dynamics at early times” refers to the evolution of the universe in an epoch starting at the Planck time. It is important to classify all possible asymptotic states at early times that are permitted by the EFEs, in order to explain how the universe may have evolved.

Two important conjectures about the asymptotic dynamics at early times have been made by Belinskii, Khalatnikov & Lifshitz, which we shall refer to as BKL I and BKL II.

BKL conjecture I

For a typical cosmological model the matter content is not dynamically significant near the initial singularity (Lifshitz & Khalatnikov 1963 [46, page 200], BKL 1970 [8, pages 532, 538]).

The implication of this conjecture is that one can use the vacuum EFEs to approximate the evolution of a typical cosmological model near the initial singularity. An example of atypical cosmologies is the set of models with an isotropic singularity (Goode & Wainwright 1985 [27], Coley *et al.* 2004 [18]). Another example is the set of models in which the matter content is a so-called stiff fluid ($p = \mu$) (Andersson & Rendall 2001 [1]).

BKL conjecture II

Near the initial singularity, the spatial derivatives in the EFEs for a typical cosmological model are not dynamically significant (BKL 1982 [9, page 656]).

The implication of this conjecture is that near the initial singularity the EFEs effectively reduce to ODEs, namely, the ODEs that describe the evolution of SH cosmologies. Hence it is plausible that SH models will play an important role in analyzing spatially inhomogeneous models.

P2. Describe the asymptotic dynamics at late times.

The phrase “dynamics at late times” refers to the dynamics in the asymptotic regime characterized by $l \rightarrow \infty$. For example, the dynamics at late times in a radiation model would describe the later stage of the radiation-dominated epoch before the universe became matter-dominated. Likewise, the dynamics at late times in an inflationary model would describe the final stage of the inflationary epoch.

P3. Describe the dynamics of close-to-FL models.

As mentioned earlier, it is usually assumed that deviations from exact isotropy and spatial inhomogeneity can be described using linear perturbations of an FL model.⁹ Linear perturbations have been used in

⁹For a review of cosmological perturbations, see Mukhanov *et al.* 1992 [55]. Other references that use a gauge-invariant approach are Bardeen 1980 [6], Bruni *et al.* 1992 [14] and Goode 1989 [26].

studying, for example, the evolution of the primordial density perturbations during the radiation-dominated epoch, and the development of large-scale structure in the distribution of galaxies. A key question is this: does linear perturbation theory correctly describe the dynamics of close-to-FL models?

1.4 Overview

This thesis is divided into two parts. The first part consists of Chapters 2–7, which provide a unified formulation of the EFEs, the background and analytical results for the dynamics of G_2 and SH cosmologies. The second part consists of Chapters 8–9, in which we present a numerical exploration of the dynamics of G_2 cosmologies.

We first establish a framework for the study of inhomogeneous cosmologies in Chapter 2. We use the orthonormal frame approach to formulate the EFEs, and introduce the appropriate normalizations for G_2 and SH models respectively, which lead to scale-invariant variables that are bounded at the initial singularity.

In Chapter 3 we present a hierarchy of subclasses within the G_2 cosmologies, and develop the links between G_2 and SH cosmologies.

A new, unified formulation for G_2 -compatible SH cosmologies is given in Chapter 4. We discuss the tilted SH cosmologies in detail, emphasizing the past asymptotic dynamics and giving conditions for the existence of Mixmaster dynamics.

Chapters 5–8 deal with analytical aspects of G_2 cosmologies. In Chapter 5 we complete the formulation for G_2 cosmologies by choosing appropriate temporal and spatial gauges. We discuss the notions of the silent boundary and asymptotic silence, which play a key role in linking G_2 dynamics with SH dynamics. Chapter 6 presents two G_2 solutions – one of which is new – that develop large spatial gradients as they approach the initial singularity. They serve as prototypes for such behaviour in typical G_2 solutions. In Chapter 7, the results of Chapters 4 and 6 are used to predict the past asymptotic dynamics of G_2 cosmologies. In particular, we discuss the existence of Mixmaster dynamics and the validity of the BKL conjecture II.

Chapter 8 is devoted to various aspects of numerical simulations of G_2 cosmologies: choosing the initial condition, devising the numerical solvers, and comparing the errors of the solvers.

In Chapter 9 we present the results from a variety of numerical simula-

tions to illustrate various facets of G_2 dynamics. In contrast to the previous numerical work on vacuum models, we investigate non-vacuum models, in which the source of the gravitational field is a radiation fluid and a cosmological constant. The main focus is on the past asymptotic regime, with a secondary focus on the future asymptotic dynamics with a positive cosmological constant and on the close-to-FL regime.

In the concluding Chapter 10 we summarize the new results in this thesis, and remark on future research.

As regards background material, we assume that the reader is familiar with the orthonormal frame formalism, although a brief review with references is given at the beginning of Chapter 2. In addition we assume familiarity with some basic concepts in the theory of dynamical systems. We refer to WE (Chapter 4) for a summary and further references. For background material on the use of scale-invariant variables and dynamical systems methods in cosmology, we also refer to WE.

Part I

Dynamics of G_2 and SH cosmologies

Chapter 2

The orthonormal frame formalism

In this chapter we introduce the orthonormal frame formalism, which is based on a 1+3 decomposition of spacetime. Our goal is to apply the formalism to give a 1+1+2 decomposition of spacetime, which provides the basis for our analysis of G_2 cosmologies.

The orthonormal frame formalism was first introduced in cosmology by Ellis 1967 [20] and subsequently developed by Ellis & MacCallum 1969 [23] and MacCallum 1973 [52]. More recently, it was extended by van Elst & Uggla 1997 [73]. Our standard references will be MacCallum 1973 [52] and van Elst & Uggla 1997 [73].

2.1 1+3 decomposition

In the orthonormal frame approach one does not use the metric \mathbf{g} directly (as done in the metric approach), but chooses at each point of the spacetime manifold $(\mathcal{M}, \mathbf{g})$ a set of four linearly independent 1-forms $\{\omega^a\}$ such that the line element can be locally expressed as $ds^2 = \eta_{ab}\omega^a\omega^b$, where $\eta_{ab} = \text{diag}(-1, 1, 1, 1)$. The corresponding vector fields $\{\mathbf{e}_a\}$ are then mutually orthogonal and of unit length – they form an orthonormal basis, with \mathbf{e}_0 being timelike (and thus defining a timelike congruence).

The gravitational field is described by the commutation functions γ^c_{ab} of

the orthonormal frame, defined by

$$[\mathbf{e}_a, \mathbf{e}_b] = \gamma^c{}_{ab} \mathbf{e}_c. \quad (2.1)$$

The first step is to perform a 1+3 decomposition of the commutation functions as follows:¹

$$[\mathbf{e}_0, \mathbf{e}_\alpha] = \dot{u}_\alpha \mathbf{e}_0 - [H\delta_\alpha^\beta + \sigma_\alpha^\beta - \epsilon_\alpha^{\beta\gamma}(\omega_\gamma - \Omega_\gamma)] \mathbf{e}_\beta, \quad (2.2)$$

$$[\mathbf{e}_\alpha, \mathbf{e}_\beta] = -2\epsilon_{\alpha\beta}{}^\mu \omega_\mu \mathbf{e}_0 + [\epsilon_{\alpha\beta\nu} n^{\mu\nu} + a_\alpha \delta_\beta^\mu - a_\beta \delta_\alpha^\mu] \mathbf{e}_\mu. \quad (2.3)$$

The variables in (2.2) and (2.3) have physical or geometrical meanings, as follows. The variable H is the Hubble scalar, $\sigma_{\alpha\beta}$ the rate of shear tensor, \dot{u}_α the acceleration vector, and ω_α the rate of vorticity vector of the timelike congruence defined by \mathbf{e}_0 , while Ω_α is the angular velocity of the spatial frame $\{\mathbf{e}_\alpha\}$ with respect to a nonrotating frame ($\Omega_\alpha = 0$). The variables $n_{\alpha\beta}$ and a_α have no direct physical or geometrical meanings in general, but if the fundamental timelike vector field \mathbf{e}_0 is hypersurface-orthogonal, then they directly determine the geometry of the spacelike 3-surfaces orthogonal to \mathbf{e}_0 (see, for example WE, Section 1.6.3). We shall thus refer to $n_{\alpha\beta}$ and a_α as the *spatial curvature variables*. Collectively, the variables above describe the gravitational field. We shall refer to them as the *gravitational field variables*, and denote them by the state vector

$$\mathbf{X}_{\text{grav}} = (H, \sigma_{\alpha\beta}, \dot{u}_\alpha, \omega_\alpha, \Omega_\alpha, n_{\alpha\beta}, a_\alpha), \quad (2.4)$$

The matter content of a cosmological model is described by the stress-energy tensor T_{ab} , which is decomposed into irreducible parts with respect to \mathbf{e}_0 in the following way (let $\mathbf{e}_0 = \mathbf{u}$ below):

$$T_{ab} = \mu u_a u_b + 2q_{(a} u_{b)} + p h_{ab} + \pi_{ab}, \quad (2.5)$$

where

$$q_a u^a = 0, \quad \pi_{ab} u^b = 0, \quad \pi_a{}^a = 0, \quad \pi_{ab} = \pi_{ba},$$

and $h_{ab} = g_{ab} + u_a u_b$ is the projection tensor which locally projects into the 3-space orthogonal to \mathbf{u} . Since we are using an orthonormal frame, we have $g_{ab} = \eta_{ab}$, $u^a = (1, 0, 0, 0)$, and $q_0 = 0 = \pi_{0a}$. The variables $(\mu, p, q_\alpha, \pi_{\alpha\beta})$

¹We follow the Ω_α sign convention of van Elst & Uggla 1997 [73, page 2676].

have physical meanings: μ is the energy density, p is the (isotropic) pressure, q_α is the energy flux density and $\pi_{\alpha\beta}$ is the anisotropic pressure (see, for example, van Elst & Uggla 1997 [73, page 2677]). We shall refer to these variables as the *matter variables*, and denote them by the state vector

$$\mathbf{X}_{\text{matter}} = (\mu, q_\alpha, p, \pi_{\alpha\beta}). \quad (2.6)$$

The dynamics of the variables in (2.4) and (2.6) is described by the EFEs, the Jacobi identities (using \mathbf{e}_a) and the contracted Bianchi identities:

$$G_{ab} + \Lambda g_{ab} = T_{ab}, \quad (2.7)$$

$$\mathbf{e}_{[c}\gamma^d{}_{ab]} - \gamma^d{}_{e[c}\gamma^e{}_{ab]} = 0, \quad (2.8)$$

$$\text{and} \quad \nabla_b T_a{}^b = 0, \quad (2.9)$$

respectively. The evolution of p and $\pi_{\alpha\beta}$ has to be specified by giving an equation of state for the matter content (e.g. perfect fluid). The variables \dot{u}_α and Ω_α correspond to the temporal and spatial gauge freedom respectively, and will be specified later.

Throughout this thesis we shall assume that *the fundamental congruence* \mathbf{e}_0 *has zero vorticity* ($\omega_\alpha = 0$), or equivalently that \mathbf{e}_0 is orthogonal to a family of spacelike 3-surfaces. We now list the system of evolution and constraint equations (also see WE, page 33, but with the opposite sign convention for Ω_α ; see van Elst & Uggla 1997 [73] for the equations with vorticity). The angle bracket used in (2.12) and (2.16) denotes traceless symmetrization – given $V_{\alpha\beta}$, $V_{\langle\alpha\beta\rangle}$ is defined by

$$V_{\langle\alpha\beta\rangle} = V_{(\alpha\beta)} - \frac{1}{3}V_\gamma{}^\gamma\delta_{\alpha\beta}. \quad (2.10)$$

The general orthonormal frame equations ($\omega_\alpha = 0$) ^a

Einstein field equations:

$$\mathbf{e}_0 H = -H^2 - \frac{1}{3}\sigma_{\alpha\beta}\sigma^{\alpha\beta} + \frac{1}{3}(\mathbf{e}_\alpha + \dot{u}_\alpha - 2a_\alpha)\dot{u}^\alpha - \frac{1}{6}(\mu + 3p) + \frac{1}{3}\Lambda \quad (2.11)$$

$$\begin{aligned} \mathbf{e}_0(\sigma_{\alpha\beta}) &= -3H\sigma_{\alpha\beta} - 2\epsilon^{\gamma\delta}{}_{(\alpha}\sigma_{\beta)\gamma}\Omega_\delta - {}^3S_{\alpha\beta} + \pi_{\alpha\beta} - \epsilon^{\gamma\delta}{}_{(\alpha}n_{\beta)\gamma}\dot{u}_\delta \\ &\quad + (\mathbf{e}_{\langle\alpha} + \dot{u}_{\langle\alpha} + a_{\langle\alpha})\dot{u}_{\beta\rangle} \end{aligned} \quad (2.12)$$

$$0 = (C_G) = 6H^2 + {}^3R - \sigma_{\alpha\beta}\sigma^{\alpha\beta} - 2\mu - 2\Lambda \quad (2.13)$$

$$0 = (C_C)_\alpha = -2\mathbf{e}_\alpha H + \mathbf{e}_\beta\sigma_\alpha{}^\beta - 3a_\beta\sigma_\alpha{}^\beta - \epsilon_\alpha{}^{\beta\gamma}n_{\beta\delta}\sigma_\gamma{}^\delta + q_\alpha, \quad (2.14)$$

where 3R and ${}^3S_{\alpha\beta}$ are the isotropic and anisotropic spatial curvature, and are given by

$${}^3R = 4\mathbf{e}_\alpha a^\alpha - 6a_\alpha a^\alpha - n_{\alpha\beta}n^{\alpha\beta} + \frac{1}{2}(n_\gamma{}^\gamma)^2 \quad (2.15)$$

$${}^3S_{\alpha\beta} = \mathbf{e}_{\langle\alpha}a_{\beta\rangle} - (\mathbf{e}_\gamma - 2a_\gamma)n_{\delta(\alpha}\epsilon_{\beta)\gamma}{}^{\delta} + 2n_{\langle\alpha}{}^\gamma n_{\beta\rangle\gamma} - n_\gamma{}^\gamma n_{\langle\alpha\beta\rangle}. \quad (2.16)$$

Jacobi identities:

$$\begin{aligned} \mathbf{e}_0(n_{\alpha\beta}) &= -Hn_{\alpha\beta} + 2\sigma^\gamma{}_{(\alpha}n_{\beta)\gamma} - 2\epsilon^{\gamma\delta}{}_{(\alpha}n_{\beta)\gamma}\Omega_\delta \\ &\quad - (\mathbf{e}_\gamma + \dot{u}_\gamma)(\epsilon^{\gamma\delta}{}_{(\alpha}\sigma_{\beta)\delta} - \delta^\gamma{}_{(\alpha}\Omega_{\beta)}) + \delta_{\alpha\beta}\Omega^\gamma \end{aligned} \quad (2.17)$$

$$\begin{aligned} \mathbf{e}_0(a_\alpha) &= (-H\delta_\alpha{}^\beta - \sigma_\alpha{}^\beta - \epsilon_\alpha{}^{\beta\gamma}\Omega_\gamma)a_\beta \\ &\quad - \frac{1}{2}(\mathbf{e}_\beta + \dot{u}_\beta)(2H\delta_\alpha{}^\beta - \sigma_\alpha{}^\beta - \epsilon_\alpha{}^{\beta\gamma}\Omega_\gamma) \end{aligned} \quad (2.18)$$

$$0 = (C_\omega)^\alpha = [\epsilon^{\alpha\beta\gamma}(\mathbf{e}_\beta - a_\beta) - n^{\alpha\gamma}]\dot{u}_\gamma \quad (2.19)$$

$$0 = (C_J)_\alpha = \mathbf{e}_\beta(n_\alpha{}^\beta + \epsilon_\alpha{}^{\beta\gamma}a_\gamma) - 2a_\beta n_\alpha{}^\beta. \quad (2.20)$$

Contracted Bianchi identities:

$$\mathbf{e}_0(\mu) = -3H(\mu + p) - \sigma_{\alpha\beta}\pi^{\alpha\beta} - (\mathbf{e}_\alpha + 2\dot{u}_\alpha - 2a_\alpha)q^\alpha \quad (2.21)$$

$$\begin{aligned} \mathbf{e}_0(q_\alpha) &= (-4H\delta_\alpha{}^\beta - \sigma_\alpha{}^\beta - \epsilon_\alpha{}^{\beta\gamma}\Omega_\gamma)q_\beta - (\mu + p)\dot{u}_\alpha - \mathbf{e}_\alpha p \\ &\quad - (\mathbf{e}_\beta + \dot{u}_\beta - 3a_\beta)\pi_\alpha{}^\beta + \epsilon_\alpha{}^{\beta\gamma}n_{\beta\delta}\pi_\gamma{}^\delta. \end{aligned} \quad (2.22)$$

^aThe letter C denotes a constraint, and the subscript denotes which one: Gauss, Codacci, vorticity and Jacobi.

Perfect fluid

This thesis focuses on cosmological models whose matter content includes a perfect fluid, which we now introduce. A *perfect fluid* has a 4-velocity $\tilde{\mathbf{u}}$ which is not necessarily aligned with the 4-velocity $\mathbf{e}_0 = \mathbf{u}$ of our fundamental observers. The stress-energy tensor T_{ab} is

$$T_{ab} = \tilde{\mu}\tilde{u}_a\tilde{u}_b + \tilde{p}(g_{ab} + \tilde{u}_a\tilde{u}_b), \quad \tilde{u}_a\tilde{u}^a = -1. \quad (2.23)$$

A *perfect fluid with a linear barotropic equation of state* specifies \tilde{p} :

$$\tilde{p} = \tilde{p}(\tilde{\mu}) = (\gamma - 1)\tilde{\mu}, \quad (2.24)$$

where γ is a constant parameter. The range

$$1 \leq \gamma < 2 \quad (2.25)$$

is of particular physical interest, since it ensures that the perfect fluid satisfies the dominant and strong energy conditions and the causality requirement that the speed of sound should be less than that of light. The values $\gamma = 1$ and $\gamma = \frac{4}{3}$ correspond to pressure-free matter (“dust”) and radiation, respectively. Since $\tilde{\mathbf{u}}$ and \mathbf{u} are not necessarily aligned, we write

$$\tilde{u}^a = \Gamma(u^a + v^a), \quad (2.26)$$

where

$$u_\alpha = 0, \quad v_0 = 0, \quad \Gamma = (1 - v^2)^{-\frac{1}{2}}, \quad v^2 = v_\alpha v^\alpha.$$

It follows from (2.5), (2.23)–(2.26) that $(\mu, p, q_\alpha, \pi_{\alpha\beta})$ are given by

$$\mu = \frac{G_+}{1 - v^2}\tilde{\mu}, \quad (2.27)$$

$$p = \frac{(\gamma - 1)(1 - v^2) + \frac{1}{3}\gamma v^2}{G_+}\mu, \quad q_\alpha = \frac{\gamma\mu}{G_+}v_\alpha, \quad \pi_{\alpha\beta} = \frac{\gamma\mu}{G_+}v_{\langle\alpha}v_{\beta\rangle}, \quad (2.28)$$

where $G_+ = 1 + (\gamma - 1)v^2$. The basic variables that we use are μ and v^α . The vector v^α is called the *tilt* of the fluid, and has three degrees of freedom.

Weyl tensor

It is useful to keep track of the Weyl curvature tensor C_{abcd} , decomposed with respect to \mathbf{e}_0 according to (see WE, page 19):

$$E_{ac} = C_{abcd}u^b u^d, \quad H_{ac} = \frac{1}{2}\eta_{ab}{}^{st}C_{stcd}u^b u^d,$$

and are given in terms of the gravitational and matter variables as follows (See WE, page 35):

$$E_{\alpha\beta} = H\sigma_{\alpha\beta} - (\sigma_{\alpha}{}^{\gamma}\sigma_{\gamma\beta} - \frac{1}{3}\sigma_{\gamma\delta}\sigma^{\gamma\delta}\delta_{\alpha\beta}) + {}^3S_{\alpha\beta} - \frac{1}{2}\pi_{\alpha\beta} \quad (2.29)$$

$$H_{\alpha\beta} = (\mathbf{e}_{\gamma} - a_{\gamma})\sigma_{\delta(\alpha}\epsilon_{\beta)}{}^{\gamma\delta} - 3\sigma^{\gamma}{}_{(\alpha}n_{\beta)\gamma} + n_{\gamma\delta}\sigma^{\gamma\delta}\delta_{\alpha\beta} + \frac{1}{2}n_{\gamma}{}^{\gamma}\sigma_{\alpha\beta}. \quad (2.30)$$

Local coordinates

For quantitative analyses, we need to express the differential operators \mathbf{e}_0 and \mathbf{e}_{α} as partial differential operators in terms of t and x^i .² The 1+3 decomposition for $\{\mathbf{e}_0, \mathbf{e}_{\alpha}\}$ is as follows:

$$\mathbf{e}_0 = N^{-1}\partial_t, \quad \mathbf{e}_{\alpha} = M_{\alpha}\partial_t + e_{\alpha}{}^i\partial_i. \quad (2.31)$$

The assumption that \mathbf{e}_0 is hypersurface-orthogonal allows us to set

$$M_{\alpha} = 0. \quad (2.32)$$

It follows that the 3-surfaces³ to which \mathbf{e}_0 is orthogonal are given by $t = \text{const.}$. See van Elst & Uggla 1997 [73, Section 2.7] for details. The variables

$$(N, e_{\alpha}{}^i) \quad (2.33)$$

are called the *frame coefficients*. When the commutators (2.2) and (2.3) act on t and x^i , they provide the equations that relate the frame coefficients to the variables in (2.4).

²We reserve the indices i, j, k , running from 1 to 3, for the local coordinate components with respect to x^i .

³For brevity we shall refer to these 3-surfaces as “slices”.

Commutators acting on t and x^i :

$$\mathbf{e}_0(e_\alpha{}^i) = (-H\delta_\alpha{}^\beta - \sigma_\alpha{}^\beta - \epsilon_\alpha{}^{\beta\gamma}\Omega_\gamma)e_\beta{}^i \quad (2.34)$$

$$0 = (C_{\dot{u}})_\alpha = N^{-1}\mathbf{e}_\alpha(N) - \dot{u}_\alpha \quad (2.35)$$

$$0 = (C_{\text{com}})^i{}_{\alpha\beta} = 2(\mathbf{e}_{[\alpha} - a_{[\alpha]}e_{\beta]}^i - \epsilon_{\alpha\beta\delta}n^{\gamma\delta}e_\gamma{}^i) . \quad (2.36)$$

The frame coefficients are directly related to the metric \mathbf{g} through

$$g^{00} = -N^{-2}, \quad g^{0i} = 0, \quad g^{ij} = \delta^{\alpha\beta}e_\alpha{}^ie_\beta{}^j. \quad (2.37)$$

This ties the variables in (2.4) to the metric.

All these equations give an autonomous system of first order PDEs involving temporal and spatial derivatives, and a set of constraint equations which involve only spatial derivatives, for the variables (2.4), (2.6) and (2.33). The system is under-determined, however, since there are no evolution equations for N , \dot{u}_α , Ω_α , p and $\pi_{\alpha\beta}$. A perfect fluid matter source with linear barotropic equation of state gives (2.28), while temporal and spatial gauges determine (N, \dot{u}_α) and Ω_α respectively.

The general orthonormal frame equations (2.11)–(2.22) describe the dynamics of G_0 cosmologies. They are also ideal for describing the dynamics of SH cosmologies of Bianchi types VIII and IX, for which the $t = \text{const.}$ slices are chosen to coincide with the G_3 group orbits (and the orthonormal frame is chosen to be *group-invariant*), so that

$$\mathbf{e}_\alpha(\mathbf{X}_{\text{grav}}) = 0, \quad \mathbf{e}_\alpha(\mathbf{X}_{\text{matter}}) = 0, \quad \dot{u}_\alpha = 0. \quad (2.38)$$

2.2 1+1+2 decomposition for G_2 cosmologies

By a G_2 cosmology, we mean a cosmological model which admits an Abelian group G_2 of isometries whose orbits are spacelike 2-surfaces. We derive the evolution and constraint equations for G_2 cosmologies by specializing the general orthonormal frame equations in the previous section. We shall preserve the vorticity-free \mathbf{e}_0 while taking full advantage of the G_2 structure to simplify the equations, namely to make the variables depend on t and x only.

Let $\boldsymbol{\xi}_1, \boldsymbol{\xi}_2$ be two independent Killing vector fields (KVF's) of the Abelian group of a G_2 cosmology. First, we choose a *group-invariant* orthonormal

frame, i.e.

$$[\mathbf{e}_a, \boldsymbol{\xi}_1] = \mathbf{0} = [\mathbf{e}_a, \boldsymbol{\xi}_2]. \quad (2.39)$$

Secondly, we also adapt the orthonormal frame $\{\mathbf{e}_a\}$ so that \mathbf{e}_2 and \mathbf{e}_3 are tangent to the G_2 orbits. The existence of such a frame is established in the proof of Theorem 3.1 in Wainwright 1979 [75] (see Hewitt 1989 [34, page 120] for a more general theorem). For a group-invariant orbit-aligned frame it follows (Wainwright 1979 [75]) that

$$\mathbf{e}_A(\gamma^a_{bc}) = 0, \quad (2.40)$$

$$\gamma^0_{0A} = \gamma^1_{0A} = 0, \quad \gamma^0_{1A} = \gamma^1_{1A} = 0, \quad \gamma^0_{23} = \gamma^1_{23} = 0. \quad (2.41)$$

Recall that Latin indices run from 0 to 3; Greek indices from 1 to 3; capital Latin indices run from 2 to 3. Writing (2.41) in terms of the irreducible variables in (2.4) gives

$$\dot{u}_A = 0, \quad \Omega_A = -\epsilon_{AB}\sigma^{1B}, \quad \omega_\alpha = 0, \quad a_A = 0, \quad n_{1\alpha} = 0. \quad (2.42)$$

Note that Ω_A is now expressed in terms of σ_{1A} , and ϵ_{AB} is the anti-symmetric permutation tensor ($\epsilon_{23} = -\epsilon_{32} = 1$).

For convenience we introduce the trace-free quantity

$$\tilde{n}_{AB} = n_{AB} - \frac{1}{2}n_C^C \delta_{AB}, \quad (2.43)$$

and its dual

$${}^*\tilde{n}_{AB} = \epsilon_{AC}\tilde{n}_B^C, \quad (2.44)$$

and similarly for σ_{AB} , ${}^3S_{AB}$ and π_{AB} . The resulting system involves the following variables:

$$\mathbf{X}_{\text{grav}} = (H, \sigma_{11}, \sigma_{1A}, \tilde{\sigma}_{AB}, n_C^C, \tilde{n}_{AB}, a_1, \dot{u}_1, \Omega_1), \quad (2.45)$$

$$\mathbf{X}_{\text{matter}} = (\mu, q_1, q_A, p, \pi_{11}, \pi_{1A}, \tilde{\pi}_{AB}). \quad (2.46)$$

By performing a 1+2 spatial decomposition of the general orthonormal frame equations in the previous section, we obtain the following equations for G_2 cosmologies.⁴ These equations arise in a fairly obvious way from the general orthonormal frame equations (2.11)–(2.22), with Ω_A replaced using (2.42).

⁴These equations generalize the system of equations in WE, pages 48–49, which are valid for OT G_2 cosmologies.

The 1+1+2 equations for G_2 cosmologies

Einstein field equations:

$$\mathbf{e}_0 H = -H^2 - \frac{1}{3}\sigma_{\alpha\beta}\sigma^{\alpha\beta} + \frac{1}{3}(\mathbf{e}_1 + \dot{u}_1 - 2a_1)\dot{u}_1 - \frac{1}{6}(\mu + 3p) + \frac{1}{3}\Lambda \quad (2.47)$$

$$\mathbf{e}_0(\sigma_{11}) = -3H\sigma_{11} - 2\sigma_{1A}\sigma^{1A} + \frac{2}{3}(\mathbf{e}_1 + \dot{u}_1 + a_1)\dot{u}_1 - {}^3S_{11} + \pi_{11} \quad (2.48)$$

$$\mathbf{e}_0(\sigma_{1A}) = -3(H - \frac{1}{2}\sigma_{11})\sigma_{1A} - (\tilde{\sigma}_{AB} - \Omega_1\epsilon_{AB})\sigma^{1B} + \pi_{1A} \quad (2.49)$$

$$\begin{aligned} \mathbf{e}_0(\tilde{\sigma}_{AB}) = & -3H\tilde{\sigma}_{AB} + 2\sigma_{1A}\sigma_{1B} - \sigma_{1C}\sigma^{1C}\delta_{AB} - 2\Omega_1{}^*\tilde{\sigma}_{AB} - \dot{u}_1{}^*\tilde{n}_{AB} \\ & - {}^3\tilde{S}_{AB} + \tilde{\pi}_{AB} \end{aligned} \quad (2.50)$$

$$0 = (C_G) = 6H^2 + {}^3R - \sigma_{\alpha\beta}\sigma^{\alpha\beta} - 2\mu - 2\Lambda \quad (2.51)$$

$$0 = (C_C)_1 = -2\mathbf{e}_1(H - \frac{1}{2}\sigma_{11}) - 3a_1\sigma_{11} - {}^*\tilde{\sigma}_{AB}\tilde{n}^{AB} + q_1 \quad (2.52)$$

$$0 = (C_C)_A = (\mathbf{e}_1 - 3a_1)\sigma_{1A} - ({}^*\tilde{n}_{AB} + \frac{1}{2}n_C{}^C\epsilon_{AB})\sigma^{1B} + q_A, \quad (2.53)$$

where

$$\sigma_{\alpha\beta}\sigma^{\alpha\beta} = \frac{3}{2}(\sigma_{11})^2 + 2\sigma_{1A}\sigma^{1A} + \tilde{\sigma}_{AB}\tilde{\sigma}^{AB} \quad (2.54)$$

$${}^3R = 4\mathbf{e}_1 a_1 - 6a_1^2 - \tilde{n}_{AB}\tilde{n}^{AB} \quad (2.55)$$

$${}^3S_{11} = \frac{2}{3}\mathbf{e}_1 a_1 - \frac{2}{3}\tilde{n}_{AB}\tilde{n}^{AB}, \quad {}^3S_{1A} = 0 \quad (2.56)$$

$${}^3\tilde{S}_{AB} = (\mathbf{e}_1 - 2a_1){}^*\tilde{n}_{AB} + n_C{}^C\tilde{n}_{AB}. \quad (2.57)$$

Jacobi identities:

$$\mathbf{e}_0(n_A{}^A) = (-H - \sigma_{11})n_A{}^A + 2\tilde{\sigma}^{AB}\tilde{n}_{AB} - 2(\mathbf{e}_1 + \dot{u}_1)\Omega_1 \quad (2.58)$$

$$\mathbf{e}_0(\tilde{n}_{AB}) = (-H - \sigma_{11})\tilde{n}_{AB} + n_C{}^C\tilde{\sigma}_{AB} - 2\Omega_1{}^*\tilde{n}_{AB} + (\mathbf{e}_1 + \dot{u}_1){}^*\tilde{\sigma}_{AB} \quad (2.59)$$

$$\mathbf{e}_0(a_1) = (-H - \sigma_{11})a_1 - (\mathbf{e}_1 + \dot{u}_1)(H - \frac{1}{2}\sigma_{11}). \quad (2.60)$$

Contracted Bianchi identities:

$$\begin{aligned} \mathbf{e}_0(\mu) = & -3H(\mu + p) - \frac{3}{2}\sigma_{11}\pi_{11} - 2\sigma_{1A}\pi^{1A} - \tilde{\sigma}_{AB}\tilde{\pi}^{AB} \\ & - (\mathbf{e}_1 + 2\dot{u}_1 - 2a_1)q_1 \end{aligned} \quad (2.61)$$

$$\begin{aligned} \mathbf{e}_0(q_1) = & (-4H - \sigma_{11})q_1 - 2\sigma_{1A}q^A - \mathbf{e}_1 p - (\mu + p)\dot{u}_1 \\ & - (\mathbf{e}_1 + \dot{u}_1 - 3a_1)\pi_{11} - {}^*\tilde{n}_{AB}\tilde{\pi}^{AB} \end{aligned} \quad (2.62)$$

$$\begin{aligned} \mathbf{e}_0(q_A) = & (-4H + \frac{1}{2}\sigma_{11})q_A - (\tilde{\sigma}_{AB} + \Omega_1\epsilon_{AB})q^B \\ & - (\mathbf{e}_1 + \dot{u}_1 - 3a_1)\pi_{1A} + ({}^*\tilde{n}_{AB} + \frac{1}{2}n_C{}^C\epsilon_{AB})\pi^{1B}. \end{aligned} \quad (2.63)$$

Perfect fluid

The 1+2 spatial decomposition of (2.28) gives

$$\begin{aligned} p &= \frac{(\gamma - 1)(1 - v^2) + \frac{1}{3}\gamma v^2}{G_+} \mu, & q_1 &= \frac{\gamma\mu}{G_+} v_1, & q_A &= \frac{\gamma\mu}{G_+} v_A, \\ \pi_{11} &= \frac{\gamma\mu}{G_+} (v_1^2 - \frac{1}{3}v^2), & \pi_{1A} &= \frac{\gamma\mu}{G_+} v_1 v_A, \\ \tilde{\pi}_{AB} &= \frac{\gamma\mu}{G_+} (v_A v_B - \frac{1}{2} v_C v^C \delta_{AB}), \end{aligned} \quad (2.64)$$

where

$$G_+ = 1 + (\gamma - 1)v^2, \quad v^2 = v_\alpha v^\alpha = v_1^2 + v_A v^A. \quad (2.65)$$

Weyl tensor

The 1+2 spatial decomposition of (2.29)–(2.30) gives

$$E_{11} = H\sigma_{11} - \frac{1}{2}\sigma_{11}^2 - \frac{1}{3}\sigma^{1A}\sigma_{1A} + \frac{1}{3}\tilde{\sigma}_{AB}\tilde{\sigma}^{AB} + {}^3S_{11} - \frac{1}{2}\pi_{11} \quad (2.66)$$

$$E_{1A} = H\sigma_{1A} - (\frac{1}{2}\sigma_{11}\sigma_{1A} + \sigma^{1B}\tilde{\sigma}_{AB}) - \frac{1}{2}\pi_{1A} \quad (2.67)$$

$$\tilde{E}_{AB} = H\tilde{\sigma}_{AB} - (\sigma_{1A}\sigma_{1B} - \frac{1}{2}\sigma_{1C}\sigma^{1C}\delta_{AB} - \sigma_{11}\tilde{\sigma}_{AB}) + {}^3\tilde{S}_{AB} - \frac{1}{2}\tilde{\pi}_{AB} \quad (2.68)$$

$$H_{11} = \tilde{n}_{AB}\tilde{\sigma}^{AB} \quad (2.69)$$

$$H_{1A} = -\frac{1}{2}(\partial_1 - a_1)\sigma_{1B}\epsilon_A^B - \frac{3}{2}\sigma^{1B}\tilde{n}_{AB} - \frac{1}{4}n_C^C\sigma_{1A} \quad (2.70)$$

$$\tilde{H}_{AB} = -(\partial_1 - a_1)^*\tilde{\sigma}_{AB} - n_C^C\tilde{\sigma}_{AB} + \frac{3}{2}\sigma_{11}\tilde{n}_{AB}. \quad (2.71)$$

Local coordinates

We choose the x -coordinate to be constant on the G_2 orbits. The 1+1+2 coordinate decomposition of the frame coefficients (2.33) is as follows:

$$\mathbf{e}_0 = N^{-1}\partial_t, \quad \mathbf{e}_1 = e_1^1\partial_x + e_1^I\partial_{x^I}, \quad \mathbf{e}_A = e_A^1\partial_x + e_A^I\partial_{x^I}.^5 \quad (2.72)$$

That x is constant on the G_2 orbits means $\mathbf{e}_A(x) = 0$, which implies

$$e_A^1 = 0, \quad (2.73)$$

⁵We reserve the indices I, J, K , running from 2 to 3, for the local coordinate components with respect to y and z .

It follows from (2.40), (2.72) and (2.73) that

$$\partial_{x^I}(\mathbf{X}_{\text{grav}}) = 0, \quad \partial_{x^I}(\mathbf{X}_{\text{matter}}) = 0, \quad (2.74)$$

which implies that in the evolution and constraint equations the operator \mathbf{e}_1 is effectively

$$\mathbf{e}_1 = e_1^1 \partial_x. \quad (2.75)$$

In conjunction with (2.42), the commutators (2.2) and (2.3) acting on t , x and x^I give the following equations for the remaining frame coefficients

$$(N, e_1^1, e_1^I, e_A^I). \quad (2.76)$$

Commutators acting on t , x and x^I :

$$0 = (C_{\dot{u}})_1 = N^{-1} \mathbf{e}_1(N) - \dot{u}_1 \quad (2.77)$$

$$\mathbf{e}_0(e_1^1) = (-H - \sigma_{11})e_1^1 \quad (2.78)$$

$$\mathbf{e}_0(e_1^I) = (-H - \sigma_{11})e_1^I - 2\sigma^{1A}e_A^I \quad (2.79)$$

$$\mathbf{e}_0(e_A^I) = -He_A^I - \sigma_A^B e_B^I - \Omega_1 \epsilon_A^B e_B^I \quad (2.80)$$

$$0 = (C_{\text{com}})^I_{1A} = (\mathbf{e}_1 - a_1)e_A^I - (*\tilde{n}_A^B + \frac{1}{2}n_C^C \epsilon_A^B)e_B^I. \quad (2.81)$$

Note that e_1^I and e_A^I decouple from the system (2.47)–(2.63).

Equations (2.47)–(2.63), (2.77) and (2.78) give a system of first order PDEs in t and x for the variables in (2.4)–(2.6) and the pair (N, e_1^1) . The system is under-determined, however, since there are no evolution equations for N , \dot{u}_1 , Ω_1 , p and $\pi_{\alpha\beta}$. A perfect fluid matter source with linear barotropic equation of state gives (2.64), while temporal and spatial gauges determine (N, \dot{u}_1) and Ω_1 respectively. These equations are used to analyze the dynamics of G_2 cosmologies and of SH cosmologies whose G_3 group has an Abelian G_2 subgroup.

2.3 Scale-invariant variables

The variables in (2.4), (2.6) and (2.33) are scale-dependent and dimensional, and are unsuitable for describing the asymptotic behaviour of cosmological models near the initial singularity, since they typically diverge. It is thus essential to introduce scale-invariant (dimensionless) variables, which

one hopes will be bounded as the initial singularity is approached. As a motivating example, consider an FL model, in which the matter density $\mu \rightarrow \infty$ at the initial singularity. One wants to introduce a corresponding scale-invariant, dimensionless density parameter $\Omega = \mu/(3H^2)$ such that $\Omega \rightarrow 1$.⁶ Another example is the Kasner models, in which the shear $\sigma_{\alpha\beta}$ satisfies $\sigma^2 \equiv \frac{1}{2}\sigma_{\alpha\beta}\sigma^{\alpha\beta} \rightarrow \infty$ at the initial singularity. One wants to introduce a corresponding shear parameter $\Sigma_{\alpha\beta} = \sigma_{\alpha\beta}/H$ such that $\Sigma^2 \equiv \sigma^2/(3H^2) \rightarrow 1$. These examples motivate the use of the Hubble scalar H as the normalizing factor.

1+3 Hubble-normalized variables

We define the Hubble-normalized gravitational and matter variables respectively as follows:

$$(\Sigma_{\alpha\beta}, \dot{U}_\alpha, R_\alpha, N_{\alpha\beta}, A_\alpha) = (\sigma_{\alpha\beta}, \dot{u}_\alpha, \Omega_\alpha, n_{\alpha\beta}, a_\alpha)/H \quad (2.82)$$

$$(\Omega, Q_\alpha, P, \Pi_{\alpha\beta}, \Omega_\Lambda) = (\mu, q_\alpha, p, \pi_{\alpha\beta}, \Lambda)/(3H^2) . \quad (2.83)$$

The differential operators (2.31) and the frame coefficients (2.33) are also redefined to be scale-invariant:

$$\partial_0 = \frac{1}{H}\mathbf{e}_0, \quad \partial_\alpha = \frac{1}{H}\mathbf{e}_\alpha, \quad (2.84)$$

$$\mathcal{N} = NH, \quad E_\alpha^i = \frac{e_\alpha^i}{H}, \quad (2.85)$$

since the frame variables have the same dimension as H . In order to transform the evolution and constraint equations, it is necessary to introduce the *deceleration parameter* q and the *Hubble gradient* r_α according to

$$q + 1 = -\frac{\partial_0 H}{H} \quad (2.86)$$

$$r_\alpha = -\frac{\partial_\alpha H}{H} . \quad (2.87)$$

In order to transform the equations, it is convenient to use the following identities. For the gravitational field variables \mathbf{X}_{grav} in (2.4), which have the

⁶Although it is sufficient to require that Ω tends to a non-zero constant, it is customary to normalize μ such that $\Omega \rightarrow 1$.

same dimension as H , we use the identities

$$\frac{1}{H^2} \mathbf{e}_0 \mathbf{X}_{\text{grav}} = [\boldsymbol{\partial}_0 - (q + 1)] \left(\frac{\mathbf{X}_{\text{grav}}}{H} \right) \quad (2.88)$$

$$\frac{1}{H^2} \mathbf{e}_\alpha \mathbf{X}_{\text{grav}} = [\boldsymbol{\partial}_\alpha - r_\alpha] \left(\frac{\mathbf{X}_{\text{grav}}}{H} \right), \quad (2.89)$$

which follow from (2.82), (2.84)–(2.87). Similarly, for the matter variables $\mathbf{X}_{\text{matter}}$ in (2.6), which have the dimension $[H^2]$, we use the identities

$$\frac{1}{3H^3} \mathbf{e}_0 \mathbf{X}_{\text{matter}} = [\boldsymbol{\partial}_0 - 2(q + 1)] \left(\frac{\mathbf{X}_{\text{matter}}}{3H^2} \right) \quad (2.90)$$

$$\frac{1}{3H^3} \mathbf{e}_\alpha \mathbf{X}_{\text{matter}} = [\boldsymbol{\partial}_\alpha - 2r_\alpha] \left(\frac{\mathbf{X}_{\text{matter}}}{3H^2} \right). \quad (2.91)$$

Then equation (2.11) for $\boldsymbol{\partial}_0 H$ decouples, and through (2.86) gives the following expression for q :

$$q = \frac{1}{3} \Sigma_{\alpha\beta} \Sigma^{\alpha\beta} + \frac{1}{2} (\Omega + 3P) - \Omega_\Lambda - \frac{1}{3} (\boldsymbol{\partial}_\alpha - r_\alpha + \dot{U}_\alpha - 2A_\alpha) \dot{U}^\alpha, \quad (2.92)$$

i.e. q is expressed in terms of the Hubble-normalized variables (2.82) and (2.83).

Equations (2.28) in Hubble-normalized form are

$$P = \frac{(\gamma - 1)(1 - v^2) + \frac{1}{3} \gamma v^2}{G_+} \Omega, \quad Q_\alpha = \frac{\gamma \Omega}{G_+} v_\alpha, \quad \Pi_{\alpha\beta} = \frac{\gamma \Omega}{G_+} v_{\langle\alpha} v_{\beta\rangle}. \quad (2.93)$$

The spatial curvature variables 3R and ${}^3S_{\alpha\beta}$ are normalized according to

$$\Omega_k = -\frac{{}^3R}{6H^2}, \quad \mathcal{S}_{\alpha\beta} = \frac{{}^3S_{\alpha\beta}}{3H^2}. \quad (2.94)$$

The Weyl curvature variables $E_{\alpha\beta}$ and $H_{\alpha\beta}$ are normalized according to

$$(\mathcal{E}_{\alpha\beta}, \mathcal{H}_{\alpha\beta}) = (E_{\alpha\beta}, H_{\alpha\beta}) / (3H^2). \quad (2.95)$$

The commutators (2.2)–(2.3) in Hubble-normalized form are

$$[\partial_0, \partial_\alpha] = (\dot{U}_\alpha - r_\alpha) \partial_0 - (-q \delta_\alpha^\beta + \Sigma_\alpha^\beta + \epsilon_\alpha^{\beta\gamma} R_\gamma) \partial_\beta, \quad (2.96)$$

$$[\partial_\alpha, \partial_\beta] = [\epsilon_{\alpha\beta\nu} N^{\mu\nu} + (A_\alpha + r_\alpha) \delta_\beta^\mu - (A_\beta + r_\beta) \delta_\alpha^\mu] \partial_\mu. \quad (2.97)$$

The 1+3 Hubble-normalized variables and equations are well-suited for analyzing G_0 cosmologies. They are also well-suited for SH cosmologies of types VIII and IX, in which (2.38) implies

$$\partial_\alpha(\mathbf{X}_{\text{grav}}/H) = 0, \quad \partial_\alpha(\mathbf{X}_{\text{matter}}/(3H^2)) = 0, \quad \dot{U}_\alpha = 0, \quad r_\alpha = 0. \quad (2.98)$$

It then follows from (2.35) and (2.84)–(2.85) that we can set

$$\mathcal{N} = 1, \quad \text{so that} \quad \partial_0 = \partial_t. \quad (2.99)$$

1+1+2 Hubble-normalized variables for G_2 -compatible SH cosmologies

For G_2 -compatible SH cosmologies, we define the Hubble-normalized 1+1+2 decomposed gravitational and matter variables as follows:

$$(\Sigma_{11}, \Sigma_{1A}, \tilde{\Sigma}_{AB}, R, N_C^C, \tilde{N}_{AB}, A) = (\sigma_{11}, \sigma_{1A}, \tilde{\sigma}_{AB}, \Omega_1, n_C^C, \tilde{n}_{AB}, a_1)/H \quad (2.100)$$

$$(\Omega, Q_1, Q_A, P, \Pi_{11}, \Pi_{1A}, \tilde{\Pi}_{AB}, \Omega_\Lambda) = (\mu, q_1, q_A, p, \pi_{11}, \pi_{1A}, \tilde{\pi}_{AB}, \Lambda)/(3H^2). \quad (2.101)$$

Equivalently, one can view this as the 1+1+2 decomposed version of the 1+3 Hubble-normalized variables in (2.82)–(2.83). Equations (2.84)–(2.98) are similarly decomposed.

1+1+2 β -normalized variables for G_2 cosmologies

For G_2 cosmologies, the area expansion of the G_2 orbits is described by

$$\Theta_{AB} \equiv H \delta_{AB} + \sigma_{AB}. \quad (2.102)$$

The average expansion rate of the G_2 orbits is described by

$$\beta \equiv \frac{1}{2} \Theta_C^C = H - \frac{1}{2} \sigma_{11}. \quad (2.103)$$

It turns out that there are some advantages in using β instead of H as the normalizing factor (see van Elst *et al.* 2002 [74]). We define the β -normalized variables as follows:

$$(\Sigma_{11}, \Sigma_{1A}, \tilde{\Sigma}_{AB}, \dot{U}, R, N_C^C, \tilde{N}_{AB}, A) = (\sigma_{11}, \sigma_{1A}, \tilde{\sigma}_{AB}, \dot{u}_1, \Omega_1, n_C^C, \tilde{n}_{AB}, a_1)/\beta \quad (2.104)$$

$$(\Omega, Q_1, Q_A, P, \Pi_{11}, \Pi_{1A}, \tilde{\Pi}_{AB}, \Omega_\Lambda) = (\mu, q_1, q_A, p, \pi_{11}, \pi_{1A}, \tilde{\pi}_{AB}, \Lambda)/(3\beta^2). \quad (2.105)$$

The differential operators are likewise normalized as follows:

$$\partial_0 = \frac{1}{\beta} \mathbf{e}_0, \quad \partial_1 = \frac{1}{\beta} \mathbf{e}_1, \quad (2.106)$$

$$\mathcal{N} = N\beta, \quad E_1^1 = \frac{e_1^1}{\beta}, \quad (2.107)$$

We define the analogous deceleration parameter q , and the β gradient r according to

$$q + 1 = -\frac{\partial_0 \beta}{\beta}, \quad r = -\frac{\partial_1 \beta}{\beta}. \quad (2.108)$$

The equations are similarly transformed using the following identities:

$$\frac{1}{\beta^2} \mathbf{e}_0 \mathbf{X}_{\text{grav}} = [\partial_0 - (q + 1)] \left(\frac{\mathbf{X}_{\text{grav}}}{\beta} \right) \quad (2.109)$$

$$\frac{1}{\beta^2} \mathbf{e}_1 \mathbf{X}_{\text{grav}} = [\partial_1 - r] \left(\frac{\mathbf{X}_{\text{grav}}}{\beta} \right) \quad (2.110)$$

$$\frac{1}{3\beta^3} \mathbf{e}_0 \mathbf{X}_{\text{matter}} = [\partial_0 - 2(q + 1)] \left(\frac{\mathbf{X}_{\text{matter}}}{3\beta^2} \right) \quad (2.111)$$

$$\frac{1}{3\beta^3} \mathbf{e}_1 \mathbf{X}_{\text{matter}} = [\partial_1 - 2r] \left(\frac{\mathbf{X}_{\text{matter}}}{3\beta^2} \right). \quad (2.112)$$

Consider the evolution equation for β , in which $\mathbf{e}_1 a_1$ is replaced using (C_G):

$$\begin{aligned} \mathbf{e}_0 \beta = & -\frac{3}{2} \beta^2 + \frac{1}{2} \sigma_{1A} \sigma^{1A} - \frac{1}{4} (\tilde{\sigma}_{AB} \tilde{\sigma}^{AB} + \tilde{n}_{AB} \tilde{n}^{AB}) + \frac{1}{2} a_1^2 - a_1 \dot{u}_1 \\ & - \frac{1}{2} (p + \pi_{11}) + \frac{1}{2} \Lambda. \end{aligned} \quad (2.113)$$

This defines the corresponding area deceleration parameter q :

$$q = \frac{1}{2} - \frac{1}{2}\Sigma_{1A}\Sigma^{1A} + \frac{1}{4}(\tilde{\Sigma}_{AB}\tilde{\Sigma}^{AB} + \tilde{N}_{AB}\tilde{N}^{AB}) - \frac{1}{2}A^2 + A\dot{U} + \frac{3}{2}(P + \Pi_{11}) - \frac{3}{2}\Omega_\Lambda. \quad (2.114)$$

The evolution equation for β decouples from the main system. The $(C_C)_1$ constraint (2.52) can be solved for r :

$$r = \frac{3}{2}(A\Sigma_{11} + {}^*\tilde{\Sigma}_{AB}\tilde{N}^{AB} - Q_1). \quad (2.115)$$

The spatial curvature variables 3R , ${}^3S_{11}$ and ${}^3S_{AB}$ are normalized according to

$$\Omega_k = -\frac{{}^3R}{6\beta^2}, \quad \mathcal{S}_{11} = \frac{{}^3S_{11}}{3\beta^2}, \quad \mathcal{S}_{AB} = \frac{{}^3S_{AB}}{3\beta^2}. \quad (2.116)$$

The Weyl curvature variables are normalized according to

$$(\mathcal{E}_{11}, \mathcal{E}_{1A}, \tilde{\mathcal{E}}_{AB}, \mathcal{H}_{11}, \mathcal{H}_{1A}, \tilde{\mathcal{H}}_{AB}) = (E_{11}, E_{1A}, \tilde{E}_{AB}, H_{11}, H_{1A}, \tilde{H}_{AB})/(3\beta^2). \quad (2.117)$$

The commutator $[\boldsymbol{\partial}_0, \boldsymbol{\partial}_1]$ is given by

$$[\boldsymbol{\partial}_0, \boldsymbol{\partial}_1] = (\dot{U} - r)\boldsymbol{\partial}_0 + (q - \frac{3}{2}\Sigma_{11})\boldsymbol{\partial}_1 - 2\Sigma_1^A\boldsymbol{\partial}_A. \quad (2.118)$$

Chapter 3

The G_2 and SH hierarchies

In this chapter we give a classification of G_2 cosmologies, and of the SH cosmologies that arise as limiting cases, using the action of the G_2 group of isometries, and the tilt degrees of freedom of the perfect fluid. Our goal is to provide a framework for describing the remarkably diverse range of dynamical behaviour that is possible within the class of G_2 cosmologies, only a small part of which has appeared in the literature to date.

3.1 The G_2 hierarchy

It is useful to classify G_2 cosmologies according to the action of the G_2 group, as determined by the properties of the KVF's associated with the G_2 group. There are four restrictions relating to the KVF's, which determine four special classes of G_2 cosmologies. If none of these restrictions is satisfied we shall refer to the G_2 cosmology as *generic*. We now give the above-mentioned restrictions, and then characterize the subclasses using the gravitational field variables (2.45).

(1) *Hypersurface-orthogonal*

This case is specified by requiring that the G_2 admits a hypersurface-orthogonal KVF ξ ,

$$\xi_{[a;b}\xi_{c]} = 0. \tag{3.1}$$

The following proposition provides a convenient way to check for the existence of a hypersurface-orthogonal KVF.

Proposition 3.1. *Consider a G_2 cosmology presented in a group-invariant orbit-aligned frame with \mathbf{e}_2 and \mathbf{e}_3 tangent to the G_2 orbits. Then the G_2 admits a hypersurface-orthogonal KVF if and only if the gravitational field variables (2.45) satisfy*

$$\tilde{\sigma}_{AB}\tilde{n}^{AB} = 0, \quad \tilde{n}_{AB}\sigma^{1A}\sigma^{1B} = 0, \quad {}^*\tilde{\sigma}_{AB}\sigma^{1A}\sigma^{1B} = 0. \quad {}^1 \quad (3.2)$$

In addition, the matter variables (2.46) satisfy

$$\epsilon^{AB}q_A\sigma_{1B} = 0, \quad \epsilon^{AB}\pi_{1A}\sigma_{1B} = 0, \quad {}^*\tilde{\pi}_{AB}\sigma^{1A}\sigma^{1B} = 0. \quad {}^2 \quad (3.3)$$

Proof. See Appendix A. □

(2) Orthogonally transitive

This case is specified by requiring that the G_2 acts orthogonally transitively,

$$\xi_{[a;b}\xi_c\eta_d] = 0, \quad \eta_{[a;b}\eta_c\xi_d] = 0, \quad (3.4)$$

where ξ and η are two linearly independent KVFs (Carter 1973 [15, page 160]). In other words, the 2-spaces orthogonal to the orbits of the G_2 are surface-forming. This is equivalent to (see WE, page 46)

$$\sigma_{1A} = 0. \quad (3.5)$$

In this class, equations (2.49) and (2.53) imply that the matter variables (2.6) are restricted as follows:

$$q_A = 0, \quad \pi_{1A} = 0. \quad (3.6)$$

(3) Diagonal

This case is specified by requiring that the G_2 admits two hypersurface-orthogonal KVFs. This class is the intersection of the first two classes, and

¹If \tilde{n}_{AB} and σ^{1A} are non-zero, then any two of the conditions in (3.2) imply the third. Furthermore, for SH cosmologies, we also have $n_C{}^C = 0$.

²It also follows from (3.2) and (3.3) that

$${}^*\tilde{\pi}_{AB}\tilde{\sigma}^{AB} = 0, \quad \tilde{\pi}_{AB}\tilde{n}^{AB} = 0.$$

is thus characterized by

$$\sigma_{1A} = 0, \quad \tilde{\sigma}_{AB}\tilde{n}^{AB} = 0, \quad (3.7)$$

as follows from (3.2) and (3.5). In this class the matter variables (2.6) are restricted as follows:

$$q_A = 0, \quad \pi_{1A} = 0, \quad {}^*\tilde{\pi}_{AB}\tilde{\sigma}^{AB} = 0. \quad (3.8)$$

The name “diagonal” reflects the fact that the line element can be written in diagonal form in this class.

(4) *Plane symmetric or locally rotationally symmetric (LRS)*

In the diagonal G_2 class, if there exists in addition a one-parameter isotropy group, then the model is locally rotationally symmetric (WE, page 43). This class is characterized by

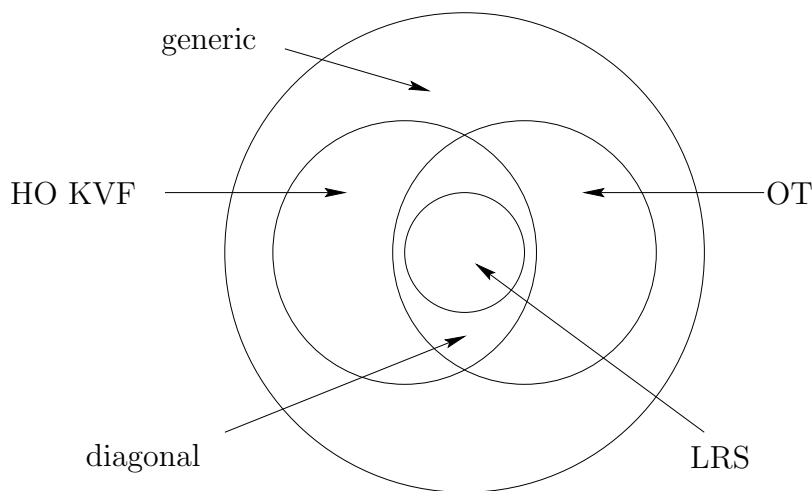
$$\sigma_{1A} = 0 = \tilde{\sigma}_{AB} = \tilde{n}_{AB}, \quad (3.9)$$

since otherwise there would exist a preferred direction in the 23-space. In this class the matter variables (2.6) are restricted as follows:

$$q_A = 0, \quad \pi_{1A} = 0, \quad \tilde{\pi}_{AB} = 0. \quad (3.10)$$

Figure 3.1 summarizes the classification of G_2 cosmologies using the action of the G_2 group and the existence of an LRS group (see WE, page 44). On account of (3.2) and (3.5) we can say that a G_2 cosmology is generic if and only if

$$\sigma_{1A}\sigma^{1A} \neq 0, \quad (\tilde{\sigma}_{AB}\tilde{n}^{AB})^2 + (\tilde{n}_{AB}\sigma^{1A}\sigma^{1B})^2 + ({}^*\tilde{\sigma}_{AB}\sigma^{1A}\sigma^{1B})^2 \neq 0. \quad (3.11)$$

Figure 3.1: Classification of G_2 cosmologies.

Assuming a perfect fluid matter content, we now show that G_2 cosmologies can be further classified using the *tilt degrees of freedom* of the perfect fluid, as described by the tilt vector v_α (see Section 2.1). From (2.49), (2.63), and using (2.53) and (2.64), one finds that the evolution equation for $\epsilon^{AB}q_A\sigma_{1B}$ is homogeneous:

$$\mathbf{e}_0(\epsilon^{AB}q_A\sigma_{1B}) = (-7H + 2\sigma_{11} - \mathbf{e}_1 v_1 - v_1 \dot{u}_1 + 6v_1 a_1 - v_1 \mathbf{e}_1)(\epsilon^{AB}q_A\sigma_{1B}). \quad (3.12)$$

Recalling from (2.64) that $q_A = \gamma G_+^{-1} \mu v_A$, equation (3.12) implies that $\epsilon^{AB}v_A\sigma_{1B} = 0$ defines an invariant set. Likewise, the evolution equation for q_A is homogeneous, on account of (2.64), implying that $v_A = 0$ forms an invariant set. These considerations lead to the hierarchy presented in Table 3.1.³

³By inspection of equations (2.62)–(2.63) and using (2.64), one finds that cases where $v_1 = 0$, $v_A \neq 0$ are not invariant.

Table 3.1: Perfect fluid hierarchy in the presence of a G_2 group.

Restriction	Description	tilt degrees of freedom
$\epsilon^{AB}v_A\sigma_{1B} \neq 0$	v_A not parallel to σ_{1A}	3
$\epsilon^{AB}v_A\sigma_{1B} = 0, v_A \neq 0$	v_A parallel to σ_{1A}	2
$v_A = 0, v_1 \neq 0$	v_α orthogonal to G_2 orbits	1
$v_\alpha = 0$	non-tilted fluid	0

Figure 3.2 summarizes the classification of G_2 cosmologies using the action of the G_2 group and the tilt degrees of freedom. Note that the matter restriction (3.3) of the class of hypersurface-orthogonal G_2 implies $\epsilon^{AB}v_A\sigma_{1B} = 0$, and restriction (3.6) of the class of OT G_2 implies $v_A = 0$. The class of hypersurface-orthogonal G_2 also contains $v_A = 0$ as an invariant subset.

3.2 G_2 -compatible SH cosmologies

Perfect fluid SH cosmologies of Bianchi type I–VII admit an Abelian G_2 subgroup (this can be inferred from Table 11.2 in MacCallum 1979 [53]). The properties of $\det n_{AB}$ and a_1 for G_2 -compatible SH cosmologies are summarized in Table 3.2. These cosmologies can be further classified according to the G_2 action (see Figure 3.1) and the tilt degrees of freedom, as in Table 3.1.⁴

Table 3.2: G_2 -compatible SH cosmologies.

	$a_1 = 0$	$a_1 \neq 0$
$\det n_{AB} > 0$	VII ₀	VII _h
$\det n_{AB} < 0$	VI ₀	VI _h
$\det n_{AB} = 0$	II	IV
$n_{AB} = 0$	I	V

⁴The parameter h in Table 3.1 will be introduced in equation (3.19).

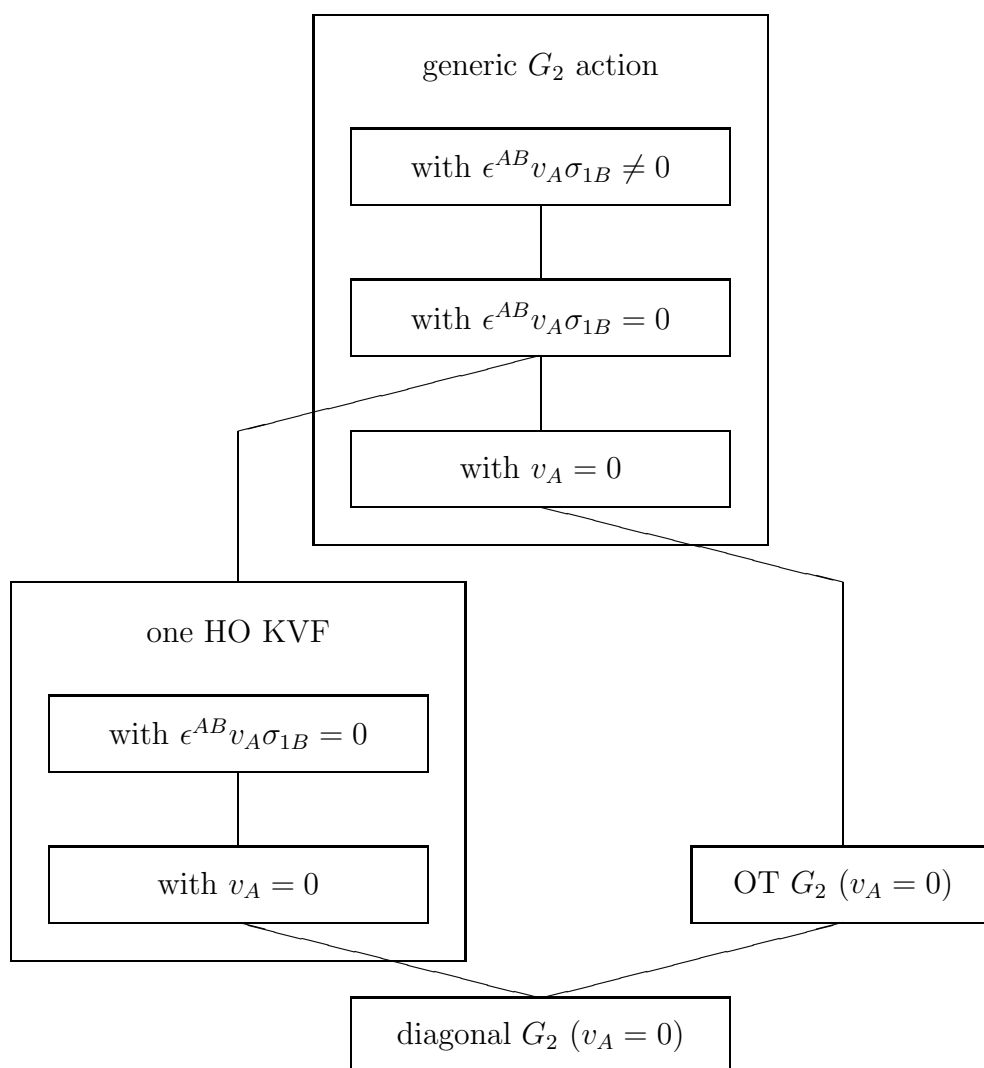


Figure 3.2: Action of the G_2 group and the tilt degrees of freedom.

SH cosmologies with generic G_2

Consider the SH cosmologies with a generic G_2 subgroup. We now show that the number of tilt degrees of freedom imposes strong restrictions on the possible Bianchi type, and that conversely, for a given Bianchi type, the tilt degrees of freedom are restricted. The results are summarized in Figure 3.3. The number on the right of each box in Figure 3.3 indicates the tilt degrees of freedom, as defined in Table 3.1.

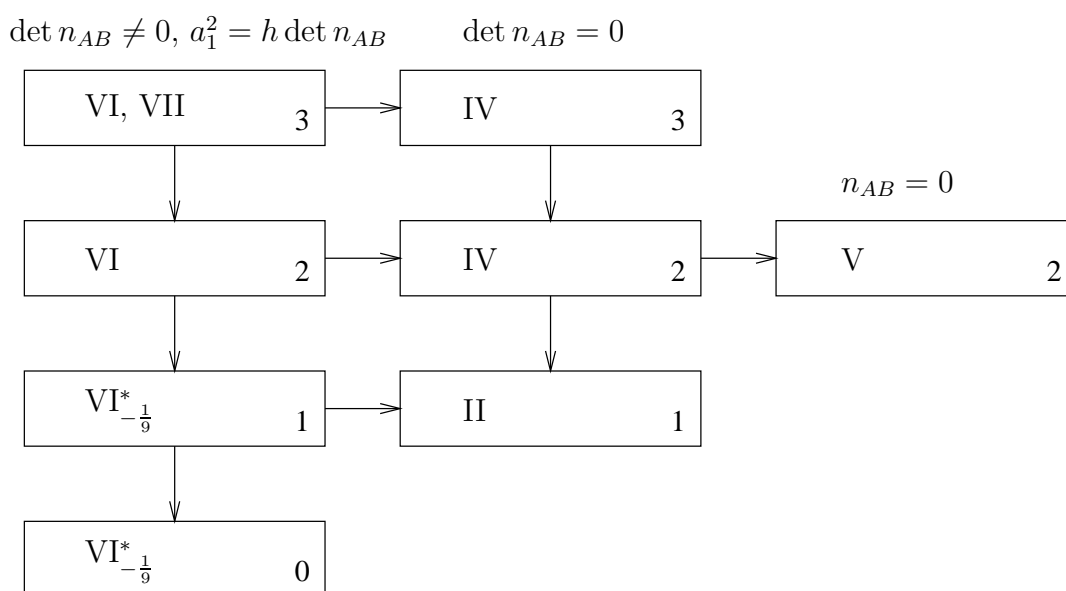


Figure 3.3: SH cosmologies with generic G_2 action. The numbers 0,1,2,3 indicate the tilt degrees of freedom.

We now justify the results in Figure 3.3. Bianchi V cosmologies with generic G_2 action necessarily have σ_{1A} parallel to q_A , as follows from (2.53). Note that Bianchi VII cosmologies with generic G_2 action necessarily have the most general tilt, as shown in the following proposition.

Proposition 3.2. *Consider a G_2 -compatible SH cosmology presented in a group-invariant orbit-aligned frame with \mathbf{e}_2 and \mathbf{e}_3 tangent to the G_2 orbits,*

and \mathbf{e}_1 tangent to the G_3 orbits. If

$$\det n_{AB} > 0 \quad \text{and} \quad \sigma_{1A}\sigma^{1A} \neq 0,$$

then

$$\epsilon^{AB}v_A\sigma_{1B} \neq 0.$$

Proof. Suppose $\epsilon^{AB}v_A\sigma_{1B} = 0$. Contract $(C_C)_A$ with $\epsilon^{AB}\sigma_{1B}$ to obtain

$$n_C{}^C\sigma_{1A}\sigma^{1A} = 2\tilde{n}_{AB}\sigma^{1A}\sigma^{1B}. \quad (3.13)$$

Assuming $\sigma_{1A}\sigma^{1A} \neq 0$, represent σ_{1A} using polar coordinates as follows:

$$\sigma_{1A} = \sigma_{\perp}K_{1A},$$

where $K_{12} = \cos \phi$, $K_{13} = \sin \phi$. Then it follows from (3.13) that

$$n_C{}^C = 2\tilde{n}_{AB}K^{1A}K^{1B}. \quad (3.14)$$

The determinant of n_{AB} , given by

$$\det(n_{AB}) = \frac{1}{4}(n_C{}^C)^2 - \frac{1}{2}\tilde{n}_{AB}\tilde{n}{}^{AB}, \quad (3.15)$$

is then expanded and simplified using (3.14) and trigonometric identities to yield

$$\det(n_{AB}) = -(*\tilde{n}_{AB}K^{1A}K^{1B})^2 \leq 0. \quad (3.16)$$

where $*\tilde{n}_{AB}$ is defined by (2.44). \square

The h parameter for Bianchi VI_h and VII_h cosmologies

We now define the h parameter for Bianchi VI_h and VII_h cosmologies. Note that the evolution equation for $\det(n_{AB})$ is given by

$$\mathbf{e}_0(\det n_{AB}) = 2(-H - \sigma_{11})\det n_{AB}, \quad (3.17)$$

as follows from (3.15) and (2.58)–(2.59). Comparing with the evolution equation (2.60) for a_1 :

$$\mathbf{e}_0(a_1) = (-H - \sigma_{11})a_1, \quad (3.18)$$

it follows that if $\det(n_{AB}) \neq 0$, there exists a constant h such that

$$a_1^2 = h \det(n_{AB}). \quad (3.19)$$

Bianchi VII $_h$ cosmologies are characterized by

$$\det(n_{AB}) > 0, \quad a_1 \neq 0,$$

requiring that h satisfies $h > 0$, while Bianchi VI $_h$ cosmologies are characterized by

$$\det(n_{AB}) < 0, \quad a_1 \neq 0,$$

requiring that h satisfies $h < 0$.

The exceptional Bianchi VI $^*_{-\frac{1}{9}}$ cosmologies

We now explain the origin of the exceptional Bianchi VI $^*_{-\frac{1}{9}}$ cosmologies. For Bianchi VI $_h$ models that also satisfy $\epsilon^{AB}v_A\sigma_{1B} = 0$, we can use (3.16) to write

$$a_1 = \pm\sqrt{-h} \, {}^* \tilde{n}_{AB} K^{1A} K^{1B}. \quad (3.20)$$

Notice that from (2.53), $(C_C)_A \sigma^{1A}$ yields

$$0 = -3[a_1 + \frac{1}{3} {}^* \tilde{n}_{AB} K^{1A} K^{1B}] + \frac{q_A K^{1A}}{\sigma_\perp} \quad (3.21)$$

for $\sigma_\perp \neq 0$. Thus, choosing $a_1 + \frac{1}{3} {}^* \tilde{n}_{AB} K^{1A} K^{1B} = 0$, which results in $h = -\frac{1}{9}$, also forces $q_A K^{1A} = 0$. In conjunction with $\epsilon^{AB}v_A\sigma_{1B} = 0$ and $\sigma_\perp \neq 0$, this yields

$$v_A = 0. \quad (3.22)$$

This class of models is referred to as the class of exceptional Bianchi VI $^*_{-\frac{1}{9}}$ cosmologies. In other words, the exceptional Bianchi VI $^*_{-\frac{1}{9}}$ cosmologies are characterized by a non-OT G_2 action ($\sigma_\perp \neq 0$) and a fluid congruence that is orthogonal to the G_2 orbits ($v_A = 0$). Note that choosing $a_1 - \frac{1}{3} {}^* \tilde{n}_{AB} K^{1A} K^{1B} = 0$ also results in $h = -\frac{1}{9}$, but does not permit $q_A K^{1A} = 0$. This class consists of the ordinary Bianchi VI $_{-\frac{1}{9}}$ cosmologies.

Bianchi IV and II cosmologies

Note that it follows from (3.16) and (3.21) that

$$\det n_{AB} = 0, \quad v_A = 0 \tag{3.23}$$

implies

$$a_1 = 0, \tag{3.24}$$

i.e. there is no Bianchi IV with generic G_2 and one tilt degree of freedom.

Lastly, we show that

$$\det n_{AB} = 0, \quad a_1 = 0 \quad \Rightarrow \quad v_A = 0, \tag{3.25}$$

i.e. Bianchi II cosmologies with generic G_2 have one tilt degree of freedom only. To see this, choose the spatial gauge (4.65). Then $\det n_{AB} = 0$ and (2.53) imply that $N_\times = 0$ and $v_A = 0$. But $v_A = 0$ is rotation-independent, so it is not an artifact of the spatial gauge choice.

Bianchi cosmologies with a generic G_2 subgroup are interesting because all of them except Bianchi V exhibit the Mixmaster dynamics, as we shall show in Section 4.1.

Bianchi cosmologies with non-generic G_2

For completeness, Bianchi cosmologies with special G_2 action are classified in Figures 3.4–3.5.

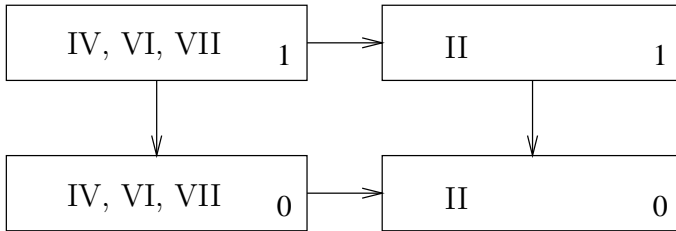


Figure 3.4: SH cosmologies with OT G_2 action. The numbers 0,1 indicate the tilt degrees of freedom.

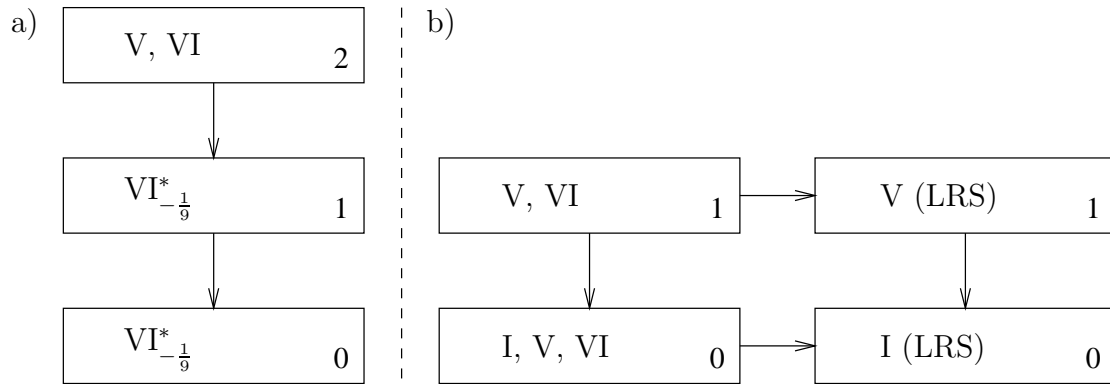


Figure 3.5: a) SH cosmologies whose G_2 admits one HO KVF. b) SH cosmologies with diagonal G_2 action. The numbers 0,1,2 indicate the tilt degrees of freedom.

Chapter 4

SH dynamics

Spatially homogeneous cosmologies are relevant in the study of G_2 cosmologies because their dynamics serves as the background dynamics of the inhomogeneous cosmologies in regimes in which the spatial derivatives are small compared with the time derivatives. In this chapter, we discuss certain aspects of the asymptotic dynamics of SH cosmologies, in particular the occurrence of Mixmaster dynamics. We introduce a unified system of evolution equations for the G_2 compatible SH cosmologies (models of Bianchi types I–VII), which enables us to predict in which classes of models Mixmaster dynamics will occur. We also mention some of the unsolved problems concerning the dynamics of SH cosmologies, which can be addressed using these evolution equations.

4.1 The standard Mixmaster dynamics

The standard Mixmaster dynamics arises in vacuum SH cosmologies of Bianchi types VIII and IX. The justification for considering vacuum cosmologies is that for typical SH cosmologies with a non-tilted perfect fluid, the matter density is dynamically insignificant in the sense that

$$\lim_{t \rightarrow -\infty} \Omega = 0, \tag{4.1}$$

where t is an appropriately defined time. (See Ringström 2001 [64] for a proof of this result for the class of non-tilted Bianchi type IX cosmologies.)

The evolution equations

The evolution equations for vacuum Bianchi VIII and IX cosmologies can be derived from the system (2.11)–(2.22) by choosing a G_3 -invariant orthonormal frame and introducing Hubble-normalized variables as in Section 2.3.

Recall from Table 1.1 that $A_\alpha = 0$ for models of Bianchi types VIII and IX. We use a time-dependent rotation of the spatial frame vectors $\{\mathbf{e}_\alpha\}$ to diagonalize $N_{\alpha\beta}$:

$$N_{\alpha\beta} = \text{diag}(N_{11}, N_{22}, N_{33}). \quad (4.2)$$

The $(C_C)_1$ constraint (2.14) implies that the shear is also diagonal. It then follows from (2.17) that the spatial frame vectors are Fermi-propagated, i.e. $R_\alpha = 0$. As in WE, Section 6.1.1, we introduce the notation

$$\Sigma_+ = \frac{1}{2}(\Sigma_{22} + \Sigma_{33}), \quad \Sigma_- = \frac{1}{2\sqrt{3}}(\Sigma_{22} - \Sigma_{33}). \quad (4.3)$$

The state vector (2.82) reduces to

$$\mathbf{X} = (\Sigma_+, \Sigma_-, N_{11}, N_{22}, N_{33}). \quad (4.4)$$

The evolution equations for \mathbf{X} are obtained by taking the appropriate linear combinations of (2.12) and by specializing (2.17):

$$\Sigma'_+ = (q - 2)\Sigma_+ - \frac{1}{6} [(N_{22} - N_{33})^2 - N_{11}(2N_{11} - N_{22} - N_{33})] \quad (4.5)$$

$$\Sigma'_- = (q - 2)\Sigma_- - \frac{1}{2\sqrt{3}}(N_{33} - N_{22})(N_{11} - N_{22} - N_{33}) \quad (4.6)$$

$$N'_{11} = (q - 4\Sigma_+)N_{11} \quad (4.7)$$

$$N'_{22} = (q + 2\Sigma_+ + 2\sqrt{3}\Sigma_-)N_{22} \quad (4.8)$$

$$N'_{33} = (q + 2\Sigma_+ - 2\sqrt{3}\Sigma_-)N_{33}, \quad (4.9)$$

where $'$ denotes the time derivative, and

$$q = 2\Sigma^2, \quad \Sigma^2 = \Sigma_+^2 + \Sigma_-^2. \quad (4.10)$$

The only remaining constraint is the Gauss constraint (2.13), which reads

$$0 = (\mathcal{C}_G) = 1 - \Omega_k - \Sigma^2, \quad (4.11)$$

where

$$\Omega_k = \frac{1}{12} [N_{11}^2 + N_{22}^2 + N_{33}^2 - 2(N_{11}N_{22} + N_{22}N_{33} + N_{33}N_{11})] . \quad (4.12)$$

The Kasner circle

The Mixmaster dynamics is generated by the stability properties of the Kasner solutions. These vacuum solutions appear as a circle of equilibrium points of the evolution equations (4.5)–(4.9), given by

$$N_{\alpha\alpha} = 0, \quad \Sigma_+^2 + \Sigma_-^2 = 1. \quad (4.13)$$

It is customary to refer to this circle as the *Kasner circle*, denoted \mathcal{K} . It follows from (4.10) and (4.13) that the Kasner solutions satisfy

$$q = 2. \quad (4.14)$$

We note that the metric for the Kasner solutions has the simple form:

$$\ell_0^{-2} ds^2 = -dT^2 + T^{2p_1} dx^2 + T^{2p_2} dy^2 + T^{2p_3} dz^2, \quad (4.15)$$

where the constants p_α satisfy

$$p_1 + p_2 + p_3 = 1 = p_1^2 + p_2^2 + p_3^2. \quad (4.16)$$

The link between the p_α and the Hubble-normalized shear is (see WE, equation (6.17))

$$p_1 = \frac{1}{3}(1 - 2\Sigma_+), \quad p_2 = \frac{1}{3}(1 + \Sigma_+ + \sqrt{3}\Sigma_-), \quad p_3 = \frac{1}{3}(1 + \Sigma_+ - \sqrt{3}\Sigma_-). \quad (4.17)$$

A typical Kasner solution is in fact represented six times on the Kasner circle. Figure 4.1a illustrates this symmetry of the Kasner circle. The grey dots connected by dashed lines are six different representations of a typical Kasner solution. The exceptions are the so-called Taub Kasner solutions ($p_\alpha = (1, 0, 0)$ and cycle), labelled T_α on the Kasner circle in Figure 4.1a, and the LRS Kasner solutions ($p_\alpha = (-\frac{1}{3}, \frac{2}{3}, \frac{2}{3})$ and cycle), labelled Q_α . See WE, Sections 6.2.2 and 9.1.1 for details.

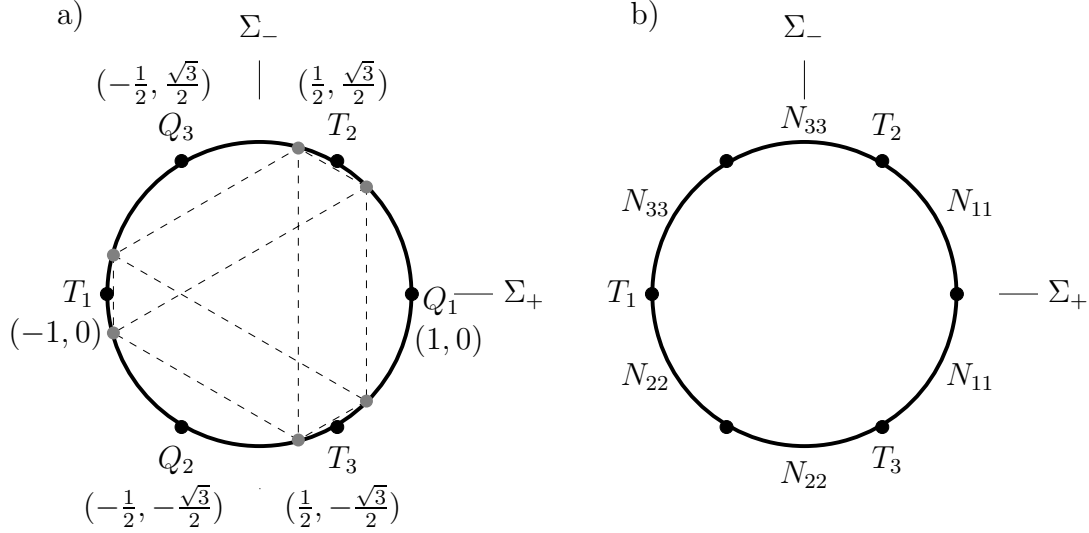


Figure 4.1: a) The Kasner circle and its six-fold symmetry. b) The triggers N_{11} , N_{22} and N_{33} and their unstable Kasner arcs.

Kasner instability and Mixmaster dynamics

In order to proceed with the analysis we restrict our consideration to solutions that are close to a Kasner solution at some time, i.e. to solutions whose orbit in the Hubble-normalized state space enters an arbitrarily small neighbourhood of the Kasner circle \mathcal{K} . Ringström 2001 [64] proved that all Bianchi IX solutions except a set of measure zero have this property.

Consider linearizing (4.7)–(4.9) on the Kasner circle (4.13). Using (4.14), we obtain

$$N'_{11} = 2(1 - 2\Sigma_+)N_{11} \quad (4.18)$$

$$N'_{22} = 2(1 + \Sigma_+ + \sqrt{3}\Sigma_-)N_{22} \quad (4.19)$$

$$N'_{33} = 2(1 + \Sigma_+ - \sqrt{3}\Sigma_-)N_{33} , \quad (4.20)$$

which imply that the $N_{\alpha\alpha}$ are unstable into the past on the following arcs:

$$N_{11} \text{ on arc}(T_2T_3), N_{22} \text{ on arc}(T_3T_1), N_{33} \text{ on arc}(T_1T_2).$$

These arcs are non-overlapping and cover all the Kasner equilibrium points

except the Taub Kasner points (see Figure 4.1b). As a result, each of these Kasner equilibrium points is unstable into the past. In the SH state space, the unstable manifold of a Kasner equilibrium point is an orbit lying on one of the ellipsoids

$$1 = \frac{1}{12}N_{\alpha\alpha}^2 + \Sigma_+^2 + \Sigma_-^2, \quad \alpha = 1, 2 \text{ or } 3, \quad (4.21)$$

as follows from the Gauss constraint (4.11). In fact, the orbits represent the Taub vacuum Bianchi II solutions, and appear as straight lines when projected onto the (Σ_+, Σ_-) plane, as illustrated in Figure 4.2. We shall refer to these orbits as the *curvature transition sets*, denoted \mathcal{T}_N . Each transition is a result of the growth (into the past) of one of $N_{\alpha\alpha}$. Therefore we call $N_{\alpha\alpha}$ the “triggers”. Because $N_{\alpha\alpha}$ represent the spatial curvature, we call them the “curvature triggers”.

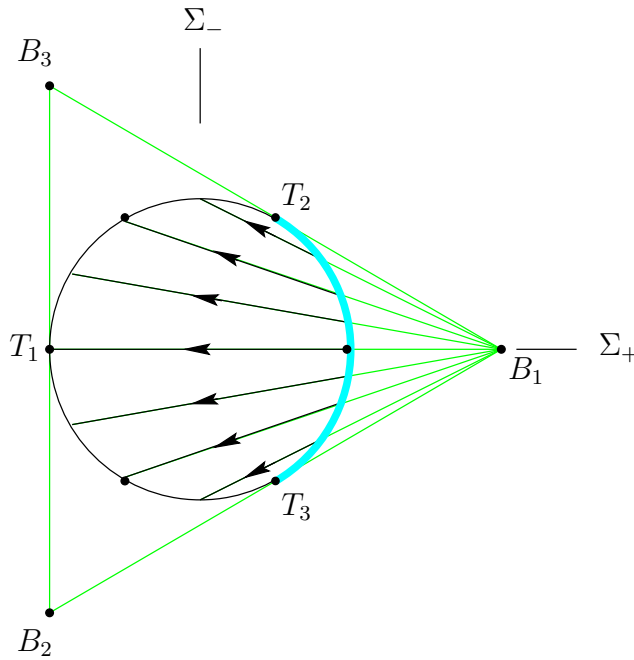


Figure 4.2: The curvature transition set and the arc of instability (into the past) of the trigger N_{11} . The transition sets for N_{22} and N_{33} are obtained by symmetry, using the points B_2 and B_3 respectively.

The evolution of a Bianchi VIII or IX cosmology is represented by an orbit in the Hubble-normalized state space. As $t \rightarrow -\infty$, a typical orbit enters a neighbourhood of the Kasner circle, but cannot be asymptotic to a Kasner equilibrium point in general. Instead it shadows the unstable manifolds of the Kasner equilibrium points, going from one Kasner equilibrium point to another. In this way, the three families of curvature transition sets sustain an endless sequence of transitions, called *Mixmaster dynamics*, in recognition of the work of Misner 1969 [54].¹ For a more detailed discussion, see Ma & Wainwright [51] and Section 6.4 of WE. The essential point is that Mixmaster dynamics will occur if for each typical Kasner equilibrium point P there is a trigger variable that renders it unstable into the past, and with the resulting unstable manifold joining P to another Kasner equilibrium point.

To summarize, the occurrence of Mixmaster dynamics and the identification of the past attractor is established by proving three results (see Ringström 2001 [64]):

$$\text{i) } \quad \lim_{t \rightarrow -\infty} \Omega = 0, \quad \lim_{t \rightarrow -\infty} \Omega_\Lambda = 0. \quad (4.22)$$

ii) A typical orbit enters an arbitrarily small neighbourhood of the Kasner circle, and

$$\text{iii) } \quad \lim_{t \rightarrow -\infty} (N_{11}N_{22}, N_{22}N_{33}, N_{33}N_{11}) = \mathbf{0}. \quad (4.23)$$

Mixmaster dynamics is initiated by Property ii), which we shall refer to as the *Kasner Attractivity Conjecture*.² It appears to play a fundamental role in the dynamics of SH cosmologies and more generally, in inhomogeneous cosmologies, although it has not been proved in more general situations. Property iii) states that the curvature transitions cannot occur simultaneously.

For Bianchi VIII and IX cosmologies, the triggers are the eigenvalues of $N_{\alpha\beta}$. If one of the triggers is zero, e.g. $N_{11} = 0$, then there is a stable arc on \mathcal{K} which is the past attractor. For G_2 -compatible SH cosmologies (Bianchi I–VII), at least one of the eigenvalues of $N_{\alpha\beta}$ is zero (see Table 1.1). Can Mixmaster dynamics occur in these cosmologies? At first sight, it does not

¹Misner discovered this behaviour by using the Hamiltonian formulation of the EFEs.

²This is stated formally later as Conjecture 4.1.

seem so. But it has been shown that in fact it can occur, although in general it requires the presence of a perfect fluid with non-zero tilt, as we shall show in Section 4.3. But first we need to derive the Hubble-normalized evolution equations for G_2 -compatible SH cosmologies, which we do in Section 4.2.

4.2 The G_2 -compatible SH evolution equations

The 1+1+2 Hubble-normalized variables (2.100)–(2.101) were introduced for the purpose of analyzing G_2 -compatible SH cosmologies. It is necessary to write out the Hubble-normalized evolution equations in component form (i.e. the 1+1+1+1 form!) rather than in the 1+1+2 form, so that we can impose a suitable spatial gauge condition. For convenience we introduce the following notation:

$$N_C{}^C = 2N_+, \quad \tilde{N}_{AB} = \sqrt{3} \begin{pmatrix} N_- & N_\times \\ N_\times & -N_- \end{pmatrix}, \quad (4.24)$$

and

$$\Sigma_{12} = \sqrt{3}\Sigma_3, \quad \Sigma_{13} = \sqrt{3}\Sigma_2. \quad (4.25)$$

The Hubble-normalized equations in component form are obtained from the 1+1+2 system (2.47)–(2.63) by expressing them in terms of the Hubble-normalized variables (2.100)–(2.101), using (2.84)–(2.85), and are given below:

G_2 -compatible SH system (Hubble-normalized)*Evolution equations for the gravitational field:*

$$\Sigma'_+ = (q - 2)\Sigma_+ + 3(\Sigma_2^2 + \Sigma_3^2) - 2(N_-^2 + N_\times^2) - \frac{3}{2} \frac{\gamma\Omega}{G_+} (v_1^2 - \frac{1}{3}v^2) \quad (4.26)$$

$$\begin{aligned} \Sigma'_- &= (q - 2)\Sigma_- + 2AN_\times - 2R\Sigma_\times - 2N_+N_- + \sqrt{3}(\Sigma_3^2 - \Sigma_2^2) \\ &\quad + \frac{\sqrt{3}}{2} \frac{\gamma\Omega}{G_+} (v_2^2 - v_3^2) \end{aligned} \quad (4.27)$$

$$\begin{aligned} \Sigma'_\times &= (q - 2)\Sigma_\times - 2AN_- + 2R\Sigma_- - 2N_+N_\times + 2\sqrt{3}\Sigma_3\Sigma_2 \\ &\quad + \sqrt{3} \frac{\gamma\Omega}{G_+} v_2v_3 \end{aligned} \quad (4.28)$$

$$\Sigma'_3 = (q - 2 - 3\Sigma_+ - \sqrt{3}\Sigma_-)\Sigma_3 - (R + \sqrt{3}\Sigma_\times)\Sigma_2 + \sqrt{3} \frac{\gamma\Omega}{G_+} v_1v_2 \quad (4.29)$$

$$\Sigma'_2 = (q - 2 - 3\Sigma_+ + \sqrt{3}\Sigma_-)\Sigma_2 + (R - \sqrt{3}\Sigma_\times)\Sigma_3 + \sqrt{3} \frac{\gamma\Omega}{G_+} v_1v_3 \quad (4.30)$$

$$N'_+ = (q + 2\Sigma_+)N_+ + 6\Sigma_-N_- + 6\Sigma_\times N_\times \quad (4.31)$$

$$N'_- = (q + 2\Sigma_+)N_- + 2N_+\Sigma_- - 2RN_\times \quad (4.32)$$

$$N'_\times = (q + 2\Sigma_+)N_\times + 2N_+\Sigma_\times + 2RN_- \quad (4.33)$$

$$A' = (q + 2\Sigma_+)A, \quad (4.34)$$

where

$$q = 2\Sigma^2 + \frac{1}{2}G_+^{-1}[(3\gamma - 2)(1 - v^2) + 2\gamma v^2]\Omega - \Omega_\Lambda \quad (4.35)$$

$$\Sigma^2 = \Sigma_+^2 + \Sigma_-^2 + \Sigma_\times^2 + \Sigma_2^2 + \Sigma_3^2 \quad (4.36)$$

$$G_\pm = 1 \pm (\gamma - 1)v^2, \quad v^2 = v_1^2 + v_2^2 + v_3^2. \quad (4.37)$$

Constraint equations:

$$0 = (\mathcal{C}_G) = 1 - N_-^2 - N_\times^2 - A^2 - \Sigma^2 - \Omega - \Omega_\Lambda \quad (4.38)$$

$$0 = (\mathcal{C}_C)_1 = 2A\Sigma_+ + 2(\Sigma_-N_\times - \Sigma_\times N_-) + \frac{\gamma\Omega}{G_+} v_1 \quad (4.39)$$

$$0 = (\mathcal{C}_C)_2 = -(3A + \sqrt{3}N_\times)\Sigma_3 - (N_+ - \sqrt{3}N_-)\Sigma_2 + \sqrt{3} \frac{\gamma\Omega}{G_+} v_2 \quad (4.40)$$

$$0 = (\mathcal{C}_C)_3 = -(3A - \sqrt{3}N_\times)\Sigma_2 + (N_+ + \sqrt{3}N_-)\Sigma_3 + \sqrt{3} \frac{\gamma\Omega}{G_+} v_3. \quad (4.41)$$

Evolution equations for the matter:

$$\Omega' = G_+^{-1}[2G_+q - (3\gamma - 2) - (2 - \gamma)v^2 - \gamma\Sigma_{\alpha\beta}v^\alpha v^\beta + 2\gamma Av_1]\Omega \quad (4.42)$$

$$v_1' = (M + 2\Sigma_+)v_1 - 2\sqrt{3}(\Sigma_3v_2 + \Sigma_2v_3) + \sqrt{3}N_\times(v_3^2 - v_2^2) + 2\sqrt{3}N_-v_2v_3 - Av^2 \quad (4.43)$$

$$v_2' = (M - \Sigma_+ - \sqrt{3}\Sigma_- + \sqrt{3}N_\times v_1)v_2 - [R + \sqrt{3}\Sigma_\times - (N_+ - \sqrt{3}N_-)v_1]v_3 \quad (4.44)$$

$$v_3' = (M - \Sigma_+ + \sqrt{3}\Sigma_- - \sqrt{3}N_\times v_1)v_3 + [R - \sqrt{3}\Sigma_\times - (N_+ + \sqrt{3}N_-)v_1]v_2 \quad (4.45)$$

$$\Omega'_\Lambda = 2(q + 1)\Omega_\Lambda, \quad (4.46)$$

where

$$M = G_-^{-1} \left[(3\gamma - 4)(1 - v^2) + (2 - \gamma)\Sigma_{\alpha\beta}v^\alpha v^\beta + [G_+ - 2(\gamma - 1)]Av_1 \right] \quad (4.47)$$

$$\Sigma_{\alpha\beta}v^\alpha v^\beta = \Sigma_+(v_2^2 + v_3^2 - 2v_1^2) + \sqrt{3}\Sigma_-(v_2^2 - v_3^2) + 2\sqrt{3}\Sigma_\times v_2v_3 + 2\sqrt{3}(\Sigma_3v_2 + \Sigma_2v_3)v_1. \quad (4.48)$$

In order to derive the v'_α equations³ from the evolution equations (2.62)–(2.63) for q_α , we first obtain Ω' and Q'_α by converting (2.61)–(2.63) to Hubble-normalized form. On differentiating $Q_\alpha = \gamma G_+^{-1}\Omega v_\alpha$, we obtain

$$Q'_\alpha = \frac{\gamma v_\alpha}{G_+}\Omega' + \frac{\gamma\Omega}{G_+}v'_\alpha - \frac{\gamma\Omega}{G_+^2}v_\alpha(G_+)' . \quad (4.49)$$

Contracting with v_α and simplifying gives

$$v^\alpha Q'_\alpha = \frac{\gamma v^2}{G_+}\Omega' + \frac{\gamma G_- \Omega}{G_+^2}(v^2)' . \quad (4.50)$$

The resulting equation for v^2 is

$$(v^2)' = \frac{2}{G_-}(1 - v^2) [(3\gamma - 4)v^2 - \Sigma_{\alpha\beta}v^\alpha v^\beta - 2(\gamma - 1)v^2 Av_1] , \quad (4.51)$$

³See van Elst & Uggla 1997 [73], page 2682.

which we use to evaluate the $\partial_0 G_+$ term in (4.49) to obtain v'_α .

It follows from (2.66)–(2.71) and (2.95) that the Hubble-normalized Weyl curvature variables are given by

$$\begin{aligned} \mathcal{E}_+ &= \frac{1}{3}(1 + \Sigma_+) \Sigma_+ + \frac{1}{6}(\Sigma_2^2 + \Sigma_3^2) - \frac{1}{3}(\Sigma_-^2 + \Sigma_\times^2) \\ &\quad + \frac{2}{3}(N_\times^2 + N_-^2) + \frac{1}{4} \frac{\gamma \Omega}{G_+} (v_1^2 - \frac{1}{3} v^2) \end{aligned} \quad (4.52)$$

$$\begin{aligned} \mathcal{E}_- &= \frac{1}{3}(1 - 2\Sigma_+) \Sigma_- - \frac{1}{2\sqrt{3}}(\Sigma_3^2 - \Sigma_2^2) \\ &\quad - \frac{2}{3} A N_\times + \frac{2}{3} N_+ N_- + \frac{1}{2\sqrt{3}} \frac{\gamma \Omega}{G_+} (v_2^2 - v_3^2) \end{aligned} \quad (4.53)$$

$$\begin{aligned} \mathcal{E}_\times &= \frac{1}{3}(1 - 2\Sigma_+) \Sigma_\times - \frac{1}{\sqrt{3}} \Sigma_3 \Sigma_2 \\ &\quad + \frac{2}{3} A N_- + \frac{2}{3} N_+ N_\times + \frac{1}{\sqrt{3}} \frac{\gamma \Omega}{G_+} v_2 v_3 \end{aligned} \quad (4.54)$$

$$\mathcal{E}_3 = \frac{1}{3}(1 + \Sigma_+ - \sqrt{3}\Sigma_-) \Sigma_3 - \frac{1}{\sqrt{3}} \Sigma_\times \Sigma_2 - \frac{1}{2} \frac{\gamma \Omega}{G_+} v_1 v_2 \quad (4.55)$$

$$\mathcal{E}_2 = \frac{1}{3}(1 + \Sigma_+ + \sqrt{3}\Sigma_-) \Sigma_2 - \frac{1}{\sqrt{3}} \Sigma_\times \Sigma_3 - \frac{1}{2} \frac{\gamma \Omega}{G_+} v_1 v_3 \quad (4.56)$$

$$\mathcal{H}_+ = -N_- \Sigma_- - N_\times \Sigma_\times \quad (4.57)$$

$$\mathcal{H}_- = \frac{1}{3} A \Sigma_\times - \frac{2}{3} N_+ \Sigma_- - \Sigma_+ N_- \quad (4.58)$$

$$\mathcal{H}_\times = -\frac{1}{3} A \Sigma_- - \frac{2}{3} N_+ \Sigma_\times - \Sigma_+ N_\times \quad (4.59)$$

$$\mathcal{H}_3 = -\frac{1}{3}(A + \sqrt{3}N_\times) \Sigma_2 - \frac{1}{\sqrt{3}} N_- \Sigma_3 + \frac{1}{2\sqrt{3}} \frac{\gamma \Omega}{G_+} v_3 \quad (4.60)$$

$$\mathcal{H}_2 = \frac{1}{3}(A - \sqrt{3}N_\times) \Sigma_3 + \frac{1}{\sqrt{3}} N_- \Sigma_2 - \frac{1}{2\sqrt{3}} \frac{\gamma \Omega}{G_+} v_2 . \quad (4.61)$$

Note that the $(\mathcal{C}_C)_2$ and $(\mathcal{C}_C)_3$ constraints have been used to simplify \mathcal{H}_2 and \mathcal{H}_3 respectively.

Recall from Section 3.2 that for SH cosmologies of Bianchi types VI and VII, the spatial curvature variables are related via

$$A^2 = h \det N_{AB}, \quad \det N_{AB} = N_+^2 - 3(N_-^2 + N_\times^2) \neq 0. \quad (4.62)$$

Thus the Bianchi VI and VII state space consists of “layers” of Bianchi VI_h and VII_h state spaces.

For SH cosmologies with generic G_2 action, a simple way to specify the spatial gauge is to use a time-dependent rotation of the spatial frame vec-

tors $\{\mathbf{e}_A\}$ to make \mathbf{e}_2 parallel to a KVF. It then follows from Lemma 1 in Appendix A that

$$N_+ = \sqrt{3}N_-, \quad R = -\sqrt{3}\Sigma_\times. \quad (4.63)$$

We shall refer to this gauge as the *Killing spatial gauge*. This gauge, however, has the disadvantage that it cannot be used for Bianchi VII cosmologies, because it entails $\det N_{AB} \leq 0$, as follows from (4.62).

A second possibility is to rotate the frame $\{\mathbf{e}_A\}$ so that $\Sigma_3 = 0$. The evolution equation (4.29) and the constraint (4.40) then give

$$\Sigma_3 = 0, \quad R = -\sqrt{3}\Sigma_\times + (N_+ - \sqrt{3}N_-)v_1. \quad (4.64)$$

We shall refer to this gauge as the *shear spatial gauge*. For the invariant set $\{v_2 = 0, \Sigma_2 \neq 0\}$, the $(\mathcal{C}_C)_2$ constraint (4.40) implies $N_+ = \sqrt{3}N_-$, and (4.64) simplifies to

$$\Sigma_3 = 0, \quad N_+ = \sqrt{3}N_-, \quad R = -\sqrt{3}\Sigma_\times. \quad (4.65)$$

On the other hand, for the invariant set $\Sigma_2 = 0$ corresponding to SH cosmologies with OT G_2 action, the $(\mathcal{C}_C)_2$ constraint (4.40) implies $v_2 = 0$, leaving (4.64) the same.

A third alternative is the *tilt spatial gauge*, where one rotates the frame $\{\mathbf{e}_A\}$ so that $v_2 = 0$. The v'_2 equation (4.44) then gives

$$v_2 = 0, \quad R = -\sqrt{3}\Sigma_\times + (N_+ - \sqrt{3}N_-)v_1. \quad (4.66)$$

Observe that the tilt spatial gauge and the shear spatial gauge have the same expression for R .

We shall use the shear spatial gauge (4.64) rather than the tilt spatial gauge because it has the advantage of displaying the tilt degrees of freedom explicitly. With this choice, the Hubble-normalized variables are

$$\mathbf{X} = (\Sigma_+, \Sigma_-, \Sigma_\times, \Sigma_2, N_+, N_-, N_\times, A, \Omega, v_1, v_2, v_3, \Omega_\Lambda), \quad (4.67)$$

together with the parameter γ . There are 13 variables and 4 constraints, making the state space 9-dimensional.⁴

⁴The state space of Bianchi VI_h or VII_h cosmologies for each fixed h is 8-dimensional, taking into account the extra constraint (4.62).

Constraints

The stability of the constraints is of great concern when doing numerical simulations. From Uggla *et al.* 2003 [72, equations (A2)–(A3)] we obtain the evolution equations for the constraints:

$$(\mathcal{C}_G)' = 2q(\mathcal{C}_G) - \frac{2}{3}A(\mathcal{C}_C)_1 \quad (4.68)$$

$$(\mathcal{C}_C)'_1 = (2q - 2 + 2\Sigma_+)(\mathcal{C}_C)_1 - 2\sqrt{3}\Sigma_3(\mathcal{C}_C)_2 - 2\sqrt{3}\Sigma_2(\mathcal{C}_C)_3 \quad (4.69)$$

$$(\mathcal{C}_C)'_2 = (2q - 2 - \Sigma_+ - \sqrt{3}\Sigma_-)(\mathcal{C}_C)_2 - (R + \sqrt{3}\Sigma_\times)(\mathcal{C}_C)_3 \quad (4.70)$$

$$(\mathcal{C}_C)'_3 = (2q - 2 - \Sigma_+ + \sqrt{3}\Sigma_-)(\mathcal{C}_C)_3 + (R - \sqrt{3}\Sigma_\times)(\mathcal{C}_C)_2 . \quad (4.71)$$

We see that the constraints are stable into the past near the Kasner circle (as the coefficients of the first terms are positive).

4.3 Generalized Mixmaster dynamics

We now predict under what circumstances Mixmaster dynamics can occur in G_2 -compatible SH cosmologies. We use the gauge choice (4.64), but we shall show that the main result, Proposition 4.1, is independent of this choice.

We begin by describing the Kasner equilibrium points. Within the state space of G_2 -compatible SH cosmologies, it is straightforward to verify that the Kasner circle \mathcal{K} , now given by

$$(\Sigma_\times, \Sigma_2, N_+, N_-, N_\times, A) = \mathbf{0}, \quad (4.72)$$

$$\Sigma_+^2 + \Sigma_-^2 = 1, \quad (4.73)$$

$$\Omega = 0 = \Omega_\Lambda, \quad v_\alpha = 0, \quad (4.74)$$

is a set of equilibrium points, and satisfies $q = 2$. In fact, by assuming

$$\Omega = 0 = \Omega_\Lambda, \quad (N_+, N_-, N_\times, A) = \mathbf{0}, \quad (4.75)$$

one quickly arrives at $\Sigma^2 = 1$ and $q = 2$ through (4.38) and (4.35). Then (4.26)–(4.30) imply

$$\Sigma_2 = \Sigma_\times = 0. \quad (4.76)$$

Evolution equations (4.43)–(4.45) and (4.51) with (4.75) and (4.76) give

$$v_1' = (M + 2\Sigma_+)v_1 \quad (4.77)$$

$$v_2' = (M - \Sigma_+ - \sqrt{3}\Sigma_-)v_2 \quad (4.78)$$

$$v_3' = (M - \Sigma_+ + \sqrt{3}\Sigma_-)v_3 \quad (4.79)$$

$$(v^2)' = \frac{2}{G_-}(1 - v^2)[(3\gamma - 4)v^2 - \Sigma_{\alpha\beta}v^\alpha v^\beta] , \quad (4.80)$$

where

$$M = G_-^{-1}[(3\gamma - 4)(1 - v^2) + (2 - \gamma)\Sigma_{\alpha\beta}v^\alpha v^\beta] \quad (4.81)$$

$$\Sigma_{\alpha\beta}v^\alpha v^\beta = \Sigma_+(v_2^2 + v_3^2 - 2v_1^2) + \sqrt{3}\Sigma_-(v_2^2 - v_3^2) . \quad (4.82)$$

Equilibrium points with $v_\alpha = 0$ give the Kasner circle \mathcal{K} . Equilibrium points with one non-zero tilt variable and $v^2 = 1$ give

$$v_\alpha = (\pm 1, 0, 0), (0, \pm 1, 0), (0, 0, \pm 1). \quad (4.83)$$

Hence we have 6 more Kasner circles $\mathcal{K}_{\pm\alpha}$ of equilibrium points, given by

$$(\Sigma_x, \Sigma_2, N_+, N_-, N_x, A) = \mathbf{0}, \quad (4.84)$$

$$\Sigma_+^2 + \Sigma_-^2 = 1, \quad (4.85)$$

$$\Omega = 0 = \Omega_\Lambda, \quad v_\alpha = (\pm 1, 0, 0), (0, \pm 1, 0), (0, 0, \pm 1). \quad (4.86)$$

The $\mathcal{K}_{\pm\alpha}$ equilibrium points are unphysical due to the extreme tilt $v^2 = 1$, but we shall see that they nevertheless play a significant role dynamically. Equilibrium points with one non-zero tilt variable and $v^2 < 1$ gives

$$\begin{cases} \Sigma_+ = -\frac{1}{2}(3\gamma - 4) & \text{if } v_1 \neq 0 \\ \Sigma_+ + \sqrt{3}\Sigma_- = 3\gamma - 4 & \text{if } v_2 \neq 0 \\ \Sigma_+ - \sqrt{3}\Sigma_- = 3\gamma - 4 & \text{if } v_3 \neq 0. \end{cases} \quad (4.87)$$

There are equilibrium points with two non-zero tilt variables, but they occur at Q_α and T_α and not on the entire Kasner circle. There are no equilibrium points with $v_1 v_2 v_3 \neq 0$, since (4.77)–(4.79) require that

$$M + 2\Sigma_+ = 0 = M - \Sigma_+ - \sqrt{3}\Sigma_- = M - \Sigma_+ + \sqrt{3}\Sigma_- ,$$

which implies $\Sigma_+ = \Sigma_- = 0$, contradicting $\Sigma_+^2 + \Sigma_-^2 = 1$. The Kasner solutions are in fact characterized by (4.75), and thus have other (non-equilibrium) representations, which we shall encounter very soon in this chapter.

In order to proceed with the analysis we first restrict our consideration to solutions that satisfy

$$\lim_{t \rightarrow -\infty} \Omega = 0, \quad \lim_{t \rightarrow -\infty} \Omega_\Lambda = 0, \quad (4.88)$$

based on the BKL conjecture I (see Section 1.3). Second, based on the Kasner Attractivity Conjecture below, we restrict our considerations to solutions whose orbit enter an arbitrarily small neighbourhood of one of the Kasner circles. Numerical simulations suggest that this property is satisfied, and hence we formalize it as a conjecture:

Conjecture 4.1 (Kasner Attractivity Conjecture). *The orbits of all G_2 -compatible SH cosmologies, except for a set of measure zero, enter an arbitrarily small neighbourhood of one of the Kasner circles.*

Consider linearizing the evolution equations (4.28), (4.30)–(4.34) for the spatial curvature and off-diagonal shear variables (4.72) on the above Kasner circles:⁵

$$\Sigma'_\times = -2\sqrt{3}\Sigma_- \Sigma_\times \quad (4.89)$$

$$\Sigma'_2 = (-3\Sigma_+ + \sqrt{3}\Sigma_-)\Sigma_2 \quad (4.90)$$

$$N'_{22} = 2(1 + \Sigma_+ + \sqrt{3}\Sigma_-)N_{22} \quad (4.91)$$

$$N'_{33} = 2(1 + \Sigma_+ - \sqrt{3}\Sigma_-)N_{33} \quad (4.92)$$

$$N'_\times = 2(1 + \Sigma_+)N_\times \quad (4.93)$$

$$A' = 2(1 + \Sigma_+)A, \quad (4.94)$$

where $(\Sigma_+, \Sigma_-) = (\cos \phi, \sin \phi)$, and ϕ is a constant. It follows that the first four variables are unstable on some arc of the Kasner circles, i.e. will act as triggers, while N_\times and A are stable on the Kasner circles, into the past. It is plausible that the stable variables tend to zero:

$$\lim_{t \rightarrow -\infty} (N_\times, A) = \mathbf{0}, \quad (4.95)$$

⁵Recall from (4.24) that $N_{22} = N_+ + \sqrt{3}N_-$, $N_{33} = N_+ - \sqrt{3}N_-$.

and this conclusion is strongly supported by numerical simulations.

We recognize that N_{22} and N_{33} are two of the curvature triggers introduced in Section 4.1. In the present situation, however, the curvature transition sets $\mathcal{T}_{N_{22}}$ and $\mathcal{T}_{N_{33}}$ also describe transitions on the Kasner circles $\mathcal{K}_{\pm\alpha}$, in addition to \mathcal{K} . The new triggers here are Σ_{\times} and Σ_2 : the off-diagonal shear components. The Σ_{\times} transition orbits lie on the sphere $\Sigma_+^2 + \Sigma_-^2 + \Sigma_{\times}^2 = 1$. Evaluating (4.26) on the sphere gives $\Sigma'_+ = 0$, which implies

$$\Sigma_+ = \text{const.} \quad (4.96)$$

on each Σ_{\times} transition orbit. Similarly, the Σ_2 transition orbits lie on the sphere $\Sigma_+^2 + \Sigma_-^2 + \Sigma_2^2 = 1$. Evaluating (4.26)–(4.27) on the sphere gives $(\Sigma_+ + \sqrt{3}\Sigma_-)' = 0$, which implies

$$\Sigma_+ + \sqrt{3}\Sigma_- = \text{const.} \quad (4.97)$$

on each Σ_2 transition orbit. The Σ_{\times} and Σ_2 transition sets are shown in Figure 4.3. By comparing Figure 4.3 with the dashed lines in Figure 4.1a, we see that these transition sets connect different representations of the same Kasner solutions. These transitions are in fact an artifact of a rotating spatial frame (non-zero Ω_{α}), and the transition sets actually represent the Kasner solutions. Therefore we shall call the off-diagonal shear components the *frame triggers*, with corresponding *frame transition sets*, denoted $\mathcal{T}_{\Sigma_{\times}}$ and \mathcal{T}_{Σ_2} .⁶

The triggers that lead to the instability of the various Kasner arcs are shown in Figure 4.4, which is obtained using Figures 4.2–4.3. The essential point is that

Mixmaster dynamics occurs if and only if each Kasner arc has at least one trigger, and so if an arc has no triggers, then it will form part of the past attractor, and Mixmaster dynamics will not occur.

Table 4.1 lists the variables for the subclasses with generic G_2 action and the additional restrictions.

⁶This artifact is beneficial. If one chooses a Fermi-propagated frame, i.e. $\Omega_{\alpha} = 0$, then the Kasner equilibrium points form a hypersphere

$$\Sigma_+^2 + \Sigma_-^2 + \Sigma_{\times}^2 + \Sigma_2^2 + \Sigma_3^2 = 1$$

instead of a circle $\Sigma_+^2 + \Sigma_-^2 = 1$.

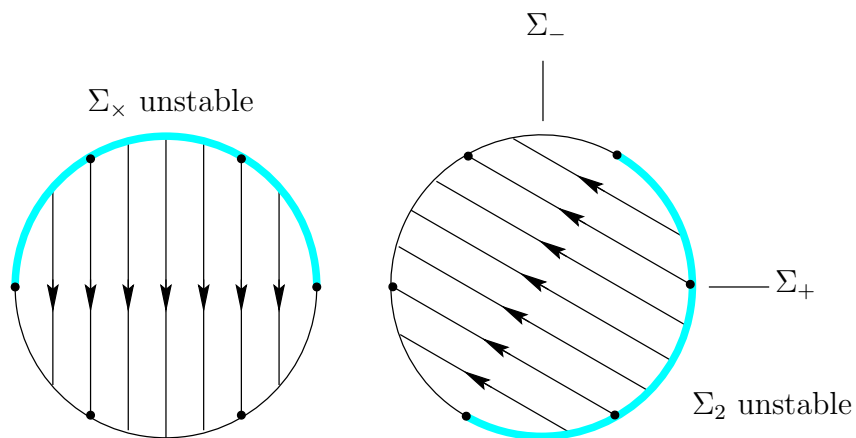


Figure 4.3: The frame transition sets corresponding to the triggers Σ_x and Σ_2 , respectively. The arrows indicate evolution into the past.

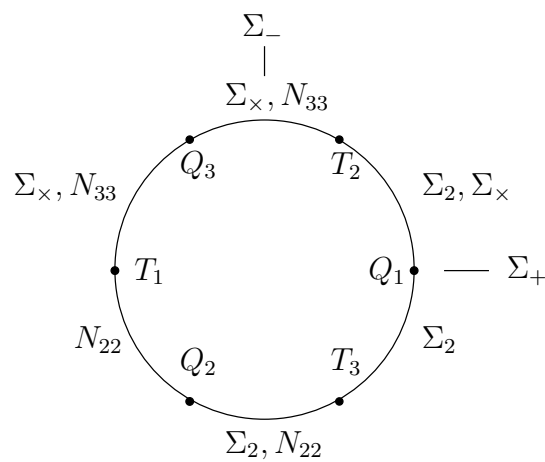


Figure 4.4: The unstable Kasner arcs and their triggers.

Table 4.1: The Hubble-normalized variables for the G_2 -compatible SH cosmologies with $\Lambda = 0$ and generic G_2 action (see Figure 3.3), relative to the shear spatial gauge. Trigger variables appear in bold. Recall that $N_{22} = N_+ + \sqrt{3}N_-$, $N_{33} = N_+ - \sqrt{3}N_-$.

Subclass	State vector \mathbf{X}	Additional restriction
With 3 tilt degrees of freedom:		
VI, VII	$(\Sigma_+, \Sigma_-, \mathbf{\Sigma}_x, \mathbf{\Sigma}_2, \mathbf{N}_+, \mathbf{N}_-, N_x, A, \Omega, v_1, v_2, v_3)$	none
IV	$(\Sigma_+, \Sigma_-, \mathbf{\Sigma}_x, \mathbf{\Sigma}_2, \mathbf{N}_+, \mathbf{N}_-, N_x, A, \Omega, v_1, v_2, v_3)$	$N_+^2 - 3(N_-^2 + N_x^2) = 0$
With 2 tilt degrees of freedom: $v_2 = 0$		
VI	$(\Sigma_+, \Sigma_-, \mathbf{\Sigma}_x, \mathbf{\Sigma}_2, \mathbf{N}_-, N_x, A, \Omega, v_1, v_3)$	$N_+ = \sqrt{3}N_-$ $N_x = -\sqrt{3}A$ if $h = -\frac{1}{9}$
IV	$(\Sigma_+, \Sigma_-, \mathbf{\Sigma}_x, \mathbf{\Sigma}_2, \mathbf{N}_-, A, \Omega, v_1, v_3)$	$N_x = 0$
V	$(\Sigma_+, \Sigma_-, \mathbf{\Sigma}_x, \mathbf{\Sigma}_2, A, \Omega, v_1, v_3)$	$N_+ = N_- = N_x = 0$
With 1 tilt degree of freedom: $v_2 = v_3 = 0$		
$\text{VI}_{-\frac{1}{9}}^*$	$(\Sigma_+, \Sigma_-, \mathbf{\Sigma}_x, \mathbf{\Sigma}_2, \mathbf{N}_-, A, \Omega, v_1)$	$N_+ = \sqrt{3}N_-$, $N_x = \sqrt{3}A$ none
II	$(\Sigma_+, \Sigma_-, \mathbf{\Sigma}_x, \mathbf{\Sigma}_2, \mathbf{N}_-, \Omega, v_1)$	$N_x = A = 0$
Non-tilted: $v_\alpha = 0$		
$\text{VI}_{-\frac{1}{9}}^*$	$(\Sigma_+, \Sigma_-, \mathbf{\Sigma}_x, \mathbf{\Sigma}_2, \mathbf{N}_-, A, \Omega)$	$N_+ = \sqrt{3}N_-$, $N_x = \sqrt{3}A$ none

Figure 4.4 and Table 4.1 provide the basis for the following proposition.

Proposition 4.1. *Consider the class of perfect fluid G_2 -compatible SH cosmologies which satisfy the Kasner Attractivity Conjecture.*

- i) If the G_2 action is generic, then Mixmaster dynamics occur if and only if the anisotropic spatial curvature $\mathcal{S}_{\alpha\beta}$ is non-zero.*
- ii) If the G_2 action is non-generic, then Mixmaster dynamics does not occur.*

Proof. From Figure 4.4 and Table 4.1, we see that for models of all Bianchi types with a generic G_2 action, each arc on the Kasner circles has at least

one trigger, unless $N_+ = N_- = N_\times = 0$ (Bianchi type V, where $\mathcal{S}_{\alpha\beta} = 0$). It follows that Mixmaster dynamics occur if and only if $\mathcal{S}_{\alpha\beta} \neq 0$.

On the other hand, if the G_2 action is non-generic, the state vector \mathbf{X} in (4.67) is restricted as follows. For SH cosmologies with OT G_2 action, from (3.5) we have

$$\Sigma_2 = 0. \quad (4.98)$$

For SH cosmologies with one HO KVF, from (3.2) we have

$$N_+ = N_- = 0 = \Sigma_\times. \quad (4.99)$$

For SH cosmologies with diagonal G_2 action, we have

$$\Sigma_2 = 0, \quad N_+ = N_- = 0 = \Sigma_\times. \quad (4.100)$$

Figure 4.4 shows that in each case there is an arc with no triggers, implying that Mixmaster dynamics does not occur.

□

Comment: To show that this result is independent of using a particular gauge, namely the shear spatial gauge (4.64), we note that the infinite sequences of transitions that arise lead to infinite sequences of changes in physically significant scalars, for example, the scalars formed from the Weyl curvature tensor, as we describe later. Since these changes are independent of the choice of gauge, the occurrence of Mixmaster dynamics is independent of the choice of gauge. However, the choice of spatial gauge does affect which triggers occur and hence the details of the dynamics.⁷ For example, in the Killing spatial gauge (4.63), the triggers are N_{22} , Σ_\times , Σ_2 and Σ_3 . It should be kept in mind that the frame transitions are merely an artifact of the rotating spatial frame, and do not lead to a change of Kasner state.⁸

⁷The real, physical dynamics, and artifacts of the rotating spatial frame both affect the triggers and other gravitational field variables. To separate these effects, we observe rotation-invariant scalars formed these variables (see (4.117)–(4.119) below).

⁸As an extreme example, an artificial type of Mixmaster dynamics consisting of an endless sequence of frame transitions occurs for models of Bianchi type V if the Killing spatial gauge (4.63) is used, since the only triggers are Σ_\times , Σ_2 and Σ_3 . The rotational freedom can be used to set $\Sigma_3 = 0$ to eliminate this artificial Mixmaster dynamics (the arc (T_1Q_2) becomes stable).

In addition to (4.95), there appear to be other limits that help to characterize the asymptotic dynamics. From the linearized equations (4.89)–(4.92) we obtain

$$(N_{22}N_{33})' = 4(1 + \Sigma_+)(N_{22}N_{33}) \quad (4.101)$$

$$(N_{22}\Sigma_\times)' = 2(1 + \Sigma_+)(N_{22}\Sigma_\times) \quad (4.102)$$

$$(N_{33}\Sigma_2)' = (2 - \Sigma_+ - \sqrt{3}\Sigma_-)(N_{33}\Sigma_2) . \quad (4.103)$$

It follows that these products are stable on the Kasner circles into the past, suggesting that they tend to zero as $t \rightarrow -\infty$:

$$\lim_{t \rightarrow -\infty} (N_{22}N_{33}, N_{22}\Sigma_\times, N_{33}\Sigma_2) = \mathbf{0} . \quad (4.104)$$

This claim is strongly supported by numerical simulations. These limits can be interpreted as stating that the two triggers in each product cannot be active simultaneously.

Multiple transitions

Returning to Figure 4.4, notice that there is more than one trigger on some Kasner arcs, which means that two triggers can become active simultaneously, leading to more complicated transitions between Kasner states. These so-called *multiple transitions* were first studied in detail by Hewitt *et al.* 2003 [36] in the context of non-tilted exceptional Bianchi VI $^*_{-1/9}$ cosmologies. The orbit of a multiple transition is not a straight line when projected on the (Σ_+, Σ_-) plane. See Figures 3 and 4 in [36]. Two of the three possible multiple transitions involve the pairs (N_{22}, Σ_2) and (N_{33}, Σ_\times) , which describe the Taub vacuum Bianchi II solutions relative to a non-Fermi-propagated frame. The third one, involving the pair $(\Sigma_2, \Sigma_\times)$, describes the Kasner solutions relative to a non-Fermi-propagated frame. The possibility of multiple transitions is a significant difference from the “standard” Mixmaster dynamics (of Bianchi VIII and IX). On the basis of detailed numerical simulations, Hewitt *et al.* conjecture that the probability of multiple transitions occurring tends to zero as $t \rightarrow -\infty$. The numerical experiments suggest that multiple transitions keep occurring as $t \rightarrow -\infty$, but that their strength, as measured by $|N_{22}\Sigma_2|$, $|N_{33}\Sigma_\times|$ and $|\Sigma_2\Sigma_\times|$, keeps decreasing, i.e. that

$$\lim_{t \rightarrow -\infty} (N_{22}\Sigma_2, N_{33}\Sigma_\times, \Sigma_2\Sigma_\times) = \mathbf{0} . \quad (4.105)$$

We caution that this result is not very conclusive, and we shall revisit multiple transitions in the context of G_2 dynamics in Chapters 7 and 9.

Tilt

What happens to the tilt variables v_α ? To determine the behaviour of v_α , linearize (4.43)–(4.45) on \mathcal{K} , and also (4.44)–(4.45) and (4.51) on $\mathcal{K}_{\pm 1}$:

$$\text{on } \mathcal{K}: \quad v'_1 = (3\gamma - 4 + 2\Sigma_+)v_1 \quad (4.106)$$

$$v'_2 = (3\gamma - 4 - \Sigma_+ - \sqrt{3}\Sigma_-)v_2 \quad (4.107)$$

$$v'_3 = (3\gamma - 4 - \Sigma_+ + \sqrt{3}\Sigma_-)v_3 \quad (4.108)$$

$$\text{on } \mathcal{K}_{\pm 1}: \quad v'_2 = (-3\Sigma_+ - \sqrt{3}\Sigma_-)v_2 \quad (4.109)$$

$$v'_3 = (-3\Sigma_+ + \sqrt{3}\Sigma_-)v_3 \quad (4.110)$$

$$(1 - v^2)' = -2\frac{3\gamma - 4 + 2\Sigma_+}{2 - \gamma}(1 - v^2). \quad (4.111)$$

For the purpose of this thesis, we shall focus on models with only one tilt degree of freedom, i.e. $v_1 \neq 0$, $v_2 = v_3 = 0$. Equations (4.106) and (4.111) give the linearized solutions

$$v_1 = (v_1)_0 e^{(3\gamma - 4 + 2\Sigma_+)t} \quad (4.112)$$

$$\sqrt{1 - v^2} = (\sqrt{1 - v^2})_0 e^{-\frac{(3\gamma - 4 + 2\Sigma_+)}{(2 - \gamma)}t}. \quad (4.113)$$

Hence, the tilt is unstable into the past on the following arcs:

$$\mathcal{K} \text{ arc}(\Sigma_+ < -\frac{1}{2}(3\gamma - 4)), \quad \mathcal{K}_{\pm 1} \text{ arc}(\Sigma_+ > -\frac{1}{2}(3\gamma - 4)). \quad (4.114)$$

This creates transition orbits between \mathcal{K} and $\mathcal{K}_{\pm 1}$, as illustrated in Figure 4.5. The unstable arcs are highlighted, and the arrows indicate evolution into the past. For convenience we augment Figure 4.4 by adding the unstable arcs for v_1 to produce Figure 4.6. There are analogous transition orbits between \mathcal{K} and $\mathcal{K}_{\pm 2}$, and between \mathcal{K} and $\mathcal{K}_{\pm 3}$. There are also transition orbits between the extreme tilt Kasner circles.⁹

⁹We refer the reader to the work by Uggla, van Elst, Wainwright & Ellis 2003 [72] in the context of G_0 cosmologies.

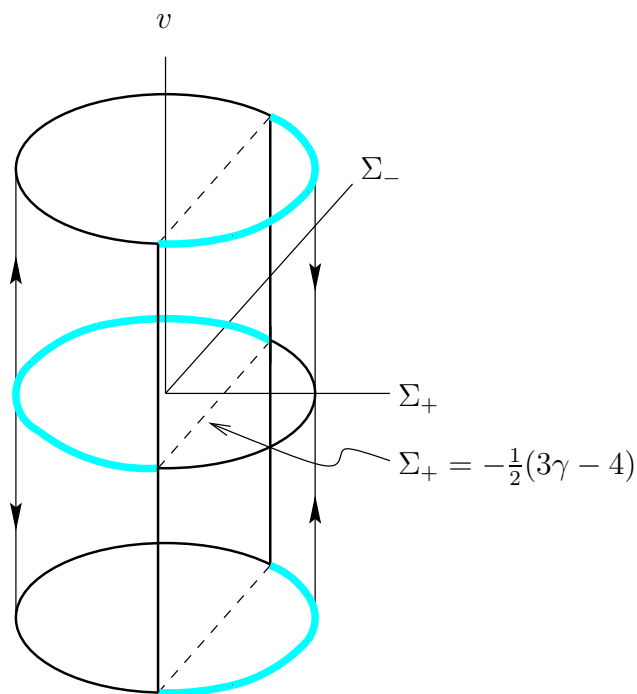


Figure 4.5: The tilt transition for v_1 .

Comments: The nature of the tilt transition means *we cannot make non-Mixmaster dynamics into Mixmaster by adding only tilt transitions*. However adding tilt degrees of freedom to a non-tilted model also adds off-diagonal shear variables and it is these variables that lead to the occurrence of Mixmaster dynamics. From Table 4.1, we see that the tilted Bianchi II cosmologies form the prototype for Mixmaster dynamics with tilt. We refer to the analysis of tilted Bianchi II cosmologies by Hewitt *et al.* 2001 [35].¹⁰ The class

¹⁰The spatial gauge used in this paper is a permutation of the one used in this thesis. The indices they use are “one lower” than ours, e.g. they have

$$N_{11} \neq 0, \quad v_3 \neq 0, \quad \Sigma_{31} = 0, \quad (4.115)$$

while we have

$$N_{22} \neq 0, \quad v_1 \neq 0, \quad \Sigma_{12} = 0. \quad (4.116)$$

They define Σ_{\pm} relative to their 23-subspace, as we do in (4.24).

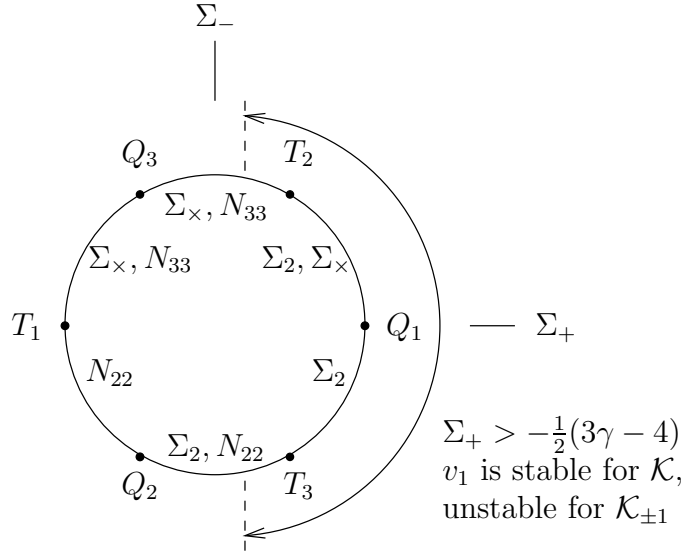


Figure 4.6: The unstable arcs on \mathcal{K} and $\mathcal{K}_{\pm 1}$ and their triggers.

of tilted exceptional Bianchi VI $^*_{-1/9}$ cosmologies has not been analyzed, but we can now predict, without additional work, that its Mixmaster dynamics is that of the tilted Bianchi II cosmologies.

Physical aspects of Mixmaster dynamics

The physical aspects of Mixmaster dynamics are described by rotation-invariant scalars, such as the shear scalar Σ and the electric and magnetic Weyl scalars \mathcal{E} and \mathcal{H} :

$$\Sigma^2 = \Sigma_+^2 + \Sigma_-^2 + \Sigma_\times^2 + \Sigma_2^2 + \Sigma_3^2 \quad (4.117)$$

$$\mathcal{E}^2 = \mathcal{E}_+^2 + \mathcal{E}_-^2 + \mathcal{E}_\times^2 + \mathcal{E}_3^2 + \mathcal{E}_2^2 \quad (4.118)$$

$$\mathcal{H}^2 = \mathcal{H}_+^2 + \mathcal{H}_-^2 + \mathcal{H}_\times^2 + \mathcal{H}_3^2 + \mathcal{H}_2^2. \quad (4.119)$$

Furthermore, the scalar $\mathcal{E}^2 - \mathcal{H}^2$ is boost-invariant. The shear scalar Σ is close to 1 except during curvature transitions. The other invariant of $\Sigma_{\alpha\beta}$ is the determinant $\det \Sigma_{\alpha\beta}$, which is also equal to $\frac{1}{3}\Sigma_{\alpha\beta}\Sigma^{\beta\gamma}\Sigma_\gamma^\alpha$. $\det \Sigma_{\alpha\beta}$ is close to constant except during curvature transitions. The electric Weyl scalar \mathcal{E}

is equal to $\sqrt{2 - \det \Sigma_{\alpha\beta}}$ when $\Sigma^2 = 1$. It is close to constant except during curvature transitions. The magnetic Weyl scalar \mathcal{H} is close to zero except during curvature transitions. We refer to WE, Section 11.4 for the graphs of these scalars under the standard Mixmaster dynamics. There are other rotation-invariant scalars, such as Ω_k , $\mathcal{S}_{\alpha\beta}\mathcal{S}^{\alpha\beta}$ and $\det \mathcal{S}_{\alpha\beta}$. The principal feature of Mixmaster dynamics is that the Hubble-normalized Weyl scalars are bounded but do not have a limit in the past asymptotic regime.

Another physical aspect is the fluid vorticity. Although the timelike congruence \mathbf{e}_0 is vorticity-free, the fluid congruence is not necessarily so. From Appendix C of Hewitt *et al.* 2001 [35], the fluid vorticity for G_2 -compatible SH cosmologies is given by

$$W_1 = \frac{1}{2B} \frac{1}{1-v^2} N^{CD} v_C v_D v_1 \quad (4.120)$$

$$W_A = \frac{1}{2B} \left[(N_A{}^C + \epsilon_A{}^C A) v_C + \frac{1}{1-v^2} N^{CD} v_C v_D v_A \right], \quad (4.121)$$

where

$$B = \frac{1 - \frac{1}{3}(v^2 + \Sigma_{\alpha\beta} v^\alpha v^\beta + 2Av_1)}{G_- \sqrt{1-v^2}}.$$

Observe that the fluid vorticity is zero if $v_2 = v_3 = 0$.

For the case $v_2 = 0$, $v_3 \neq 0$, the spatial gauge is given by (4.65), which implies $N^{CD} v_C v_D = 0$. It follows that the only non-zero vorticity component is

$$W_2 = \frac{1}{2B} (\sqrt{3}N_\times + A)v_3. \quad (4.122)$$

The limit (4.95) then implies that W_2 tends to zero.

For the case with three tilt degrees of freedom, since the limit of $N^{CD} v_C v_D$ does not exist, the limit of the fluid vorticity does not exist as $t \rightarrow -\infty$, i.e. Mixmaster dynamics is reflected in the fluid vorticity.

Thus we have the following proposition.

Proposition 4.2. *Consider G_2 -compatible SH cosmologies with generic G_2 action.*

- *If there is one tilt degree of freedom (i.e. $v_A = 0$), then the fluid vorticity is zero.*
- *If there are two tilt degrees of freedom, then the fluid vorticity tends to zero as $t \rightarrow -\infty$.*

- *If there are three tilt degrees of freedom, then the limit of the fluid vorticity does not exist as $t \rightarrow -\infty$.*

We revisit Figure 3.3 and include the total number of curvature and frame triggers, the dimension of the state space, and the asymptotic behaviour of the fluid vorticity (see Figure 4.7). Note that for Bianchi VI and VII cosmologies, the dimension listed is for the state space with a fixed parameter h . For $\Lambda > 0$, increase the dimension by one.

Before giving a summary we note that there is some uncertainty as regards the behaviour of the tilt as $t \rightarrow -\infty$. The analysis of the triggers and of the tilt transitions suggests that along a typical infinite sequence of transitions, the tilt scalar v will not approach a limit:

$$\lim_{t \rightarrow -\infty} v \text{ does not exist.} \quad (4.123)$$

However, while performing numerical simulations of Bianchi II models with $\gamma = \frac{4}{3}$, Bridson 1997 [13] discovered that, despite the existence of tilt transitions from $\mathcal{K}_{\pm 1}$ to \mathcal{K} that transform v from ± 1 to 0, v tends to get stuck at ± 1 . He argued that, due to the arrangement of the transition orbits, the state vector \mathbf{X} spends more time close to the part of $\mathcal{K}_{\pm 1}$ where $1 - v^2$ is stable and hence $1 - v^2$ is forced even closer to zero, so that when it has an opportunity to activate, i.e. when \mathbf{X} is close to the unstable arc on $\mathcal{K}_{\pm 1}$ for $1 - v^2$, it needs more time to do so and loses out to the curvature and frame triggers. This tendency will, however, depend significantly on the value of γ . If γ is close to 2, then v should have a strong tendency to stay close to zero, for two reasons: $(1 - v^2)$ is unstable on most of $\mathcal{K}_{\pm 1}$, and also has a high growth rate into the past due to the $(2 - \gamma)$ factor in the denominator (see equation (4.113)). Hence one expects that somewhere between $\gamma = \frac{4}{3}$ and $\gamma = 2$ there is a critical value of γ where one tendency replaces the other.

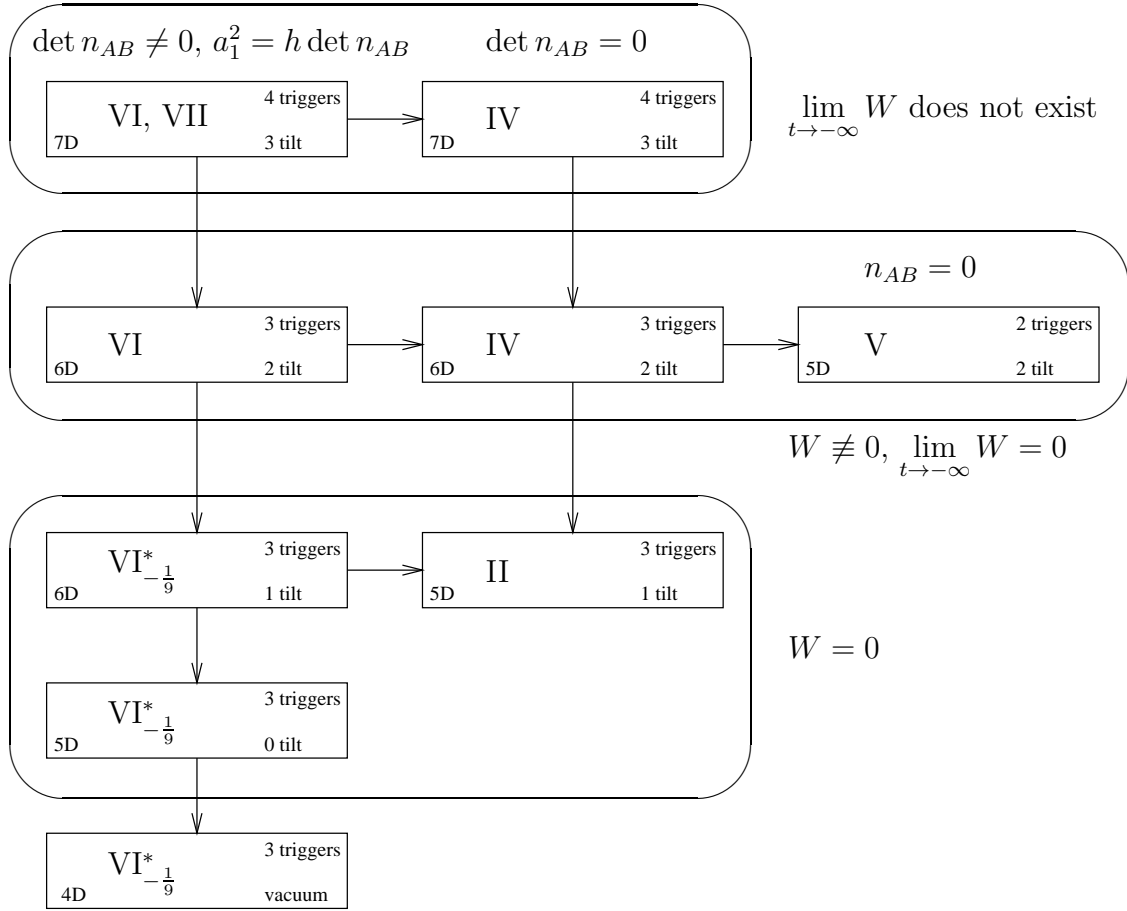


Figure 4.7: SH cosmologies with generic G_2 action, indicating the Bianchi group type, the dimension of the Hubble-normalized state space, the number of triggers and the number of tilt degrees of freedom. Here W is the Hubble-normalized fluid vorticity scalar, defined by $W^2 = W_1^2 + W_A W^A$.

Summary

To recapitulate, the *generalized Mixmaster dynamics* that we have discussed in this section can be described by the following limits:

$$\text{BKL conjecture I:} \quad \lim_{t \rightarrow -\infty} \Omega = 0, \quad \lim_{t \rightarrow -\infty} \Omega_\Lambda = 0, \quad (4.124)$$

$$\text{Stable variables:} \quad \lim_{t \rightarrow -\infty} (A, N_\times) = \mathbf{0}, \quad (4.125)$$

$$\text{Non-overlapping triggers:} \quad \lim_{t \rightarrow -\infty} (N_{22}N_{33}, N_{22}\Sigma_\times, N_{33}\Sigma_2) = \mathbf{0}, \quad (4.126)$$

$$\text{Trigger variables:} \quad \lim_{t \rightarrow -\infty} (N_{22}, N_{33}, \Sigma_2, \Sigma_\times) \quad \text{do not exist.} \quad (4.127)$$

Unlike the case of standard Mixmaster dynamics discussed in Section 4.1, to date no proofs have been given concerning generalized Mixmaster dynamics (e.g. the limits (4.124)–(4.126) which serve to restrict the past attractor). The non-tilted Bianchi VI_{-1/9}^{*} solutions and the tilted Bianchi II solutions are prototypes for the new features of generalized Mixmaster dynamics. Understanding these two special cases, and having our formulation of the evolution equations for the whole hierarchy, gives qualitative information about the dynamics of the whole class and provides equations for doing detailed analyses, and perhaps for providing proofs of some of the above limits.

4.4 Non-Mixmaster dynamics

In this section, we discuss the past asymptotic dynamics of SH subclasses with non-generic G_2 action. The conditions for OT G_2 action, HO KVF and diagonal G_2 action are given by (4.98)–(4.100) respectively. Figures 3.4–3.5 summarized the hierarchy for these SH subclasses. Tables 4.2–4.4 list the variables and the additional restrictions.

For each entry in Tables 4.2–4.4, we combine the unstable arcs of the curvature, frame and tilt transition sets in Figure 4.6 and look for the remaining stable arcs on the Kasner circles \mathcal{K} and $\mathcal{K}_{\pm 1}$. In each case, sequences of transition sets will terminate at some stable arc. For each class the past attractor is an arc or union of arcs on the Kasner circles. The result is that each orbit, except for a set of measure zero, is past asymptotic to a Kasner equilibrium point.

For SH cosmologies with OT G_2 action (4.98), the Σ_2 trigger is zero,

Table 4.2: The Hubble-normalized variables for the G_2 -compatible SH cosmologies with $\Lambda = 0$ and OT G_2 action (see Figure 3.4). Triggers appear in bold.

Subclass	State vector \mathbf{X}	Additional restriction
With 1 tilt degree of freedom: $v_2 = v_3 = 0$		
VII	$(\Sigma_+, \Sigma_-, \mathbf{\Sigma}_x, \mathbf{N}_+, \mathbf{N}_-, N_x, A, \Omega, v_1)$	$\Sigma_2 = 0$ none
VI	$(\Sigma_+, \Sigma_-, \mathbf{\Sigma}_x, \mathbf{N}_-, N_x, A, \Omega, v_1)$	$N_+ = \sqrt{3}N_-$
IV	$(\Sigma_+, \Sigma_-, \mathbf{\Sigma}_x, \mathbf{N}_-, A, \Omega, v_1)$	$N_+ = \sqrt{3}N_-$, $N_x = 0$
II	$(\Sigma_+, \Sigma_-, \mathbf{\Sigma}_x, \mathbf{N}_-, \Omega, v_1)$	$N_+ = \sqrt{3}N_-$, $N_x = 0 = A$
Non-tilted: $v_\alpha = 0$		
VII	$(\Sigma_+, \Sigma_-, \mathbf{\Sigma}_x, \mathbf{N}_+, \mathbf{N}_-, N_x, A, \Omega)$	$\Sigma_2 = 0$ none
VI	$(\Sigma_+, \Sigma_-, \mathbf{\Sigma}_x, \mathbf{N}_-, N_x, A, \Omega)$	$N_+ = \sqrt{3}N_-$
IV	$(\Sigma_+, \Sigma_-, \mathbf{\Sigma}_x, \mathbf{N}_-, A, \Omega)$	$N_+ = \sqrt{3}N_-$, $N_x = 0$
II	$(\Sigma_+, \Sigma_-, \mathbf{N}_-, \Omega)$	$N_+ = \sqrt{3}N_-$, $N_x = 0 = A = \Sigma_x$

making the Kasner arc (T_3Q_1) on \mathcal{K} in Figure 4.6 stable. The corresponding arc on $\mathcal{K}_{\pm 1}$ is unstable due to the tilt. Thus the conjectured past attractor is given by

$$\mathcal{A}^- = \mathcal{K} \text{ arc}(T_3Q_1). \quad (4.128)$$

The past attractor for the non-tilted case (i.e. $v_1 = 0$) is also given by (4.128), except for Bianchi II, whose past attractor is a bigger set

$$\mathcal{A}^- = \mathcal{K} \text{ arc}(T_1Q_3T_2Q_1T_3). \quad (4.129)$$

For SH cosmologies with one HO KVF (4.99), there is only one trigger, Σ_2 . With one tilt degree of freedom, from Figure 4.6, we see that the conjectured past attractor is given by

$$\begin{aligned} \mathcal{A}^- = & \left[\mathcal{K} \text{ arc}(\Sigma_+ > -\frac{1}{2}(3\gamma - 4)) \cap \mathcal{K} \text{ arc}(Q_2T_1Q_3T_2) \right] \\ & \cup \left[\mathcal{K}_{\pm 1} \text{ arc}(\Sigma_+ < -\frac{1}{2}(3\gamma - 4)) \cap \mathcal{K}_{\pm 1} \text{ arc}(Q_2T_1Q_3T_2) \right]. \end{aligned} \quad (4.130)$$

For non-tilted models, the past attractor is the point $(\Sigma_+, \Sigma_-) = (-\frac{\sqrt{3}}{2}, \frac{1}{2})$ on

Table 4.3: The Hubble-normalized variables for the G_2 -compatible SH cosmologies with $\Lambda = 0$ and one HO KVF (see Figure 3.5). Σ_2 is the only trigger.

Subclass	State vector \mathbf{X}	Additional restriction
With 2 tilt degrees of freedom: $v_2 = 0$		$N_+ = \sqrt{3}N_- = 0 = \Sigma_\times$
VI	$(\Sigma_+, \Sigma_-, \mathbf{\Sigma}_2, N_\times, A, \Omega, v_1, v_3)$	$N_\times = -\sqrt{3}A$ if $h = -\frac{1}{9}$
V	$(\Sigma_+, \Sigma_-, \mathbf{\Sigma}_2, A, \Omega, v_1, v_3)$	$N_\times = 0$
With 1 tilt degree of freedom: $v_2 = v_3 = 0$		$N_+ = \sqrt{3}N_- = 0 = \Sigma_\times, N_\times = \sqrt{3}A$
$\text{VI}^*_{-\frac{1}{9}}$	$(\Sigma_+, \Sigma_-, \mathbf{\Sigma}_2, A, \Omega, v_1)$	none
Non-tilted: $v_\alpha = 0$		$N_+ = \sqrt{3}N_- = 0 = \Sigma_\times, N_\times = \sqrt{3}A,$ $\Sigma_+ = -\sqrt{3}\Sigma_-$
$\text{VI}^*_{-\frac{1}{9}}$	$(\Sigma_-, \mathbf{\Sigma}_2, A, \Omega)$	none

\mathcal{K} . Finally, we note that the past attractor for the case with two tilt degrees of freedom is also given by (4.130).¹¹

For SH cosmologies with diagonal G_2 action (4.100), there are no triggers. From Figure 4.5, we see that for tilted models ($v_1 \neq 0$) the conjectured past attractor is given by

$$\mathcal{A}^- = \mathcal{K} \text{ arc}(\Sigma_+ > -\frac{1}{2}(3\gamma - 4)) \cup \mathcal{K}_{\pm 1} \text{ arc}(\Sigma_+ < -\frac{1}{2}(3\gamma - 4)). \quad (4.131)$$

¹¹It turns out that the set for stable arcs on $\mathcal{K}_{\pm 3}$, given by

$$\mathcal{K}_{\pm 3} \text{ arc}(\Sigma_+ - \sqrt{3}\Sigma_- > 3\gamma - 4) \cap \mathcal{K}_{\pm 3} \text{ arc}(Q_3T_2Q_1T_3) \cap \mathcal{K}_{\pm 3} \text{ arc}(Q_2T_1Q_3T_2),$$

is empty, and the arcs for which $v_3 = 0$ is stable on $\mathcal{K}_{\pm 1}$ is identical to $\mathcal{K}_{\pm 1} \text{ arc}(Q_2T_1Q_3T_2)$ (compare (4.108) with (4.90)). Finally, the stable arcs on \mathcal{K} , given by

$$\mathcal{K} \text{ arc}(\Sigma_+ > -\frac{1}{2}(3\gamma - 4)) \cap \mathcal{K} \text{ arc}(\Sigma_+ - \sqrt{3}\Sigma_- < 3\gamma - 4) \cap \mathcal{K} \text{ arc}(Q_2T_1Q_3T_2),$$

simplifies to

$$\mathcal{K} \text{ arc}(\Sigma_+ > -\frac{1}{2}(3\gamma - 4)) \cap \mathcal{K} \text{ arc}(Q_2T_1Q_3T_2).$$

Table 4.4: The Hubble-normalized variables for the G_2 -compatible SH cosmologies with $\Lambda = 0$ and diagonal G_2 action (see Figure 3.5).

Subclass	State vector \mathbf{X}	Additional restriction
With 1 tilt degree of freedom: $v_2 = v_3 = 0$		$\Sigma_2 = 0, N_+ = \sqrt{3}N_- = 0 = \Sigma_\times$
VI	$(\Sigma_+, \Sigma_-, N_\times, A, \Omega, v_1)$	none
V	$(\Sigma_+, \Sigma_-, A, \Omega, v_1)$	$N_\times = 0$
V (LRS)	$(\Sigma_+, A, \Omega, v_1)$	$N_\times = 0 = \Sigma_-$
Non-tilted: $v_\alpha = 0$		$\Sigma_2 = 0, N_+ = \sqrt{3}N_- = 0 = \Sigma_\times$
VI	$(\Sigma_+, \Sigma_-, N_\times, A, \Omega)$	none
V	(Σ_-, A, Ω)	$N_\times = 0 = \Sigma_+$
I	$(\Sigma_+, \Sigma_-, \Omega)$	$N_\times = 0 = A$
I (LRS)	(Σ_+, Ω)	$N_\times = 0 = A = \Sigma_-$

With zero tilt, the past attractor is given by

$$\mathcal{A}^- = \mathcal{K} , \quad (4.132)$$

except for Bianchi V, whose past attractor is a smaller set

$$\mathcal{A}^- = \{\Sigma_+ = 0, \Sigma_- = \pm 1\}. \quad (4.133)$$

4.5 Future asymptotics

In this section we discuss the future asymptotic dynamics of G_2 -compatible SH cosmologies.

The role of Λ

The presence of a cosmological constant $\Lambda > 0$ simplifies the future asymptotic dynamics of SH cosmologies dramatically, as shown by Wald 1983 [80]. He proved, for all SH cosmologies excluding Bianchi type IX, subject to cer-

tain restrictions on the matter content, that

$$\lim_{t \rightarrow \infty} H = \sqrt{\frac{\Lambda}{3}}, \quad \lim_{t \rightarrow \infty} \sigma_{\alpha\beta} = 0, \quad (4.134)$$

where H is the Hubble scalar and $\sigma_{\alpha\beta}$ is the shear tensor. In other words, the cosmological models are asymptotic to the de Sitter solution.

Starobinskiĭ 1983 [67] discussed the asymptotic dynamics of cosmologies without symmetry assumptions and provided a conjecture for behaviour of the tilt variables, an issue that Wald had not addressed. He called the positive cosmological constant “the best isotropizer”.

Our goal is to describe the effect of including a positive cosmological constant Λ from the perspective of the Hubble-normalized state space. First, including Λ increases the dimension of the Hubble-normalized state space by one, by adjoining the Hubble-normalized variable Ω_Λ . Second, the Gauss constraint (4.38) implies

$$0 < \Omega_\Lambda \leq 1. \quad (4.135)$$

The condition

$$\Omega_\Lambda = 1 \quad (4.136)$$

with (4.38) and (4.35) implies that

$$\Omega = 0, \quad \Sigma^2 = 0, \quad N_- = 0 = N_\times = A, \quad q = -1, \quad (4.137)$$

and the evolution equation (4.46) for Ω_Λ is identically satisfied. Equations (4.136)–(4.137) thus define an invariant set. The evolution equation (4.31) evaluated on the invariant set (4.136)–(4.137) gives

$$N'_+ = -N_+, \quad (4.138)$$

which implies that equilibrium points must satisfy

$$N_+ = 0. \quad (4.139)$$

Evolution equations (4.43)–(4.45) and (4.51) evaluated on this invariant set

give

$$v'_\alpha = \frac{(3\gamma - 4)}{G_-}(1 - v^2)v_\alpha \quad (4.140)$$

$$(v^2)' = \frac{2(3\gamma - 4)}{G_-}(1 - v^2)v^2, \quad (4.141)$$

which imply that the equilibrium points are

$$\begin{cases} v_\alpha = 0 \quad \text{or} \quad v^2 = 1 & \text{if } \gamma \neq \frac{4}{3} \\ v_\alpha = \text{const.}, \quad 0 \leq v^2 \leq 1 & \text{if } \gamma = \frac{4}{3}. \end{cases} \quad (4.142)$$

We shall refer to the set (4.136)–(4.137), (4.139) and (4.142) as the *de Sitter invariant set*.

The evolution equation (4.46) for Ω_Λ , (4.35) and (4.135) imply that

$$\Omega'_\Lambda = (q + 1)\Omega_\Lambda > 0, \quad (4.143)$$

which implies that Ω_Λ is monotone increasing, and

$$\lim_{t \rightarrow \infty} \Omega_\Lambda = 1, \quad \lim_{t \rightarrow -\infty} \Omega_\Lambda = 0. \quad (4.144)$$

The presence of Ω_Λ thus has no effect on the past asymptotic dynamics, but destabilizes all equilibrium points on the set $\Omega_\Lambda = 0$ into the future. That $\lim_{t \rightarrow \infty} \Omega_\Lambda = 1$ implies

$$\lim_{t \rightarrow \infty} \Omega = 0, \quad \lim_{t \rightarrow \infty} \Sigma^2 = 0, \quad \lim_{t \rightarrow \infty} (N_+, N_-, N_\times, A) = \mathbf{0}. \quad (4.145)$$

As a result, the Weyl curvature variables also tend to zero:

$$\lim_{t \rightarrow \infty} \mathcal{E}_{\alpha\beta} = 0, \quad \lim_{t \rightarrow \infty} \mathcal{H}_{\alpha\beta} = 0. \quad (4.146)$$

Since there are no equilibrium points with $0 < \Omega_\Lambda < 1$, as $t \rightarrow \infty$ the solutions must approach the de Sitter invariant set. The tilt variables have

the following limits:

$$\begin{cases} \lim_{t \rightarrow \infty} v_\alpha = 0 & \text{if } \gamma < \frac{4}{3} \\ \lim_{t \rightarrow \infty} v_\alpha = \text{const.} & \text{if } \gamma = \frac{4}{3} \\ \lim_{t \rightarrow \infty} v_\alpha = \text{const.}, \quad \lim_{t \rightarrow \infty} v^2 = 1 & \text{if } \frac{4}{3} < \gamma < 2. \end{cases} \quad (4.147)$$

See Lim *et al.* 2004 [48], Appendix B for a proof.

The case $\Lambda = 0$

The future dynamics in the case $\Lambda = 0$ is much more complicated than in the case $\Lambda > 0$, and depends significantly on the Bianchi type and on the equation of state parameter γ . The future dynamics for the non-tilted case has been completely analyzed,¹² but much remains to be done as regards the tilted case. Based on the known cases – the Bianchi II and VI₀ subclasses (see [35] and [32] respectively), non-tilted equilibrium points in the interior ($\Omega > 0$) of the state space, which act as the future attractor for non-tilted models, are destabilized by the tilt as γ increases. The resulting bifurcations lead to the creation of tilted equilibrium points that act as the future attractor.

Table 4.5 gives an overview of the work on tilted G_2 -compatible SH cosmologies (all with $\Lambda = 0$) using Hubble-normalized variables.¹³ Hervik and Coley 2004 [33] are currently analyzing the future dynamics of tilted Bianchi VI_h cosmologies, and a preliminary result suggests that a complicated, periodic orbit attractor exists for a certain range of γ .

The class of SH cosmologies of Bianchi type VII is of particular interest because it contains the flat and open FL cosmologies as isotropic special cases (flat FL as a special case of VII₀ and open FL as a special case of VII_h).

The Bianchi VII₀ state space is unbounded: N_+ is not bounded by the Gauss constraint (4.38). This is not an artifact of a bad choice of spatial frame, since the Weyl curvature scalars become unbounded as $N_+ \rightarrow \infty$ (N_+ appears in (4.53)–(4.54) and (4.58)–(4.59)). In other words, the Hubble-normalized Weyl curvature scalars are unbounded on the Bianchi VII₀ state space. The detailed analysis of the non-tilted Bianchi VII₀ cosmologies shows

¹²See WE, Wainwright, Hancock & Uggla 1999 [78], Nilsson, Hancock & Wainwright 2000 [56], Horwood *et al.* 2003 [38] and Hewitt *et al.* 2003 [36].

¹³See WE for references to work on tilted SH cosmologies using other approaches.

Table 4.5: Previous work on G_2 -compatible SH cosmologies with tilt and $\Lambda = 0$.

Bianchi type	G_2 action	paper
Bianchi V	generic G_2	Harnett 1996 [30]
	HO KVF	Harnett 1996 [31]
	tilted diagonal	Hewitt & Wainwright 1992 [37]
	LRS tilted diagonal	Collins & Ellis 1979 [19]
Bianchi II	generic G_2	Hewitt <i>et al.</i> 2001 [35]
Bianchi VI ₀	generic G_2	Hervik 2004 [32]

that if $\gamma \leq \frac{4}{3}$, they isotropize as regards the shear (i.e. $\Sigma_{\pm} \rightarrow 0$ as $r \rightarrow \infty$) even though $N_+ \rightarrow \infty$, but that the Weyl curvature diverges if $\gamma > 1$ [78] [56]. Preliminary investigation of the tilted models [47] indicates that no tilted equilibrium points exist for Bianchi VII₀ cosmologies. We expect that if $\gamma \leq \frac{4}{3}$, they isotropize as regards the shear. This matter requires further investigation.

Chapter 5

The state space for G_2 cosmologies

In this chapter, we use the 1+1+2 orthonormal frame formalism as developed in Section 2.2 to formulate the evolution equations for G_2 cosmologies. We also introduce the notion of *asymptotic silence* and the *silent boundary*, which provides the link between G_2 dynamics and SH dynamics.

5.1 The evolution equations

The starting point for deriving the evolution equations for G_2 cosmologies is the 1+1+2 form of the orthonormal frame equations. As discussed in Section 2.3 we normalize the variables for G_2 cosmologies using the area expansion rate β , as motivated by van Elst *et al.* 2002 [74]. β -normalization is advantageous only when used in conjunction with the so-called *separable area gauge*, introduced by van Elst *et al.* 2002 [74] in the context of OT G_2 cosmologies.

The separable area gauge condition is given by

$$\dot{U} = r. \tag{5.1}$$

By using the $(C_{\dot{u}})_1$ constraint (2.77) we find that \mathcal{N} , introduced in (2.107), is independent of x , which implies that we may reparametrize t to set

$$\mathcal{N} = 1. \tag{5.2}$$

A special case of the separable area gauge is the *timelike area gauge*, for which

$$\dot{U} = r, \quad \mathcal{N} = 1, \quad A = 0. \quad (5.3)$$

This gauge is equivalent to the one that has been widely used in the study of vacuum OT G_2 cosmologies using the metric approach (see, for example, Rendall & Weaver 2001 [62]). Although the timelike area gauge is simpler than the separable area gauge in a number of respects (see Sections 8.1, 8.2 and 8.3), we shall resist setting $A = 0$, since the separable area gauge enables one to include all G_2 -compatible SH cosmologies as special cases, as will be explained in Section 5.2.

As in Section 4.2, for convenience we introduce the following notation:

$$N_C{}^C = 2N_+, \quad \tilde{N}_{AB} = \sqrt{3} \begin{pmatrix} N_- & N_\times \\ N_\times & -N_- \end{pmatrix}, \quad (5.4)$$

and

$$\Sigma_{12} = \sqrt{3}\Sigma_3, \quad \Sigma_{13} = \sqrt{3}\Sigma_2. \quad (5.5)$$

The 1+1+1+1 β -normalized evolution equations and constraints then follow from the system (2.47)–(2.63), and are given below. In the process, we replace H by β using the relation

$$H = (1 - \Sigma_+) \beta \quad (5.6)$$

(see (2.103)), and normalize the variables using (2.100)–(2.101). The variables q and r are introduced and are given by (2.114) and (2.115) respectively. We remind the reader that

$$\partial_1 = E_1{}^1 \partial_x. \quad (5.7)$$

G_2 system (β -normalized)*Evolution equations for the gravitational field:*

$$\partial_t E_1^1 = (q + 3\Sigma_+)E_1^1 \quad (5.8)$$

$$\partial_t A = (q + 3\Sigma_+)A \quad (5.9)$$

$$\begin{aligned} \partial_t \Sigma_+ = & -(q + 3\Sigma_+)(1 - \Sigma_+) + 2(\Sigma_+ + \Sigma_-^2 + \Sigma_\times^2 + \Sigma_2^2 + \Sigma_3^2) \\ & + \frac{1}{2}G_+^{-1}[(3\gamma - 2) + (2 - \gamma)v^2]\Omega - \Omega_\Lambda - \frac{1}{3}(\boldsymbol{\theta}_1 - 2A)r \end{aligned} \quad (5.10)$$

$$\partial_t N_+ = (q + 3\Sigma_+)N_+ + 6\Sigma_-N_- + 6\Sigma_\times N_\times - \boldsymbol{\theta}_1 R \quad (5.11)$$

$$\begin{aligned} \partial_t \Sigma_- + \boldsymbol{\theta}_1 N_\times = & (q + 3\Sigma_+ - 2)\Sigma_- + 2AN_\times - 2R\Sigma_\times - 2N_+N_- \\ & + \sqrt{3}(\Sigma_3^2 - \Sigma_2^2) + \frac{\sqrt{3}}{2}\frac{\gamma\Omega}{G_+}(v_2^2 - v_3^2) \end{aligned} \quad (5.12)$$

$$\partial_t N_\times + \boldsymbol{\theta}_1 \Sigma_- = (q + 3\Sigma_+)N_\times + 2N_+\Sigma_\times + 2RN_- \quad (5.13)$$

$$\begin{aligned} \partial_t \Sigma_\times - \boldsymbol{\theta}_1 N_- = & (q + 3\Sigma_+ - 2)\Sigma_\times - 2AN_- + 2R\Sigma_- - 2N_+N_\times \\ & + 2\sqrt{3}\Sigma_3\Sigma_2 + \sqrt{3}\frac{\gamma\Omega}{G_+}v_2v_3 \end{aligned} \quad (5.14)$$

$$\partial_t N_- - \boldsymbol{\theta}_1 \Sigma_\times = (q + 3\Sigma_+)N_- + 2N_+\Sigma_- - 2RN_\times \quad (5.15)$$

$$\partial_t \Sigma_3 = (q - 2 - \sqrt{3}\Sigma_-)\Sigma_3 - (R + \sqrt{3}\Sigma_\times)\Sigma_2 + \sqrt{3}\frac{\gamma\Omega}{G_+}v_1v_2 \quad (5.16)$$

$$\partial_t \Sigma_2 = (q - 2 + \sqrt{3}\Sigma_-)\Sigma_2 + (R - \sqrt{3}\Sigma_\times)\Sigma_3 + \sqrt{3}\frac{\gamma\Omega}{G_+}v_1v_3, \quad (5.17)$$

where

$$\begin{aligned} q = \frac{1}{2} \left[1 + 3(-\Sigma_2^2 - \Sigma_3^2 + \Sigma_-^2 + \Sigma_\times^2 + N_-^2 + N_\times^2) - A^2 + 2Ar \right. \\ \left. + 3G_+^{-1}[(\gamma - 1)(1 - v^2) + \gamma v_1^2]\Omega - 3\Omega_\Lambda \right] \end{aligned} \quad (5.18)$$

$$r = -3A\Sigma_+ - 3(N_\times\Sigma_- - N_-\Sigma_\times) - \frac{3}{2}\frac{\gamma\Omega}{G_+}v_1 \quad (5.19)$$

$$G_\pm = 1 \pm (\gamma - 1)v^2, \quad v^2 = v_1^2 + v_2^2 + v_3^2. \quad (5.20)$$

Constraint equations:

$$\begin{aligned} 0 = (\mathcal{C}_G) = & 1 - 2\Sigma_+ - \Sigma_-^2 - \Sigma_\times^2 - \Sigma_2^2 - \Sigma_3^2 - \Omega - \Omega_\Lambda \\ & - N_-^2 - N_\times^2 + \frac{2}{3}(\boldsymbol{\theta}_1 - r)A - A^2 \end{aligned} \quad (5.21)$$

$$0 = (\mathcal{C}_C)_2 = (\boldsymbol{\theta}_1 - r)\Sigma_3 - (3A + \sqrt{3}N_\times)\Sigma_3 - (N_+ - \sqrt{3}N_-)\Sigma_2 + \sqrt{3}\frac{\gamma\Omega}{G_+}v_2 \quad (5.22)$$

$$0 = (\mathcal{C}_C)_3 = (\boldsymbol{\theta}_1 - r)\Sigma_2 - (3A - \sqrt{3}N_\times)\Sigma_2 + (N_+ + \sqrt{3}N_-)\Sigma_3 + \sqrt{3}\frac{\gamma\Omega}{G_+}v_3 \quad (5.23)$$

$$0 = (\mathcal{C}_\beta) = (\boldsymbol{\theta}_1 - 2r)\Omega_\Lambda. \quad (5.24)$$

Evolution equations for the matter:

$$\begin{aligned} \partial_t \Omega = & -\frac{\gamma v_1}{G_+} \boldsymbol{\partial}_1 \Omega + \frac{\gamma \Omega}{G_+} \left[2 \frac{G_+}{\gamma} (q+1) - 3(1 - \Sigma_+) (1 + \frac{1}{3} v^2) \right. \\ & \left. - \Sigma_{\alpha\beta} v^\alpha v^\beta - \boldsymbol{\partial}_1 v_1 + v_1 \boldsymbol{\partial}_1 \ln G_+ + 2A v_1 \right] \end{aligned} \quad (5.25)$$

$$\begin{aligned} \partial_t v_1 = & -v_1 \boldsymbol{\partial}_1 v_1 + \boldsymbol{\partial}_1 \ln G_+ - \frac{\gamma - 1}{\gamma} (1 - v^2) (\boldsymbol{\partial}_1 \ln \Omega - 2r) - r \\ & + (M + 2\Sigma_+) v_1 - 2\sqrt{3}(\Sigma_3 v_2 + \Sigma_2 v_3) \\ & + \sqrt{3} N_\times (v_3^2 - v_2^2) + 2\sqrt{3} N_- v_2 v_3 - A v^2 \end{aligned} \quad (5.26)$$

$$\begin{aligned} \partial_t v_2 = & -v_1 \boldsymbol{\partial}_1 v_2 + (M - \Sigma_+ - \sqrt{3}\Sigma_- + \sqrt{3}N_\times v_1) v_2 \\ & - [R + \sqrt{3}\Sigma_\times - (N_+ - \sqrt{3}N_-) v_1] v_3 \end{aligned} \quad (5.27)$$

$$\begin{aligned} \partial_t v_3 = & -v_1 \boldsymbol{\partial}_1 v_3 + (M - \Sigma_+ + \sqrt{3}\Sigma_- - \sqrt{3}N_\times v_1) v_3 \\ & + [R - \sqrt{3}\Sigma_\times - (N_+ + \sqrt{3}N_-) v_1] v_2 \end{aligned} \quad (5.28)$$

$$\partial_t \Omega_\Lambda = 2(q+1)\Omega_\Lambda, \quad (5.29)$$

where

$$\begin{aligned} M = G_-^{-1} \left[(\gamma - 1)(1 - v^2) \boldsymbol{\partial}_1 v_1 - (2 - \gamma) v_1 \boldsymbol{\partial}_1 \ln G_+ \right. \\ \left. + \frac{\gamma - 1}{\gamma} (2 - \gamma)(1 - v^2) v_1 (\boldsymbol{\partial}_1 \ln \Omega - 2r) + G_- r v_1 \right. \\ \left. + (3\gamma - 4)(1 - v^2)(1 - \Sigma_+) + (2 - \gamma) \Sigma_{\alpha\beta} v^\alpha v^\beta \right. \\ \left. + [G_+ - 2(\gamma - 1)] A v_1 \right], \end{aligned} \quad (5.30)$$

$$\begin{aligned} \Sigma_{\alpha\beta} v^\alpha v^\beta = & \Sigma_+ (v_2^2 + v_3^2 - 2v_1^2) + \sqrt{3}\Sigma_- (v_2^2 - v_3^2) + 2\sqrt{3}\Sigma_\times v_2 v_3 \\ & + 2\sqrt{3}(\Sigma_3 v_2 + \Sigma_2 v_3) v_1. \end{aligned} \quad (5.31)$$

Note that we have used the $(C_C)_1$ constraint (2.52) to solve for r , giving (5.19). The (C_β) constraint (5.24) is an immediate consequence of the definitions (2.108) and $\Omega_\Lambda = \Lambda/(3\beta^2)$. Equation (5.8) is the β -normalized form of equation (2.78). The evolution equations for v_α are derived in the same manner as explained in Section 4.2 for SH cosmologies. They were first derived by Weaver 2002 [81] for generic G_2 cosmologies.

Three useful auxiliary equations are

$$q + 3\Sigma_+ = 2(1 - A^2) + \boldsymbol{\partial}_1 A - 3(\Sigma_2^2 + \Sigma_3^2) - \frac{3}{2}(2 - \gamma) \frac{(1 - v^2)}{G_+} \Omega - 3\Omega_\Lambda \quad (5.32)$$

$$\begin{aligned} \partial_t(v^2) = & -v_1 \boldsymbol{\partial}_1(v^2) + \frac{2}{G_-}(1 - v^2) \left[v_1 \boldsymbol{\partial}_1 \ln G_+ + (\gamma - 1)v^2 \boldsymbol{\partial}_1 v_1 \right. \\ & - \frac{\gamma - 1}{\gamma}(1 - v^2)v_1(\boldsymbol{\partial}_1 \ln \Omega - 2r) - G_- r v_1 \\ & \left. + (3\gamma - 4)v^2(1 - \Sigma_+) - \Sigma_{\alpha\beta} v^\alpha v^\beta - 2(\gamma - 1)v^2 A v_1 \right] \quad (5.33) \end{aligned}$$

$$\partial_t r = (q + 3\Sigma_+)r + \boldsymbol{\partial}_1 q. \quad (5.34)$$

Equation (5.32) is derived from (5.18) and (5.21), while (5.34) is derived from the commutator $[\boldsymbol{\partial}_0, \boldsymbol{\partial}_1]$ in (2.118) acting on β . Equation (5.32) becomes algebraic and convenient to use in the timelike area gauge (5.3). Equation (5.34) is not used for numerical simulations, but is useful for analysis.

It follows from (2.66)–(2.71) and (2.117) that the Weyl curvature variables are given by

$$\begin{aligned} \mathcal{E}_+ = & \frac{1}{3}\Sigma_+ + \frac{1}{6}(\Sigma_2^2 + \Sigma_3^2) - \frac{1}{3}(\Sigma_-^2 + \Sigma_\times^2) \\ & - \frac{1}{9}(\boldsymbol{\partial}_1 - r)A + \frac{2}{3}(N_\times^2 + N_-^2) + \frac{1}{4} \frac{\gamma\Omega}{G_+} (v_1^2 - \frac{1}{3}v^2) \quad (5.35) \end{aligned}$$

$$\begin{aligned} \mathcal{E}_- = & \frac{1}{3}(1 - 3\Sigma_+)\Sigma_- - \frac{1}{2\sqrt{3}}(\Sigma_3^2 - \Sigma_2^2) \\ & + \frac{1}{3}(\boldsymbol{\partial}_1 - r - 2A)N_\times + \frac{2}{3}N_+N_- + \frac{1}{2\sqrt{3}} \frac{\gamma\Omega}{G_+} (v_2^2 - v_3^2) \quad (5.36) \end{aligned}$$

$$\begin{aligned} \mathcal{E}_\times = & \frac{1}{3}(1 - 3\Sigma_+)\Sigma_\times - \frac{1}{\sqrt{3}}\Sigma_3\Sigma_2 \\ & - \frac{1}{3}(\boldsymbol{\partial}_1 - r - 2A)N_- + \frac{2}{3}N_+N_\times + \frac{1}{\sqrt{3}} \frac{\gamma\Omega}{G_+} v_2 v_3 \quad (5.37) \end{aligned}$$

$$\mathcal{E}_3 = \frac{1}{3}(1 - \sqrt{3}\Sigma_-)\Sigma_3 - \frac{1}{\sqrt{3}}\Sigma_\times\Sigma_2 - \frac{1}{2} \frac{\gamma\Omega}{G_+} v_1 v_2 \quad (5.38)$$

$$\mathcal{E}_2 = \frac{1}{3}(1 + \sqrt{3}\Sigma_-)\Sigma_2 - \frac{1}{\sqrt{3}}\Sigma_\times\Sigma_3 - \frac{1}{2} \frac{\gamma\Omega}{G_+} v_1 v_3 \quad (5.39)$$

$$\mathcal{H}_+ = -N_- \Sigma_- - N_\times \Sigma_\times \quad (5.40)$$

$$\mathcal{H}_- = -\frac{1}{3}(\boldsymbol{\theta}_1 - r - A)\Sigma_\times - \frac{2}{3}N_+ \Sigma_- - \Sigma_+ N_- \quad (5.41)$$

$$\mathcal{H}_\times = \frac{1}{3}(\boldsymbol{\theta}_1 - r - A)\Sigma_- - \frac{2}{3}N_+ \Sigma_\times - \Sigma_+ N_\times \quad (5.42)$$

$$\mathcal{H}_3 = -\frac{1}{3}(A + \sqrt{3}N_\times)\Sigma_2 - \frac{1}{\sqrt{3}}N_- \Sigma_3 + \frac{1}{2\sqrt{3}}\frac{\gamma\Omega}{G_+}v_3 \quad (5.43)$$

$$\mathcal{H}_2 = \frac{1}{3}(A - \sqrt{3}N_\times)\Sigma_3 + \frac{1}{\sqrt{3}}N_- \Sigma_2 - \frac{1}{2\sqrt{3}}\frac{\gamma\Omega}{G_+}v_2 . \quad (5.44)$$

Note that the $(\mathcal{C}_C)_2$ and $(\mathcal{C}_C)_3$ constraints have been used to simplify \mathcal{H}_2 and \mathcal{H}_3 respectively.

At this stage the β -normalized state vector is

$$(E_1^1, \Sigma_+, \Sigma_-, \Sigma_\times, \Sigma_2, \Sigma_3, N_+, N_-, N_\times, A, R, \Omega, v_1, v_2, v_3, \Omega_\Lambda). \quad (5.45)$$

The variable R is to be determined by choosing a spatial gauge, and the final form of the state vector depends on this choice, as we now describe.

The spatial gauge

We use a (t, x) -dependent rotation (see Appendix B) to rotate the spatial frame vectors $\{\mathbf{e}_A\}$ so that $\Sigma_3 = 0$. The evolution equation (5.16) and the constraint (5.22) then give

$$\Sigma_3 = 0, \quad R = -\sqrt{3}\Sigma_\times + (N_+ - \sqrt{3}N_-)v_1 . \quad (5.46)$$

This is the *shear spatial gauge* (4.64) introduced for G_2 -compatible SH cosmologies. Alternatively, we can use the Killing spatial gauge (4.63):

$$N_+ = \sqrt{3}N_-, \quad R = -\sqrt{3}\Sigma_\times . \quad (5.47)$$

Both gauges specialize to (4.65) for generic G_2 cosmologies with fewer than three tilt degrees of freedom. The motivation for using the shear spatial gauge rather than the Killing spatial gauge is the compatibility of the former with all G_2 -compatible SH cosmologies.

Using the shear spatial gauge (5.46), the final β -normalized state vector for G_2 cosmologies is

$$\mathbf{X} = (E_1^1, \Sigma_+, \Sigma_-, \Sigma_\times, \Sigma_2, N_+, N_-, N_\times, A, \Omega, v_1, v_2, v_3, \Omega_\Lambda), \quad (5.48)$$

together with the parameter γ .

Separating E_1^1 from the rest of the variables as follows,

$$\mathbf{X} = E_1^1 \oplus \mathbf{Y} , \quad (5.49)$$

where

$$\mathbf{Y} = (\Sigma_+, \Sigma_-, \Sigma_\times, \Sigma_2, N_+, N_-, N_\times, A, \Omega, v_1, v_2, v_3, \Omega_\Lambda), \quad (5.50)$$

we can write the system of evolution equations and constraints (5.8)–(5.29) in a concise symbolic form.

Evolution equations and constraints:

$$\partial_t E_1^1 = B(\mathbf{Y}) E_1^1 \quad (5.51)$$

$$\partial_t \mathbf{Y} + M(\mathbf{Y}) E_1^1 \partial_x \mathbf{Y} = g(\mathbf{Y}) \quad (5.52)$$

$$\mathcal{C}(\mathbf{Y}, E_1^1 \partial_x \mathbf{Y}) = 0 . \quad (5.53)$$

In addition we write the expression (5.19) for the spatial gradient r of the normalization factor β symbolically as

$$r = F(\mathbf{Y}). \quad (5.54)$$

Features of β -normalization and separable area gauge

The principal advantage of using β -normalized variables and the associated separable area gauge is that it leads to evolution equations that are first order in the spatial derivatives as well as the time derivatives, i.e. a first order quasi-linear system of PDEs, which is desirable for numerical simulations. In contrast, if we were to use Hubble-normalized variables and the associated separable volume gauge (see Uggla *et al.* 2003 [72]), then the evolution equations would contain second spatial derivative terms. The reason for this difference is that (5.19) gives an algebraic expression for r , whereas when using Hubble-normalized variables and the associated separable volume gauge, the expression for r contains first order spatial derivatives, which lead to second spatial derivatives since the equation for $\partial_t \Sigma_+$ contains the spatial derivative $\partial_1 r$. A minor variation of the formulation (5.49)–(5.54) is possible

due to the fact that (5.21) is linear in Σ_+ , allowing one to replace Σ_+ by

$$\Sigma_+ = \left[1 - A^2 + \frac{2}{3}\partial_1 A + A \frac{\gamma^v}{G_+} \Omega + 2A(N_\times \Sigma_- - N_- \Sigma_\times) - \Sigma_-^2 - \Sigma_\times^2 - \Sigma_2^2 - N_\times^2 - N_-^2 - \Omega - \Omega_\Lambda \right] / [2(1 - A^2)] \quad (5.55)$$

(substitute (5.19) in (5.21) and solve for Σ_+).¹ Coupled with the fact that $\partial_1 \Sigma_+$ does not appear in the evolution equations, this again leads to a first order quasi-linear system of PDEs. We shall make use of this possibility when doing numerical simulations.

5.2 Invariant subsets of the β -normalized state space

In this section, we explain the important invariant sets and equilibrium points within the G_2 state space, and the link with the SH state space.

The G_2 hierarchy

We now revisit the hierarchy of the action of the G_2 group and the tilt degrees of freedom, as shown in Figure 3.2, and give the defining conditions in terms of the state variables (5.50).

For OT G_2 cosmologies, (3.5) and (5.46) imply

$$\Sigma_2 = 0. \quad (5.56)$$

For G_2 cosmologies with one HO KVF, (3.2) and (5.46) imply

$$N_+ = N_- = 0 = \Sigma_\times. \quad (5.57)$$

For diagonal G_2 cosmologies, (5.56) and (5.57) imply

$$\Sigma_2 = 0, \quad N_+ = N_- = 0 = \Sigma_\times. \quad (5.58)$$

The hierarchy of invariant sets is summarized in Table 5.1, which lists the

¹We restrict to models with $A^2 < 1$, i.e. models with a timelike gradient vector of the G_2 area density. See van Elst *et al.* 2002 [74], equation (62).

Table 5.1: The β -normalized variables for G_2 cosmologies.

Invariant set	State vector \mathbf{Y}	Additional restriction
Generic G_2 with 3 tilt degrees of freedom:	$(\Sigma_+, \Sigma_-, \Sigma_\times, \Sigma_2, N_+, N_-, N_\times, A, \Omega, v_1, v_2, v_3)$	none
Generic G_2 with 2 tilt degrees of freedom: $v_2 = 0$	$(\Sigma_+, \Sigma_-, \Sigma_\times, \Sigma_2, N_-, N_\times, A, \Omega, v_1, v_3)$	$N_+ = \sqrt{3}N_-$
Generic G_2 with 1 tilt degree of freedom: $v_2 = v_3 = 0$	$(\Sigma_+, \Sigma_-, \Sigma_\times, \Sigma_2, N_-, N_\times, A, \Omega, v_1)$	$N_+ = \sqrt{3}N_-$
OT G_2 with 1 tilt degree of freedom: $v_2 = v_3 = 0$	$(\Sigma_+, \Sigma_-, \Sigma_\times, N_+, N_-, N_\times, A, \Omega, v_1)$	$N_+ = \sqrt{3}N_-, \Sigma_2 = 0$
One HO KVF with 2 tilt degrees of freedom: $v_2 = 0$	$(\Sigma_+, \Sigma_-, \Sigma_2, N_\times, A, \Omega, v_1, v_3)$	$(N_+, N_-, \Sigma_\times) = \mathbf{0}$
One HO KVF with 1 tilt degree of freedom: $v_2 = v_3 = 0$	$(\Sigma_+, \Sigma_-, \Sigma_2, N_\times, A, \Omega, v_1)$	$(N_+, N_-, \Sigma_\times) = \mathbf{0}$
Diagonal G_2 with 1 tilt degree of freedom: $v_2 = v_3 = 0$	$(\Sigma_+, \Sigma_-, N_\times, A, \Omega, v_1)$	$(N_+, N_-, \Sigma_\times, \Sigma_2) = \mathbf{0}$

variables and the additional restrictions. We have omitted Ω_Λ in Table 5.1 for simplicity and ease of comparison with Tables 4.1–4.4 for G_2 -compatible SH cosmologies.

SH dynamics again

To specialize to G_2 -compatible SH models (see Figures 3.3–3.5), one sets

$$\partial_x \mathbf{Y} = 0, \quad r = 0. \quad (5.59)$$

Then the separable area gauge (5.1) coincides with the G_3 -adapted gauge of SH cosmologies. The system (5.52)–(5.54) simplifies to

$$\partial_t \mathbf{Y} = g(\mathbf{Y}) \quad (5.60)$$

$$\mathcal{C}(\mathbf{Y}, 0) = 0, \quad F(\mathbf{Y}) = 0, \quad (5.61)$$

and (5.51) decouples. The system (5.60)–(5.61), given in detail by (5.8)–(5.29) subject to (5.59), describes the dynamics of G_2 -compatible SH cosmologies, but in β -normalized variables, and is fully equivalent to the Hubble-normalized system, given by (4.26)–(4.46).

The silent boundary

The evolution equations (5.8) and (5.34),

$$\partial_t E_1^1 = (q + 3\Sigma_+)E_1^1, \quad \partial_t r = (q + 3\Sigma_+)r + E_1^1 \partial_x q \quad (5.62)$$

imply that the conditions

$$E_1^1 = 0, \quad r = 0 \quad (5.63)$$

define an invariant subset of the evolution equations, which we shall call the *silent boundary*.²

It follows by setting $E_1^1 = 0$ and $r = 0$ in (5.52)–(5.54), that the SH evolution equations (5.60)–(5.61) describe the dynamics in the silent boundary, but now with

$$\partial_x \mathbf{Y} \quad \text{unrestricted (subject to (5.61))}. \quad (5.64)$$

In Section 5.3 we shall present evidence that the dynamics in the silent boundary approximates the dynamics of G_2 cosmologies in the asymptotic regimes ($t \rightarrow -\infty$ or, $\Lambda > 0$ and $t \rightarrow \infty$) in the sense that E_1^1 and r tend to zero asymptotically. An important aspect of this approximation is that equilibrium points for the SH evolution equations are also equilibrium points for the G_2 evolution equations on the silent boundary.

²van Elst *et al.* 2002 [74] define the silent boundary to be $E_1^1 = 0$, with no restrictions on r . Using this definition, Andersson *et al.* 2004 [3] relate the vacuum G_2 dynamics to the dynamics of *spatially self-similar* cosmologies (see sets (2) and (3) on page S39 of [3]). The difference here does not affect the past asymptotic dynamics, as spatially self-similar cosmologies and SH cosmologies have the same past asymptotic dynamics.

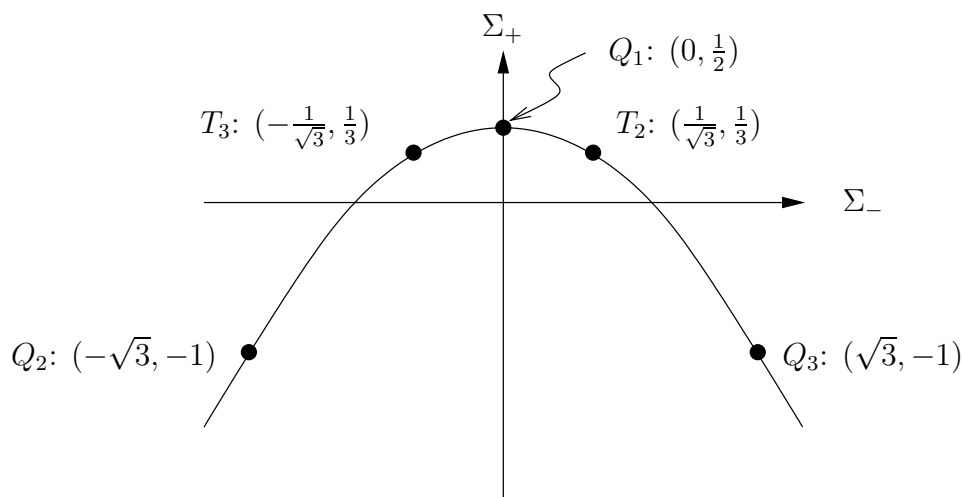


Figure 5.1: The Kasner parabola in the β -normalized state space.

The Kasner equilibrium points

On the silent boundary in the β -normalized G_2 state space, the Kasner solutions are described by a parabola of equilibrium points (see Figure 5.1), given by

$$\Omega = 0 = \Omega_\Lambda, \quad (N_+, N_-, N_\times, A, \Sigma_\times, \Sigma_2) = 0, \quad (5.65)$$

and

$$0 = 1 - 2\Sigma_+ - \Sigma_-^2. \quad (5.66)$$

The latter equation follows from (5.21). From (5.32), the deceleration parameter q is given by

$$q = -3\Sigma_+. \quad (5.67)$$

The parabola (5.66) is equivalent to the circle

$$(\Sigma_+^H)^2 + (\Sigma_-^H)^2 = 1 \quad (5.68)$$

in the Hubble-normalized state space, as follows from (5.73) below. The Taub Kasner point T_1 (where $\beta = 0$) is not represented on the parabola, because the β -normalized variables are undefined there. The corresponding

transitions and Mixmaster dynamics can be described in the β -normalized state space, but their representation in the Hubble-normalized state space is simpler geometrically.

The de Sitter equilibrium points

On the silent boundary in the β -normalized G_2 state space, the de Sitter equilibrium points are given by

$$\Omega_\Lambda = 1, \quad \Omega = 0, \quad \Sigma^2 = 0, \quad N_+ = N_- = 0 = N_\times = A \quad (5.69)$$

$$\begin{cases} v_\alpha = 0 \quad \text{or} \quad v^2 = 1 & \text{if } \gamma \neq \frac{4}{3} \\ v_\alpha = v_\alpha(x), \quad 0 \leq v^2 \leq 1 & \text{if } \gamma = \frac{4}{3}, \end{cases} \quad (5.70)$$

which are the same as (4.136)–(4.137), (4.139) and (4.142), except v_α are functions of x rather than constants. From (5.18), the deceleration parameter is given by

$$q = -1. \quad (5.71)$$

The β -normalized and the Hubble-normalized variables coincide here because $\Sigma_+ = 0$ (see equation (5.72) below).

Visualization of SH and G_2 cosmologies

In the SH state space, an SH cosmology at a fixed time is represented by a point, and its evolution in time by an orbit. A G_2 cosmology at a fixed time can be represented by an arc of points in the SH state space, parametrized by the spatial variable x . The evolution of a G_2 cosmology along one timeline is represented by an orbit in the SH state space, and the full evolution of a G_2 cosmology is represented by a moving arc of points. We shall use this representation in Chapters 6 and 9 to illustrate G_2 solutions in the SH state space.

As discussed in Section 5.1, β -normalized variables have the major advantage of leading to evolution equations that are first order in the spatial derivatives, and will thus be used for analysis and numerical simulations. On the other hand, Hubble-normalized variables are directly related to the standard observational parameters, and give a simpler representation of the Kasner solutions. We shall thus use them for displaying the state space and

most of the plotted figures in Chapter 9.

To avoid possible confusion between the notation of the Hubble-normalized variables in Section 4.2 and of the β -normalized variables here, we shall use a superscript H for Hubble-normalized variables for the rest of Part I and Part II of this thesis. Note that from (2.103),

$$\frac{H}{\beta} = 1 - \Sigma_+ = \frac{1}{1 + \Sigma_+^H}. \quad (5.72)$$

Using this relation, β -normalized variables can be converted into Hubble-normalized variables as follows:

$$\Sigma_-^H = \frac{\Sigma_-}{1 - \Sigma_+}, \quad \Omega^H = \frac{\Omega}{(1 - \Sigma_+)^2}, \quad \text{etc.} \quad (5.73)$$

In addition, the gradients of H and β , defined by (2.86)–(2.87) and (2.108), are related according to

$$q^H + 1 = \frac{q + 1}{1 - \Sigma_+} + \frac{\partial_t \Sigma_+}{(1 - \Sigma_+)^2} \quad (5.74)$$

$$r^H = \frac{r}{1 - \Sigma_+} + \frac{E_1^1 \partial_x \Sigma_+}{(1 - \Sigma_+)^2}. \quad (5.75)$$

It is important to note, however, that converting β -normalized variables to Hubble-normalized variables does not change the temporal or spatial gauge (we are still using the separable area gauge and the shear spatial gauge).

When the separable area gauge (5.1)–(5.2) and the G_3 -adapted gauge coincide,³ the time variable t for the separable area gauge is related to the time variable t^H for the G_3 -adapted gauge according to

$$t^H = (1 - \Sigma_+)t. \quad (5.76)$$

5.3 Asymptotic silence

There is considerable analytical and numerical evidence that the silent boundary plays a significant role in determining the asymptotic dynamics of G_2

³This happens for SH cosmologies, and in the silent boundary of G_2 cosmologies (see below).

cosmologies in the following sense: E_1^1 and r tend to zero along almost all timelines as $t \rightarrow -\infty$, and if there is a positive cosmological constant, as $t \rightarrow \infty$. The significance of this behaviour is that the asymptotic dynamics of G_2 cosmologies will then be approximated locally, i.e. along individual timelines, by the dynamics in the silent boundary, i.e by SH dynamics.

Past asymptotic silence

We now define past asymptotic silence as

$$\lim_{t \rightarrow -\infty} E_1^1 = 0, \quad \lim_{t \rightarrow -\infty} r = 0. \quad ^4 \quad (5.77)$$

On the basis of numerical simulations and physical considerations about the existence of particle horizons (see below), we conjecture that generic G_2 cosmologies are asymptotically silent into the past:

Conjecture 5.1 (Past asymptotic silence). *A typical G_2 cosmology is asymptotically silent into the past along almost all timelines.*

Some analytical evidence for asymptotic silence is provided by the evolution equations. In the special case of vacuum OT G_2 cosmologies with $A = 0$, the evolution equation (5.8) for E_1^1 simplifies to

$$\partial_t E_1^1 = 2E_1^1, \quad (5.78)$$

which gives

$$E_1^1 = (E_1^1)_0 e^{2t} \rightarrow 0 \quad \text{as } t \rightarrow -\infty, \quad (5.79)$$

where $(E_1^1)_0$ is a positive function of x . We note that for a timeline whose orbit is past asymptotic to the Taub Kasner point T_1 , t tends to a finite limit t_s (see Section 6.1). So E_1^1 tends to zero along orbits that are not past asymptotic to T_1 . The evolution equation (5.34) for r also simplifies to

$$\partial_t r = 2r + E_1^1 \partial_x q. \quad (5.80)$$

⁴We note that, away from the Taub Kasner point T_1 (where $\beta = 0$), Hubble-normalized and β -normalized variables only differ by a finite factor. Equation (5.77) is thus equivalent to

$$\lim_{t \rightarrow -\infty} (E_1^1)^H = 0, \quad \lim_{t \rightarrow -\infty} r^H = 0,$$

since the limits are zero.

On the invariant set $E_1^1 = 0$, this equation reduces to

$$\partial_t r = 2r, \quad (5.81)$$

and hence along orbits on the invariant set $E_1^1 = 0$, $r \rightarrow 0$ as $t \rightarrow -\infty$.

Future asymptotic silence

Similarly, we define future asymptotic silence as

$$\lim_{t \rightarrow \infty} E_1^1 = 0, \quad \lim_{t \rightarrow \infty} r = 0. \quad (5.82)$$

On the basis of numerical simulations, we expect that typical G_2 cosmologies with $\Lambda > 0$ are future asymptotic to the de Sitter solution. Evaluating (5.8) and (5.34) on the de Sitter invariant set (5.69)–(5.70), we obtain

$$\partial_t E_1^1 = -E_1^1, \quad \partial_t r = -r, \quad (5.83)$$

which imply that

$$\lim_{t \rightarrow \infty} E_1^1 = 0, \quad \lim_{t \rightarrow \infty} r = 0. \quad (5.84)$$

Thus we expect that G_2 cosmologies that are asymptotic to the de Sitter invariant set are asymptotically silent into the future.

Physical interpretation of asymptotic silence

The coordinate speed of light in the x -direction is given by

$$\frac{dx}{dt} = \pm \mathcal{N} E_1^1, \quad ^5 \quad (5.85)$$

⁵The easiest way to see this is from the metric

$$ds^2 = -N^2 dt^2 + (e_1^1)^{-2} dx^2 + \dots$$

For null geodesics in the x -direction, set $ds = 0 = dy = dz$, and we obtain

$$\frac{dx}{dt} = \pm N e_1^1 = \pm \mathcal{N} E_1^1.$$

and it depends on the choice of temporal gauge and the parametrization of the t - and x -coordinates. In using the separable area gauge (5.1)–(5.2), we have set $\mathcal{N} = 1$. We also note that the slope of the light cone in the x -direction is the inverse of the coordinate speed of light:

$$\frac{dt}{dx} = \pm \frac{1}{\mathcal{N}E_1^1} . \quad (5.86)$$

The physical speed of light has been set to unity by using geometrized units.

If there exists a particle horizon in the x -direction, then its coordinate distance (from the observer at $x = 0$) at t_0 is given by

$$x_H(t_0) = \int_{-\infty}^{t_0} E_1^1 \mathcal{N} dt. {}^6 \quad (5.87)$$

The physical distance of the horizon at t_0 from the observer is given by

$$d_H(t_0) = \int_0^{x_H(t_0)} \frac{1}{\beta(t_0, x) E_1^1(t_0, x)} dx , \quad (5.88)$$

where $x_H(t_0)$ is given by (5.87).

With $\mathcal{N} = 1$, if a particle horizon exists, then $x_H(t_0)$ is finite and (assuming a bounded derivative) E_1^1 must tend to zero as $t \rightarrow -\infty$. If we also have r tending to zero, then we have past asymptotic silence. Thus, *past asymptotic silence is interpreted as the existence of a particle horizon*.

Similarly, if there exists an event horizon in the x -direction, then its coordinate and physical distances are given by

$$x_{EH}(t_0) = \int_{t_0}^{\infty} E_1^1 \mathcal{N} dt \quad (5.89)$$

$$d_{EH}(t_0) = \int_0^{x_{EH}(t_0)} \frac{1}{\beta(t_0, x) E_1^1(t_0, x)} dx . \quad (5.90)$$

With $\mathcal{N} = 1$, if an event horizon exists, then $x_{EH}(t_0)$ is finite and (assuming a bounded derivative) E_1^1 must tend to zero as $t \rightarrow \infty$. If we also have

⁶More precisely, $x_H(t_0)$ is given by $\int_{-\infty}^{t_0} E_1^1(t, x_{\text{light}}(t)) \mathcal{N}(t, x_{\text{light}}(t)) dt$, where $x_{\text{light}}(t)$ is the path of the light that reaches the observer at t_0 . See Lim *et al.* 2004 [48] for the equations of the null geodesics.

r tending to zero, then we have future asymptotic silence. Thus, *future asymptotic silence is interpreted as the existence of an event horizon.*

The significance of the spatial average of $1/E_1^1$

At a fixed time t , consider a spatial inhomogeneity with a coordinate wavelength of $\Delta x = 2\pi$. Its physical wavelength is given by

$$L(t) = \int_0^{2\pi} \frac{1}{\beta(t, x) E_1^1(t, x)} dx . \quad (5.91)$$

Suppose that a particle horizon exists. We can make a rough approximation of the ratio of this physical wavelength to the distance to the particle horizon. By assuming that βE_1^1 does not vary dramatically with x , it follows from (5.88) and (5.91) that

$$\frac{L}{d_H} \approx \frac{2\pi}{x_H} . \quad (5.92)$$

Under a change of x -coordinate

$$\hat{x} = f(x) , \quad (5.93)$$

E_1^1 transforms as follows:

$$\hat{E}_1^1 = f'(x) E_1^1 . \quad (5.94)$$

Note that the spatial average of $\frac{1}{E_1^1}$ (on $x \in [0, 2\pi]$ for example), given by

$$\left\langle \frac{1}{E_1^1} \right\rangle = \frac{\int_0^{2\pi} \frac{1}{E_1^1} dx}{\int_0^{2\pi} dx} , \quad (5.95)$$

is preserved under (5.93) provided that

$$f(0) = 0, \quad f(2\pi) = 2\pi, \quad f'(x) > 0 \quad \text{on } x \in [0, 2\pi]. \quad (5.96)$$

This average has physical significance, as we now explain.

We choose $f(x)$ such that

$$\frac{1}{\hat{E}_1^1} = \text{const.} = \left\langle \frac{1}{E_1^1} \right\rangle . \quad (5.97)$$

Assuming that E_1^{-1} has an exponential growth rate from $t = -\infty$ up to time t (e.g. in the past asymptotic regime), (5.87) reduces to $x_H \approx E_1^{-1}$, and (5.92) reduces to

$$\frac{L}{d_H} \approx 2\pi \left\langle \frac{1}{E_1^{-1}} \right\rangle. \quad (5.98)$$

The spatial average of $\frac{1}{E_1^{-1}}$ is thus a measure of the ratio of the scale of spatial inhomogeneities and the distance to the particle horizon. The bigger E_1^{-1} is, the shorter the wavelength is relative to the horizon distance.

This understanding will be helpful in interpreting the numerical simulations in Chapter 9, in which we prescribe periodic boundary conditions by identifying $x = 2\pi$ with $x = 0$.⁷ In this situation the maximum coordinate wavelength is $\Delta x = 2\pi$.

⁷In doing so, we do not regard the universe as being spatially finite, but rather as an infinite universe with repetitive patterns. In this way, we consider the particle horizon still exists even when $x_H > 2\pi$.

Chapter 6

Explicit G_2 cosmologies

In this chapter we give two explicit G_2 solutions that can develop large spatial gradients on approach to the initial singularity. In the first solution, the asymptotic form of the (Hubble-normalized) state vector can have jump discontinuities or “steps”, while in the second solution the asymptotic form can have “spike” discontinuities. The explicit solutions allow us to analyze the development of large spatial gradients in detail.

6.1 An explicit solution with “steps”

In this section, we discuss an explicit LRS G_2 dust solution, which can develop step-like structures as it approaches the initial singularity.

The framework

We consider the class of LRS G_2 cosmologies which are defined by the condition (3.9):

$$\Sigma_2 = 0 = \Sigma_3 = \Sigma_- = \Sigma_\times = N_- = N_\times, \quad v_2 = 0 = v_3, \quad (6.1)$$

and we drop the index on v_1 . We use the timelike area gauge (5.3):

$$\dot{U} = r, \quad \mathcal{N} = 1, \quad A = 0. \quad (6.2)$$

Recall that the spatial gauge is given by (4.64), which now simplifies to

$$N_+ = 0, \quad R = 0. \quad (6.3)$$

With these restrictions the evolution equations (5.8)–(5.29) simplify dramatically. Firstly the Gauss constraint (5.21) defines Σ_+ according to

$$\Sigma_+ = \frac{1}{2}(1 - \Omega - \Omega_\Lambda), \quad (6.4)$$

and the remaining constraints are satisfied identically. Secondly, the expressions (5.18) and (5.19) for q and r become

$$q = \frac{1}{2} \left[1 + 3G_+^{-1} [(\gamma - 1)(1 - v^2) + \gamma v^2] \Omega - 3\Omega_\Lambda \right] \quad (6.5)$$

$$r = -\frac{3}{2} \frac{\gamma \Omega}{G_+} v, \quad G_\pm = 1 \pm (\gamma - 1)v^2. \quad (6.6)$$

The state vector (5.48) reduces to

$$\mathbf{X} = (E_1^1, \Omega, v, \Omega_\Lambda). \quad (6.7)$$

Using (6.1)–(6.6) the evolution equations (5.8), (5.25), (5.26) and (5.29) for these variables reduce to the following:

$$\partial_t E_1^1 = (q + 3\Sigma_+) E_1^1 \quad (6.8)$$

$$\begin{aligned} \partial_t \Omega + \frac{\gamma v}{G_+} \partial_1 \Omega + \frac{\gamma G_-}{G_+^2} \Omega \partial_1 v \\ = \frac{2\gamma}{G_+} \Omega \left[\frac{G_+}{\gamma} (q + 1) - \frac{1}{2} (1 - 3\Sigma_+) (1 + v^2) - 1 \right] \end{aligned} \quad (6.9)$$

$$\begin{aligned} \partial_t v + \frac{(\gamma - 1)}{\gamma G_-} (1 - v^2)^2 \partial_1 \ln \Omega - [(3\gamma - 4) - (\gamma - 1)(4 - \gamma)v^2] \frac{v}{G_+ G_-} \partial_1 v \\ = -\frac{(1 - v^2)}{\gamma G_-} \left[(2 - \gamma) G_+ r - \gamma v [3\gamma - 4 + 3(2 - \gamma)\Sigma_+] \right] \end{aligned} \quad (6.10)$$

$$\partial_t \Omega_\Lambda = 2(q + 1)\Omega_\Lambda. \quad (6.11)$$

An explicit solution

Consider the ansatz $v = 0$, and with $\partial_1 \Omega \neq 0$. Equation (6.6) implies $r = 0$, and then (6.10) implies $\gamma = 1$ (otherwise $\Omega = \Omega(t)$). Equation (6.5) simplifies to

$$q = \frac{1}{2}(1 - 3\Omega_\Lambda). \quad (6.12)$$

Note that $r = 0$ also implies $\beta = \beta(t)$ and $\Omega_\Lambda = \Omega_\Lambda(t)$, in accordance with equations (2.108) and (5.24). Equations (6.8)–(6.15) reduce to the following evolution equations:

$$\partial_t E_1^1 = (2 - \frac{3}{2}\Omega - 3\Omega_\Lambda)E_1^1 \quad (6.13)$$

$$\partial_t \Omega = \frac{3}{2}(1 - \Omega - 3\Omega_\Lambda)\Omega \quad (6.14)$$

$$\partial_t \Omega_\Lambda = 3(1 - \Omega_\Lambda)\Omega_\Lambda . \quad (6.15)$$

These equations can be solved explicitly, yielding

$$\Omega_\Lambda = \frac{\Lambda \ell^2}{\Lambda \ell^2 + e^{-3t}} \quad (6.16)$$

$$\Omega = \frac{e^{-3t}}{(\Lambda \ell^2 + e^{-3t}) [1 + f(x)\sqrt{\Lambda \ell^2 + e^{-3t}}]} \quad (6.17)$$

$$E_1^1 = \frac{e^{-t}}{\sqrt{\Lambda \ell^2 + e^{-3t}} [1 + f(x)\sqrt{\Lambda \ell^2 + e^{-3t}}]} \quad (6.18)$$

where ℓ is a constant with dimension [length], and $f(x)$ is an essential arbitrary function, which is required to satisfy

$$1 + f(x)\sqrt{\Lambda \ell^2} > 0. \quad (6.19)$$

This condition ensures that $\Omega > 0$ for t sufficiently large. If $f(x) > 0$, then t assumes all real values while if $f(x) < 0$, then t satisfies

$$t_s(x) < t < \infty, \quad (6.20)$$

where

$$t_s(x) = -\frac{1}{3} \ln(f(x)^{-2} - \Lambda \ell^2) . \quad (6.21)$$

An arbitrary multiplicative function of x in (6.18) has been absorbed by means of x -reparametrization. The shear is given by

$$\Sigma_+ = \frac{\frac{1}{2}f(x)e^{-3t}}{\sqrt{\Lambda \ell^2 + e^{-3t}} [1 + f(x)\sqrt{\Lambda \ell^2 + e^{-3t}}]} . \quad (6.22)$$

If $f(x) = \text{const.}$, the solution is an LRS Bianchi I dust solution with $\Lambda > 0$. In addition, if $f(x) \equiv 0$, the solution is a flat FL solution with $\Omega + \Omega_\Lambda = 1$.

Structure of the singularity

For simplicity we shall analyze the structure of the singularity using the explicit solution (6.16)–(6.18). To show that an initial singularity exists, we show that the matter density $\mu \rightarrow \infty$. Using the definition of Ω and Ω_Λ and equations (6.16)–(6.17), it follows that

$$\mu\ell^2 = \frac{e^{-3t}}{1 + f(x)\sqrt{\Lambda\ell^2 + e^{-3t}}} \rightarrow \begin{cases} \infty & \text{as } t \rightarrow t_s(x)^+, \text{ if } f(x) < 0 \\ \infty & \text{as } t \rightarrow -\infty, \text{ if } f(x) \geq 0. \end{cases} \quad (6.23)$$

In order to determine the asymptotic state of the singularity, it is helpful to calculate the Hubble-normalized shear. Equations (6.22) and (5.73) lead to

$$\Sigma_+^H = \frac{e^{-3t}f(x)}{2\sqrt{\Lambda\ell^2 + e^{-3t}} + f(x)(2\Lambda\ell^2 + e^{-3t})}. \quad (6.24)$$

It follows that

$$\Sigma_+^H \rightarrow \begin{cases} -1 \text{ as } t \rightarrow t_s(x)^+ & \text{for } f(x) < 0 \text{ (Taub Kasner)} \\ 0 \text{ as } t \rightarrow -\infty & \text{for } f(x) = 0 \text{ (flat FL)} \\ 1 \text{ as } t \rightarrow -\infty & \text{for } f(x) > 0 \text{ (LRS Kasner)}. \end{cases} \quad (6.25)$$

Crucially, if $f(x)$ has both signs, the limit of Σ_+^H at the singularity has a jump discontinuity, i.e. a “step”. Thus the solution can develop step-like structures as it approaches the initial singularity.

One can gain insight into the creation of “steps” by thinking of the LRS G_2 dust solution as an “inhomogenized” LRS Bianchi I dust solution. The Hubble-normalized state space for the LRS Bianchi I solutions is shown¹ in Figure 6.1. In terms of evolution into the past, the flat FL equilibrium point is a saddle point, and the de Sitter equilibrium point is a source. The line going from the de Sitter equilibrium point to the flat FL equilibrium point is the stable manifold of the flat FL equilibrium point. At a given time, an LRS G_2 dust solution is represented by a segment of points in the LRS Bianchi I state space. If $f(x) > 0$ for all x , then $\Sigma_+^H > 0$ and hence the segment lies to the right of the stable manifold of the FL equilibrium point, and follows the arrows to the LRS Kasner equilibrium point as $t \rightarrow -\infty$.

¹The state space follows from a routine analysis of equations (6.14)–(6.15), and then making use of (6.4).

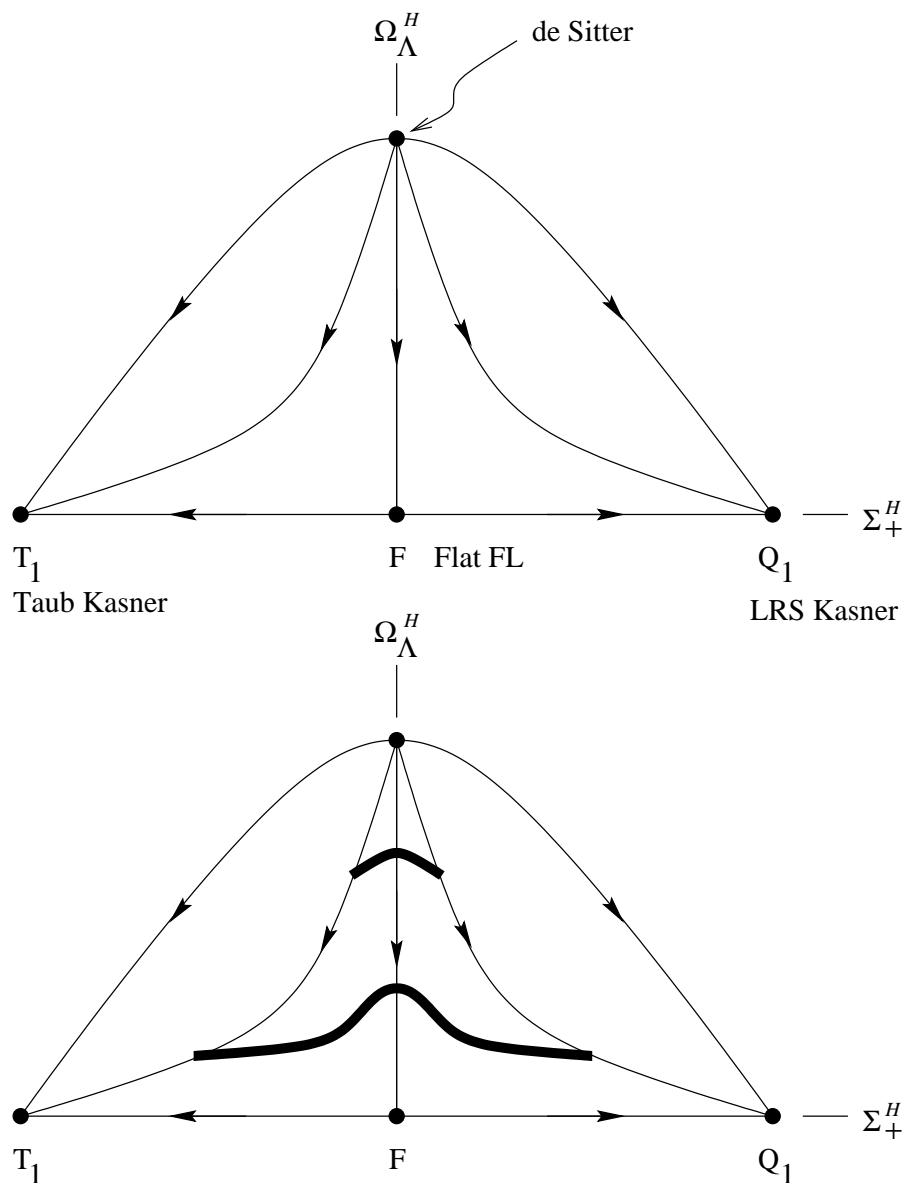


Figure 6.1: The LRS Bianchi I state space ($\Lambda > 0$), and an LRS dust solution as an “inhomogenized” solution at two different times. Arrows indicate evolution into the past.

Likewise, if $f(x) < 0$ for all x , then the segment lies to the left of the stable manifold of the FL equilibrium point, and follows the arrows to the Taub Kasner equilibrium point as $t \rightarrow t_s(x)$. Crucially, if $f(x)$ has both signs, then the segment straddles the stable manifold of the FL equilibrium point. As t tends to $t_s(x)$ or $-\infty$, the segment is stretched out more and more. The part of the segment straddling the stable manifold of the flat FL equilibrium point is being stretched the most, giving a step-like structure in the spatial profile of Σ_+^H .

This solution is a special case of the Szekeres solution (see Krasinski 1997 [44, page 25], the case $k = \beta' = 0$). It is first given explicitly by Barrow & Stein-Schabes 1984 [7, case $k = \beta' = 0$]. They however did not discuss the past asymptotic dynamics. A special case of this solution, with $\Lambda = 0$, is first given explicitly by Bonnor & Tomimura 1976 [12, Model PI with $\mu \neq 0$, $\beta = 0$]. They discussed the past asymptotic dynamics, but overlooked the possibility that models can be past asymptotic to the Taub Kasner point.

6.2 An explicit solution with “spikes”

In this section, we obtain a new explicit vacuum OT G_2 solution that develops “spikes” as $t \rightarrow -\infty$. Spikes are narrow spatial structures with steep slopes appearing on an otherwise mild profile of a variable of a cosmological solution (see Berger & Moncrief 1993 [11]). To generate this spiky solution, we apply a transformation introduced by Rendall & Weaver 2001 [62] to the Wainwright-Marshman solution (see Wainwright & Marshman 1979 [79], Case I with $m = -\frac{3}{16}$).

The framework

We consider the class of vacuum OT G_2 cosmologies which are defined by the conditions

$$\Omega = 0, \quad v_\alpha = 0, \quad \Omega_\Lambda = 0, \quad \Sigma_2 = 0 \quad (6.26)$$

(see (5.56) for the OT condition). We use the timelike area gauge (5.3):

$$\dot{U} = r, \quad \mathcal{N} = 1, \quad A = 0. \quad (6.27)$$

Recall that the spatial gauge is (4.64):

$$N_+ = \sqrt{3}N_-, \quad R = -\sqrt{3}\Sigma_\times. \quad (6.28)$$

With these restrictions the evolution equations (5.8)–(5.29) simplify dramatically. Firstly the Gauss constraint (5.21) defines Σ_+ according to

$$\Sigma_+ = \frac{1}{2}(1 - \Sigma_-^2 - \Sigma_\times^2 - N_-^2 - N_\times^2), \quad (6.29)$$

and the remaining constraints are satisfied identically. Secondly, the expressions (5.18) and (5.19) for q and r become

$$q = 2 - 3\Sigma_+ \quad (6.30)$$

$$r = -3(N_\times\Sigma_- - N_-\Sigma_\times). \quad (6.31)$$

The state vector (5.48) reduces to

$$\mathbf{X} = (E_1^1, \Sigma_-, \Sigma_\times, N_-, N_\times). \quad (6.32)$$

Using (6.26)–(6.31) the evolution equations (5.8), (5.12)–(5.15) for these variables reduce to the following equations:

$$\partial_t E_1^1 = 2E_1^1 \quad (6.33)$$

$$\partial_t \Sigma_- + E_1^1 \partial_x N_\times = 2\sqrt{3}(\Sigma_\times^2 - N_-^2) \quad (6.34)$$

$$\partial_t N_\times + E_1^1 \partial_x \Sigma_- = 2N_\times \quad (6.35)$$

$$\partial_t \Sigma_\times - E_1^1 \partial_x N_- = -2\sqrt{3}(N_- N_\times + \Sigma_- \Sigma_\times) \quad (6.36)$$

$$\partial_t N_- - E_1^1 \partial_x \Sigma_\times = 2N_- + 2\sqrt{3}(\Sigma_- N_- + N_\times \Sigma_\times). \quad (6.37)$$

Equation (6.33) can be solved explicitly to give

$$E_1^1 = e^{g(x)} e^{2t}, \quad (6.38)$$

and we reparametrize x to set $g(x) = 0$ for simplicity. Since $E_1^1 \rightarrow 0$ as $t \rightarrow -\infty$, the solutions are asymptotically silent (see Section 5.2). The metric in this temporal and spatial gauge can be written in this form (see,

e.g. van Elst *et al.* 2002 [74, Appendix A.3]):

$$ds^2 = \beta^{-2}[-dt^2 + (E_1^{-1})^{-2}dx^2] + \ell_0^2 e^{2t} [e^{P(t,x)}(dy + Q(t,x)dz)^2 + e^{-P(t,x)}dz^2] , \quad (6.39)$$

where the variables $(\Sigma_-, N_\times, \Sigma_\times, N_-)$ are defined in terms of P and Q (see van Elst *et al.* 2002 [74, equations (180) and (181)], which are derived from the constraint (2.81)):

$$(\Sigma_-, N_\times) = \frac{1}{2\sqrt{3}}(\partial_t, -E_1^{-1}\partial_x)P, \quad (\Sigma_\times, N_-) = \frac{1}{2\sqrt{3}}e^P(\partial_t, E_1^{-1}\partial_x)Q. \quad (6.40)$$

The transformation method

Rendall & Weaver 2001 [62] introduce a two-step solution-generating method.

The first step of the method is to perform the following transformation on the metric functions P and Q :²

$$e^{\hat{P}} = e^{-P}[(Qe^P)^2 + 1] \quad (6.41)$$

$$\hat{Q} = -\frac{Qe^{2P}}{(Qe^P)^2 + 1}. \quad (6.42)$$

The second step is to perform the so-called Gowdy-to-Ernst transformation. Rendall & Weaver 2001 [62]) define this transformation in terms of its effect on P and Q :

$$\hat{P} = -P - 2t \quad (6.43)$$

$$\hat{Q}_t = e^{2(P+2t)}Q_x \quad (6.44)$$

$$\hat{Q}_x = e^{2P}Q_t, \quad (6.45)$$

which generates a new solution,³ although in general \hat{Q} cannot be obtained explicitly.

We now describe the transformations in the framework of the orthonormal frame formalism. First, we show that the transformation (6.41)–(6.42) is a rotation of the frame vectors $\{\mathbf{e}_2, \mathbf{e}_3\}$, and describe it in terms of β -

²We have changed the sign of (6.42) from equation (4) of [62].

³This is the same transformation as equation (7) of Rendall & Weaver 2001 [62], but looks slightly different because the time variable τ in [62] is related to our time variable t via $\tau = -2t$.

normalized variables.

Consider a rotation of the frame vectors $\{\mathbf{e}_2, \mathbf{e}_3\}$ (see Appendix B),

$$\begin{pmatrix} \hat{\mathbf{e}}_2 \\ \hat{\mathbf{e}}_3 \end{pmatrix} = \begin{pmatrix} \cos \phi & \sin \phi \\ -\sin \phi & \cos \phi \end{pmatrix} \begin{pmatrix} \mathbf{e}_2 \\ \mathbf{e}_3 \end{pmatrix}. \quad (6.46)$$

To preserve the spatial gauge condition (6.28), it follows from (B.2)–(B.7) that the angle ϕ must satisfy

$$\partial_t \phi = \sqrt{3}(-\sin 2\phi \Sigma_- + \cos 2\phi \Sigma_\times) - \sqrt{3}\Sigma_\times \quad (6.47)$$

$$E_1^{-1} \partial_x \phi = \sqrt{3}(\cos 2\phi N_- + \sin 2\phi N_\times) - \sqrt{3}N_- . \quad (6.48)$$

It turns out that these equations are satisfied if the rotation angle ϕ is related to P and Q according to

$$\cos 2\phi = \frac{(Qe^P)^2 - 1}{(Qe^P)^2 + 1}, \quad \sin 2\phi = \frac{2Qe^P}{(Qe^P)^2 + 1}, \quad (6.49)$$

as follows from differentiating (6.49) and using (6.40). The transformation (B.6)–(B.7), with ϕ given by (6.49), is in fact equivalent to performing the transformation (6.41)–(6.42). This statement can be verified by differentiating (6.41)–(6.42) and expressing them in terms of $(\Sigma_-, N_\times, \Sigma_\times, N_-)$ using (6.40), then comparing with (B.6)–(B.7) to obtain (6.49).

The Gowdy-to-Ernst transformation (6.43)–(6.45) is much simpler in terms of $(\Sigma_-, N_\times, \Sigma_\times, N_-)$, as follows from (6.40):

$$\hat{\Sigma}_- = -\Sigma_- - \frac{1}{\sqrt{3}} \quad (6.50)$$

$$\hat{N}_\times = -N_\times \quad (6.51)$$

$$\hat{\Sigma}_\times = N_- \quad (6.52)$$

$$\hat{N}_- = \Sigma_\times . \quad (6.53)$$

It is easily verified that this transformation preserves the form of the evolution equations (6.34)–(6.37).

Composing the transformations (B.6)–(B.7) with (6.49) and (6.50)–(6.53)

leads to

$$\tilde{\Sigma}_- = -(\cos 2\phi \Sigma_- + \sin 2\phi \Sigma_\times) - \frac{1}{\sqrt{3}} \quad (6.54)$$

$$\tilde{N}_\times = \sin 2\phi N_- - \cos 2\phi N_\times \quad (6.55)$$

$$\tilde{\Sigma}_\times = \cos 2\phi N_- + \sin 2\phi N_\times \quad (6.56)$$

$$\tilde{N}_- = -\sin 2\phi \Sigma_- + \cos 2\phi \Sigma_\times \quad (6.57)$$

where ϕ is given by (6.49).

In summary, *given a solution $(\Sigma_-, N_\times, \Sigma_\times, N_-)$ of (6.34)–(6.37), the metric functions P and Q are determined by (6.40). Then (6.54)–(6.57), with ϕ determined by P and Q according to (6.49), determines a new solution.*

The Wainwright-Marshman solution

Consider the ansatz

$$\Sigma_\times + N_- = 0 \quad (N_- \neq 0). \quad (6.58)$$

It follows from (6.36)–(6.37) that $\Sigma_- = N_\times - \frac{1}{2\sqrt{3}}$. Then (6.34)–(6.35) imply $N_\times = 0$. Solving (6.36) then gives $\Sigma_\times = \frac{1}{\sqrt{3}}e^t f'(e^{2t} - 2x)$, where $f : \mathbb{R} \rightarrow \mathbb{R}$ is freely specifiable, and $e^{2t} - 2x$ is the argument of the function f' . To recapitulate, we have

$$\Sigma_- = -\frac{1}{2\sqrt{3}}, \quad N_\times = 0, \quad \Sigma_\times = -N_- = \frac{1}{\sqrt{3}}e^t f'(e^{2t} - 2x). \quad (6.59)$$

We can now obtain P and Q via (6.40):

$$P = -t, \quad Q = f(e^{2t} - 2x). \quad (6.60)$$

This is the Wainwright-Marshman (WM) solution (see Wainwright & Marshman 1979 [79], Case I with $m = -\frac{3}{16}$).⁴

⁴The Gowdy-to-Ernst transformation leaves the WM solution essentially invariant – it changes only the sign of f .

The transformed Wainwright-Marshman solution

We apply the transformation (6.54)–(6.57) to the WM solution and obtain a new explicit solution of the evolution equations (6.33)–(6.37):

$$\tilde{\Sigma}_- = -\left(-\frac{1}{2\sqrt{3}} \cos 2\phi + \frac{1}{\sqrt{3}} \sin 2\phi e^t f'\right) - \frac{1}{\sqrt{3}} \quad (6.61)$$

$$\tilde{N}_\times = -\frac{1}{\sqrt{3}} \sin 2\phi e^t f' \quad (6.62)$$

$$\tilde{\Sigma}_\times = -\frac{1}{\sqrt{3}} \cos 2\phi e^t f' \quad (6.63)$$

$$\tilde{N}_- = \frac{1}{2\sqrt{3}} \sin 2\phi + \frac{1}{\sqrt{3}} \cos 2\phi e^t f' \quad (6.64)$$

where

$$\cos 2\phi = \frac{(fe^{-t})^2 - 1}{(fe^{-t})^2 + 1}, \quad \sin 2\phi = \frac{2fe^{-t}}{(fe^{-t})^2 + 1}, \quad f = f(e^{2t} - 2x). \quad (6.65)$$

Structure of the singularity

What solution(s) does the transformed WM solution tend to as $t \rightarrow -\infty$? From (6.65), we see that for a fixed x ,

$$\lim_{t \rightarrow -\infty} \cos 2\phi = \begin{cases} -1 & \text{if } f(-2x) = 0 \\ 1 & \text{if } f(-2x) \neq 0, \end{cases} \quad (6.66)$$

and $\sin 2\phi \rightarrow 0$ only pointwise because

$$\sin 2\phi = \pm 1 \quad \text{whenever} \quad f(e^{2t} - 2x)e^{-t} = \pm 1. \quad (6.67)$$

Then from (6.61)–(6.65), we obtain (assuming that $f(e^{2t} - 2x)$ is smooth):

$$\lim_{t \rightarrow -\infty} (\tilde{\Sigma}_-, \tilde{N}_\times, \tilde{\Sigma}_\times, \tilde{N}_-) = \begin{cases} (-\frac{\sqrt{3}}{2}, 0, 0, 0) & \text{for } f(-2x) = 0 \\ (-\frac{1}{2\sqrt{3}}, 0, 0, 0) & \text{for } f(-2x) \neq 0. \end{cases} \quad (6.68)$$

In terms of Hubble-normalized variables, we obtain

$$\lim_{t \rightarrow -\infty} (\tilde{\Sigma}_+^H, \tilde{\Sigma}_-^H) = \begin{cases} (\frac{1}{7}, -\frac{4\sqrt{3}}{7}) & \text{for } f(-2x) = 0 \\ (\frac{11}{13}, -\frac{4\sqrt{3}}{13}) & \text{for } f(-2x) \neq 0. \end{cases} \quad (6.69)$$

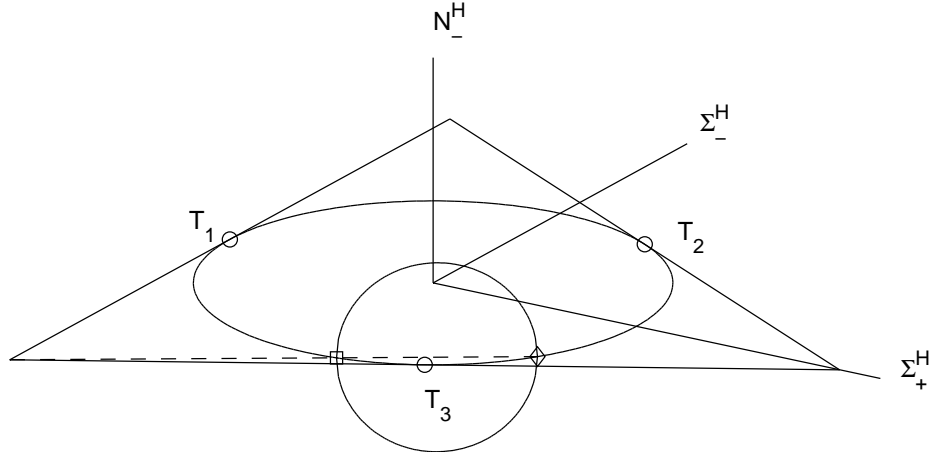


Figure 6.2: The two N_-^H transition orbits shadowed by the transformed WM solution. $(\Sigma_+^H, \Sigma_-^H) = (\frac{1}{7}, -\frac{4\sqrt{3}}{7})$ is marked by a square, and $(\Sigma_+^H, \Sigma_-^H) = (\frac{11}{13}, -\frac{4\sqrt{3}}{13})$ is marked by a diamond.

i.e. the transformed WM solution tends pointwise to two distinct Kasner solutions if f has both signs. These two Kasner solutions are shown in the SH state space in Figure 6.2, and are in fact connected by two N_-^H transition orbits. Recall that it follows from (4.21) that the two N_-^H transition orbits lie on the sphere

$$1 = (N_-^H)^2 + (\Sigma_+^H)^2 + (\Sigma_-^H)^2, \quad (6.70)$$

going from $(\tilde{\Sigma}_+^H, \tilde{\Sigma}_-^H) = (\frac{1}{7}, -\frac{4\sqrt{3}}{7})$ to $(\tilde{\Sigma}_+^H, \tilde{\Sigma}_-^H) = (\frac{11}{13}, -\frac{4\sqrt{3}}{13})$ as $t \rightarrow -\infty$. We can think of the transformed WM solution as represented by a segment of points in the SH state space in Figure 6.2. If f has both signs, then this segment gets stretched along the two N_-^H transition orbits as $t \rightarrow -\infty$, thus creating spiky structures in the variables.

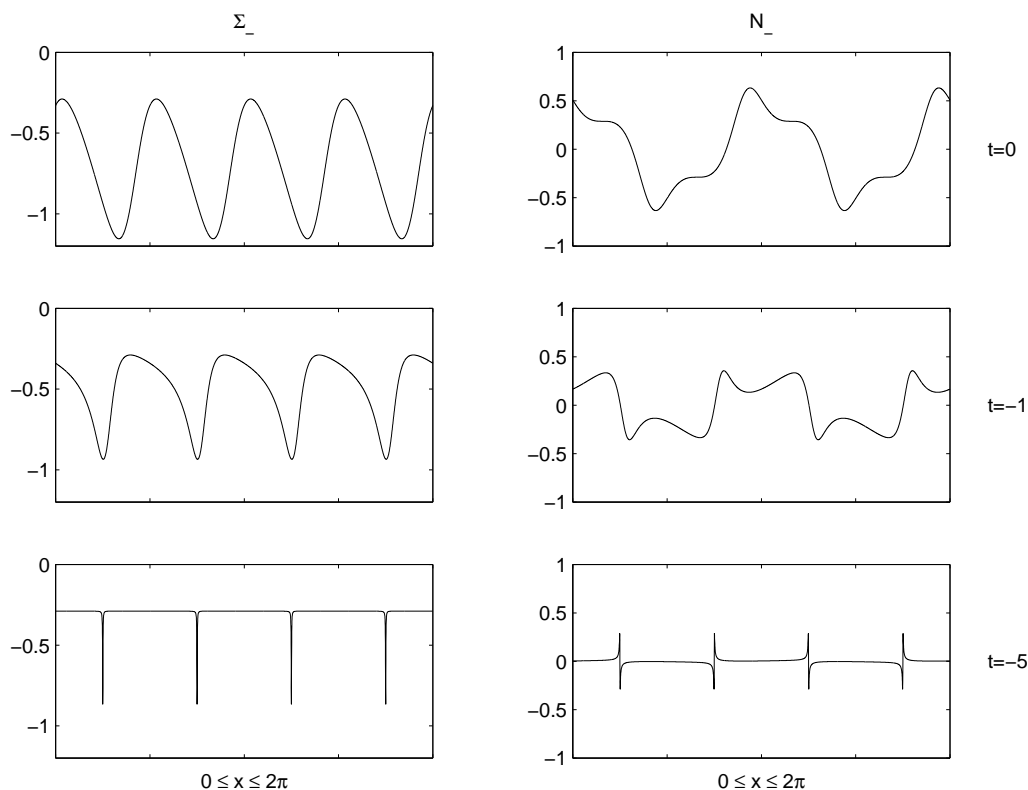


Figure 6.3: Snapshots of the variables $\tilde{\Sigma}_-$ and \tilde{N}_- for $f(\bullet) = \cos(\bullet)$.

To see this clearly, consider the example $f(e^{2t} - 2x) = \cos(e^{2t} - 2x)$. Figure 6.3 shows the snapshots of $\tilde{\Sigma}_-$ and \tilde{N}_- at $t = 0, -1, -5$. The variable $\tilde{\Sigma}_-$ tends to $-\frac{\sqrt{3}}{2}$ for $x = \frac{\pi}{4}, \frac{3\pi}{4}, \frac{5\pi}{4}, \frac{7\pi}{4}$, and $-\frac{1}{2\sqrt{3}}$ otherwise. The variable \tilde{N}_- tends to zero pointwise, but not uniformly. The height of the spikes in \tilde{N}_- is $\frac{1}{2\sqrt{3}}$. We note that spikes also form in \tilde{N}_x and $\tilde{\Sigma}_x$, but these variables still tend to zero uniformly.

In Section 8.3 we shall use both the WM solution and the transformed WM solution to test the accuracy of three numerical schemes. The transformed WM solution also provides a simple way to analyze the nature of spikes. We shall return to this in Section 7.2.

6.3 Spiky and step-like structures

Spikes and step-like structures are governed by the same mechanism. They have one thing in common – they form because the solution shadows two disjoint branches of the unstable manifold (of an unstable equilibrium point). The meaning of a “trigger”, introduced in Section 4.1, can be extended to include the variable whose axis is parallel to the directions of the branches above. In the language of triggers, consider a trigger of an unstable equilibrium point. It assumes a certain value (we call it an “inactive value”) at the unstable equilibrium point. Now consider a G_2 solution in which the trigger of an unstable equilibrium point straddles its inactive value, e.g. the LRS dust solution in which Σ_+^H straddles its inactive value of zero, and the transformed WM solution in which \tilde{N}_- straddles its inactive value of zero. Then the trigger activates on both sides of the inactive value, but by continuity there exists some point $x_{\text{intercept}}$ in the middle where it cannot activate. Over time, a steep slope forms at $x_{\text{intercept}}$. How the profile of the trigger extends further is determined by the unstable manifolds of the saddle point, whose orbits may lead directly to the sinks or indirectly through a sequence of saddle points. If these orbits are such that the trigger develops a monotone profile, then we see a step-like structure. Otherwise the profile resembles a non-monotone, spiky structure. Figure 6.4 illustrates the initial smooth profile and the asymptotic formation of a steep slope at $x_{\text{intercept}}$, and either a step-like structure or a generic spiky structure.

We end this chapter with the following conjecture on what causes the formation of spiky or step-like structures.

Conjecture 6.1. *Consider a class of G_2 cosmologies and their invariant subset of SH cosmologies. In an asymptotically silent regime, the G_2 cosmologies locally approach the attractor of their SH subset. Step-like or spiky structures will form if a G_2 solution, represented by a segment of points in the SH state space, straddles the stable manifold of a saddle point.*

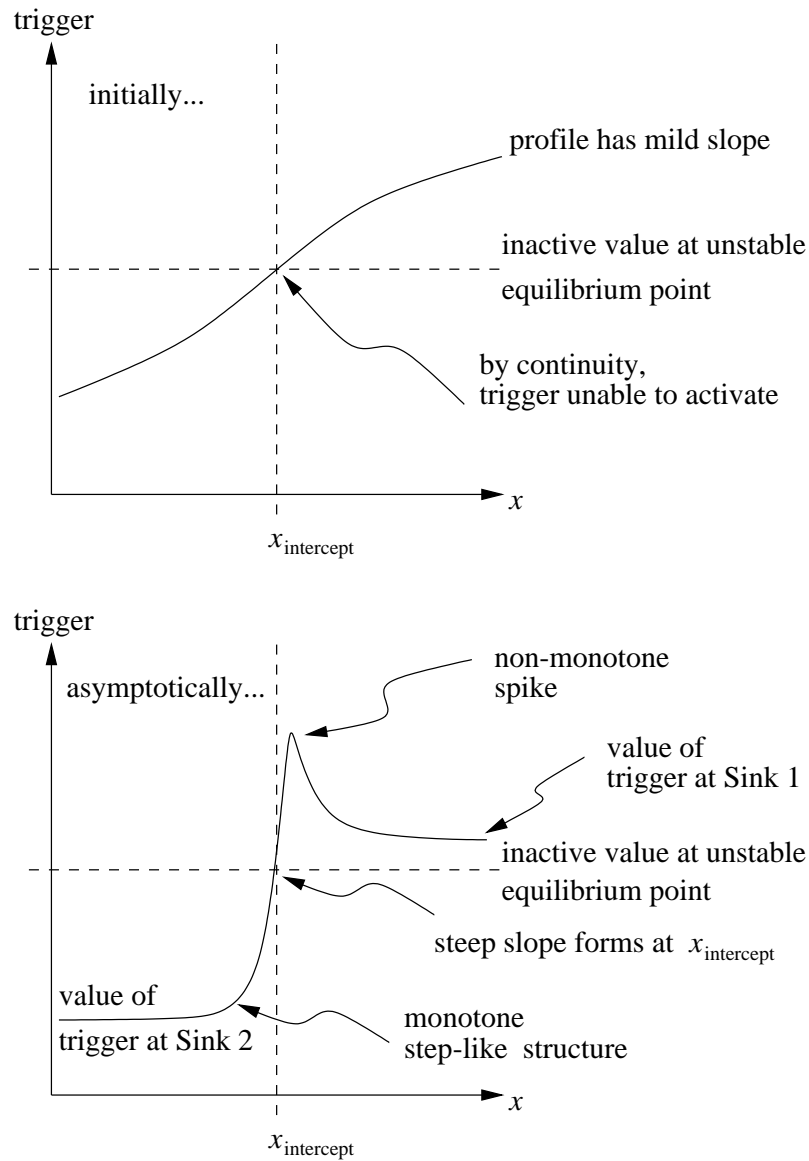


Figure 6.4: Formation of spiky and step-like structures.

Chapter 7

Dynamics in the past asymptotic regime

In this chapter, we make predictions about the dynamics in the past asymptotic regime of G_2 cosmologies, based on a heuristic analysis of the equations. Recall that we wrote the system (5.8)–(5.29) symbolically as (5.51)–(5.54):

$$\partial_t E_1^1 = B(\mathbf{Y})E_1^1 \quad (7.1)$$

$$\partial_t \mathbf{Y} + M(\mathbf{Y})E_1^1 \partial_x \mathbf{Y} = g(\mathbf{Y}) \quad (7.2)$$

$$\mathcal{C}(\mathbf{Y}, E_1^1 \partial_x \mathbf{Y}) = 0, \quad r = F(\mathbf{Y}), \quad (7.3)$$

where \mathbf{Y} is the state vector in (5.48). In analyzing the dynamics, we shall consider three types of behaviour:

- the background dynamics,
- the effects of saddle points, and
- the effects of spatial derivative terms.

The background dynamics is governed by the SH system (5.60)–(5.61):

$$\partial_t \mathbf{Y} = g(\mathbf{Y}) \quad (7.4)$$

$$\mathcal{C}(\mathbf{Y}, 0) = 0, \quad F(\mathbf{Y}) = 0, \quad (7.5)$$

which we regard as governing the dynamics in the silent boundary (5.63):

$$E_1^1 = 0, \quad r = 0. \quad (7.6)$$

We shall show that the saddle points of the SH system can combine with inhomogeneity to initiate some interesting effects in this system. Furthermore, under the right conditions, the term $M(\mathbf{Y})E_1^{-1}\partial_x\mathbf{Y}$ becomes active and the system (7.2) exhibits some fascinating behaviour. We explain each type of dynamical behaviour in the sections below, and present numerical simulations that illustrate the behaviour in Chapter 9.

7.1 Background dynamics: role of algebraic terms

In Section 5.3, we conjectured that a typical G_2 cosmology is asymptotically silent into the past, suggesting that SH dynamics plays a major role in the past asymptotic dynamics of G_2 cosmologies. The separable area gauge for G_2 cosmologies also coincides with the G_2 adapted gauge for SH cosmologies as $t \rightarrow -\infty$, since asymptotic silence entails $r \rightarrow 0$.

Mixmaster dynamics

With asymptotic silence, it is plausible that G_2 cosmologies, like SH cosmologies, also satisfy the BKL conjecture I and the Kasner Attractivity Conjecture, which will now refer to tilted Kasner circles $\mathcal{K}_{\pm\alpha}$ as well as the standard Kasner circle \mathcal{K} .

BKL conjecture I

Along almost all local orbits of a typical G_2 cosmology,

$$\lim_{t \rightarrow -\infty} \Omega = 0, \quad \lim_{t \rightarrow -\infty} \Omega_\Lambda = 0. \quad (7.7)$$

Kasner Attractivity Conjecture

Almost all local orbits of a typical G_2 cosmology enter a neighbourhood of one of the Kasner circles.

We emphasize that at this time there has been no progress in proving these conjectures for G_2 cosmologies. They are, however, strongly supported by our numerical simulations. We believe that they are fundamentally important as regards the dynamics in the past asymptotic regime.

Once the G_2 orbits enter a neighbourhood of one of the Kasner circles, Mixmaster dynamics takes over along each individual orbit, in accordance with SH dynamics. Proposition 4.1 concerning the occurrence of Mixmaster dynamics in G_2 -compatible SH cosmologies now leads directly to the following proposition.

Proposition 7.1. *Consider G_2 cosmologies that satisfy the Kasner Attractivity Conjecture.*

- i) If the G_2 is generic, Mixmaster dynamics occurs along typical timelines.¹*
- ii) If the G_2 is non-generic, Mixmaster dynamics does not occur.*

For generic G_2 cosmologies, the background dynamics is that of SH cosmologies of Bianchi type VI and VII.

To recapitulate, the limits (4.125)–(4.127) for G_2 -compatible SH cosmologies should also hold locally (i.e. along typical timelines) for G_2 cosmologies:

$$\text{Stable variables:} \quad \lim_{t \rightarrow -\infty} (A, N_\times) = 0, \quad (7.8)$$

$$\text{Non-overlapping triggers:} \quad \lim_{t \rightarrow -\infty} (N_{22}N_{33}, N_{22}\Sigma_\times, N_{33}\Sigma_2) = 0, \quad (7.9)$$

$$\text{Trigger variables:} \quad \lim_{t \rightarrow -\infty} (N_-, \Sigma_2, \Sigma_\times) \quad \text{do not exist.} \quad (7.10)$$

Again we emphasize that no progress has been made in proving Proposition 7.1 and the limits (7.8)–(7.10). The limits (7.7), (7.8) and (7.9), which assert that almost all local G_2 orbits shadow the unstable manifolds of the Kasner equilibrium points, provide the foundation of Mixmaster dynamics in G_2 cosmologies.

Non-Mixmaster dynamics

For more special G_2 actions, there are too few triggers to sustain Mixmaster dynamics as some of the arcs on the Kasner circle become sinks (into the past) in the smaller state space.

¹We note that in contrast to the case of SH cosmologies, $N_{\alpha\beta} = 0$ is not an invariant set in G_2 cosmologies, due to the presence of the terms $\partial_1 \Sigma_-$ and $\partial_1 \Sigma_\times$ in the $\partial_t N_\times$ and $\partial_t N_-$ equations.

For OT G_2 cosmologies, the background dynamics is that of OT SH cosmologies of type VI and VII. Thus we expect the local past attractor to be given by (4.128):

$$\mathcal{A}^- = \mathcal{K} \operatorname{arc}(T_3 Q_1). \quad (7.11)$$

By the phrase “local past attractor” we mean that almost all local orbits of a typical OT G_2 cosmology are past asymptotic to the arc (7.11). As an example, the transformed WM solution tends to two distinct Kasner solutions, as given by (6.69). The local orbit of a spike point tends to the Kasner solution $(\Sigma_+^H, \Sigma_-^H) = (\frac{1}{7}, -\frac{4\sqrt{3}}{7})$, which does not lie on $\mathcal{K} \operatorname{arc}(T_3 Q_1)$, but other local orbits tend to the Kasner solution $(\Sigma_+^H, \Sigma_-^H) = (\frac{11}{13}, -\frac{4\sqrt{3}}{13})$, which lies on $\mathcal{K} \operatorname{arc}(T_3 Q_1)$.

For G_2 cosmologies with one HO KVF, the background dynamics is that of SH cosmologies of type VI with one HO KVF. We expect the local past attractor to be given by (4.130):

$$\begin{aligned} \mathcal{A}^- = & \left[\mathcal{K} \operatorname{arc}(\Sigma_+^H > -\frac{1}{2}(3\gamma - 4)) \cap \mathcal{K} \operatorname{arc}(Q_2 T_1 Q_3 T_2) \right] \\ & \cup \left[\mathcal{K}_{\pm 1} \operatorname{arc}(\Sigma_+^H < -\frac{1}{2}(3\gamma - 4)) \cap \mathcal{K}_{\pm 1} \operatorname{arc}(Q_2 T_1 Q_3 T_2) \right]. \end{aligned} \quad (7.12)$$

For diagonal G_2 cosmologies, the background dynamics is that of diagonal SH cosmologies of type VI. Thus we expect the local past attractor to be given by (4.131):

$$\mathcal{A}^- = \mathcal{K} \operatorname{arc}(\Sigma_+^H > -\frac{1}{2}(3\gamma - 4)) \cup \mathcal{K}_{\pm 1} \operatorname{arc}(\Sigma_+^H < -\frac{1}{2}(3\gamma - 4)). \quad (7.13)$$

Isenberg & Moncrief 1990 [41] proved that \mathcal{K} contains the past attractor for vacuum diagonal G_2 cosmologies. Anguige 2000 [5] gave the asymptotic expansions for a generic class of perfect fluid diagonal G_2 cosmologies that are past asymptotic to $\mathcal{K} \operatorname{arc}(\Sigma_+^H > -\frac{1}{2}(3\gamma - 4))$.

7.2 Effects of spatial inhomogeneity I: role of saddles

Recall that the state of a G_2 solution at a fixed time is represented by an arc of points in the SH state space. We have seen in Chapter 6 that if this arc straddles the stable manifold of a saddle point then the solution will develop steep spatial gradients. In the language of triggers, if a trigger variable

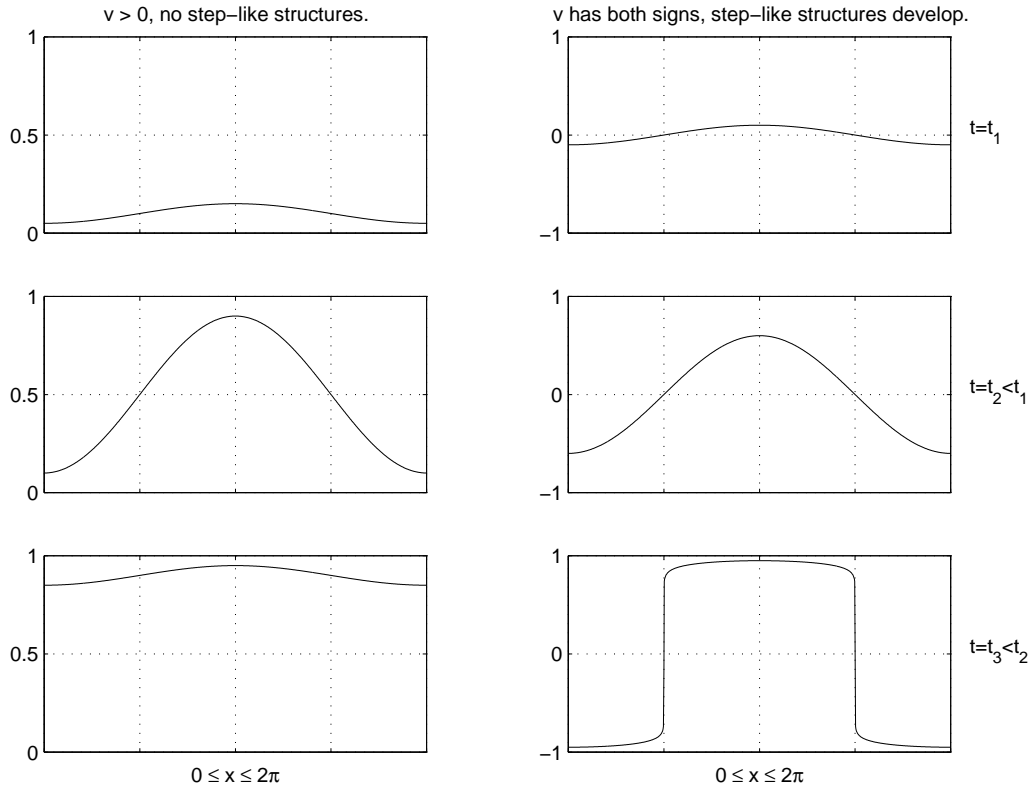


Figure 7.1: The tilt variable v can develop step-like structures into the past.

has both signs, then when the trigger activates, steep spatial gradients will develop in the neighbourhood of the point where the trigger variable is zero.

In this section we discuss the steep spatial gradients in more detail, with a view to confirming the validity of BKL conjecture II. We shall see that a mild initial inhomogeneity plus a zero in a trigger variable can lead to a strong asymptotic inhomogeneity, via local SH dynamics.

Step-like structures

The tilt variable v assumes a value close to 0 or ± 1 when it is inactive, and undergoes transitions between 0 and ± 1 when it activates. If v has both signs on an arc of the Kasner circle \mathcal{K} when it activates, it develops step-like

structures, as illustrated schematically in Figure 7.1. This is not unlike the step-like structures in the LRS dust solution in Section 6.1, since the tilt transition will change $v = \epsilon > 0$ to $v = 1 - \epsilon$, and $v = -\epsilon < 0$ to $v = -1 + \epsilon$, where $0 < \epsilon \ll 1$.

Spiky structures

The curvature trigger N_- and the frame triggers Σ_\times and Σ_2 assume a value close to zero when they are inactive, and become of order unity when they activate. If such a trigger has both signs on a Kasner arc when it activates, it develops spikes, as illustrated schematically in Figure 7.2. The spikes shown in Figure 6.3 for the transformed WM solution are a simple prototype.

In the case of the transformed WM solution (6.61)–(6.65), the spikes are *permanent* – their amplitude does not tend to zero as $t \rightarrow -\infty$. The spikes in the transformed WM solution form in a neighbourhood of isolated points where $f(e^{2t} - 2x) = 0$, called “spike points”, defined by

$$f(e^{2t} - 2x_{\text{spike}}(t)) = 0. \quad (7.14)$$

Since t appears in the argument of f , a spike point depends on t and moves toward a limiting spike point $x_{\text{spike}}(-\infty)$ as $t \rightarrow -\infty$:

$$x_{\text{spike}}(t) = x_{\text{spike}}(-\infty) + \frac{1}{2}e^{2t}. \quad (7.15)$$

Despite the fact that $E_1^1 \rightarrow 0$ exponentially fast, the steep slopes of the spikes ensure that $M(\mathbf{Y})E_1^1\partial_x\mathbf{Y}$ in (7.2) is comparable to $g(\mathbf{Y})$ in size, as shown by the asymptotic expansion of the transformed WM solution below.

The decay rates as $t \rightarrow -\infty$ along the timeline $x = x_{\text{spike}}(-\infty)$ are as follows (dropping tildes in (6.61)–(6.64)):

$$\Sigma_- = -\frac{\sqrt{3}}{2} + \mathcal{O}(e^{2t}) \quad (7.16)$$

$$N_\times = -\frac{2\sqrt{3}}{3}f_1^2 e^{2t} + \mathcal{O}(e^{4t}) \quad (7.17)$$

$$\Sigma_\times = \frac{\sqrt{3}}{3}f_1 e^t + \mathcal{O}(e^{3t}) \quad (7.18)$$

$$N_- = \frac{\sqrt{3}}{3}(f_1^3 - \frac{1}{2}f_2) e^{3t} + \mathcal{O}(e^{5t}) \quad (7.19)$$

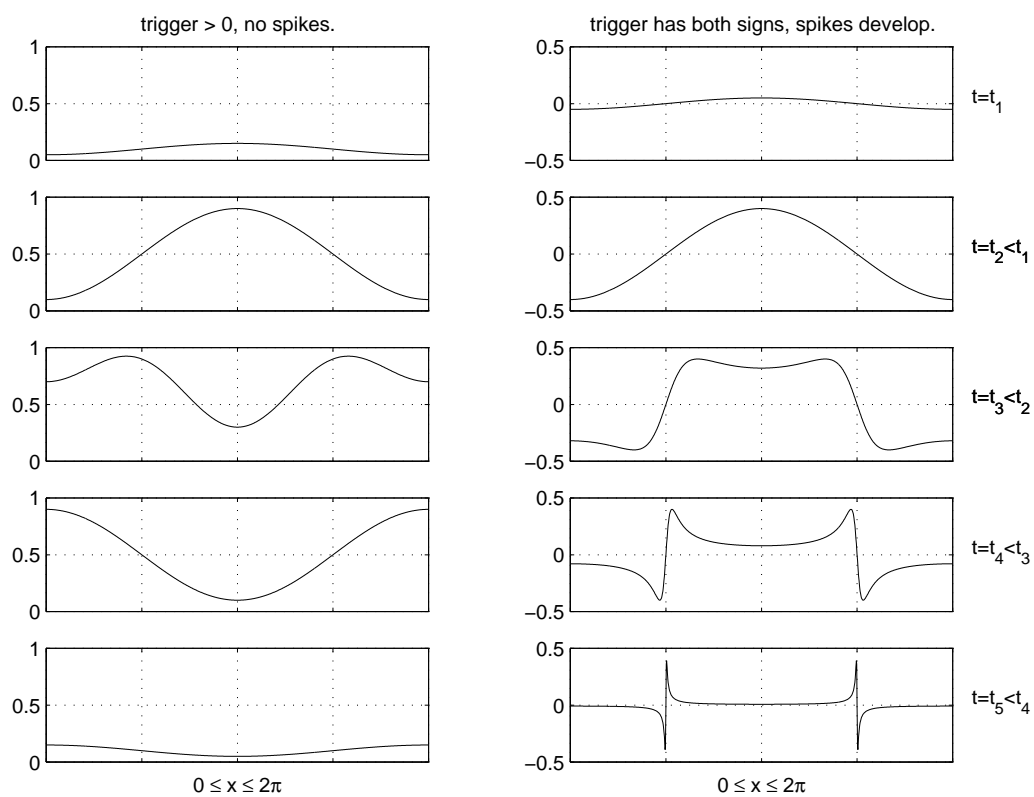


Figure 7.2: The triggers N_- and Σ_x can develop spikes into the past, as illustrated schematically in the above snapshots.

$$\partial_t \Sigma_- = -\frac{2\sqrt{3}}{3} f_1^2 e^{2t} + \mathcal{O}(e^{4t}) \quad \partial_1 N_\times = \frac{4\sqrt{3}}{3} f_1^2 e^{2t} + \mathcal{O}(e^{4t}) \quad (7.20)$$

$$\partial_t N_\times = -\frac{4\sqrt{3}}{3} f_1^2 e^{2t} + \mathcal{O}(e^{4t}) \quad \partial_1 \Sigma_- = \frac{4\sqrt{3}}{3} (-f_1^4 + \frac{3}{2} f_2 f_1) e^{4t} + \mathcal{O}(e^{6t}) \quad (7.21)$$

$$\partial_t \Sigma_\times = \frac{\sqrt{3}}{3} f_1 e^t + \mathcal{O}(e^{3t}) \quad \partial_1 N_- = -\frac{2\sqrt{3}}{3} f_1 e^t + \mathcal{O}(e^{3t}) \quad (7.22)$$

$$\partial_t N_- = \sqrt{3} (f_1^3 - \frac{1}{2} f_2) e^{3t} + \mathcal{O}(e^{5t}) \quad \partial_1 \Sigma_\times = \frac{2\sqrt{3}}{3} (4f_1^3 - f_2) e^{3t} + \mathcal{O}(e^{5t}), \quad (7.23)$$

where $f_1 = f'(-2x_{\text{spike}}(-\infty))$ and $f_2 = f''(-2x_{\text{spike}}(-\infty))$.

For comparison, the following are the decay rates as $t \rightarrow -\infty$ along a typical timeline $x = a$, where $f(-2a) \neq 0$:

$$\Sigma_- = -\frac{\sqrt{3}}{6} + \mathcal{O}(e^{2t}) \quad (7.24)$$

$$N_\times = -\frac{2\sqrt{3}}{3} \frac{f_1}{f_0} e^{2t} + \mathcal{O}(e^{4t}) \quad (7.25)$$

$$\Sigma_\times = -\frac{\sqrt{3}}{3} f_1 e^t + \mathcal{O}(e^{3t}) \quad (7.26)$$

$$N_- = \frac{\sqrt{3}}{3} \left[f_1 + \frac{1}{f_0} \right] e^t + \mathcal{O}(e^{3t}) \quad (7.27)$$

$$\partial_t \Sigma_- = -\frac{2\sqrt{3}}{3} \left[2\frac{f_1}{f_0} + \frac{1}{f_0^2} \right] e^{2t} + \mathcal{O}(e^{4t}) \quad \partial_1 N_\times = \frac{4\sqrt{3}}{3} \left[-\frac{f_1^2}{f_0^2} + \frac{f_2}{f_0} \right] e^{4t} + \mathcal{O}(e^{6t}) \quad (7.28)$$

$$\partial_t N_\times = -\frac{4\sqrt{3}}{3} \frac{f_1}{f_0} e^{2t} + \mathcal{O}(e^{4t}) \quad \partial_1 \Sigma_- = \frac{4\sqrt{3}}{3} \left[-\frac{f_1}{f_0^3} - \frac{f_1^2}{f_0^2} + \frac{f_2}{f_0} \right] e^{4t} + \mathcal{O}(e^{6t}) \quad (7.29)$$

$$\partial_t \Sigma_\times = -\frac{\sqrt{3}}{3} f_1 e^t + \mathcal{O}(e^{3t}) \quad \partial_1 N_- = -\frac{2\sqrt{3}}{3} \left[-\frac{f_1}{f_0^2} + f_2 \right] e^{3t} + \mathcal{O}(e^{5t}) \quad (7.30)$$

$$\partial_t N_- = \frac{\sqrt{3}}{3} \left[f_1 + \frac{1}{f_0} \right] e^t + \mathcal{O}(e^{3t}) \quad \partial_1 \Sigma_\times = \frac{2\sqrt{3}}{3} f_2 e^{3t} + \mathcal{O}(e^{5t}), \quad (7.31)$$

where $f_1 = f'(-2a)$, $f_2 = f''(-2a)$ and $f_0 = f(-2a)$.

For typical points, from (7.28)–(7.31), we see that the spatial derivative terms are negligible compared with the time derivative and algebraic terms in the evolution equations (6.34)–(6.37). This supports the BKL conjecture II in Section 1.3 that the spatial derivatives in the EFEs for a typical cosmological model are not dynamically significant in the past asymptotic regime.

For spike points, however, (7.20), (7.22) and (7.23) show that despite

asymptotic silence, the spatial derivative terms are of the same order as the algebraic terms in the evolution equations (6.34), (6.36) and (6.37) respectively. This limits the validity of the BKL conjecture II within this class of models to typical timelines.

For a general class of vacuum OT G_2 solutions, Kichenassamy & Rendall 1998 [42, equations (5)–(6)] gave an asymptotic expansion for the metric functions P and Q (see (6.39)–(6.40)) as $t \rightarrow -\infty$. Rendall & Weaver 2001 [62] transformed this expansion to produce expansions for \tilde{P} , \tilde{Q}_t and \tilde{Q}_x for a spiky solution. In order to obtain asymptotic expansions for the derivative terms in the evolution equations (6.34)–(6.37), we found it necessary to increase the accuracy of their asymptotic expansions, as is done in Appendix C.

For typical points, the leading orders for the time and spatial derivatives are ²

$$\partial_t \tilde{\Sigma}_- = \Theta(e^{4kt} + e^{4(1-k)t}) \quad \partial_1 \tilde{N}_x = \Theta(-te^{4t}) \quad (7.32)$$

$$\partial_t \tilde{N}_x = \Theta(-te^{2t}) \quad \partial_1 \tilde{\Sigma}_- = \Theta(e^{2t}) \quad (7.33)$$

$$\partial_t \tilde{\Sigma}_x = \Theta(e^{2(1-k)t}) \quad \partial_1 \tilde{N}_- = \Theta(-te^{2(1+k)t}) \quad (7.34)$$

$$\partial_t \tilde{N}_- = \Theta(e^{2kt}) \quad \partial_1 \tilde{\Sigma}_x = \Theta(-te^{2(2-k)t}), \quad (7.35)$$

where $k(x)$ satisfies $0 < k < 1$. We see that the spatial derivatives terms tend to zero as $t \rightarrow -\infty$ faster than the corresponding time derivatives in the evolution equations (6.34)–(6.37). ³

For spike points, the leading orders for the time and spatial derivatives are

$$\partial_t \tilde{\Sigma}_- = \Theta(e^{4(1-k)t}) \quad \partial_1 \tilde{N}_x = \Theta(e^{4(1-k)t}) \quad (7.36)$$

$$\partial_t \tilde{N}_x = \Theta(-te^{2t}) \quad \partial_1 \tilde{\Sigma}_- = \Theta(e^{2t}) \quad (7.37)$$

$$\partial_t \tilde{\Sigma}_x = \Theta(e^{2(1-k)t}) \quad \partial_1 \tilde{N}_- = \Theta(e^{2(1-k)t}) \quad (7.38)$$

$$\partial_t \tilde{N}_- = \Theta(e^{6kt} + e^{2(2-k)t}) \quad \partial_1 \tilde{\Sigma}_x = \Theta(-te^{2(2-k)t}), \quad (7.39)$$

where $k(x)$ satisfies $0 < k < 1$. Equations (7.36) and (7.38) show that, despite asymptotic silence, the spatial derivative terms are of the same order as the

²The big Θ below is defined as follows: $f(t) = \Theta(g(t))$ means there exist constants c_1 and c_2 such that $f(t)$ satisfies $c_1 g(t) < f(t) < c_2 g(t)$ for all t greater (or less) than t_0 .

³ $\partial_1 \tilde{\Sigma}_-$ has a marginal impact on $\partial_t \tilde{N}_x$.

algebraic terms in the evolution equations (6.34) and (6.36) respectively. On the other hand, (7.39) shows that $\partial_1 \tilde{\Sigma}_\times$ dominates $\partial_t \tilde{N}_-$ in the case $k \geq \frac{1}{2}$. This casts more doubts on the BKL conjecture II along the timelines corresponding to the spike points.

It should be noted that the results (7.32)–(7.39) do not reduce exactly to the WM results because the WM solutions are special in a number of respects. For proper reduction, set $k(x) = \frac{1}{2}$ in the more detailed expansions in Appendix C.

The main investigators of spikes (so-called Gowdy spikes in the context of vacuum G_2 cosmologies) are Berger, Moncrief, Isenberg and their collaborators. Berger & Moncrief 1993 [11] first discovered spikes in numerical experiments. A more detailed numerical analysis is performed by Berger & Garfinkle 1998 [10].

7.3 Effects of spatial inhomogeneity II: role of spatial derivative terms

In this section, we discuss inherently non-SH dynamics.

Spike transitions

Not all spikes are permanent. In Garfinkle & Weaver 2003 [25], numerical simulations show that for vacuum OT G_2 cosmologies, spikes which develop during certain Kasner epochs are transient in the sense that they recede to a smooth profile via *spike transitions*.⁴ Eventually, however, new spikes may appear at exactly the same spike point $x_{\text{spike}}(t)$, and may be permanent. Unfortunately we have been unable to provide analytical heuristics to predict spike transitions.

In Chapter 9, we shall illustrate transient spikes in G_2 cosmologies with generic G_2 action, and describe spike transitions in more detail. We shall see that $\partial_1 N_-$ is larger than at permanent spikes, enough to change the sign of $\partial_t \Sigma_\times$ and initiate a spike transition.

⁴More precisely, spikes (as identified by their peak in the profile of Σ_-^H) that form near the Kasner arc spanning from T_2 counter-clockwise to the point $(\Sigma_+^H, \Sigma_-^H) = (-\frac{1}{7}, -\frac{4\sqrt{3}}{7})$ are transient.

Shock waves

Shock waves can form if there are short-wavelength fluctuations with large enough amplitude in the perfect fluid variables. Heuristically, this can be explained as follows. For G_2 cosmologies with one tilt degree of freedom, the evolution equation (5.26) for the tilt v has the following form:

$$\partial_t v - \frac{[(3\gamma - 4) - (\gamma - 1)(4 - \gamma)v^2]}{G_+ G_-} v E_1^{-1} \partial_x v = \dots \quad (7.40)$$

While other terms are not negligible, the left hand side of (7.40) behaves like an inviscid Burgers' equation:

$$\partial_t u + u \partial_x u = 0. \quad (7.41)$$

It is well-known that solutions of Burgers' equation can develop shock waves, depending on the initial conditions (see, for example, Whitham 1974 [84], in which Chapter 4 is dedicated to Burgers' equation). We predict that G_2 cosmologies can develop shock waves in the perfect fluid variables if the conditions are right, namely the occurrence of short-wavelength fluctuations with large enough amplitude in the perfect fluid variables (Ω, v) . In other words, the larger $E_1^{-1} \partial_x v$ is, the sooner v develops shock waves.

Part II

Numerical exploration of G_2 cosmologies

Chapter 8

Equations for numerical simulations

In the remaining two chapters, we show a variety of numerical simulations to support our analysis in Chapter 7, and to explore new phenomena.

For simplicity we restrict our considerations to perfect fluid models with one tilt degree of freedom:

$$v_2 = v_3 = 0, \quad (8.1)$$

although for some experiments we shall use vacuum models. In doing so, the shear spatial gauge (5.46) simplifies to

$$\Sigma_3 = 0, \quad N_+ = \sqrt{3}N_-, \quad R = -\sqrt{3}\Sigma_\times . \quad (8.2)$$

As discussed in Section 4.2 in the context of SH dynamics, the stability of the constraints is of great concern when doing numerical simulations. The concern is even greater for simulations of PDEs, which are less accurate than simulations of ODEs. Numerical experiments of G_2 cosmologies show that the Gauss constraint (5.21) is the most unstable one during the transient regime, and the resulting error is unacceptably large. We remedy this problem by using (5.21) to determine Σ_+ . The decision to use the $(\mathcal{C}_C)_1$ constraint to determine r (see (5.19)) also turns out to be equally important. The remaining $(\mathcal{C}_C)_3$ and (\mathcal{C}_β) constraints yield small, acceptable errors during the transient regime, and are stable in the asymptotic regimes. Ideally, the errors should be minimized, and the difficulties in doing so are discussed in Section 8.4.

With the restrictions (8.1)–(8.2) and solving $(\mathcal{C}_G) = 0$ for Σ_+ , the state

vector (5.48) reduces to the following for numerical purposes:

$$\mathbf{X} = (E_1^{-1}, A, \Sigma_-, N_\times, \Sigma_\times, N_-, \Sigma_2, \Omega, v_1, \Omega_\Lambda), \quad (8.3)$$

together with the parameter γ , and we drop the index on v_1 . The full system of 10 evolution equations and 2 constraint equations is given in Appendix D. We write the system of evolution equations (D.3)–(D.11) symbolically as

$$\partial_t \mathbf{X} + M(\mathbf{X}) \partial_x \mathbf{X} = g(\mathbf{X}). \quad (8.4)$$

Boundary conditions are required for simulations of PDEs. We shall prescribe *periodic boundary condition*, i.e. the numerical solutions are required to satisfy

$$\mathbf{X}(t, 0) = \mathbf{X}(t, 2\pi) \quad \text{for all } t. \quad (8.5)$$

It is customary to do so for numerical simulations of G_2 cosmologies.

By identifying $x = 2\pi$ with $x = 0$, we have used up some but not all of the freedom in the choice of x -coordinate. A change of x -coordinate that satisfies (5.96) preserves this identification. We want to use all the freedom in the choice of x when specifying the initial conditions. Making $E_1^{-1} = \text{const.}$ in the initial conditions achieves this, and also makes the simulations more efficient.

8.1 Specifying the initial conditions

To perform a numerical simulation, we must first specify initial conditions that satisfy the boundary condition (8.5) and the remaining constraints $(\mathcal{C}_C)_3$ and (\mathcal{C}_β) :

$$0 = (\mathcal{C}_C)_3 = E_1^{-1} \partial_x \Sigma_2 - (r + 3A - \sqrt{3}N_\times) \Sigma_2 \quad (8.6)$$

$$0 = (\mathcal{C}_\beta) = (E_1^{-1} \partial_x - 2r) \Omega_\Lambda. \quad (8.7)$$

A good way to specify the initial conditions is the following. We first specify the following eight variables:

$$(E_1^{-1}, r, A, \Sigma_-, N_\times, \Sigma_\times, N_-, \Omega) \quad (8.8)$$

on the interval $x \in [0, 2\pi]$, and the parameter γ .¹ Because we are using the periodic boundary condition (8.5), the initial data must be 2π -periodic. Then we calculate successively the following four variables

$$(\Omega_\Lambda, \Sigma_2, \Sigma_+, Q), \quad (8.9)$$

where

$$Q = \frac{\gamma v}{G_+} \Omega, \quad G_+ = 1 + (\gamma - 1)v^2, \quad (8.10)$$

from the constraints (8.7), (8.6), (5.21) and (5.19) respectively:

$$\Omega_\Lambda = (\Omega_\Lambda)_0 \exp\left(\int_0^x \frac{2r}{E_1^1} dx\right) \quad (8.11)$$

$$\Sigma_2 = (\Sigma_2)_0 \exp\left(\int_0^x \frac{r + 3A - \sqrt{3}N_\times}{E_1^1} dx\right) \quad (8.12)$$

$$\Sigma_+ = \frac{1}{2}[1 - \Sigma_-^2 - \Sigma_\times^2 - \Sigma_2^2 - \Omega_k - \Omega - \Omega_\Lambda] \quad (8.13)$$

$$Q = \frac{2}{3}[-3A\Sigma_+ - 3N_\times\Sigma_- + 3N_-\Sigma_\times - r], \quad (8.14)$$

where $(\Omega_\Lambda)_0$ and $(\Sigma_2)_0$ are freely specifiable positive constants, and

$$\Omega_k = N_-^2 + N_\times^2 - \frac{2}{3}(E_1^1 \partial_x - r)A + A^2. \quad (8.15)$$

We often specify initial conditions which are so simple that Ω_Λ and Σ_2 can be computed by hand. We must make sure that (8.11) and (8.12) yield 2π -periodic Ω_Λ and Σ_2 , i.e. we must ensure that (8.8) satisfies²

$$\int_0^{2\pi} \frac{2r}{E_1^1} dx = 0 \quad (8.16)$$

$$\int_0^{2\pi} \frac{r + 3A - \sqrt{3}N_\times}{E_1^1} dx = 0. \quad (8.17)$$

The tilt v is obtained by solving (8.10), which is a quadratic equation for v ,

¹Although during the simulation we use (5.19) to calculate r in terms of the state variables \mathbf{X} , when specifying the initial conditions it is more convenient to specify r and use (5.19) to calculate Q and hence v .

²If $\Lambda = 0$, then r does not have to satisfy (8.16). Likewise if $\Sigma_2 = 0$, then $r + 3A - \sqrt{3}N_\times$ does not have to satisfy (8.17).

giving

$$v = \frac{2(Q/\Omega)}{\gamma + \sqrt{\gamma^2 - 4(\gamma - 1)(Q/\Omega)^2}} .^3 \quad (8.18)$$

We must make sure that (8.8) and $(\Sigma_2)_0$ yield a v that satisfies

$$-1 < v < 1, \quad \text{or equivalently,} \quad -1 < \frac{Q}{\Omega} < 1 .^4 \quad (8.19)$$

One way to ensure this is to specify a large Ω , as we now explain.

Consider the following format for the initial data, which we shall use in most numerical simulations in the next chapter:

$$\begin{aligned} E_1^1 &= (E_1^1)_0, \quad r = \epsilon \sin x, \quad A = A_0 + \epsilon \sin x, \quad \Sigma_- = (\Sigma_-)_0 + \epsilon \sin x, \\ N_\times &= \sqrt{3}A_0 + \frac{\epsilon}{\sqrt{3}} \sin x, \quad N_- = (N_-)_0 + \epsilon \sin x, \quad \Sigma_\times = (\Sigma_\times)_0 + \epsilon \sin x, \\ \Omega &= \Omega_0 + \epsilon \sin x, \end{aligned} \quad (8.20)$$

where the subscript 0 indicates a constant, and ϵ is a small positive constant. Note that we have made the choice $r_0 = 0$ and $(N_\times)_0 = \sqrt{3}A_0$ in order to satisfy (8.16)–(8.17). The remaining variables are determined by (8.11)–(8.14) and (8.18). Equations (8.11) and (8.12) simplify to

$$\Omega_\Lambda = (\Omega_\Lambda)_0 \exp \left[-2 \frac{\epsilon}{(E_1^1)_0} \cos x \right], \quad \Sigma_2 = (\Sigma_2)_0 \exp \left[-3 \frac{\epsilon}{(E_1^1)_0} \cos x \right], \quad (8.21)$$

while Σ_+ and v have complicated expressions. Expanding $\frac{Q}{\Omega}$ as a power series in ϵ , we obtain

$$\begin{aligned} \frac{Q}{\Omega} &= A_0 + 2(N_-)_0(\Sigma_\times)_0 - 2\sqrt{3}A_0(\Sigma_-)_0 \\ &\quad - A_0[1 - 4A_0^2 - (N_-)_0^2 - (\Sigma_-)_0^2 - (\Sigma_\times)_0^2 - (\Sigma_2)_0^2]/\Omega_0 + \mathcal{O}(\epsilon). \end{aligned} \quad (8.22)$$

One can ensure $v^2 < 1$ by choosing a sufficiently small ϵ and a sufficiently large Ω_0 . It also helps to specify a small A_0 (assuming $A_0 > 0$).

³The second solution for v does not satisfy $v^2 \leq 1$.

⁴One can prove this by plotting (8.18) on the box $-1 \leq \frac{Q}{\Omega} \leq 1$, $1 \leq \gamma \leq 2$, and by plotting (8.10) on the box $-1 \leq v \leq 1$, $1 \leq \gamma \leq 2$ using MAPLE.

Timelike area gauge $A = 0$

If we use the timelike area gauge ($A = 0$), there is a simpler scheme. We first specify

$$(E_1^1, \Sigma_-, N_\times, \Sigma_\times, N_-, \Omega, v) \quad (8.23)$$

and γ . Then we calculate successively

$$(r, \Omega_\Lambda, \Sigma_2, \Sigma_+), \quad (8.24)$$

from (5.19), (8.7), (8.6) and (5.21) respectively:

$$r = -3(N_\times \Sigma_- - N_- \Sigma_\times) - \frac{3}{2} \frac{\gamma \Omega}{G_+} v \quad (8.25)$$

$$\Omega_\Lambda = (\Omega_\Lambda)_0 \exp\left(\int_0^x \frac{2r}{E_1^1} dx\right) \quad (8.26)$$

$$\Sigma_2 = (\Sigma_2)_0 \exp\left(\int_0^x \frac{r - \sqrt{3} N_\times}{E_1^1} dx\right) \quad (8.27)$$

$$\Sigma_+ = \frac{1}{2} [1 - \Sigma_-^2 - \Sigma_\times^2 - \Sigma_2^2 - N_-^2 - N_\times^2 - \Omega - \Omega_\Lambda], \quad (8.28)$$

where $(\Omega_\Lambda)_0$ and $(\Sigma_2)_0$ are freely specifiable positive constants. Note that in order to ensure that Ω_Λ and Σ_2 are periodic, equations (8.16)–(8.17) with $A = 0$ must be satisfied.

Vacuum subcase

The scheme for the generic case does not apply to vacuum initial conditions, while the scheme for the $A = 0$ subcase above does. We now provide a way to specify vacuum initial conditions with $A > 0$. We choose $N_\times = 0$ and specify

$$(E_1^1, A, \Sigma_\times, N_-, \Sigma_2). \quad (8.29)$$

Then the $(\mathcal{C}_C)_3$ and (\mathcal{C}_G) constraints (5.23) and (5.21) are solved for Σ_+ and Σ_- in sequence, yielding

$$\Sigma_+ = 1 - (\frac{1}{3} E_1^1 \partial_x \ln \Sigma_2 - N_- \Sigma_\times) / A \quad (8.30)$$

$$\Sigma_- = [1 - \Omega_k - 2\Sigma_+ - \Sigma_\times^2 - \Sigma_2^2]^{1/2}, \quad (8.31)$$

where

$$\Omega_k = N_-^2 - \frac{2}{3}(E_1^{-1}\partial_x - r)A + A^2, \quad r = -3A\Sigma_+ + 3N_-\Sigma_\times. \quad (8.32)$$

8.2 Is the system hyperbolic?

We ask the following question: does the system of equations (8.4) lead to a well-posed initial value problem? To answer this we rely on a theorem that states that if (8.4) is symmetric hyperbolic, then it leads to a well-posed IVP (see Friedrich & Rendall 2000 [24, pages 147–157]). By symmetric hyperbolic we mean $M(\mathbf{X})$ is symmetric, or more generally, that (8.4) can be multiplied by a symmetric positive definite matrix $A(\mathbf{X})$ so that $A(\mathbf{X})M(\mathbf{X})$ is symmetric (see Friedrich & Rendall 2000 [24, pages 148, 157]). One important notion of hyperbolicity is strong hyperbolicity, which means $M(\mathbf{X})$ is diagonalizable. Strongly hyperbolic systems are also symmetric hyperbolic in the general sense (see Friedrich & Rendall 2000 [24, page 161]). To our knowledge there are no other proofs of well-posedness for quasi-linear systems of PDEs that satisfy other notions of hyperbolicity. See Gustafsson *et al.* 1995 [28, page 119] for these notions in the context of linear PDEs.

The presence of $\partial_x A$ (contained in q and Σ_+) in $M(\mathbf{X})$ complicates the matrix. As a result we have been unable to determine whether the system (8.4) is symmetric hyperbolic.⁵ We comment that if we use the timelike area gauge, where A is identically zero, then the system is symmetric hyperbolic,⁶ and thus has a well-posed IVP. Since we find that the numerical results obtained in this gauge and in the separable area gauge are qualitatively the same, we are confident that the separable area gauge is suitable for simulations.

⁵The system is not strongly hyperbolic, because although $M(\mathbf{X})$ has real eigenvalues, it is not diagonalizable on a set of points with measure zero.

⁶This is proved by van Elst *et al.* 2002 [74] for OT G_2 cosmologies. This result generalizes to the class of generic G_2 cosmologies with one tilt degree of freedom, because the evolution equations for OT G_2 are augmented by the $\partial_t \Sigma_2$ equation (D.8), which has a zero characteristic speed of propagation.

8.3 Accuracy of numerical schemes

In our numerical experiments, we make use of the following three numerical schemes:

- i) the fourth order Runge-Kutta method (RK4),
- ii) the 3-step iterative Crank-Nicholson method (ICN), and
- iii) the CLAWPACK code

(see Gustafsson *et al.* 1995 [28, page 241], Teukolsky 2000 [70], and LeVeque 2002 [45] respectively). RK4 is a classic numerical solver for ODEs, but is suggested for application to PDEs by Gustafsson *et al.*. ICN is a new method developed by Choptuik, but is not well-documented. CLAWPACK is developed by LeVeque, and is well-documented in [45].

We now explain the algorithm for each method briefly, and describe some tests of their accuracy when applied to the system (8.4). To conform with the notation in the literature on numerical algorithms for PDEs, we denote the state vector \mathbf{X} by y and rewrite the symbolic equation (8.4) as

$$\partial_t y = f(y, \partial_x y). \quad (8.33)$$

We denote the grid size by Δx and the step size by Δt . First, we have to decide how to discretize the spatial partial derivative $\partial_x y$. The central differencing scheme for the derivative gives

$$\partial_x y(t, x) = \frac{y(t, x + \Delta x) - y(t, x - \Delta x)}{2\Delta x} + \mathcal{O}((\Delta x)^2), \quad (8.34)$$

which is second order accurate, i.e. the error is of order $(\Delta x)^2$. The central differencing on five grid points is fourth order accurate:

$$\begin{aligned} \partial_x y(t, x) = & \frac{4}{3} \frac{y(t, x + \Delta x) - y(t, x - \Delta x)}{2\Delta x} \\ & - \frac{1}{3} \frac{y(t, x + 2\Delta x) - y(t, x - 2\Delta x)}{4\Delta x} + \mathcal{O}((\Delta x)^4) \end{aligned} \quad (8.35)$$

(see, e.g., Gustafsson *et al.* 1995 [28, pages 19, 247]).

Secondly, we have to give a scheme for time-stepping, i.e. to compute $y(t + \Delta t, x)$, given $y(t, x)$. Let y_n and y_{n+1} denote the computed values for

$y(t)$ and $y(t + \Delta t)$ respectively. The fourth order Runge-Kutta method (RK4) is described as follows (see, e.g., Gustafsson *et al.* 1995 [28, page 241]). For brevity we write $f(y_n, \partial_x y_n)$ as $f(y_n)$ (or think of f as an operator).

$$\begin{aligned} k_1 &= \Delta t f(y_n) \\ k_2 &= \Delta t f(y_n + \frac{1}{2}k_1) \\ k_3 &= \Delta t f(y_n + \frac{1}{2}k_2) \\ k_4 &= \Delta t f(y_n + k_3) \\ y_{n+1} &= y_n + \frac{1}{6}(k_1 + 2k_2 + 2k_3 + k_4). \end{aligned}$$

Using Taylor polynomials, it is straightforward to show that RK4 is fourth order accurate (the error in the spatial derivatives may for the moment be ignored):

$$y_{n+1} = y(t + \Delta t, x) + \mathcal{O}((\Delta t)^5), \quad (8.36)$$

i.e. the power of Δt in the error term is four orders higher than that in the formula for y_{n+1} . Now combining RK4 with the 5-grid central difference scheme, one obtains a fourth order accurate finite difference scheme.

The 3-step iterative Crank-Nicholson method (ICN) is described as follows:

$$\begin{aligned} k_1 &= \Delta t f(y_n) \\ k_2 &= \Delta t f(y_n + \frac{1}{2}k_1) \\ k_3 &= \Delta t f(y_n + \frac{1}{2}k_2) \\ y_{n+1} &= y_n + k_3. \end{aligned}$$

ICN is second order accurate.⁷ Now combining ICN with the 3-grid central difference scheme, one obtains a second order accurate finite difference scheme. Since RK4 evaluates the equations four times at each time step while ICN only three, it takes RK4 $4/3$ times as long to run as it takes ICN.

⁷See Teukolsky 2000 [70]. While an n -th order Runge-Kutta method is n -th order accurate, Teukolsky's analysis shows that all ICN methods are only second order accurate, and the 3-step ICN method is the cheapest stable method among them (see Teukolsky 2000 [70]). We note that there are more sophisticated implementations of the iterative Crank-Nicholson method (Choptuik 2004 [16]). Teukolsky claims that there is no benefit in applying more iterations. Choptuik, however, has reservations about this claim, on the basis that Teukolsky's idealized analysis is incomplete.

The CLAWPACK code (see LeVeque 2002 [45]) handles the evolution equations (8.4) in two stages for each time step, using the so-called Godunov splitting (see LeVeque 2002 [45, pages 380-388]). In the first stage, CLAWPACK solves the following system (referring to (8.4)):

$$\partial_t y + M(y)\partial_x y = 0, \quad (8.37)$$

where $M(y)$ must be diagonalizable. i.e. it can be written as

$$M = QDQ^{-1}, \quad (8.38)$$

where D is a diagonal matrix of real eigenvalues, and Q is a matrix constructed from the corresponding eigenvectors. The upwind finite volume method (see LeVeque 2002 [45, page 73]) is then used to discretize (8.37). To explain the discretization, consider rewriting (8.37) as

$$\partial_t w + D\partial_x w = 0, \quad w = Q^{-1}y, \quad (8.39)$$

pretending that Q is constant. Since D is diagonal, this system decouples into independent advection equations, and the eigenvalues determine the velocities (and hence the upwind directions) of the waves in the characteristic eigenfields w . So we are able to determine the upwind direction for each wave. In finite volume methods, an x -interval is divided into cells, and fluxes are computed at the interface of two adjacent cells. To obtain the data at the interface, some averaging scheme must be used (see LeVeque 2002 [45, Section 15.3]), and here we simply take the arithmetic average. The discretization of (8.37) yields

$$y_i^{n+1} = y_i^n - \frac{\Delta t}{\Delta x} \left[\mathcal{A}_{i-\frac{1}{2}}^{+n}(y_i^n - y_{i-1}^n) + \mathcal{A}_{i+\frac{1}{2}}^{-n}(y_{i+1}^n - y_i^n) \right], \quad (8.40)$$

where

$$\mathcal{A}_{i-\frac{1}{2}}^{\pm n} = Q_{i-\frac{1}{2}}^n D_{i-\frac{1}{2}}^{\pm n} (Q_{i-\frac{1}{2}}^n)^{-1}, \quad (8.41)$$

and $D = D^+ + D^-$, where D^+ contains only positive eigenvalues while D^- contains only negative eigenvalues. The vector $\mathcal{A}_{i-\frac{1}{2}}^+(y_i - y_{i-1})/\Delta x$ describes fluxes to the right from the $(i-1)$ -th cell to the i -th cell, etc. For details see LeVeque 2002 [45, pages 78–82]. The first stage is first order accurate.

In the second stage, **CLAWPACK** solves the system

$$\partial_t y = g(y). \quad (8.42)$$

This part can be discretized by any ODE solver. We solve this part by using the explicit Euler method,

$$y_{n+1} = y_n + \Delta t g(y_n),$$

which is first order accurate.

Overall, **CLAWPACK** is first order accurate. While **RK4** and **ICN** do poorly in simulating shock waves (Taylor polynomials do not apply at points of discontinuity), **CLAWPACK** sacrifices high accuracy for smooth solutions for the ability to simulate shock waves reasonably well. The error analysis of **CLAWPACK** near shock waves is based on conservative systems of the form:

$$\partial_t y + \partial_x(G(y)) = g(y).$$

However, the system (D.3)–(D.11) is not conservative, due to the presence of inhomogeneity in E_1^1 and the non-conservative pair $(\ln \Omega, \operatorname{arctanh} v)$. This will likely reduce the accuracy of **CLAWPACK** when simulating shock waves. Another more serious abuse of **CLAWPACK** is that we have put $\partial_x A$ (contained in q and Σ_+) in the right hand side of the equations ($g(y)$ becomes $g(y, \partial_x y)$),⁸ which makes it unsuitable for shock waves simulations. The best we can do is to simulate shock waves using the timelike area gauge $A = 0$. The abuse becomes relatively harmless if E_1^1 is small. For example, **CLAWPACK** does a better job than the other two schemes at simulating permanent spikes under low resolution (see Section 8.4), so there is value in keeping **CLAWPACK**.

To measure the rate of convergence for each method, we make three runs, using 512, 1024 and 4096 spatial grid points. The data using 4096 spatial grid points serves as the reference, and the errors of the two runs with cruder

⁸**CLAWPACK** requires a coefficient matrix $M(y)$ that is diagonalizable. By putting $\partial_x A$ in the left hand side, **CLAWPACK** is liable to crash due to unbounded determinant of the Q matrix in (8.38).

grids are compared. We use both L_2 and L_∞ norms to measure the errors.⁹

Table 8.1: The rate of convergence of numerical methods: errors relative to the solution on 4096 grid points as measured in the L_∞ norm.

Method	error (512)	error (1024)	ratio	convergence
RK4	2.9746×10^{-7}	1.9852×10^{-8}	14.9839	fourth order
ICN	2.2908×10^{-3}	5.3947×10^{-4}	4.2464	second order
CLAWPACK	1.7974×10^{-1}	7.8783×10^{-2}	2.2814	first order

In Table 8.1 we present the errors in L_∞ norm. A method is said to be n -th order accurate in time if its error (approximately) shrinks by a factor of 2^{-n} when the number of grid points is doubled. Errors in L_2 norm are of similar size and are not presented. The initial data is chosen to be (8.20) with $\gamma = \frac{4}{3}$ and

$$\begin{aligned} \epsilon &= 0.01, \quad (E_1^1)_0 = 1, \quad A_0 = 0.2, \quad (\Sigma_-)_0 = 0.2, \quad (\Sigma_\times)_0 = 0.4, \\ (N_-)_0 &= -0.4, \quad \Omega_0 = 0.5, \quad (\Omega_\Lambda)_0 = 0.7, \quad (\Sigma_2)_0 = 0.1. \end{aligned} \quad (8.43)$$

The simulations run from $t = 0$ to $t = -1$. Longer simulations will see the formation of spikes. The order of accuracy is derived from Taylor polynomial approximation. With decreasing resolution around the spikes, the approximation becomes poorer and poorer, and eventually becomes totally useless. Higher resolution will be needed to prolong simulations. The CFL stability condition (see Gustafsson *et al.* 1995 [28, page 54]) is set at $\Delta t \leq$

⁹Let y_i^m be the m -th component of the vector y evaluated at the i -th grid point. Then the L_2 norm of the error in y is given by

$$\|y - y_{\text{ref}}\|_2 = \sqrt{\frac{1}{N} \sum_{i,m} (y_i^m - (y_{\text{ref}})_i^m)^2},$$

where N is the number of grid points. The L_∞ norm of the error in y is given by

$$\|y - y_{\text{ref}}\|_\infty = \max_{i,m} |y_i^m - (y_{\text{ref}})_i^m|.$$

$\Delta x / \max E_1^1$. This serves as a cap for the step size Δt to maintain the stability of the solution.¹⁰ The preferred value for Δt is set at $\Delta t = 0.9\Delta x / \max E_1^1$, i.e. the step size is computed as follows:

$$\Delta t = 0.9\Delta x / \max E_1^1(t, x). \quad (8.44)$$

After the data at time $t + \Delta t$ is obtained, we check that

$$\Delta t \leq \Delta x / \max E_1^1(t + \Delta t, x). \quad (8.45)$$

If this is satisfied, we continue; otherwise we recalculate the data with a smaller step size

$$\Delta t_{\text{smaller}} = 0.9\Delta x / \max E_1^1(t + \Delta t, x). \quad (8.46)$$

This smaller step size will satisfy the CFL condition:

$$\Delta t_{\text{smaller}} \leq \Delta x / \max E_1^1(t + \Delta t_{\text{smaller}}, x). \quad (8.47)$$

Now since the reference solution is computed by the same method, we can only conclude that each method converges at the respective rate. Do they all converge to the real solution? To answer this we need an exact solution against which the error of the methods can be measured. Unfortunately there are no exact generic G_2 solutions available thus far. The most suitable possible test solution is the WM solution (see Section 6.2), which is an exact vacuum OT G_2 solution, containing one arbitrary function $f : \mathbb{R} \rightarrow \mathbb{R}$. It is given by (6.59):

$$\Sigma_- = -\frac{1}{2\sqrt{3}}, \quad N_\times = 0 = A, \quad \Sigma_\times = -N_- = \frac{1}{\sqrt{3}}e^t f(e^{2t} - 2x), \quad E_1^1 = e^{2t}. \quad (8.48)$$

For the test, we choose

$$f(e^{2t} - 2x) = \sin(e^{2t} - 2x) \quad \text{with} \quad 0 \leq x \leq 2\pi. \quad (8.49)$$

The solution then satisfies periodic boundary conditions. The simulations run from $t = 0$ to $t = -1$. The CFL condition is set at $\Delta t \leq \Delta x / \max E_1^1$, and the preferred value for Δt at $\Delta t = 0.9\Delta x / \max E_1^1$. In Table 8.2 we

¹⁰We also impose an absolute cap to the time step: $\Delta t \leq 0.1$ for stability.

present the errors in Σ_\times in the L_∞ norm. Errors in the L_2 norm are similar and are not presented.

Table 8.2: The accuracy of numerical methods: errors in the simulated Σ_\times for the WM solution as measured in the L_∞ norm.

Method	error (512)	error (1024)	ratio	accuracy
RK4	9.5834×10^{-9}	6.2809×10^{-10}	15.2581	fourth order
ICN	9.8275×10^{-6}	2.7601×10^{-6}	3.5605	second order
CLAWPACK	4.3212×10^{-3}	2.2423×10^{-3}	1.9272	first order

Table 8.3: The accuracy of numerical methods: errors in the simulated Σ_- for the transformed WM solution as measured in the L_∞ norm.

Method	error (512)	error (1024)	ratio	accuracy
RK4	1.5157×10^{-5}	9.7292×10^{-7}	15.5789	fourth order
ICN	2.6242×10^{-3}	6.6930×10^{-4}	3.9208	second order
CLAWPACK	2.4204×10^{-2}	1.2511×10^{-2}	1.9347	first order

The WM solution can be transformed into a new solution (see Section 6.2). We test the codes against this solution, using the initial condition for the WM solution above. In Table 8.3 we present the errors in Σ_- in L_∞ norm.

The tests confirm that the methods produce solutions that converge to the exact solution at the expected rates, which gives us some confidence that the methods are reliable.

8.4 Unsatisfactory aspects of the numerical simulations

Instability of $(\mathcal{C}_C)_3$

The evolution equation for $(\mathcal{C}_C)_3$ is given by

$$\partial_t(\mathcal{C}_C)_3 = (2q - 2 + 3\Sigma_+ + \sqrt{3}\Sigma_-)(\mathcal{C}_C)_3. \quad (8.50)$$

This constraint is stable into the past near Kasner equilibrium points. However, when Σ_2 is large, $(\mathcal{C}_C)_3$ grows as $t \rightarrow -\infty$. This is a cause for concern especially when $(\mathcal{C}_C)_3$ grows at the beginning of the simulation (i.e. before entering the asymptotic regime). Using finer grids or taking smaller time steps reduces the size of $(\mathcal{C}_C)_3$, but is very inefficient. Unfortunately, we find that adding the constraint in the evolution equations¹¹ does not change its instability. Constraint instability is a recurring problem in numerical relativity. For other methods in controlling constraint instability, see Lindblom *et al.* 2004 [50].

Resolution

As we have not implemented an adaptive mesh refinement scheme, high-resolution simulations are expensive for the numerical schemes we have. This imposes a severe limitation when spikes occur. Without mesh refinement, we can only adequately simulate spikes for a short time before the spikes become too narrow to resolve numerically. If E_1 ¹ is sufficiently large near a spike, RK4 can generate spurious oscillations, while ICN also generate some overshoot. Only CLAWPACK handles spikes reasonably well in all situations.

The dust case

For dust ($\gamma = 1$) the equations are not strongly hyperbolic (the matrix $M(\mathbf{X})$ is not diagonalizable at any point in spacetime), regardless of whether $A = 0$ or not. We shall not simulate the dust case in this thesis.

¹¹For example,

$$\partial_t \Sigma_2 = (q - 2 + \sqrt{3}\Sigma_-)\Sigma_2 + (\mathcal{C}_C)_3 .$$

The Taub Kasner point T_1

The Taub Kasner point T_1 given by $\beta = 0$ causes difficulties for numerical simulations. It causes blow-up in the β -normalized variables because β is zero here. This problem cannot be avoided by using Hubble-normalized variables or other gauges, because the Taub Kasner point is qualitatively different from other Kasner points, namely it is non-silent in the x -direction. We can only simulate solutions that do not get too close to the Taub Kasner point during the period of interest. As a general rule of thumb, the more inhomogeneous the initial condition is, the more likely we will run into the Taub Kasner point at an early stage in numerical simulations.

Chapter 9

Numerical simulations

In this chapter, we present a variety of numerical simulations of G_2 cosmologies that confirm the analytical predictions made in Chapter 7. The numerical results also illustrate the spike transitions, which we were unable to predict analytically in Chapter 7. In addition we describe simulations of the future asymptotic approach to de Sitter, and the close-to-FL regime.

For most of the simulations,¹ we shall specify initial conditions by following the format (8.20) introduced in Chapter 8:

$$\begin{aligned} E_1^1 &= (E_1^1)_0, & r &= \epsilon \sin x, & A &= A_0 + \epsilon \sin x, & \Sigma_- &= (\Sigma_-)_0 + \epsilon \sin x, \\ N_\times &= \sqrt{3}A_0 + \frac{\epsilon}{\sqrt{3}} \sin x, & N_- &= (N_-)_0 + \epsilon \sin x, & \Sigma_\times &= (\Sigma_\times)_0 + \epsilon \sin x, \\ & & \Omega &= \Omega_0 + \epsilon \sin x, \end{aligned} \tag{9.1}$$

where the subscript 0 indicates a constant. Ω_Λ and Σ_2 are given by (8.21):

$$\Omega_\Lambda = (\Omega_\Lambda)_0 \exp \left[-2 \frac{\epsilon}{(E_1^1)_0} \cos x \right], \quad \Sigma_2 = (\Sigma_2)_0 \exp \left[-3 \frac{\epsilon}{(E_1^1)_0} \cos x \right], \tag{9.2}$$

while Σ_+ and v are computed numerically using (D.13), (8.14) and (8.18), and have complicated expressions. For more special G_2 actions, we set the appropriate variables to zero.

While β -normalized variables are used in the simulations, Hubble-normalized variables are displayed in most of the plots.

¹The exceptions are the simulation of vacuum models in Section 9.2.3, the shock wave simulation in Section 9.4.2, and the close-to-FL simulation in Section 9.6.

9.1 Asymptotic silence

In this section we shall provide evidence to support the occurrence of asymptotic silence not only as $t \rightarrow -\infty$, namely,

$$\lim_{t \rightarrow -\infty} E_1^1 = 0, \quad \lim_{t \rightarrow -\infty} r = 0, \quad (9.3)$$

but also as $t \rightarrow \infty$ in the presence of a cosmological constant.

Using the format (9.1) for initial conditions, consider the following initial data at $t = 0$, with $\gamma = \frac{4}{3}$:

$$\begin{aligned} \epsilon = 0.01, \quad (E_1^1)_0 = 1, \quad A_0 = 0.2, \quad (\Sigma_-)_0 = 0.2, \quad (\Sigma_\times)_0 = 0.4, \\ (N_-)_0 = 0.4, \quad \Omega_0 = 0.5, \quad (\Omega_\Lambda)_0 = 0.7, \quad (\Sigma_2)_0 = 0.1. \end{aligned} \quad (9.4)$$

We ran ICN with 512 grid points, from $t = 0$ to $t = -50$, and from $t = 0$ to $t = 5$ storing data at intervals of $t = 0.1$. First, we plot the maximum and minimum of $\ln(E_1^1)^H$ and $\ln|r|$ against t in Figure 9.1 We see that $(E_1^1)^H$ and r decay exponentially both into the past and into the future, supporting the conjecture that the past and future dynamics are asymptotically silent.² Thus it is reasonable to say that the local background dynamics of G_2 cosmologies is the SH dynamics.

9.2 Background dynamics

In this section we illustrate the role of SH dynamics in G_2 dynamics.

9.2.1 Local Mixmaster dynamics

Still using the initial data (9.4), we plot the maximum and minimum of $\ln(\Omega^H)$ and $\ln(\Omega_\Lambda^H)$ against t in Figure 9.2. We see that Ω^H and Ω_Λ^H decay exponentially into the past, supporting the BKL conjecture I.

Figures 9.3–9.4 show the evolution along a fixed timeline $x = \text{const.}$ (the grid point 100 of 512). They show the generalized Mixmaster dynamics into the past and the approach to de Sitter into the future.

²Actually, this is only true along almost all timelines. In Section 9.4.1, we shall see that along some timelines r can become large, but the spatial resolution in this run is too low to simulate it correctly.

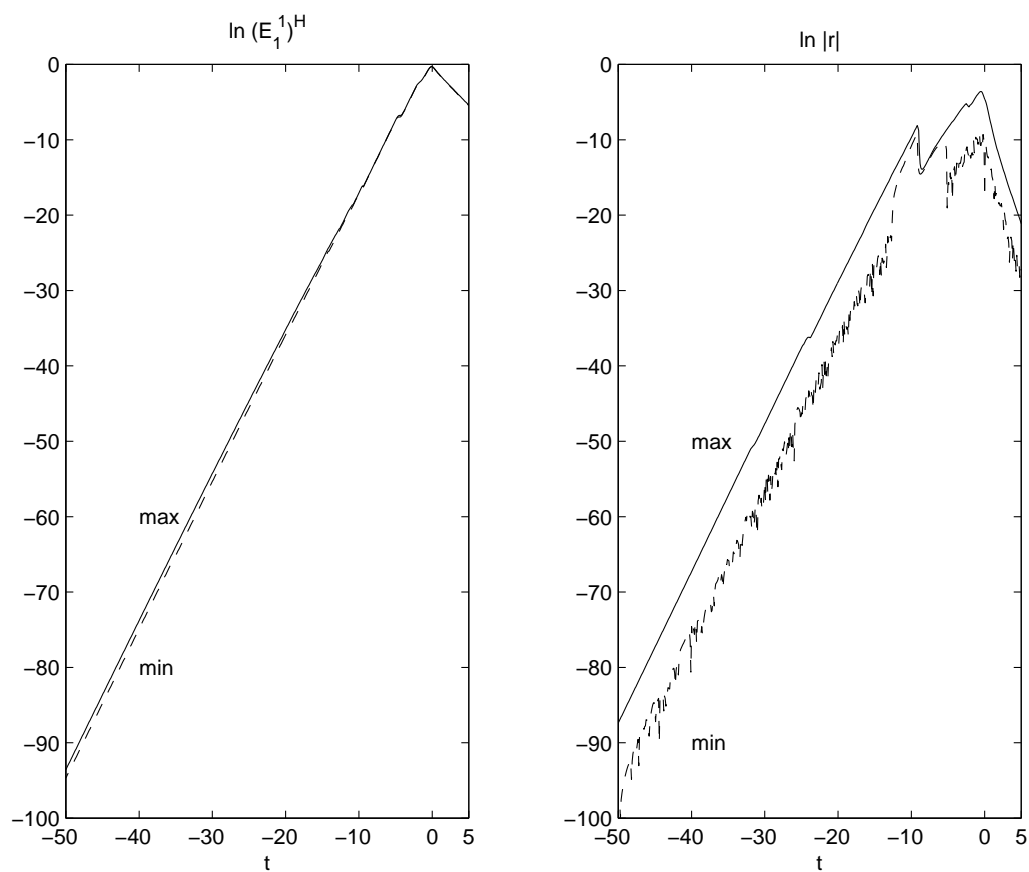


Figure 9.1: Exponential decay of $(E_1^1)^H$ and r as $t \rightarrow -\infty$ and as $t \rightarrow \infty$, showing the maximum and minimum values of $\ln(E_1^1)^H$ and $\ln |r|$. The graph for $\min_{0 \leq x \leq 2\pi} \ln |r|$ is broken because r has both signs.

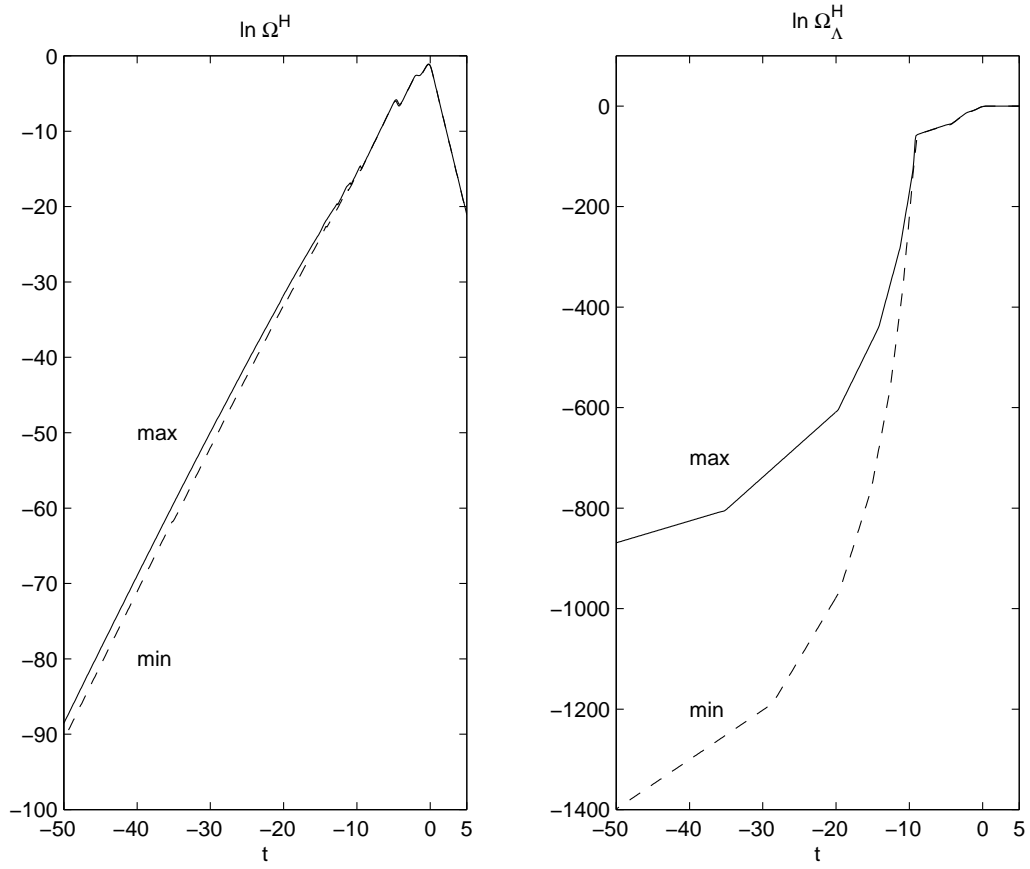


Figure 9.2: Exponential decay of Ω^H and Ω_Λ^H as $t \rightarrow -\infty$, showing the maximum and minimum values of $\ln \Omega^H$ and $\ln \Omega_\Lambda^H$.

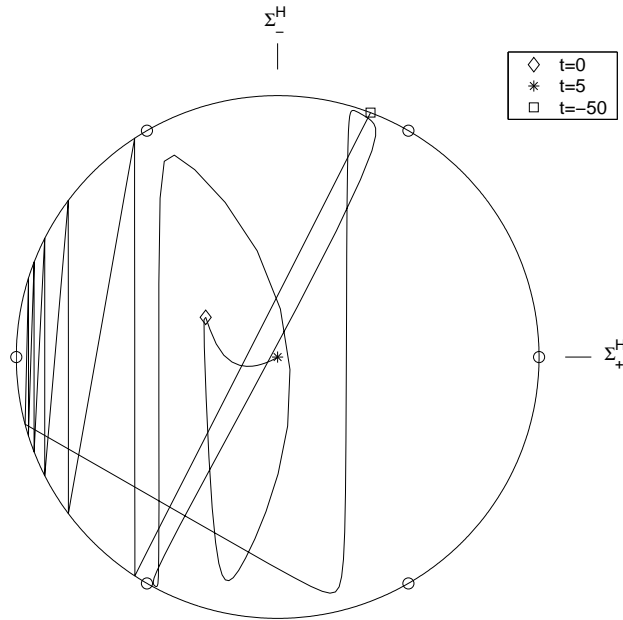


Figure 9.3: Typical evolution along a fixed timeline, showing the transition orbits.

Evolving into the past from $t = 0$, the solution enters the Kasner regime at about $t = -3$. One prominent Σ_2 transition is observed at about $t = -9$, followed by an alternating sequence of N_- and Σ_\times transitions (see also Figure 9.4 below).

Figure 9.4 shows that v is stuck at $v = 1$ as $t \rightarrow -\infty$, and tends to a non-zero limit as $t \rightarrow \infty$. For more details about the future asymptotics, see Section 9.5.

Table 9.1 shows the expected and actual growth rates into the past (positive value indicates growth into the past) along grid point 100, at two selected times. The actual rates are in good agreement with the expected rates, which can be inferred from the β -normalized version of (4.89)–(4.91).

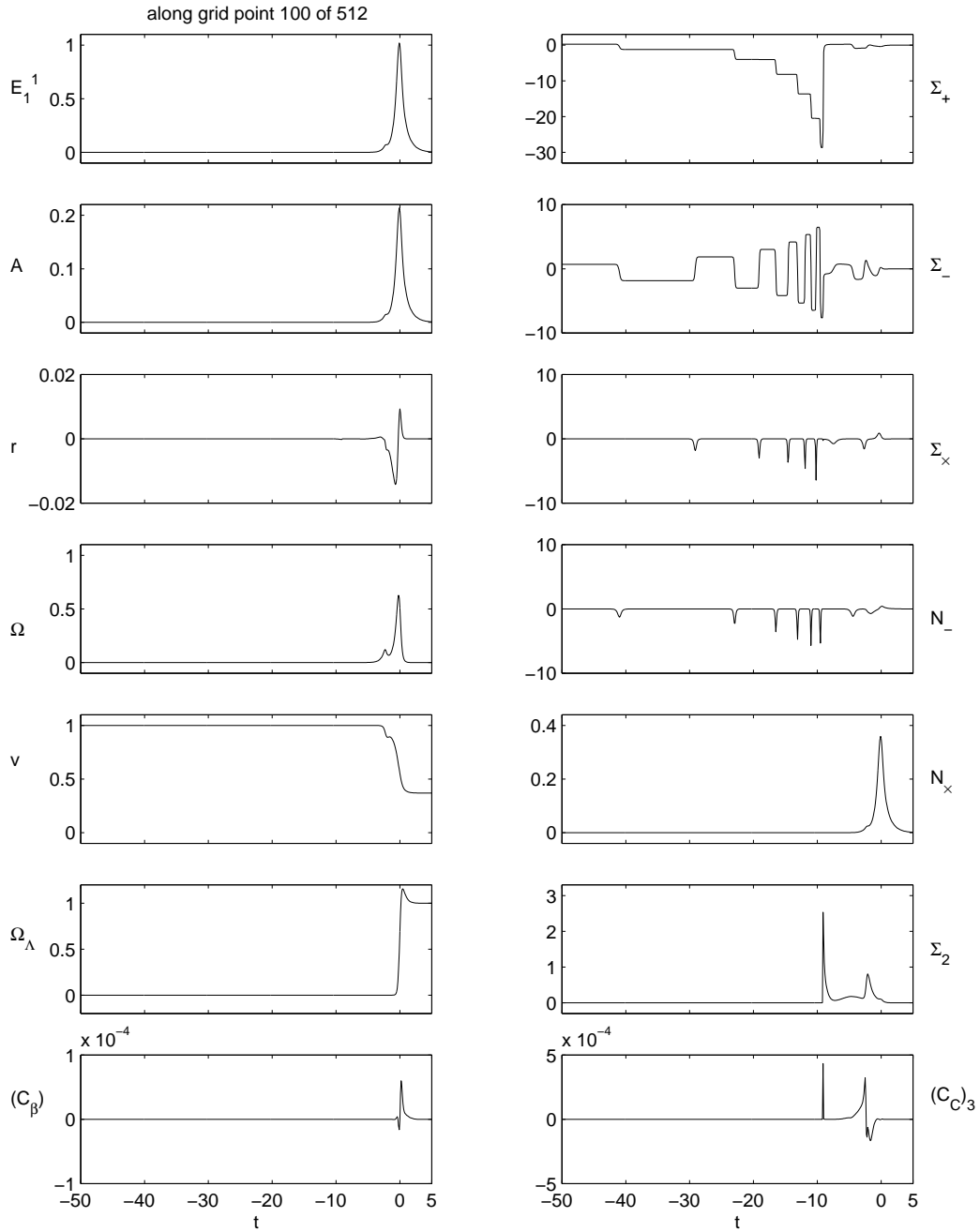


Figure 9.4: Typical evolution along a fixed timeline.

Table 9.1: Predicted and actual growth rates of the triggers into the past (positive value indicates growth into the past) along grid point 100 of 512.

Triggers	N_-	Σ_\times	Σ_2	$\sqrt{1-v^2}$
At $t = -50$ ($\phi = 1.2076$ or 69.2°)				
Expected rate	-4.3894	2.3894	-0.4083	0.7864
Actual rate	-4.4174	2.3920	-0.4083	0.7864
At $t = -35$ ($\phi = 4.1341$ or 236.9°)				
Expected rate	4.3976	-6.3976	-0.4173	-3.6161
Actual rate	4.4040	-6.4323	-0.4173	-3.6161

9.2.2 Spatial variation in the background dynamics

The timing of the transitions in Mixmaster dynamics varies from one timeline to another. Continuing with the initial data (9.4), Figure 9.5 shows some snapshots of the triggers Σ_\times^H and N_-^H , illustrating this variation in the timing. The variation in the timing leads to a pulse-like profile of the triggers.

As discussed in Section 5.3, the particle horizon is given by $\int_{-\infty}^0 E_1^1 dt$. Since $E_1^1 = 1$ at $t = 0$ here and decays like e^{2t} , $\int_{-\infty}^0 E_1^1 dt$ is approximately equal to $\frac{1}{2}$, and so information can travel only a finite distance of $\Delta x \approx \frac{1}{2}$ as $t \rightarrow \infty$. But the pulses in Figure 9.5 travel more than $\Delta x = \frac{1}{2}$, which is only possible if they propagate faster than light. How is this possible? In fact, the apparent superluminal speed is an illusion created by the variation in the background SH dynamics from one timeline to another (e.g. variation in the timing of the transitions in Mixmaster dynamics). An analogy to this phenomenon is a Mexican wave in a stadium.

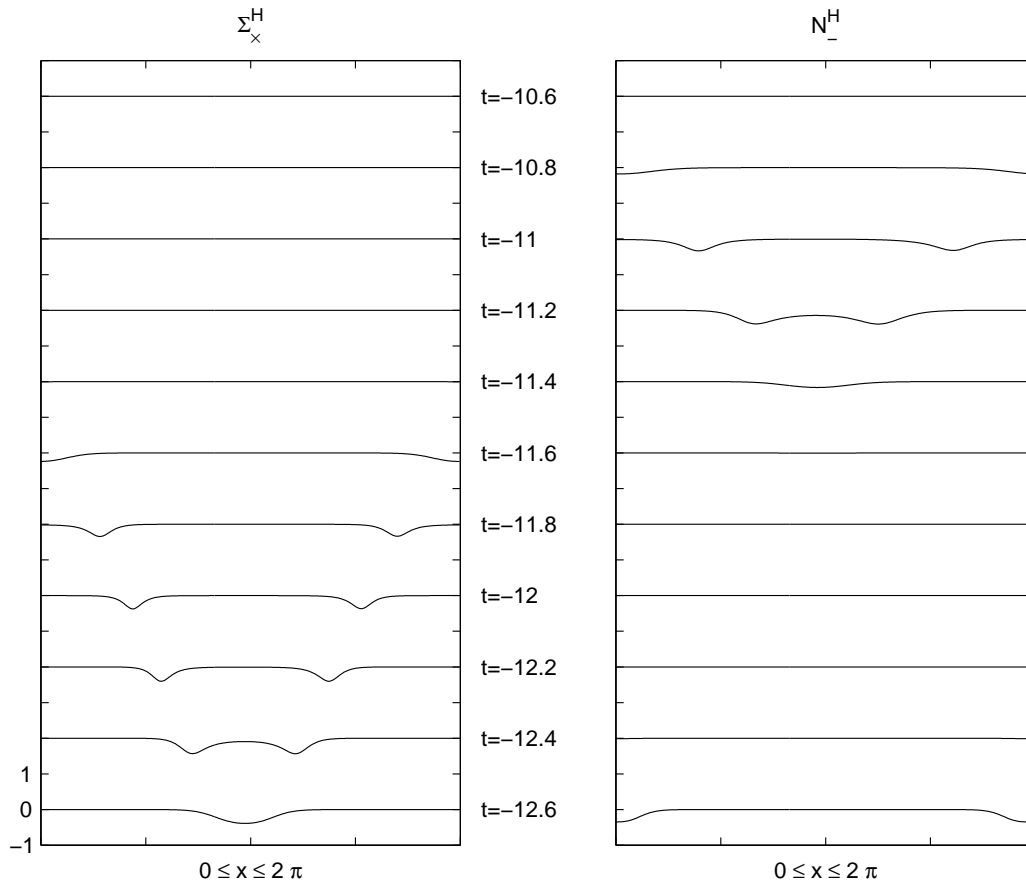


Figure 9.5: Snapshots of triggers Σ_x^H and N_-^H , showing pulses apparently travelling at superluminal speeds.

9.2.3 Multiple transitions

It is simplest to analyze multiple transitions in the absence of spikes or step-like structures. Since it is difficult to produce a spike-free solution over a very long run in a perfect fluid solution,³ we resort to simulating vacuum solutions.

Using the scheme for the vacuum case in Section 8.1, we choose $N_\times = 0$ and specify the following vacuum initial condition:

$$\begin{aligned} E_1^1 &= A = 0.1 + 0.01 \sin x, \\ \Sigma_\times &= -N_- = 0.8 + 0.1 \sin x, \quad \Sigma_2 = 0.1. \end{aligned} \tag{9.5}$$

Then Σ_+ , Σ_- and r are given by (8.30)–(8.32).

We ran `CLAWPACK` with 512 grid points, from $t = 0$ to $t = -50$, storing data at intervals of $t = 0.1$. Figure 9.6 shows bands of level curves indicating the activation of the triggers Σ_2 , Σ_\times and N_- . The result is spike-free up to $t = -33$. Spikes occur in the lower right quarter of Figure 9.6.

In Figure 9.5 of the previous section, we saw that there is variation in the timing of the transitions in Mixmaster dynamics, due to spatial inhomogeneity. Figure 9.6 shows that the sequence of the transitions can also vary from one timeline to another. For example, proceeding along the timeline $x = \pi$ as $t \rightarrow -\infty$, the solution undergoes an N_- transition first at about $t = -10$ before undergoing a Σ_2 transition at about $t = -20$. In comparison, proceeding along the timeline $x = \frac{3\pi}{4}$ as $t \rightarrow -\infty$, the solution undergoes a Σ_2 transition first at about $t = -17$ before undergoing an N_- transition at about $t = -18$. Thus, by continuity, there must be timelines between $x = \pi$ and $x = \frac{3\pi}{4}$ that undergo both Σ_2 and N_- transitions at the same time, i.e. they undergo a multiple transition.

The intersection of the bands indicates multiple transitions. We see that such intersections are inevitable in the global picture. Thus multiple transitions will occur from time to time globally, as $t \rightarrow -\infty$. Locally along a fixed timeline, it is possible that the probability of multiple transitions occurring will tend to zero as $t \rightarrow -\infty$, in agreement with the multiple transitions conjecture in SH dynamics, but we cannot make a strong claim in this regard.

³That the initial condition for Ω is large (see the comment following (8.19)) makes it difficult to predict whether a solution will be spike-free and will stay away from the Taub Kasner point for a long period of time.

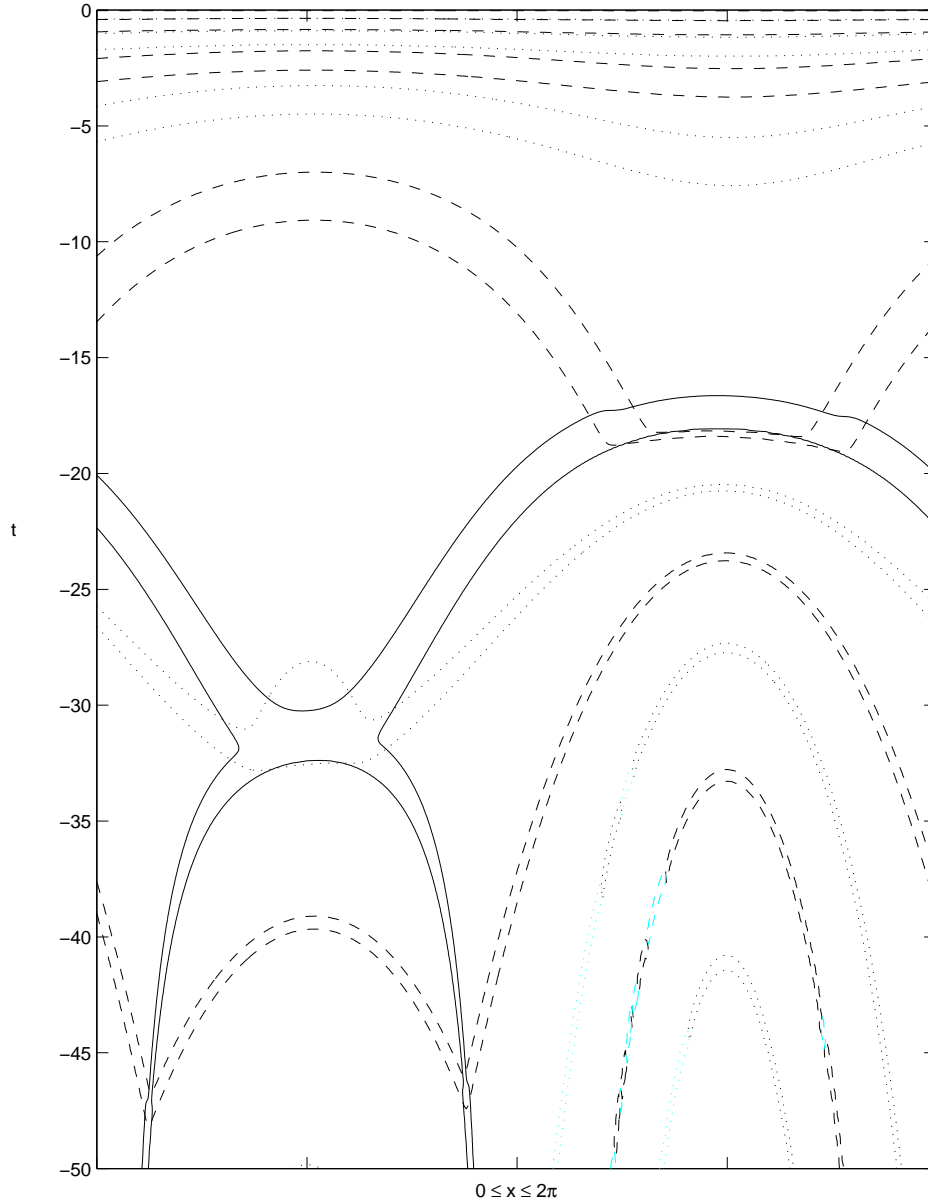


Figure 9.6: The level curves of $\Sigma_2^H = 0.1$ (solid), $N_-^H = -0.1$ (dashed) and $\Sigma_x^H = 0.1$ (dotted), indicating the activation of the triggers. Multiple transitions occur when two bands overlap. For example, in a neighbourhood of $t = -32$ and $x = \pi/4$, the solid band and the dotted band overlap, indicating a multiple transition involving Σ_2^H and Σ_x^H .

9.3 Effects of spatial inhomogeneity I: role of saddles

In this section, we illustrate the role of saddle points in creating step-like or spiky structures. We also take this opportunity to illustrate the past attractors of diagonal and OT G_2 cosmologies.

9.3.1 Step-like structures

We now illustrate step-like structures in the tilt variable v in diagonal G_2 cosmologies, and provide evidence to support the claim that the past attractor is given by (7.13):

$$\mathcal{A}^- = \mathcal{K} \operatorname{arc}(\Sigma_+^H > -\frac{1}{2}(3\gamma - 4)) \cup \mathcal{K}_{\pm 1} \operatorname{arc}(\Sigma_+^H < -\frac{1}{2}(3\gamma - 4)). \quad (9.6)$$

Recall that diagonal G_2 cosmologies satisfy (5.58):

$$\Sigma_2 = 0 = \Sigma_x = N_- . \quad (9.7)$$

Consider the following initial data at $t = 0$ with $\gamma = \frac{4}{3}$ (in conjunction with (9.1) and (9.7)):

$$\begin{aligned} \epsilon = 0.3, \quad (E_1^1)_0 = 1, \quad A_0 = 0, \quad (\Sigma_-)_0 = 0.2, \quad \Sigma_x \equiv 0, \\ N_- \equiv 0, \quad \Omega_0 = 0.6, \quad (\Omega_\Lambda)_0 = 0.1, \quad \Sigma_2 \equiv 0. \end{aligned} \quad (9.8)$$

We ran `CLAWPACK` with 512 grid points, from $t = 0$ to $t = -10$, storing data at intervals of $t = 0.1$. Figure 9.7 shows the snapshots of the tilt variable v at $t = -4$, $t = -5$ and $t = -10$. We see the strong suggestion that three step-like structures develop as $t \rightarrow -\infty$: one between $v = \pm 1$, and two between $v = 0$ and $v = 1$. The one between $v = \pm 1$ involves an unstable state $v = 0$, while the two between $v = 0$ and $v = 1$ involve a string of Kasner equilibrium points with $\Sigma_+^H = 0$ and $-1 \leq v \leq 1$ that connect the stable arcs $\mathcal{K} \operatorname{arc}(\Sigma_+^H > 0)$ and $\mathcal{K}_{\pm 1} \operatorname{arc}(\Sigma_+^H < 0)$.

Figures 9.8–9.10 show the snapshots of the variables $(\Sigma_+^H, \Sigma_-^H, v)$ in the $(\Sigma_+^H, \Sigma_-^H, v)$ space. Each dot represents the state at a grid point. We see that the state vector approaches the past attractor (4.131).

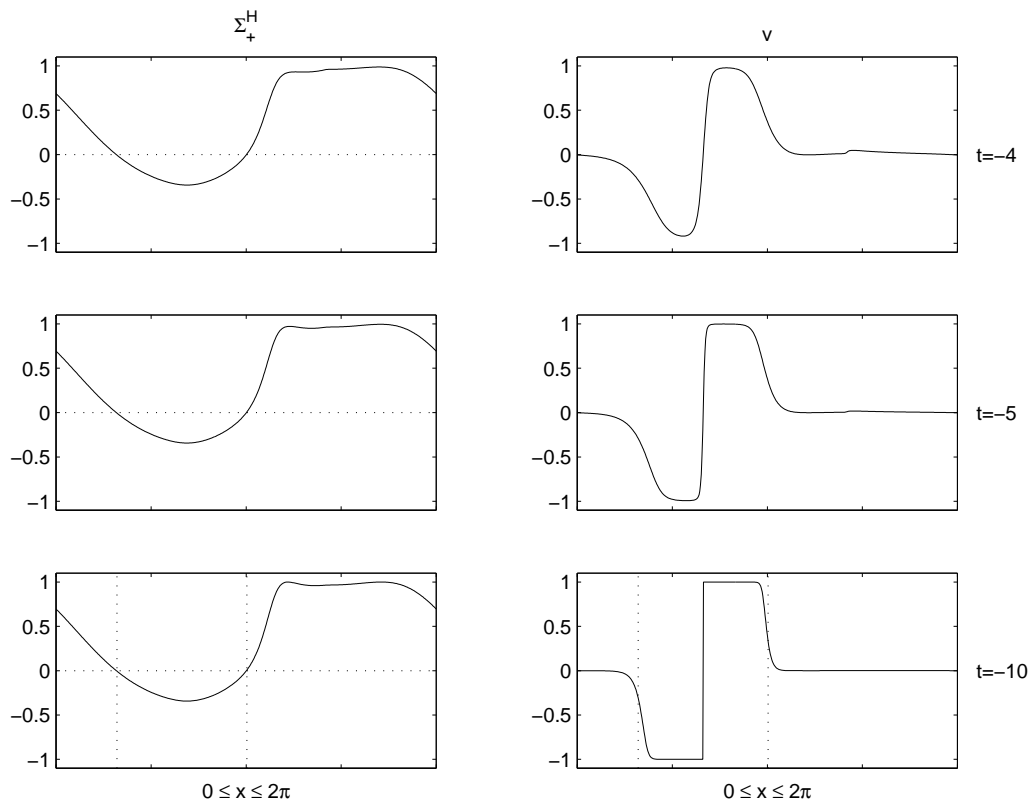


Figure 9.7: Snapshots of Σ_+^H and v in a diagonal G_2 cosmology, showing step-like structures in v .

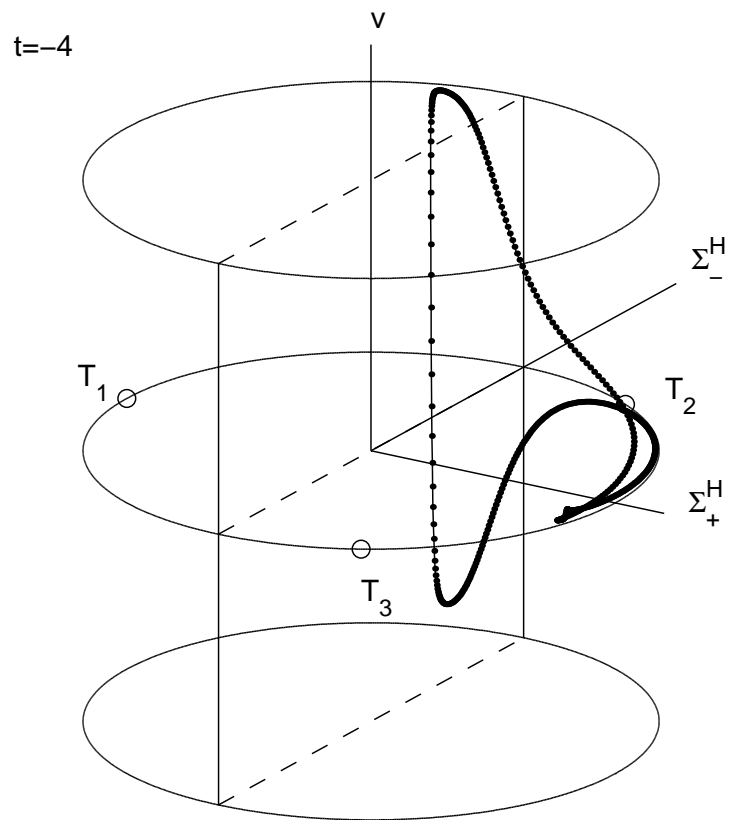


Figure 9.8: Snapshot of the variables $(\Sigma_+^H, \Sigma_-^H, v)$ in a diagonal G_2 cosmology at $t = -4$.

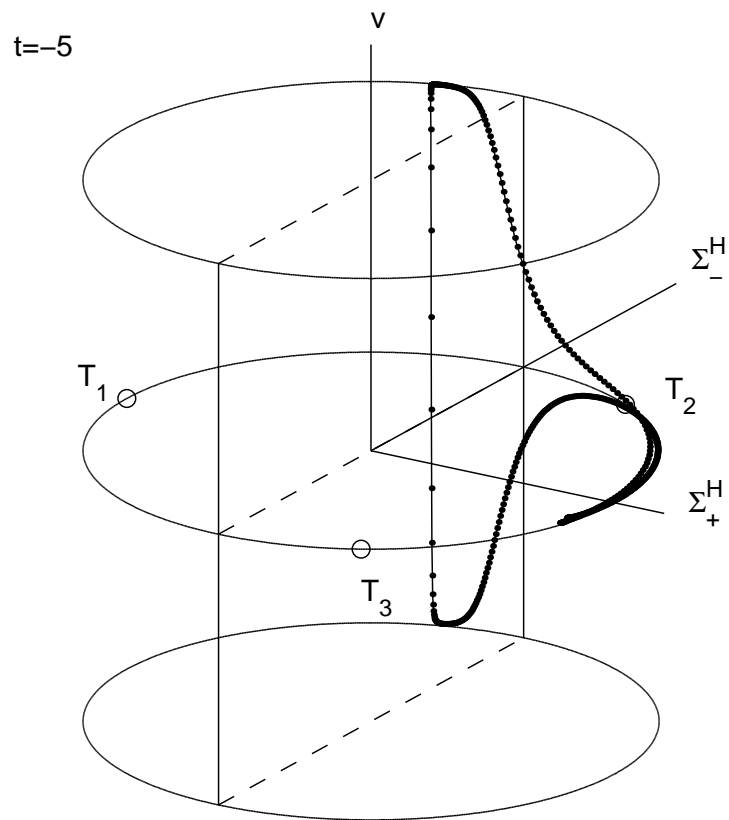


Figure 9.9: Snapshot of the variables $(\Sigma_+^H, \Sigma_-^H, v)$ in a diagonal G_2 cosmology at $t = -5$.

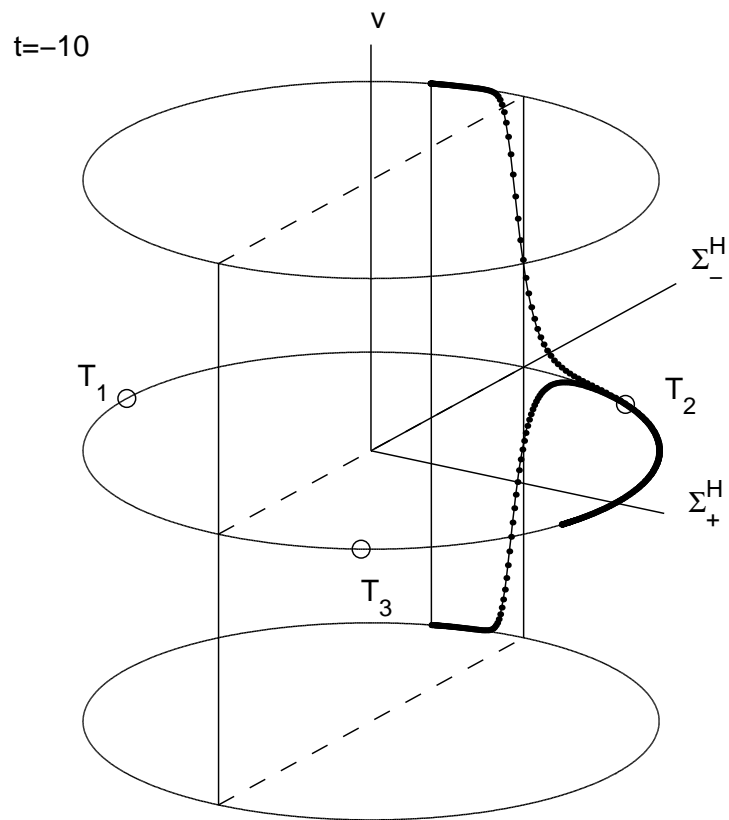


Figure 9.10: Snapshot of the variables $(\Sigma_+^H, \Sigma_-^H, v)$ in a diagonal G_2 cosmology at $t = -10$.

9.3.2 Spiky structures

We now illustrate spiky structures in the trigger N_- in OT G_2 cosmologies, and provide evidence to support the claim that the past attractor is given by (7.11):

$$\mathcal{A}^- = \mathcal{K} \operatorname{arc}(T_3 Q_1). \quad (9.9)$$

Recall that OT G_2 cosmologies satisfy (5.56):

$$\Sigma_2 = 0. \quad (9.10)$$

Consider the following initial data at $t = 0$ with $\gamma = \frac{4}{3}$ (in conjunction with (9.1) and (9.10)):

$$\begin{aligned} \epsilon = 0.1, \quad (E_1^1)_0 = 1, \quad A_0 = 0, \quad (\Sigma_-)_0 = 0.2, \quad (\Sigma_\times)_0 = 0.2, \\ (N_-)_0 = 0, \quad \Omega_0 = 0.6, \quad (\Omega_\Lambda)_0 = 0.1, \quad \Sigma_2 \equiv 0. \end{aligned} \quad (9.11)$$

We ran **CLAWPACK** with 512 grid points, from $t = 0$ to $t = -10$, storing data at intervals of $t = 0.1$. Figure 9.11 shows the snapshots of Σ_- and the trigger N_- at $t = -2$, $t = -6$ and $t = -8$. We see the strong suggestion that spikes develop as $t \rightarrow -\infty$. Figure 9.12 shows the snapshots of the variables $(\Sigma_+^H, \Sigma_-^H, N_-^H)$ in the $(\Sigma_+^H, \Sigma_-^H, N_-^H)$ space. Each dot represents the state at a grid point. We see that the solution shadows the Taub vacuum Bianchi II orbits on the sphere (6.70):

$$1 = (N_-^H)^2 + (\Sigma_+^H)^2 + (\Sigma_-^H)^2$$

along some grid points, as it approaches the stable Kasner arc between T_3 and Q_1 . This may be compared with the Taub vacuum Bianchi II orbits shadowed by the transformed WM solution in Figure 6.2. There are two points stuck on the arc to the left of the T_3 Taub Kasner point, creating two spikes. Along all other grid points, the orbits approach the past attractor (9.9). The points closest to T_3 take the longest to traverse the Taub vacuum Bianchi II orbits.

The simulations also confirm that

$$\lim_{t \rightarrow -\infty} \partial_1 \mathbf{X} = 0, \quad (9.12)$$

along spike points, despite large spatial gradients. Thus asymptotic silence

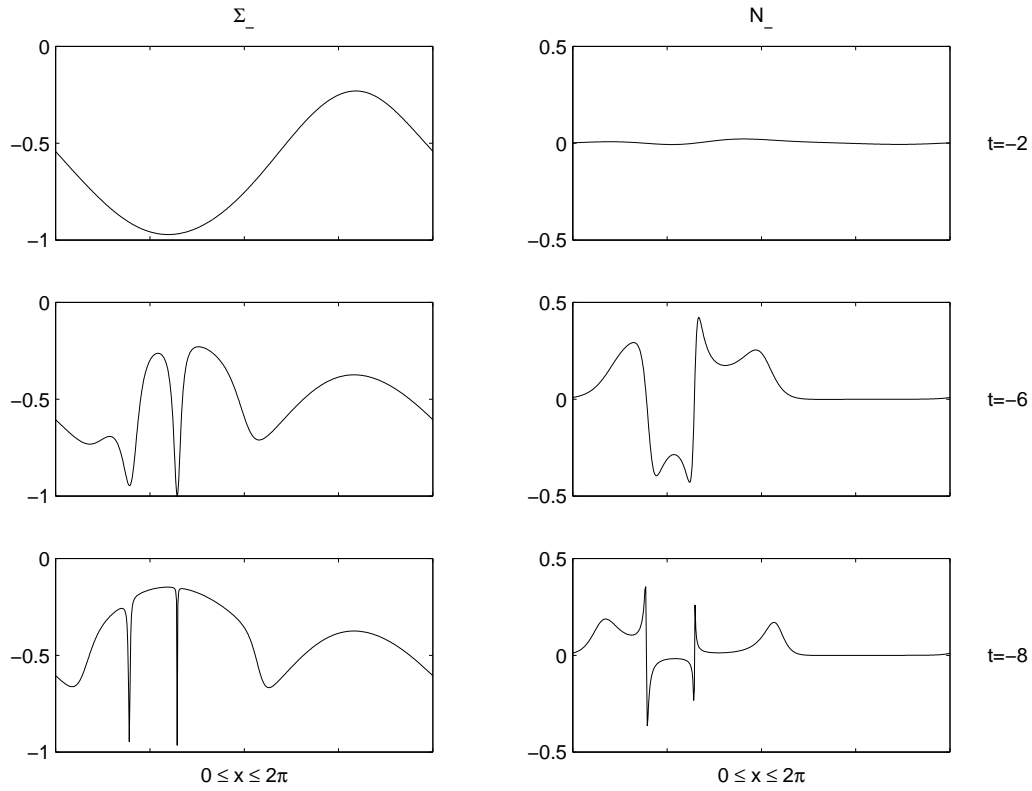


Figure 9.11: Snapshots of Σ_- and the trigger N_- at $t = -2$, $t = -6$ and $t = -8$, showing the asymptotic signature $(\Sigma_-)_{\text{sig}}(x)$ and the formation of permanent spikes in N_- .

holds along spike points. Our result has been mentioned in Andersson *et al.* 2004 [3, page S50].

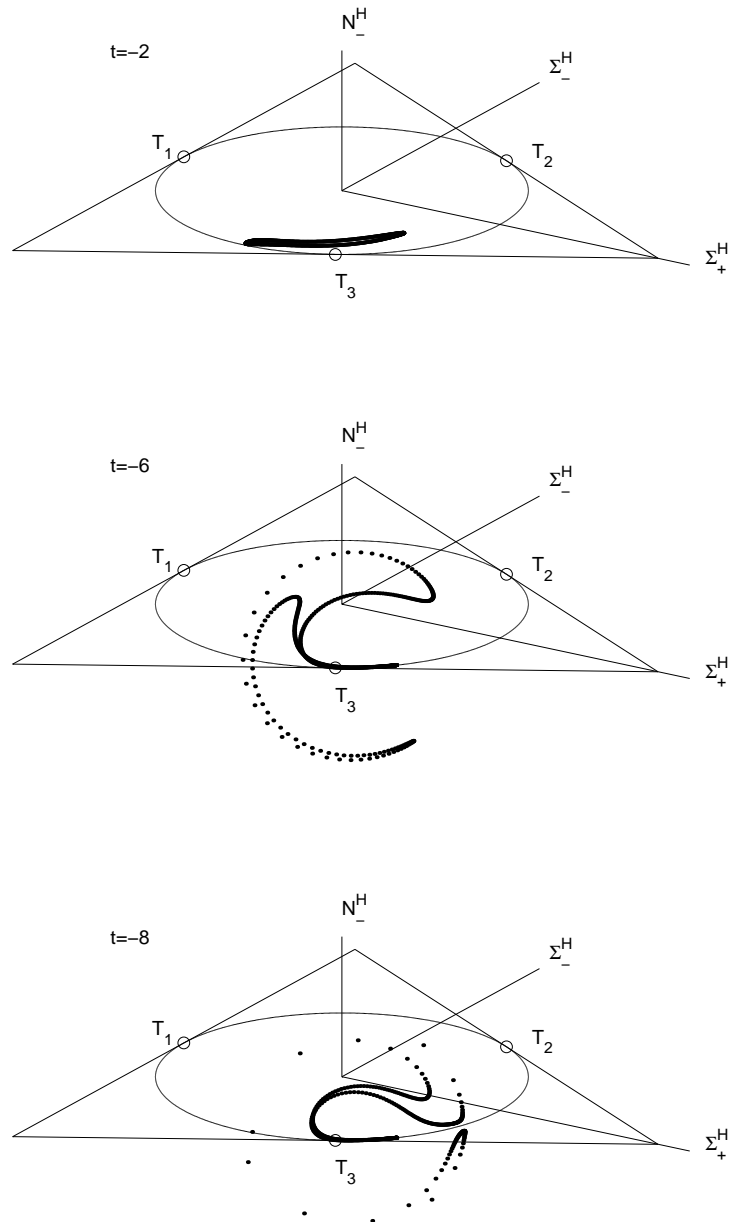


Figure 9.12: Snapshots of the variables $(\Sigma_+^H, \Sigma_-^H, N_-^H)$ in the $(\Sigma_+^H, \Sigma_-^H, N_-^H)$ space. Each dot represents the solution at a grid point.

9.4 Effects of spatial inhomogeneity II: role of spatial derivative terms

In this section, we illustrate the role of spatial derivative terms in creating spike transitions and shock waves.

9.4.1 Spike transitions

Consider the following initial data at $t = 0$ with $\gamma = \frac{4}{3}$ (in conjunction with (9.1)):

$$\begin{aligned} \epsilon = 0.1, \quad (E_1^1)_0 = 1, \quad A_0 = 0, \quad (\Sigma_-)_0 = 0.2, \quad (\Sigma_\times)_0 = 0.2, \\ (N_-)_0 = 0, \quad \Omega_0 = 0.6, \quad (\Omega_\Lambda)_0 = 0.1, \quad (\Sigma_2)_0 = 0.1. \end{aligned} \quad (9.13)$$

High resolution is essential to simulate a spike transition correctly. We ran CLAWPACK with 16384 grid points, from $t = 0$ to $t = -4$, storing data at intervals of $t = 0.1$.⁴

Figure 9.13 shows the orbits along three grid points: two typical points at grid number 3000 and 3500, and the spike point at grid number 3267. The typical points undergo a sequence of three transitions, while the spike point undergoes a spike transition. The spike transition orbit is a straight line, taking the solution to the Kasner point that is reached by the sequence of $N_- - \Sigma_\times - N_-$ transitions, in about the same time.

Figure 9.14 shows the snapshots of Σ_+^H , the triggers N_-^H , Σ_\times^H and the spatial derivative terms $(E_1^1)^H \partial_x N_-^H$, $(E_1^1)^H \partial_x \Sigma_\times^H$ on the interval between grid point 3000 and grid point 3500. A spike forms at $t = -2.6$ in all of the variables, but Σ_\times^H also activates at the spike point (grid point 3267), and develops a very steep gradient. In addition, $(E_1^1)^H \partial_x N_-^H$ and $(E_1^1)^H \partial_x \Sigma_\times^H$ develop spikes that have bigger amplitudes than the spikes in both N_-^H and Σ_\times^H . A reversal of the spike in N_-^H occurs some time between $t = -2.6$ and $t = -2.7$. The dynamics appears to be inherently inhomogeneous.

We now take a closer look at the dynamics. Figures 9.15–9.16 show the β -normalized terms in the evolution equations (D.6)–(D.7) for the pair (Σ_\times, N_-) . First, a spike forms in N_- with the same mechanism as permanent N_- spikes. From Figure 9.15, we see that $\partial_1 N_-$ is significant enough

⁴The simulation in Section 9.1 does not have high enough resolution to correctly simulate spike transitions, but was acceptable for the typical background SH dynamics.

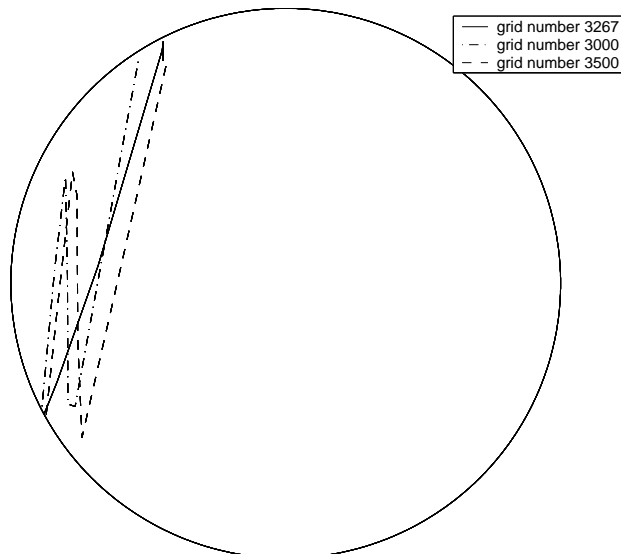


Figure 9.13: The orbit of an N_- spike transition along x_{spike} , from $t = -2.2$ to $t = -3.3$, projected onto the (Σ_+^H, Σ_-^H) plane, shown as a solid line. The orbits of a sequence of $N_- - \Sigma_\times - N_-$ transitions along two nearby grid points are shown as a dashed line and a dash-dot line.

that, when added to the algebraic terms on the right hand side of the $\partial_t \Sigma_\times$ equation, it leads to a sign change in $\partial_t \Sigma_\times$ at the spike point, which then activates Σ_\times at the spike point to start the spike transition. From Figure 9.16, we see that an active Σ_\times at the spike point in turn gives a $\partial_1 \Sigma_\times$ large enough that, when added to the algebraic terms on the right hand side of the $\partial_t N_-$ equation, it leads to a sign change in $\partial_t N_-$ at the spike point, which causes the reversal of the spike in N_- .

What separates transient spikes like these from the permanent spikes that we observed in OT G_2 cosmologies? Here, $\partial_1 N_-$ is large enough to activate Σ_\times at the spike point. In permanent spikes, $\partial_1 N_-$ is too small, so Σ_\times still decays to zero at the spike point. Whether $\partial_1 N_-$ is large enough depends on the Kasner point where the spike occurs (see Section 7.3).

The terminology *spike transition* is introduced by the author and was first referred to by Andersson *et al.* 2004 [3, page S50], who gave a survey of regular transitions in vacuum OT G_2 cosmologies, using Hubble-normalized

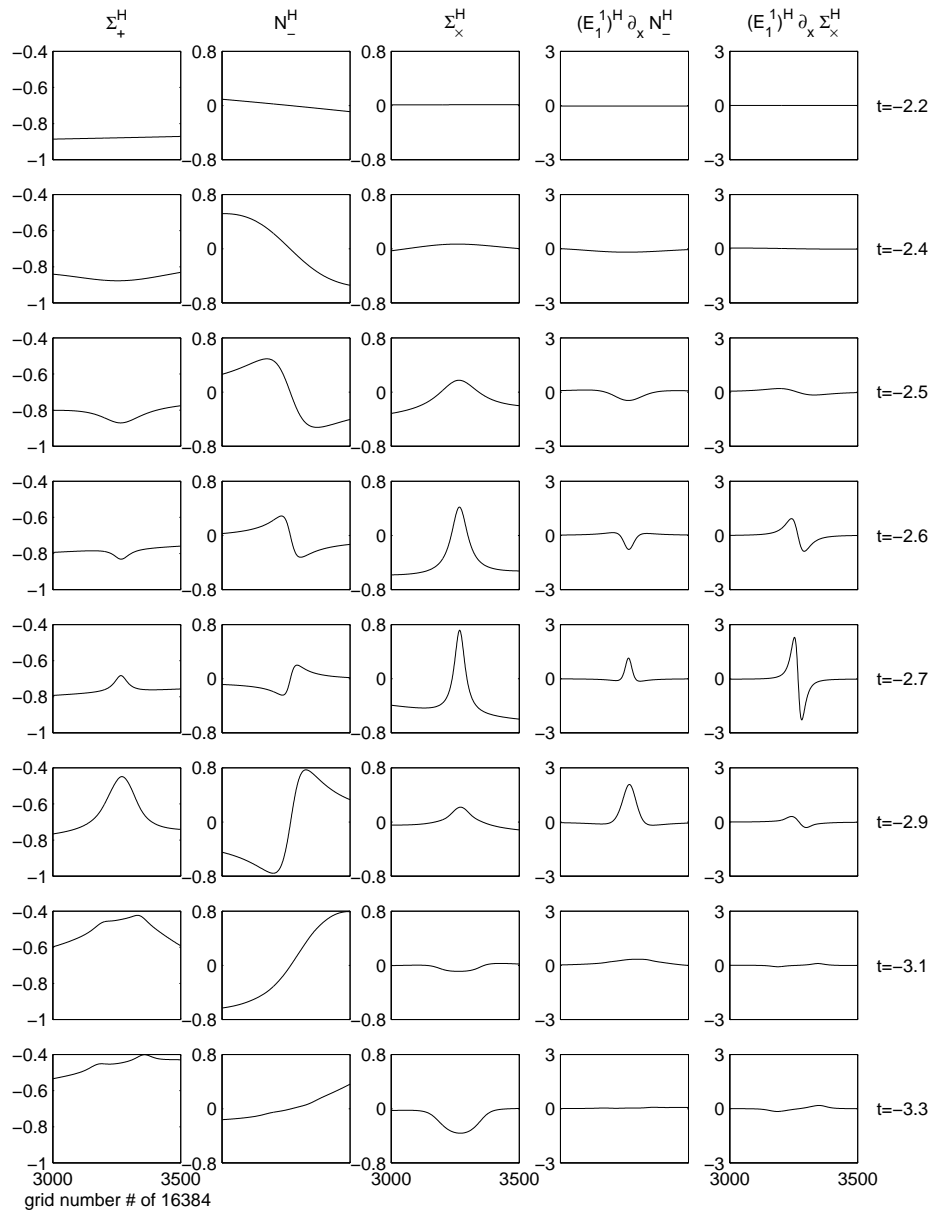


Figure 9.14: An N_- spike transition. Hubble-normalized variables are plotted. A reversal of the N_- spike occurs between $t = -2.6$ and $t = -2.7$.

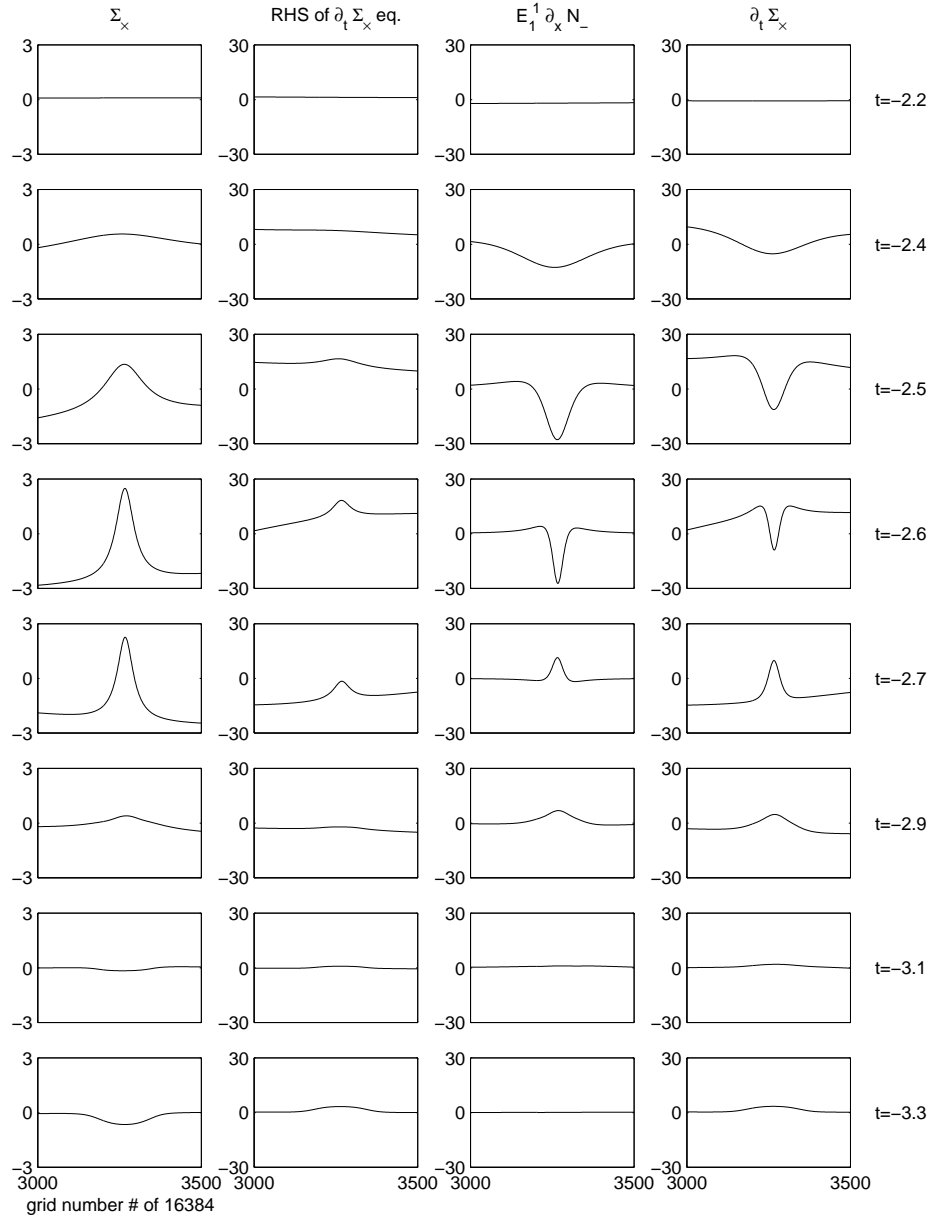


Figure 9.15: Influence of $E_1^1 \partial_x N_-$ on $\partial_t \Sigma_x$. At $t = -2.4$, $E_1^1 \partial_x N_-$ is large enough along the spike point that $\partial_t \Sigma_x$ changes sign, causing Σ_x to develop a spike.

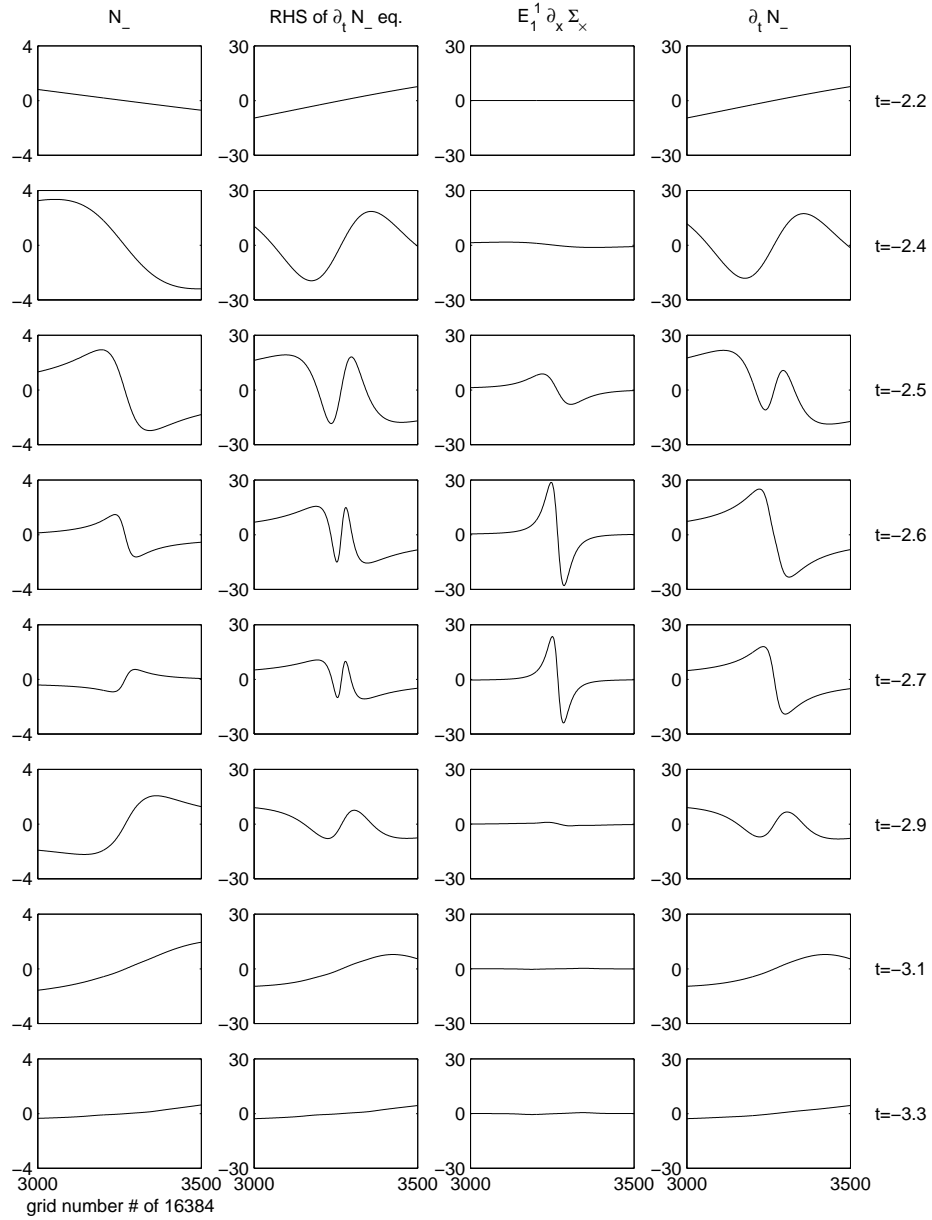


Figure 9.16: Influence of $E_1^1 \partial_x \Sigma_x$ on $\partial_t N_-$. The Σ_x spike that was started by a large $E_1^1 \partial_x N_-$ at $t = -2.4$, now becomes large enough at $t = -2.6$ that the slope of $\partial_t N_-$ changes sign, causing the reversal of the N_- spike at $t = -2.7$.

variables. By examining the interplay between N_- and Σ_\times , we shed new light on the mechanism of spike transitions, building on the work of Garfinkle & Weaver 2003 [25]. What we have seen here is the transition of a so-called high-velocity spike.⁵ In OT G_2 cosmologies, a high-velocity spike is by definition a transient spike, which either reappears as a permanent, low-velocity spike eventually or disappears [25].

Similarly, a transient spike can occur in Σ_\times , and will undergo a spike transition that is equivalent to a sequence of $\Sigma_\times - N_- - \Sigma_\times$ transitions.

The simulation also suggests that spike transitions may violate asymptotic silence: as $t \rightarrow -\infty$, E_1^1 tends to zero, but r becomes large during a spike transition, due to the term $N_- \Sigma_\times$ (see equation (D.14)).⁶ In other words, during a spike transition, the orbit does not shadow the silent boundary. If spike transitions occur indefinitely as $t \rightarrow -\infty$, then asymptotic silence is violated. Inadequate numerical spatial resolution confines the simulations to very short times, so we have not been able to accurately simulate two consecutive spike transitions.⁷ We shall leave this for future research.

There are still questions about what happens to low-velocity spikes in generic G_2 cosmologies. Will they be permanent or will they undergo transitions? We have been unable to specify initial conditions that produce such transitions before numerical resolution becomes inadequate. We shall also leave this for future research.

⁵The so-called velocity is equal to $\sqrt{3}\sqrt{\Sigma_-^2 + \Sigma_\times^2}$, and a spike transition is called a “slide-down” in the velocity in [25] because $\Sigma_-^2 + \Sigma_\times^2$ decreases by a predicted amount during a spike transition. Garfinkle & Weaver also recognized that a sign change in the evolution equations is crucial for a spike transition.

⁶When doing linearization on the Kasner circles, we dropped the spatial derivative terms. The linearized evolution equations for N_- and Σ_\times indicate that $N_- \Sigma_\times$ tends to zero into the past. This linearization does not hold when the spatial derivative terms are large enough, as in the case of spike transitions.

⁷For a fixed grid size Δx , the largest gradient of a jump in a variable Y that can be represented is $(Y_{\max} - Y_{\min})/\Delta x$. A finer grid size is needed if the numerical gradient of a spike is observed to approach this upper bound and $E_1^1(Y_{\max} - Y_{\min})/\Delta x$ is observed to be growing, otherwise the numerical solution can underestimate $\partial_1 Y$ and thus can delay or even prevent a spike transition from occurring. This can mislead one to predict that spike transitions will eventually stop as $t \rightarrow -\infty$, or that $\partial_1 Y$ tends to zero as $t \rightarrow -\infty$ (see Andersson *et al.* 2004b [4], Figure 2).

9.4.2 Shock waves

Numerical experiments with shock waves show that the constraints $(\mathcal{C}_C)_3$ and (\mathcal{C}_β) (see (D.16)–(D.17)) are unstable numerically near shock waves. To avoid this problem, we shall set Ω_Λ and Σ_2 to zero. As mentioned in Section 8.2, the presence of $\partial_1 A$ on the right hand side may prevent the system from being symmetric hyperbolic, which may be bad for simulations of shock waves. To avoid this problem we shall set $A = 0$.

Consider the following initial data at $t = 0$ with $\gamma = \frac{4}{3}$ (using the scheme for the case $A = 0$ in Section 8.1.

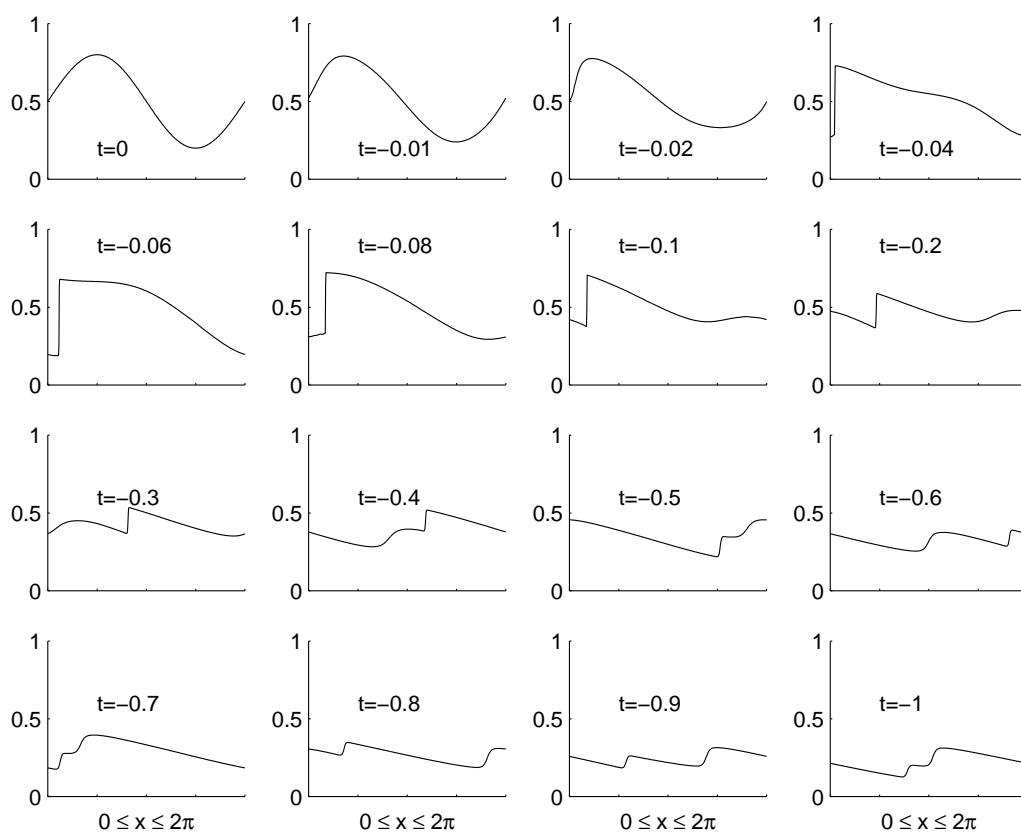
$$\begin{aligned} A &= 0 = \Sigma_2 = \Omega_\Lambda \\ E_1^{-1} &= 100, \quad \Sigma_- = 0.1, \quad \Sigma_\times = 0.01, \\ N_- &= 0.01, \quad N_\times = 0.01, \quad \Omega = 0.01, \quad v = 0.5 + 0.3 \sin x. \end{aligned} \quad (9.14)$$

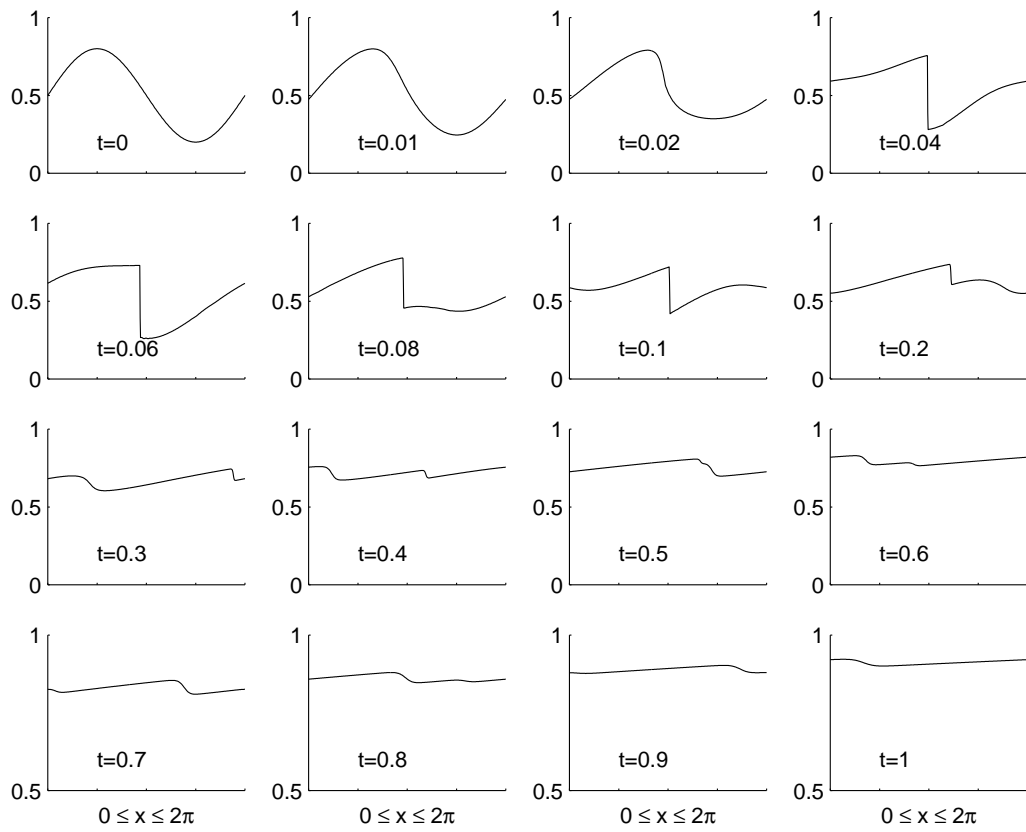
Here, a large E_1^{-1} is chosen to create inhomogeneities with a short-wavelength (relative to the horizon). The amplitude in the fluctuation of v is also chosen to be large. These conditions are favourable for the formation of shock waves.

We ran CLAWPACK with 512 grid points, from $t = 0$ to $t = -1$, and from $t = 0$ to $t = 1$ storing data at intervals of $t = 0.01$. Figures 9.17–9.18 show the formation of a shock wave in the tilt variable v into the past and into the future respectively.

The shock wave subsequently smoothes out or dissipates asymptotically. The mechanism of this dissipation is not clear. SH dynamics cannot dissipate a discontinuity, but would a small $\partial_1 \mathbf{X}$ term dissipate it?

Figure 9.19 shows a snapshot of all the variables into the future (at $t = 0.06$). We see that shock waves also appear in the profiles of Ω , Σ_+ , q and r , but not in Σ_\times , N_- and N_\times , which seem to become non-differentiable at the location of the shock wave, but still continuous. The profiles of E_1^{-1} and Σ_- seem smooth, but it could be that their non-differentiability is barely visible. Also plotted in Figure 9.19 are the β -normalized Weyl scalar $\mathcal{E}^2 - \mathcal{H}^2$ and the Hubble-normalized Weyl scalar $(\mathcal{E}^H)^2 - (\mathcal{H}^H)^2$.

Figure 9.17: Shock wave in v into the past.

Figure 9.18: Shock wave in v into the future.

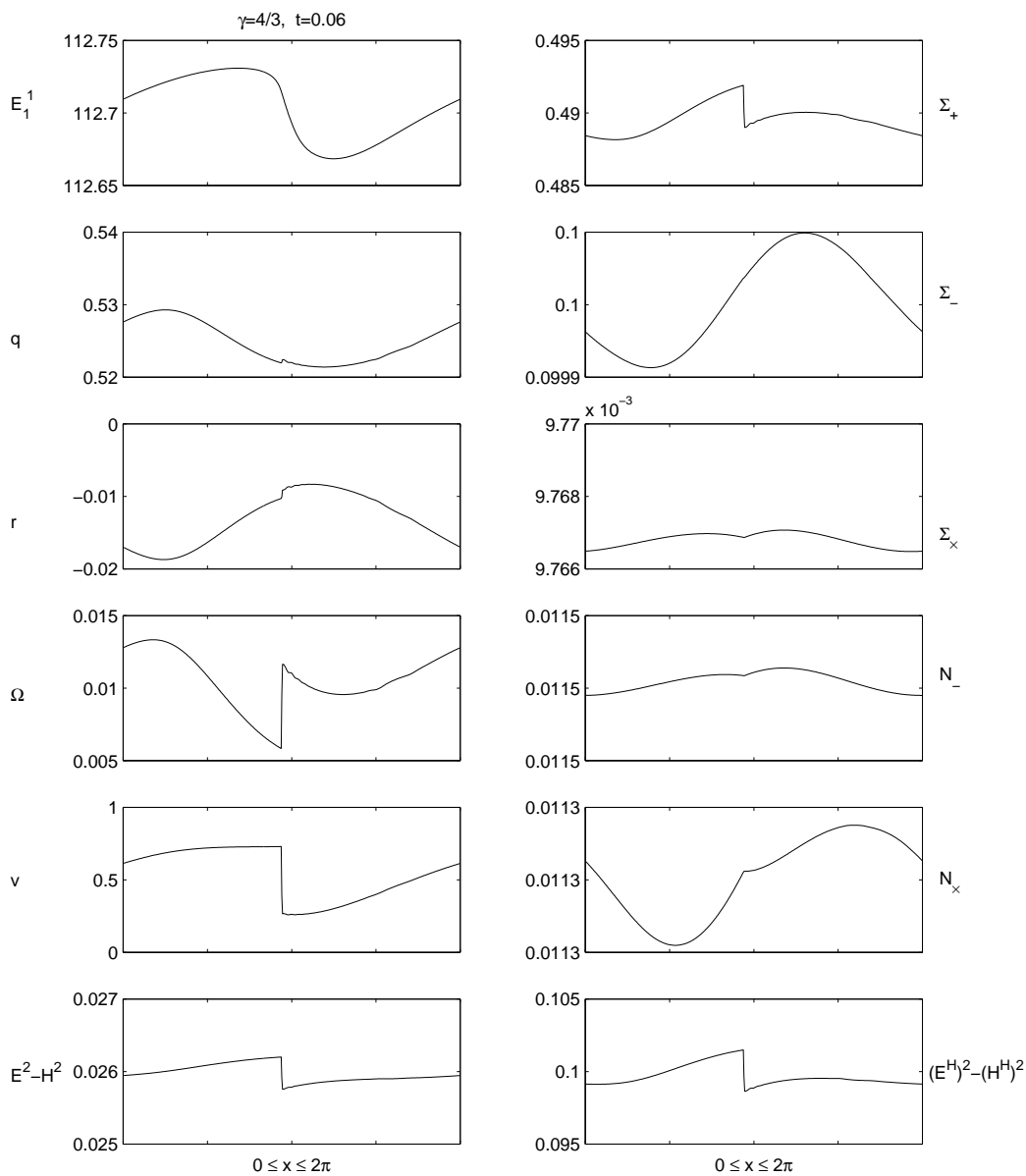


Figure 9.19: Snapshot of all variables, showing shock waves or non-differentiability into the future.

9.5 Future asymptotics

In this section, we illustrate the future asymptotic behaviour of the tilt variable v , as predicted by (5.70).

Consider three sets of the following initial data at $t = 0$, with $\gamma = 1.2, \frac{4}{3}$ and 1.5 (in conjunction with (9.1)):

$$\begin{aligned} \epsilon = 0.09, \quad (E_1^1)_0 = 1, \quad A_0 = 0.1, \quad (\Sigma_-)_0 = 0.2, \quad (\Sigma_\times)_0 = 0.2, \\ (N_-)_0 = 0.2, \quad \Omega_0 = 0.4, \quad (\Omega_\Lambda)_0 = 0.01, \quad (\Sigma_2)_0 = 0.1. \end{aligned} \quad (9.15)$$

Changing γ affects only the initial condition for v .

We ran ICN with 512 grid points, from $t = 0$ to $t = 10$, storing data at intervals of $t = 0.1$.

As predicted by (5.70), the limit of the tilt variable v depends on the parameter γ . Figure 9.20 plots the snapshots of v for the three solutions. This confirms that if $\gamma < \frac{4}{3}$, v tends to zero; if $\gamma = \frac{4}{3}$, v tends to a function of x that depends on the initial condition; for $\gamma > \frac{4}{3}$, v tends to ± 1 , depending on the initial condition.⁸

As mentioned in Section 9.1, the evolution is asymptotically silent as $t \rightarrow \infty$:

$$E_1^1 \rightarrow 0, \quad r \rightarrow 0, \quad (9.16)$$

and the solutions tend to

$$\Omega_\Lambda = 1, \quad (\Omega, A, \Sigma_+, \Sigma_-, \Sigma_\times, \Sigma_2, N_-, N_\times) = \mathbf{0}. \quad (9.17)$$

The numerical decay rates agree with the analytical results of Lim *et al.* 2004 [48]. Table 9.2 gives the predicted growth rates from [48], and the typical absolute errors of the numerical decay rates. The errors are small, indicating excellent agreement between numerical and analytical results. Note that for the case $\frac{4}{3}$, since v tends to an arbitrary function, we take $v(10, x)$ as the signature function, and determine the decay rate of $v(t, x) - v(10, x)$ at $t = 5$.

⁸That step-like structures can develop in the case $\gamma > \frac{4}{3}$ was first predicted by Rendall 2003 [61].

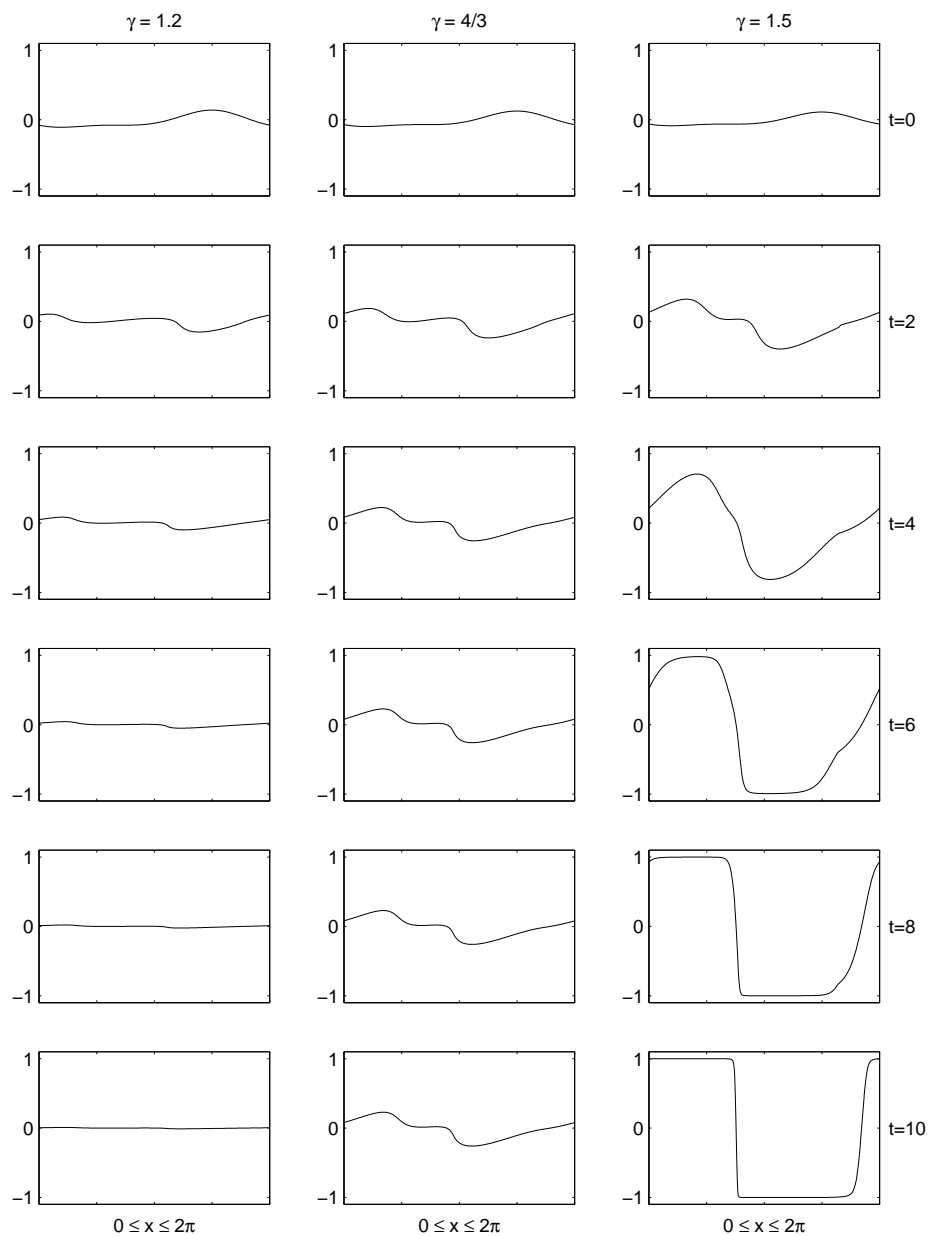


Figure 9.20: Snapshots of v for three solutions with $\gamma = 1.2$, $\frac{4}{3}$ and 1.5 , showing the asymptotic signature $v_{\text{sig}}(x)$ in the case $\gamma \geq \frac{4}{3}$.

Table 9.2: Predicted and actual growth rates at $t = 10$. Errors are obtained along typical timelines, ignoring irregular growth rates along timelines where a variable crosses zero.

Variable	predicted growth rate	Absolute error (order)		
		$\gamma = 1.2$	$\gamma = \frac{4}{3}$	$\gamma = 1.5$
E_1^1	-1	10^{-8}	10^{-8}	10^{-8}
A	-1	10^{-8}	10^{-8}	10^{-8}
r	-1	10^{-5}	10^{-3}	10^{-3}
Σ_+	-2	10^{-3}	10^{-3}	10^{-3}
Σ_-	-2	10^{-5}	10^{-5}	10^{-3}
Σ_\times	-2	10^{-3}	10^{-3}	10^{-3}
Σ_2	-3	10^{-9}	10^{-9}	10^{-9}
N_-	-1	10^{-5}	10^{-5}	10^{-5}
N_\times	-1	10^{-5}	10^{-5}	10^{-5}
$\Omega_\Lambda - 1$	-2	10^{-3}	10^{-5}	10^{-3}
Ω	-3γ	10^{-5}		
	-4		10^{-5}	
	-4			10^{-3}
v	$3\gamma - 4$	10^{-3}		
$v - v_{\text{sig}}(x)$	-1		10^{-2}	
$1 - v^2$	$\frac{2(3\gamma-4)}{2-\gamma}$			10^{-4}

9.6 Close-to-FL epoch

In this section, we describe the evolution of a cosmological model that is close to the flat FL solution at $t = 0$. By “close to flat FL” we mean the Hubble-normalized shear and the Weyl scalars are sufficiently small, and Ω is sufficiently close to 1 (see WE, page 62).

Consider the following initial data at $t = 0$ for an OT G_2 cosmology

($\Sigma_2 = 0$) with $\gamma = \frac{4}{3}$ (using the scheme for the case $A = 0$ in Section 8.1).

$$\begin{aligned} E_1^1 &= 1, & \Sigma_- &= 0.01 \sin 3x, & \Sigma_\times &= 0.01 \sin 5x, & N_- &= 0, & N_\times &= 0, \\ v &= 0.01 \sin x, & \Omega &= 0.98G_+, & G_+ &= 1 + (\gamma - 1)v^2, \\ r &= -2(0.98)(0.01) \sin x, \\ \Omega_\Lambda &= 10^{-6} \exp\left[-\frac{8}{E_1^1}(0.98)(0.01) \sin^2 \frac{x}{2}\right]. \end{aligned} \quad (9.18)$$

The initial value for Ω is chosen so that the initial value for Σ_+ is close to zero (see Figure 9.24).

We ran CLAWPACK with 512 grid points, from $t = 0$ to $t = -15$, storing data at intervals of $t = 0.1$, and from $t = 0$ to $t = 15$, storing data at intervals of $t = 0.005$.

Figure 9.21 shows the evolution along the grid point 100 of 512. The graphs of $\ln(E_1^1)^H$ and q^H show three distinct epochs – two asymptotic and one intermediate. They are the Kasner asymptotic epoch from $t = -15$ to $t = -4$, the flat FL intermediate epoch from $t = -4$ to $t = 3.48$, and the de Sitter asymptotic epoch from $t = 3.48$ to $t = 15$. The fact that the flat FL epoch is of finite duration is a reflection of the fact that the flat FL model is unstable⁹ into the future and into the past. The transition from the flat FL epoch to the de Sitter asymptotic epoch is rapid, with steep slopes in the graphs of Ω^H and Ω_Λ^H . The transition from the Kasner epoch to the flat FL epoch is less rapid, with a milder slope in the graph of Ω^H . The growth rate of E_1^1 is as expected, since $E_1^1 = (E_1^1)_0 e^{2t}$ for the Kasner solutions, $E_1^1 = (E_1^1)_0 e^t$ for the flat FL solution with $\gamma = \frac{4}{3}$, and $E_1^1 = (E_1^1)_0 e^{-t}$ for the de Sitter solution. As t increases, E_1^1 grows exponentially until $\Omega \approx \frac{1}{2}$ at $t = 3.48$, when E_1^1 reaches a maximum of 23.7902 and starts to decrease exponentially.¹⁰

Evolving into the past from $t = 0$, the solution enters the Kasner asymptotic regime and approaches the Kasner arc (T_3Q_1). A snapshot of the spatial profile at $t = -15$ would show two spikes forming in Σ_\times , and the asymptotic spatial signature, i.e. the dependence of Σ_- on x . This asymptotic behaviour

⁹In the Hubble-normalized SH state space, the flat FL solution is described by an equilibrium point that is a saddle point, reflecting its instability within the SH context. The simulations also reflect unstable inhomogeneous modes.

¹⁰Notice that the $(C_\beta)^H$ constraint has an unacceptably large error at about $t = 3.48$. As a result, the simulation loses accuracy temporarily. As mentioned in Section 8.4, stability of constraints is still an open issue in numerical simulations.

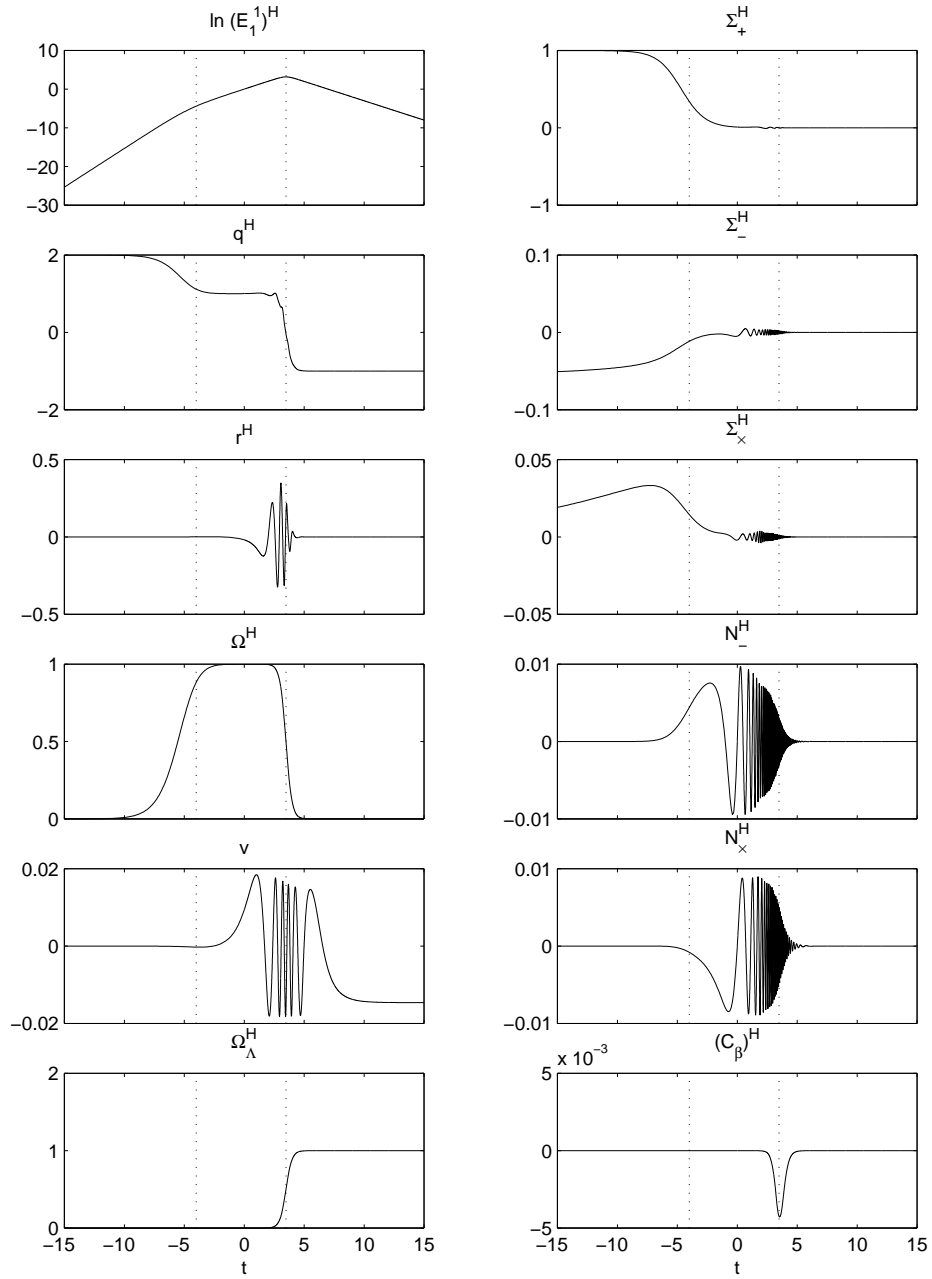


Figure 9.21: Evolution along a fixed timeline – from the past asymptote to the future asymptote.

is similar to the one shown in Figure 9.11.

Evolving far into the future, the solution approaches the de Sitter solution. A snapshot of the spatial profile at $t = 15$ would show the asymptotic spatial signature, i.e. the dependence of v on x . This asymptotic behaviour is qualitatively the same as the one shown in Figure 9.20.

We now take a detailed look at the close-to-FL intermediate epoch. Evolving into the future from $t = 0$, we observe oscillations in the variables. Figure 9.22 shows in detail the evolution during the close-to-FL epoch and the earlier part of the de Sitter epoch, during which these oscillations occur. We see 45 oscillations in the pair (Σ_\times, N_-) , 27 in (Σ_-, N_\times) , and 5 in v .¹¹ How do these numbers relate to the wavelengths of spatial inhomogeneities? Figure 9.25 shows the snapshot at $t = 3.48$, revealing that the wavelength of spatial inhomogeneities is $2\pi/5$ in the pair (Σ_\times, N_-) , $2\pi/3$ in (Σ_-, N_\times) , and 2π in (Ω, v) . $(\Sigma_-, N_\times, \Sigma_\times, N_-)$ are gravitational field variables, whose characteristic speed of propagation is the speed of light, while v is a matter field variable, whose characteristic speed of propagation is the speed of sound, given by $\sqrt{\gamma - 1}$ times the speed of light.¹² Comparing the numbers of oscillations with the wavelengths and taking into account the speeds of propagation, we have excellent agreement – we see $\frac{3}{5}$ as many oscillations in (Σ_-, N_\times) as in (Σ_\times, N_-) , because the wavelength of spatial inhomogeneities in (Σ_-, N_\times) is $\frac{5}{3}$ times as long. Since $\gamma = \frac{4}{3}$, we can predict that there should be $\sqrt{\frac{4}{3} - 1} \times \frac{1}{3} \approx 0.5774 \times \frac{1}{3}$ as many oscillations in v as in (Σ_-, N_\times) , because waves in v travel 0.5774 as fast as (Σ_-, N_\times) do, and the wavelength of spatial inhomogeneities in v is 3 times as long. The simulations agree with the prediction.

We also observe that the oscillations are most rapid at $t = 3.48$, when E_1^1 reaches its maximum. This is expected, because the frequency is equal to the speed of propagation divided by the wavelength. Recall from (5.85) that the coordinate speed of light is $E_1^1 \mathcal{N}$. Since we have chosen a t -coordinate such that $\mathcal{N} = 1$, for a fixed wavelength the frequency is proportional to E_1^1 . We note that the frequency depends on the choice of t -coordinate, and the physical frequency should be computed with respect to the clock time, for

¹¹There are also oscillations in Ω , approximately of amplitude 0.02, but these are not visible in the graph because of the scale.

¹²For characteristic eigenfields and their corresponding characteristic velocities of propagation, see van Elst *et al.* 2002 [74].

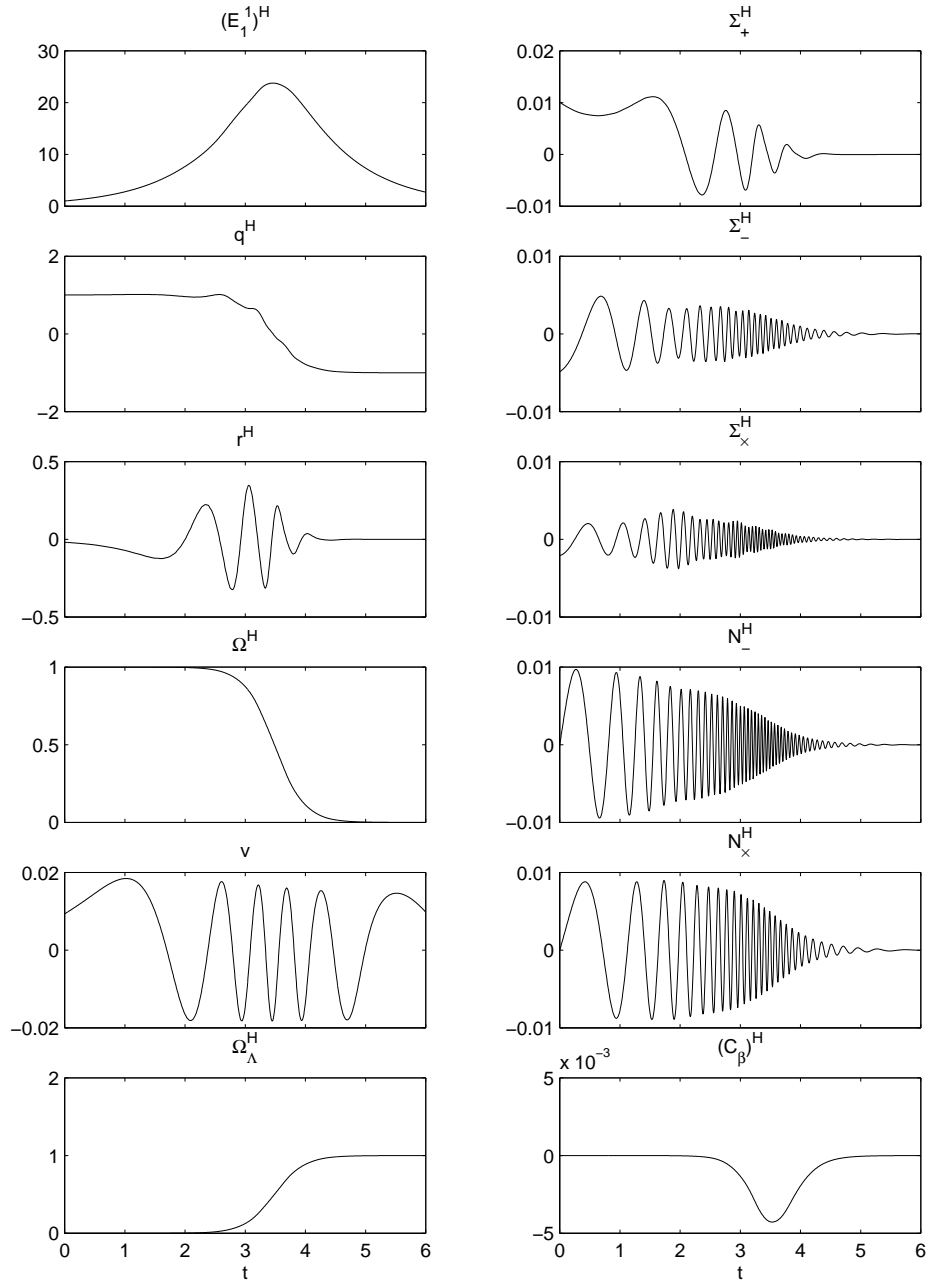


Figure 9.22: Evolution along a fixed timeline – details of the close-to-FL epoch.

which $\mathcal{N} = \beta$. Since $\beta \rightarrow \infty$ into the past and $\beta \rightarrow \sqrt{\frac{\Lambda}{3}}$ into the future, the physical frequency actually decreases with time.

With the shear and spatial curvature variables staying close to zero during the flat FL epoch and subsequently during the de Sitter epoch, the instability of the flat FL model appears to be primarily due to the growth of E_1^1 into the future, leading to growth in the Weyl curvature, which describes anisotropy in the free gravitational field.¹³ The spatial derivative terms are the largest at $t = 3.48$, when E_1^1 attains a maximum. The largest spatial derivative terms are $E_1^1 \partial_x \Sigma_\times$ and $E_1^1 \partial_x N_-$, both of which have magnitudes approximately equal to

$$\begin{aligned} \text{magnitude} &\approx \max\left(E_1^1(\Sigma_\times, N_-)\right) \times \frac{2\pi}{\text{wavelength}} \\ &\approx (24 \times 0.005) \times 5 = 0.6 . \end{aligned}$$

Thus the Weyl scalars \mathcal{E} and \mathcal{H} (see (4.117) and (5.35)–(5.44)), which contain spatial derivative terms, are approximately $\frac{1}{3} \times 0.6 = 0.2$ at $t = 3.48$. This growth in the Weyl curvature scalars mirrors the growth of E_1^1 and the decrease of the wavelength of inhomogeneities relative to the particle horizon. From $t = 3.48$ onwards, the Weyl curvature scalars decrease, reflecting the decrease of E_1^1 and the increase of the wavelength of inhomogeneities relative to the event horizon. Figure 9.23 shows the evolution of the Weyl scalars along the grid point 100 of 512, confirming the above argument.

We have performed a variety of simulations of G_2 cosmologies with a close-to-FL epoch. Decreasing the initial size of Ω_Λ will increase the duration of the flat FL epoch, defined by $\Omega \approx 1$, $\Sigma \approx 0$, into the future. On the other hand, this change will allow more time for E_1^1 to grow, which will in turn increase the Weyl scalars significantly. Increasing the initial value of E_1^1 will also increase the Weyl scalars. We comment that there are three modes (with two fields in each mode) that develop oscillations, namely (Ω, v) describing acoustic waves, and (Σ_-, N_\times) and (Σ_\times, N_-) describing gravitational waves. In the initial condition (9.18) we introduced three different wavelengths into the three modes ($\sin x$, $\sin 3x$ and $\sin 5x$). Coupling between these three modes does occur, but is rather weak. For example if $v = 0$ ini-

¹³Such behaviour can also occur in SH cosmologies of Bianchi type VII₀ (see Nilsson *et al.* 1999 [57]), i.e. the Hubble-normalized Weyl curvature can be large even though the Hubble-normalized shear is close to zero.

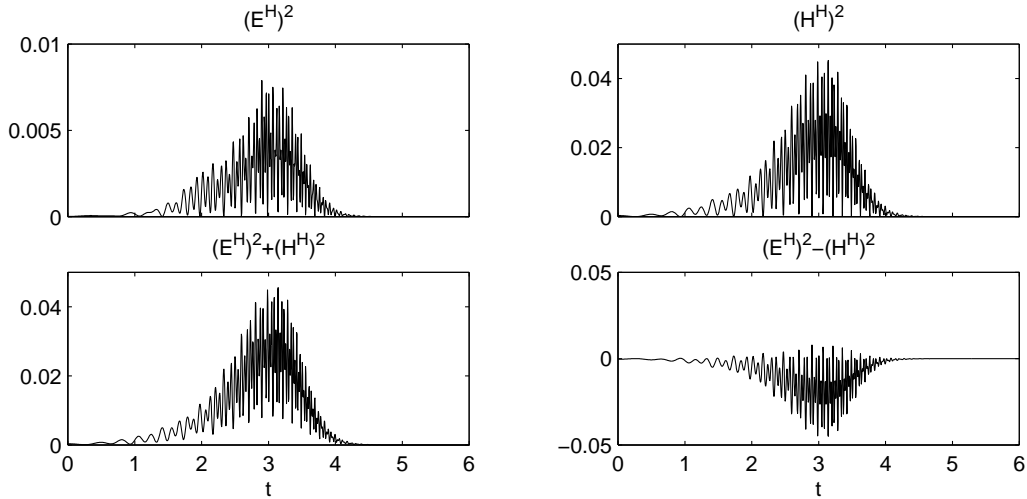


Figure 9.23: Evolution of the Hubble-normalized Weyl scalars along a fixed timeline, showing growth as E_1^1 increases.

tially the gravitational wave modes will subsequently turn v on, with $\sin 3x$ and $\sin 5x$ modes. We note that the two fields in each mode can have different wavelengths.

In conclusion we note that the simulations during the close-to-FL epoch $-4 \leq t \leq 3.48$ can be viewed as non-linear perturbations of the flat FL model. It would be interesting to use simulations of this nature to test the validity of the linear perturbations of the flat FL model that are used extensively in cosmology.

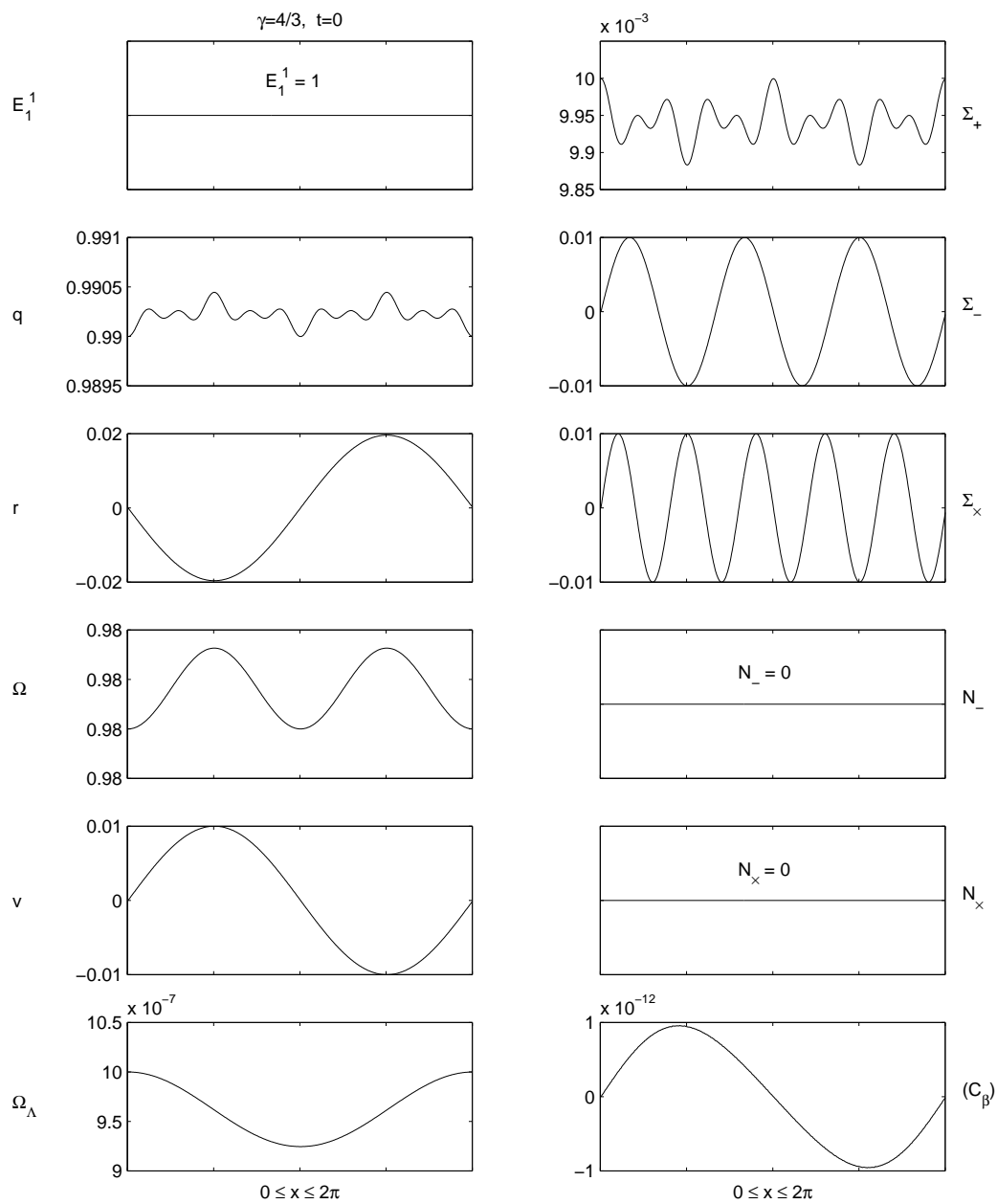


Figure 9.24: Snapshot of the initial condition at $t = 0$, showing a small Σ_+ .

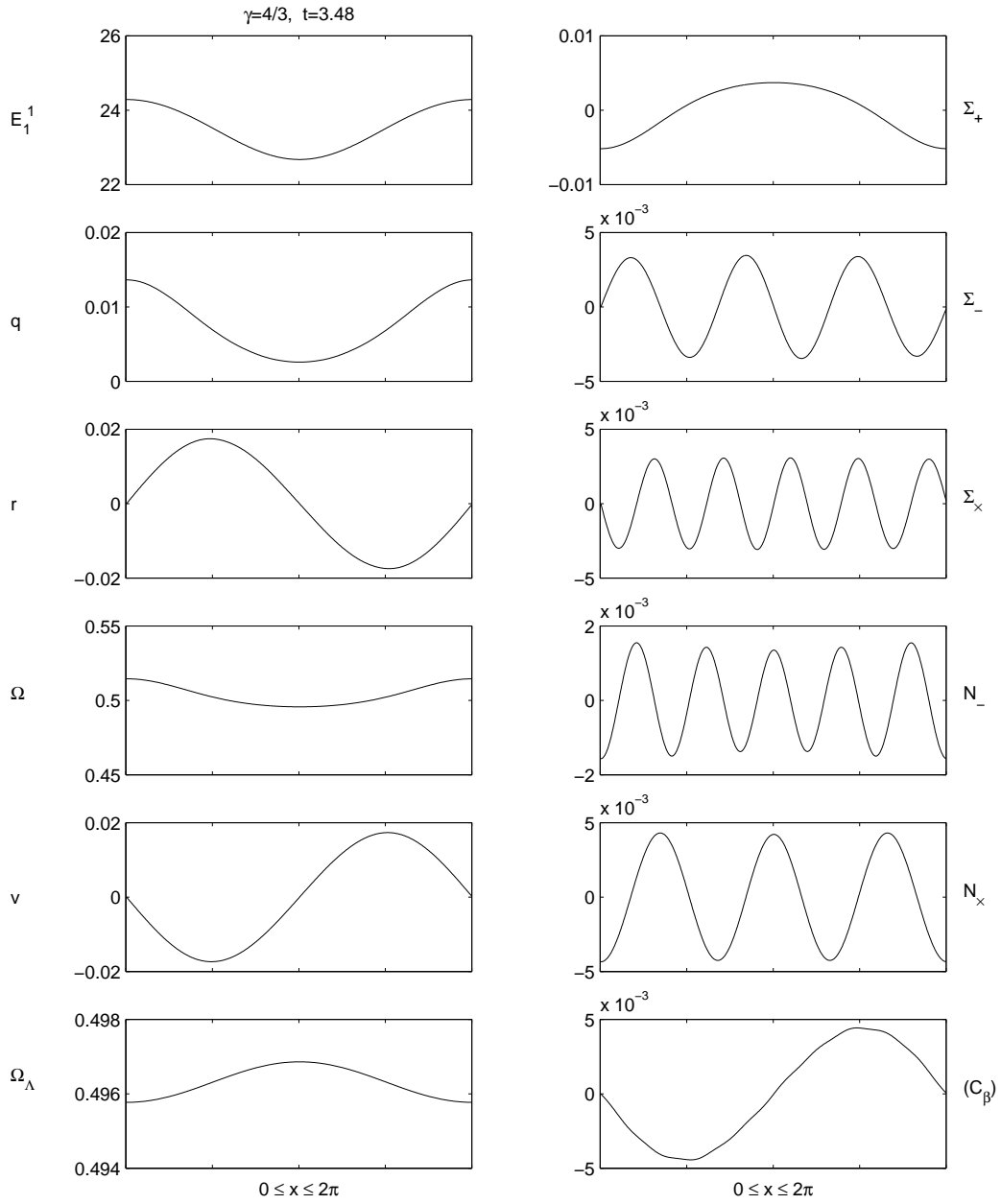


Figure 9.25: Snapshot at $t = 3.48$, showing the wavelengths in the different modes.

Chapter 10

Conclusion

In this thesis, by constructing a unified framework, analyzing explicit solutions, providing heuristic arguments, and performing numerical simulations, we have made considerable progress in understanding the dynamics of inhomogeneous cosmologies with one spatial degree of freedom, the so-called G_2 cosmologies. We have highlighted the role of spatially homogeneous cosmologies, in particular the tilted models, in providing the background dynamics.

The dynamics of tilted SH cosmologies is still not well-understood. In Chapter 3, we have given a unified classification scheme for G_2 cosmologies and for G_2 -compatible SH cosmologies, based on the G_2 action and on the tilt degrees of freedom. In Chapter 4, this classification leads to a unified system of equations and spatial gauge choice that is valid for G_2 -compatible SH cosmologies of all Bianchi types. By analyzing the stability of the Kasner equilibrium points, we have shown that the occurrence of Mixmaster dynamics is determined by the G_2 action, and that the tilt determines whether the fluid vorticity is dynamically significant near the initial singularity.

The notion of asymptotic silence provides the link between G_2 and SH dynamics. This link enabled us to establish that Mixmaster dynamics occurs in a G_2 cosmology if and only if the G_2 action is generic, by making use of the analysis of Mixmaster dynamics in SH cosmologies. We have also given the past attractors for subclasses of G_2 cosmologies that do not permit Mixmaster dynamics.

We have made significant progress in understanding the development of steep spatial gradients. In Chapter 6, we have given a detailed analysis of two classes of explicit solutions, the first one with step-like structures, and the second one with spikes. The second one is new, and is the only known

explicit G_2 solution with spikes. We have made a detailed comparison of the asymptotic size of different terms in the evolution equations, which revealed that spatial derivative terms are not always negligible. Furthermore, the growth of spatial derivative terms triggers the so-called spike transitions. As a result, the BKL conjecture II does not hold in general for G_2 cosmologies.

All numerical simulations of G_2 cosmologies to date have considered vacuum models, and have used a metric formulation. Chapter 9 is one of two pieces of work, the other being Andersson *et al.* 2004 [4] [2], in which numerical simulations of G_2 cosmologies have been performed in a dynamical system framework. Our work complements that of Andersson *et al.* in that they consider the past asymptotic dynamics of vacuum G_2 cosmologies, whereas we have considered the full range of the dynamics for non-vacuum models in which the matter content is a radiation perfect fluid and a positive cosmological constant.

Our simulations show that, for models that are close to FL at some time, the evolution consists of three distinct epochs, namely the past and future asymptotic epochs and the close-to-FL intermediate epoch. The numerical results support the following conclusions, within these epochs.

- Past asymptotic silence, future asymptotic silence (if $\Lambda > 0$), the BKL conjecture I, and the Kasner Attractivity Conjecture are valid along almost all orbits of a typical G_2 cosmology.
- Mixmaster dynamics occurs along a typical timeline of a typical G_2 cosmology in the past asymptotic regime, provided that the group action is generic.
- The dynamics in asymptotically silent regimes consists of the background SH dynamics and a spectrum of inhomogeneous phenomena, in which the trigger variables and the wavelengths of inhomogeneities play crucial roles.
- A trigger variable that has both signs causes step-like or spiky structures to form.
- A spike transition occurs if the spatial derivative of a trigger causes the time derivative in the evolution equation to change sign.
- Sufficiently short wavelength spatial inhomogeneities in the matter variables can lead to the formation of shock waves.

- A long enough close-to-FL epoch allows the wavelength of spatial inhomogeneities to decrease, which leads to wave-like phenomena and potentially a large Weyl curvature.
- Wave-like phenomena disappear as the solution enters the past asymptotic regime or the de Sitter future asymptotic regime, which is asymptotically silent.

We conclude by commenting on future research that this thesis leads to. Firstly, the unified formulation that we have given provides a framework for proving the conjectures, in particular the asymptotic silence conjecture, the BKL conjecture I, and the Kasner Attractivity Conjecture, that appear to govern the asymptotic dynamics of tilted SH and G_2 cosmologies. Secondly, the analysis of the tilted SH cosmologies can now be completed using the unified formulation. Thirdly, it is possible that further analysis of the close-to-FL simulations, which represent non-linear perturbations of the flat FL model, may shed light on an important question: how reliable are the standard linear perturbation analyses of the flat FL model, which play a fundamental role in cosmology?

Appendix A

G_2 action

In this appendix, we prove Proposition 3.1 in Section 3.1 about G_2 models with a hypersurface-orthogonal KVF. We split the proposition into two parts: Proposition A.1 and its corollary.

Proposition A.1. *Consider a G_2 model presented in a group-invariant orbit-aligned frame with \mathbf{e}_2 and \mathbf{e}_3 tangent to the G_2 orbits. Then the G_2 admits a hypersurface-orthogonal KVF if and only if*

$$\tilde{\sigma}_{AB}\tilde{n}^{AB} = 0, \quad \tilde{n}_{AB}\sigma^{1A}\sigma^{1B} = 0, \quad *\tilde{\sigma}_{AB}\sigma^{1A}\sigma^{1B} = 0. \quad (\text{A.1})$$

Proof. “ \Rightarrow ”: Let ξ be a HO KVF, i.e.

$$\xi_{[a;b}\xi_{c]} = 0. \quad (\text{A.2})$$

Expanding this yields

$$\xi_C\epsilon^{CB}\mathbf{e}_0(\xi_B) + \epsilon^{AB}\xi_B\gamma^C{}_{0A}\xi_C = 0 \quad (\text{A.3})$$

$$\xi_C\epsilon^{CB}\mathbf{e}_1(\xi_B) + \epsilon^{AB}\xi_B\gamma^C{}_{1A}\xi_C = 0 \quad (\text{A.4})$$

$$\gamma^C{}_{01}\xi_C = 0. \quad (\text{A.5})$$

Using (2.42), equations (A.5) simplifies to

$$\sigma_{1A}\xi^A = 0. \quad (\text{A.6})$$

The group-invariant frame yields

$$\mathbf{e}_0(\xi^B) + \gamma^B{}_{0A}\xi^A = 0 \quad (\text{A.7})$$

$$\mathbf{e}_1(\xi^B) + \gamma^B{}_{1A}\xi^A = 0, \quad (\text{A.8})$$

which are then contracted with $\xi_C \epsilon^C{}_B$ and substituted into (A.3) and (A.4) to obtain

$${}^*\tilde{\sigma}_{AB}\xi^A\xi^B = 0 \quad \text{and} \quad \tilde{n}_{AB}\xi^A\xi^B = 0 \quad (\text{A.9})$$

respectively. Equations (A.6) and (A.9) combine to yield (A.1). \square

“ \Leftarrow ”: Assuming (A.1), use the rotation freedom to set ¹

$$n_- = 0. \quad (\text{A.12})$$

Then (A.1) yields

$$\sigma_{12} = 0, \quad \sigma_\times = 0. \quad (\text{A.13})$$

The evolution equations for n_- , σ_{12} and σ_\times , and the $(C_C)_2$ constraint then imply that

$$n_+ = 0, \quad \Omega_1 = 0. \quad (\text{A.14})$$

Equations (A.12)–(A.14) imply that the frame vector \mathbf{e}_2 is hypersurface-orthogonal. We also have, trivially,

$$\Omega_1 = -\sqrt{3}\sigma_\times, \quad n_+ = \sqrt{3}n_-. \quad (\text{A.15})$$

Using Lemma 1 below, this means \mathbf{e}_2 is parallel to a KVF. Thus this KVF is also hypersurface-orthogonal, and is independent of the choice (A.12). \square

¹For convenience we introduce the following notation:

$$n_C{}^C = 2n_+, \quad \tilde{n}_{AB} = \sqrt{3} \begin{pmatrix} n_- & n_\times \\ n_\times & -n_- \end{pmatrix}, \quad (\text{A.10})$$

and

$$\sigma_{12} = \sqrt{3}\sigma_3, \quad \sigma_{13} = \sqrt{3}\sigma_2. \quad (\text{A.11})$$

Lemma 1

Consider a G_2 model presented in a group-invariant orbit-aligned frame with \mathbf{e}_2 and \mathbf{e}_3 tangent to the G_2 orbits. Then

$$\Omega_1 = -\sqrt{3}\sigma_\times, \quad n_+ = \sqrt{3}n_- \quad (\text{A.16})$$

if and only if \mathbf{e}_2 is parallel to a KVF.

Proof. Let $\boldsymbol{\xi}$ and $\boldsymbol{\eta}$ be KVFs. As seen in the proof of the Proposition, the group-invariant frame yields

$$\mathbf{e}_0(\xi^B) + \gamma^B_{0A}\xi^A = 0 \quad (\text{A.17})$$

$$\mathbf{e}_1(\xi^B) + \gamma^B_{1A}\xi^A = 0, \quad (\text{A.18})$$

and likewise for $\boldsymbol{\eta}$.

“ \Leftarrow ”: Assuming $\boldsymbol{\xi}$ is parallel to \mathbf{e}_2 , we have $\xi_3 = 0$. Then (A.17)–(A.18) imply that

$$\gamma^3_{02} = 0 = \gamma^3_{12}, \quad (\text{A.19})$$

or equivalently (A.16), as required to prove. \square

“ \Rightarrow ”: Assuming (A.16), or equivalently,

$$\gamma^3_{02} = 0 = \gamma^3_{12}, \quad (\text{A.20})$$

we obtain the following:

$$\mathbf{e}_0(\xi_3) + \gamma^3_{03}\xi_3 = 0, \quad \mathbf{e}_1(\xi_3) + \gamma^3_{13}\xi_3 = 0, \quad (\text{A.21})$$

and likewise for $\boldsymbol{\eta}$. Equation (A.21) has a very special form. If $\xi_3 = 0$ at one point in spacetime, then (A.21) implies that $\xi_3 = 0$ at every point in spacetime.

If $\xi_3 = 0$ or $\eta_3 = 0$, then $\boldsymbol{\xi}$ or $\boldsymbol{\eta}$ is parallel to \mathbf{e}_2 and we are done. If not, pick any point P and a constant K so that

$$\xi_3 + K\eta_3 = 0 \quad \text{at P.} \quad (\text{A.22})$$

But $\xi_3 + K\eta_3$ satisfies the equations

$$\mathbf{e}_0(\xi_3 + K\eta_3) + \gamma^3_{03}(\xi_3 + K\eta_3) = 0, \quad \mathbf{e}_1(\xi_3 + K\eta_3) + \gamma^3_{13}(\xi_3 + K\eta_3) = 0, \quad (\text{A.23})$$

which now implies

$$\xi_3 + K\eta_3 = 0 \quad (\text{A.24})$$

at every point in spacetime. Thus $\xi + K\eta$ is parallel to \mathbf{e}_2 and we are done. \square

Corollary of Proposition A.1

Consider a G_2 model presented in a group-invariant orbit-aligned frame with \mathbf{e}_2 and \mathbf{e}_3 tangent to the G_2 orbits. If the G_2 admits a hypersurface-orthogonal KVF, then

$$\epsilon^{AB}q_A\sigma_{1B} = 0, \quad \epsilon^{AB}\pi_{1A}\sigma_{1B} = 0, \quad *\tilde{\pi}_{AB}\sigma^{1A}\sigma^{1B} = 0. \quad (\text{A.25})$$

Proof. Using (A.6) and (A.9), we simplify (A.7) and (A.8) to the following:

$$\mathbf{e}_0(\xi^A) = \Omega_1\epsilon_{AB}\xi^B \quad (\text{A.26})$$

$$\mathbf{e}_1(\xi^A) = \frac{1}{2}n_C{}^C\epsilon_{AB}\xi^B. \quad (\text{A.27})$$

We shall then differentiate (A.6) and (A.9). First, using (2.49) and (A.26), $\mathbf{e}_0(\sigma_{1A}\xi^A) = 0$ yields

$$\pi_{1A}\xi^A = 0, \quad (\text{A.28})$$

which implies

$$\epsilon^{AB}\pi_{1A}\sigma_{1B} = 0. \quad (\text{A.29})$$

Next, using (2.53) and (A.27), $\mathbf{e}_1(\sigma_{1A}\xi^A) = 0$ yields

$$q_A\xi^A = 0, \quad (\text{A.30})$$

which implies

$$\epsilon^{AB}q_A\sigma_{1B} = 0. \quad (\text{A.31})$$

Similarly, using (2.50) and (A.26), $\mathbf{e}_0(*\tilde{\sigma}_{AB}\xi^A\xi^B) = 0$ and $\mathbf{e}_1(\tilde{n}_{AB}\xi^A\xi^B) = 0$ combine to yield

$$*\tilde{\pi}_{AB}\xi^a\xi^B = 0, \quad (\text{A.32})$$

which implies

$$*\tilde{\pi}_{AB}\sigma^{1A}\sigma^{1B} = 0, \quad (\text{A.33})$$

as required. It also follows from (A.1) and (A.25) that

$$*\tilde{\pi}_{AB}\tilde{\sigma}^{AB} = 0, \quad \tilde{\pi}_{AB}\tilde{n}^{AB} = 0. \quad ^2 \tag{A.34}$$

□

²To show this, use the notation (A.10) and introduce the notation

$$(n_-, n_\times) = (n \cos \phi, n \sin \phi), \quad (\sigma_{12}, \sigma_{13}) = (\sigma \cos \theta, \sigma \sin \theta),$$

and similarly for $\tilde{\pi}_{AB}$.

Appendix B

Rotation formulae

For G_2 cosmologies, the spatial gauge freedom is represented by a position-dependent rotation of the spatial frame vectors $\{\mathbf{e}_2, \mathbf{e}_3\}$:

$$\begin{pmatrix} \hat{\mathbf{e}}_2 \\ \hat{\mathbf{e}}_3 \end{pmatrix} = \begin{pmatrix} \cos \phi & \sin \phi \\ -\sin \phi & \cos \phi \end{pmatrix} \begin{pmatrix} \mathbf{e}_2 \\ \mathbf{e}_3 \end{pmatrix}, \quad \phi = \phi(t, x). \quad (\text{B.1})$$

For G_2 -compatible SH cosmologies, the rotation is restricted to $\phi = \phi(t)$.

Writing the commutators using (B.1) gives the formulae for the transformation of the variables (regardless of β - or Hubble-normalization) under a rotation:

$$\hat{R} = R - \partial_t \phi, \quad (\text{B.2})$$

$$\hat{N}_+ = N_+ + \boldsymbol{\partial}_1 \phi, \quad (\text{B.3})$$

$$\begin{pmatrix} \hat{\Sigma}_3 \\ \hat{\Sigma}_2 \end{pmatrix} = \begin{pmatrix} \cos \phi & \sin \phi \\ -\sin \phi & \cos \phi \end{pmatrix} \begin{pmatrix} \Sigma_3 \\ \Sigma_2 \end{pmatrix}, \quad (\text{B.4})$$

$$\begin{pmatrix} \hat{v}_3 \\ \hat{v}_2 \end{pmatrix} = \begin{pmatrix} \cos \phi & \sin \phi \\ -\sin \phi & \cos \phi \end{pmatrix} \begin{pmatrix} v_2 \\ v_3 \end{pmatrix}, \quad (\text{B.5})$$

$$\begin{pmatrix} \hat{\Sigma}_- \\ \hat{\Sigma}_\times \end{pmatrix} = \begin{pmatrix} \cos 2\phi & \sin 2\phi \\ -\sin 2\phi & \cos 2\phi \end{pmatrix} \begin{pmatrix} \Sigma_- \\ \Sigma_\times \end{pmatrix}, \quad (\text{B.6})$$

$$\begin{pmatrix} \hat{N}_- \\ \hat{N}_\times \end{pmatrix} = \begin{pmatrix} \cos 2\phi & \sin 2\phi \\ -\sin 2\phi & \cos 2\phi \end{pmatrix} \begin{pmatrix} N_- \\ N_\times \end{pmatrix}. \quad (\text{B.7})$$

Other variables, namely E_1^1 , A , Σ_+ , r , q , Ω , v_1 and Ω_Λ , are not affected by the rotation.

Note that the determinant of N_{AB} , given by

$$\det N_{AB} = N_+^2 - 3(N_-^2 + N_\times^2), \quad (\text{B.8})$$

is invariant if $\phi = \phi(t)$, but will change if ϕ also depends on x . The sign of $\det N_{AB}$ is thus significant for G_2 -compatible SH cosmologies, but not for G_2 cosmologies.

Appendix C

Asymptotic expansions at spike points

For a general vacuum OT G_2 solution, Kichenassamy & Rendall 1998 [42, equations (5)–(6)] gave a generic expansion for the metric functions P and Q (see (6.39)–(6.40)):

$$P = -2k(x)t - \phi(x) + \dots \quad (\text{C.1})$$

$$Q = X_0(x) + e^{4k(x)t}\psi(x) + \dots, \quad (\text{C.2})$$

where $k(x)$ satisfies $0 < k(x) < 1$. The above expansion is inadequate in satisfying the evolution equations (6.34)–(6.37). To obtain an adequate expansion, we start with the vacuum Bianchi II solution

$$\Sigma_- = \frac{-\frac{2-k}{\sqrt{3}} - \frac{k}{\sqrt{3}}F^2}{1 + F^2}, \quad N_- = \pm \frac{\frac{2}{\sqrt{3}}(1-k)F}{1 + F^2}, \quad \Sigma_\times = N_\times = 0, \quad (\text{C.3})$$

where $F = F_0 e^{-2(1-k)t}$. We replace the constants k and F_0 by arbitrary functions of x and integrate the evolution equations (6.34)–(6.37) to obtain updated N_\times , Σ_\times , N_- and Σ_- in succession. Finally, we integrate the asymptotic expansion for Σ_- and Σ_\times to obtain the asymptotic expansion for P and Q , using (6.40).

The necessary expansion for P and Q is as follows:

$$P = -2k(x)t - \phi(x) + A(x)e^{4k(x)t} + B(x)e^{4(1-k)t} + C(x)e^{8k(x)t} + \dots \quad (\text{C.4})$$

$$Q = X_0(x) + \psi(x)e^{4k(x)t} + \theta(x)e^{8k(x)t} + \chi(x)e^{12k(x)t} \\ + \xi(x)te^{4t} + \zeta(x)e^{4t} + \dots, \quad (\text{C.5})$$

where

$$A = \psi^2 e^{-2\phi}, \quad B = -\frac{(X'_0)^2 e^{-2\phi}}{16(1-k)^2}, \quad C = -\frac{1}{2}A^2, \quad (\text{C.6})$$

$$\theta = -A\psi, \quad \chi = A^2\psi, \quad \xi = -\frac{k'X'_0}{4(1-k)}, \quad (\text{C.7})$$

$$\zeta = -2kB\psi + \frac{X''_0}{16(1-k)} - \frac{\phi'X'_0}{8(1-k)} - \frac{(2-k)}{4(1-k)}\xi. \quad (\text{C.8})$$

Rendall & Weaver 2001 [62] transform the Kichenassamy-Rendall expansion (C.1)–(C.2) to produce expansions for \tilde{P} , \tilde{Q}_t and \tilde{Q}_x for the transformed solution.¹ We shall transform (C.4)–(C.5) to obtain a consistent expansion for the transformed solutions $(\tilde{\Sigma}_-, \tilde{N}_x, \tilde{\Sigma}_x, \tilde{N}_-)$. The resulting expansions for the transformed solution are as follows. Along $x = x_{\text{spike}}(-\infty)$, where $X_0(x_{\text{spike}}(-\infty)) = 0$:²

$$\tilde{\Sigma}_- = -\frac{1}{\sqrt{3}}(1+k) + \frac{2}{\sqrt{3}}(1-k)Be^{4(1-k)t} + \mathcal{O}(e^{12kt} + e^{8(1-k)t} - te^{4t}) \quad (\text{C.9})$$

$$\tilde{N}_x = -\frac{1}{\sqrt{3}}k'(-te^{2t}) + \frac{1}{2\sqrt{3}}(2X'_0\psi e^{-2\phi} + \phi')e^{2t} + \mathcal{O}(-te^{2(1+2k)t}) \quad (\text{C.10})$$

$$\tilde{\Sigma}_x = -\frac{1}{2\sqrt{3}}X'_0e^{-\phi}e^{2(1-k)t} + \mathcal{O}(e^{2(1+k)t} + e^{6(1-k)t}) \quad (\text{C.11})$$

$$\tilde{N}_- = \frac{2}{\sqrt{3}}(1-k)\xi e^{-\phi}(-te^{2(2-k)t}) \\ - \frac{1}{2\sqrt{3}}e^{-\phi}[\xi + 4(1-k)\zeta + 8(1-k)B\psi]e^{2(2-k)t} \\ + \mathcal{O}(e^{14kt} - te^{2(4-3k)t} - te^{2(2+k)t}) \quad (\text{C.12})$$

¹The temporal and spatial coordinates used by Rendall & Weaver 2001 [62] are τ and x_{RW} , which are related to ours according to $\tau = -2t$, $x_{RW} = 2x$. For example, $X'_0(x)$ here would correspond to $2X'_0(x_{RW})$ in [62].

²It turns out that the asymptotic expansions for $\partial_t \tilde{\Sigma}_-$, $\partial_t \tilde{N}_x$, $\partial_t \tilde{\Sigma}_x$ and $\partial_t \tilde{N}_-$ are the same as the time derivative of the asymptotic expansions (C.9)–(C.12), and so we do not list them.

$$\partial_1 \tilde{N}_\times = \frac{1}{\sqrt{3}}(X'_0)^2 e^{-2\phi} e^{4(1-k)t} + \mathcal{O}(e^{8(1-k)t} - te^{4t}) \quad (\text{C.13})$$

$$\begin{aligned} \partial_1 \tilde{\Sigma}_- &= -\frac{1}{\sqrt{3}}k'e^{2t} + \frac{4}{\sqrt{3}}(1-k) [X'_0 \xi e^{-2\phi} + 2k'B] (-te^{2(3-2k)t}) \\ &\quad + \left[-\frac{1}{\sqrt{3}}X'_0 \xi e^{-2\phi} + \frac{2}{\sqrt{3}}(1-k)B' - \frac{2}{\sqrt{3}}[4(1-k)X'_0 \psi e^{-2\phi} + k']B \right. \\ &\quad \left. - \frac{4}{\sqrt{3}}(1-k)X'_0 \zeta e^{-2\phi} \right] e^{2(3-2k)t} \\ &\quad + \mathcal{O}(-te^{2(5-4k)t} - te^{2(1+6k)t}) \end{aligned} \quad (\text{C.14})$$

$$\partial_1 \tilde{N}_- = \frac{2}{\sqrt{3}}kX'_0 e^{-\phi} e^{2(1-k)t} + \mathcal{O}(e^{6(1-k)t}) \quad (\text{C.15})$$

$$\begin{aligned} \partial_1 \tilde{\Sigma}_\times &= -\sqrt{3}k'X'_0 e^{-\phi} (-te^{2(2-k)t}) \\ &\quad + \frac{1}{2\sqrt{3}} [4(X'_0)^2 \psi e^{-3\phi} - X''_0 e^{-\phi} + 3X'_0 \phi' e^{-\phi}] e^{2(2-k)t} \\ &\quad + \mathcal{O}(-te^{2(4-3k)t} - te^{2(2+k)t}) . \end{aligned} \quad (\text{C.16})$$

Along typical points: ³

$$\begin{aligned} \tilde{\Sigma}_- &= -\frac{1}{\sqrt{3}}(1-k) - \frac{2}{\sqrt{3}}k\left(\frac{e^{2\phi}}{X_0^2} + 2\frac{\psi}{X_0} + A\right)e^{4kt} - \frac{2}{\sqrt{3}}(1-k)Be^{4(1-k)t} \\ &\quad + \mathcal{O}(e^{8kt} + e^{8(1-k)t} - te^{4t}) \end{aligned} \quad (\text{C.17})$$

$$\tilde{N}_\times = \frac{1}{\sqrt{3}}k'(-te^{2t}) + \frac{1}{2\sqrt{3}} \left[2\frac{X'_0}{X_0} - \phi' \right] e^{2t} + \mathcal{O}(-te^{2(1+2k)t} - te^{2(3-2k)t}) \quad (\text{C.18})$$

$$\tilde{\Sigma}_\times = \frac{1}{2\sqrt{3}}X'_0 e^{-\phi} e^{2(1-k)t} + \mathcal{O}(-te^{2(1+k)t} + e^{6(1-k)t}) \quad (\text{C.19})$$

$$\tilde{N}_- = \frac{2}{\sqrt{3}}k\left(\frac{e^\phi}{X_0} + \psi e^{-\phi}\right)e^{2kt} + \mathcal{O}(e^{6kt} - te^{2(2-k)t}) . \quad (\text{C.20})$$

The above expansion is consistent with the evolution equations (6.34)–(6.37). To simplify to the expansion for the transformed WM solution in Section 7.2, set

$$k = \frac{1}{2}, \quad \phi = 0, \quad \psi = f_1, \quad X'_0 = -2f_1, \quad X''_0 = 4f_2 . \quad (\text{C.21})$$

In this case, the $A(x)$ and $B(x)$ terms have the same power and they cancel each other in the expansion for P , since $A(x) = -B(x)$ from (C.6) and (C.21).

The above expansion is a new result, and provides the asymptotic expansion in the framework of the orthonormal frame formalism.

³It turns out that the asymptotic expansions for the temporal and spatial derivatives of $\tilde{\Sigma}_-$, \tilde{N}_\times , $\tilde{\Sigma}_\times$ and \tilde{N}_- are the same as the temporal and spatial derivatives of the asymptotic expansions (C.17)–(C.20), and so we do not list them.

Appendix D

Equations for numerical simulations of G_2 models

Following the derivation in Section 5.1, we arrive at a system of equations (5.8)–(5.29) with β -normalized variables for G_2 cosmologies. As mentioned at the beginning of Chapter 8, we shall restrict our considerations to G_2 cosmologies with one tilt degree of freedom. In doing so, the shear spatial gauge (5.46) simplifies to (8.2):

$$\Sigma_3 = 0, \quad N_+ = \sqrt{3}N_-, \quad R = -\sqrt{3}\Sigma_\times . \quad (\text{D.1})$$

We drop the index on the remaining tilt variable v_1 , and simplify the evolution equation (5.33) for v^2 by collecting the $\partial_1(v^2)$, $\partial_1 \ln G_+$ and $\partial_1 v_1$ terms into an $E_1^1 \partial_x v$ term. As explained in Chapter 8, we solve the constraint (5.21) to determine Σ_+ .

Since E_1^1 and A have the same evolution equation, we can save numerical resources by writing

$$A = B(x)E_1^1 \quad (\text{D.2})$$

and evolve E_1^1 only, and obtain $B(x)$ from the initial conditions. See Section 8.1 for more discussion of the initial conditions.

Numerical experiments show that E_1^1 , Σ_2 , Ω and v are prone to getting out of range, e.g. Ω becoming negative. To prevent this we evolve $\ln E_1^1$, $\ln \Sigma_2$, $\ln \Omega$ and $\text{arctanh } v$ instead.

The resulting system for numerical simulations, given below, consists of 9 evolution equations (D.3)–(D.11) and two constraint equation (D.16)–(D.17).

Evolution equations:

$$\partial_t \ln E_1^1 = q + 3\Sigma_+ \quad (\text{D.3})$$

$$\partial_t \Sigma_- + E_1^1 \partial_x N_\times = (q + 3\Sigma_+ - 2)\Sigma_- + 2AN_\times + 2\sqrt{3}(\Sigma_\times^2 - N_-^2) - \sqrt{3}\Sigma_2^2 \quad (\text{D.4})$$

$$\partial_t N_\times + E_1^1 \partial_x \Sigma_- = (q + 3\Sigma_+)N_\times \quad (\text{D.5})$$

$$\partial_t \Sigma_\times - E_1^1 \partial_x N_- = (q + 3\Sigma_+ - 2 - 2\sqrt{3}\Sigma_-)\Sigma_\times - 2AN_- - 2\sqrt{3}N_\times N_- \quad (\text{D.6})$$

$$\partial_t N_- - E_1^1 \partial_x \Sigma_\times = (q + 3\Sigma_+ + 2\sqrt{3}\Sigma_-)N_- + 2\sqrt{3}\Sigma_\times N_\times \quad (\text{D.7})$$

$$\partial_t \ln \Sigma_2 = q - 2 + \sqrt{3}\Sigma_- \quad (\text{D.8})$$

$$\begin{aligned} \partial_t \ln \Omega + \frac{\gamma v}{G_+} E_1^1 \partial_x \ln \Omega + \frac{\gamma G_- (1 - v^2)}{G_+^2} E_1^1 \partial_x (\text{arctanh } v) \\ = \frac{2\gamma}{G_+} \left[\frac{G_+}{\gamma} (q + 1) - \frac{1}{2} (1 - 3\Sigma_+) (1 + v^2) - 1 + Av \right] \end{aligned} \quad (\text{D.9})$$

$$\begin{aligned} \partial_t (\text{arctanh } v) + \frac{(\gamma - 1)(1 - v^2)}{\gamma G_-} E_1^1 \partial_x \ln \Omega \\ - \frac{[(3\gamma - 4) - (\gamma - 1)(4 - \gamma)v^2]v}{G_+ G_-} E_1^1 \partial_x (\text{arctanh } v) \\ = -(\gamma G_-)^{-1} \left[(2 - \gamma)G_+ r - \gamma v [3\gamma - 4 + 3(2 - \gamma)\Sigma_+] \right. \\ \left. + 2\gamma(\gamma - 1)Av^2 \right] \end{aligned} \quad (\text{D.10})$$

$$\partial_t \ln \Omega_\Lambda = 2(q + 1) , \quad (\text{D.11})$$

where

$$q + 3\Sigma_+ = 2(1 - A^2) + E_1^1 \partial_x A - 3\Sigma_2^2 - \frac{3}{2}(2 - \gamma) \frac{(1 - v^2)}{G_+} \Omega - 3\Omega_\Lambda \quad (\text{D.12})$$

$$\begin{aligned} \Sigma_+ = & \left[1 - A^2 + \frac{2}{3} E_1^1 \partial_x A + A \frac{\gamma v}{G_+} \Omega + 2A(N_\times \Sigma_- - N_- \Sigma_\times) \right. \\ & \left. - \Sigma_-^2 - \Sigma_\times^2 - \Sigma_2^2 - N_\times^2 - N_-^2 - \Omega - \Omega_\Lambda \right] / [2(1 - A^2)] \quad (\text{D.13}) \end{aligned}$$

$$r = -3A\Sigma_+ - 3N_\times \Sigma_- + 3N_- \Sigma_\times - \frac{3}{2} \frac{\gamma v}{G_+} \Omega \quad (\text{D.14})$$

$$G_\pm = 1 \pm (\gamma - 1)v^2 . \quad (\text{D.15})$$

Constraint equations:

$$0 = (\mathcal{C}_C)_3 = E_1^1 \partial_x \Sigma_2 - (r + 3A - \sqrt{3}N_\times) \Sigma_2 \quad (\text{D.16})$$

$$0 = (\mathcal{C}_\beta) = (E_1^1 \partial_x - 2r) \Omega_\Lambda . \quad (\text{D.17})$$

For simulations in the de Sitter asymptotic regime (where $\Omega_\Lambda - 1$ and $q + 1$ tend to zero), we use $\Omega_\Lambda - 1$ and $q + 1$ as variables to maintain numerical precision.

Bibliography

- [1] L. Andersson and A. D. Rendall, “Quiescent cosmological singularities”, 2001, *Commun. Math. Phys.*, **218**, 479–511.
- [2] L. Andersson, H. van Elst, W. C. Lim, and C. Uggla, “The past attractor in vacuum G_2 cosmology: a picture story”, in preparation, 2004.
- [3] L. Andersson, H. van Elst, and C. Uggla, “Gowdy phenomenology in scale-invariant variables”, 2004, *Class. Quant. Grav.*, **21**, S29–S57.
- [4] L. Andersson, H. van Elst, and C. Uggla, “Past asymptotic dynamics in vacuum G_2 cosmology”, 2004, *arXiv.org: gr-qc/0402051*.
- [5] K. Anguige, “A class of perfect-fluid cosmologies with polarised Gowdy symmetry and a Kasner-like singularity”, 2000, *arXiv.org: gr-qc/0005086*.
- [6] J. M. Bardeen, “Gauge-invariant cosmological perturbations”, 1980, *Phys. Rev. D*, **22**, 1882–905.
- [7] J. D. Barrow and J. Stein-Schabes, “Inhomogeneous cosmologies with cosmological constant”, 1984, *Phys. Lett. A*, **103**, 315–7.
- [8] V. A. Belinskii, I. M. Khalatnikov, and E. M. Lifschitz, “Oscillatory approach to a singular point in the relativistic cosmology”, 1970, *Adv. Phys.*, **19**, 525–73.
- [9] V. A. Belinskii, I. M. Khalatnikov, and E. M. Lifschitz, “A general solution of the Einstein equations with a time singularity”, 1982, *Adv. Phys.*, **31**, 639–67.
- [10] B. K. Berger and D. Garfinkle, “Phenomenology of the Gowdy model on $T^3 \times R$ ”, 1998, *Phys. Rev. D*, **57**, 4767–77.

- [11] B. K. Berger and V. Moncrief, “Numerical investigation of cosmological singularities”, 1993, *Phys. Rev. D*, **48**, 4676–87.
- [12] W. B. Bonnor and N. Tomimura, “Evolution of Szekeres’s cosmological models”, 1976, *Mon. Not. Roy. Astr. Soc.*, **175**, 85–93.
- [13] R. Bridson, unpublished work, 1997.
- [14] M. Bruni, P. K. S. Dunsby, and G. F. R. Ellis, “Cosmological perturbations and the physical meaning of gauge-invariant variables”, 1992, *Astrophys. J.*, **395**, 34–53.
- [15] B. Carter, “Black Hole Equilibrium State”, In C. DeWitt and B. S. DeWitt, editors, *Black Holes*, pages 57–214, New York, 1973. Gordon and Breach Science Publishers.
- [16] M. Choptuik, private communication, 2004.
- [17] P. Coles and F. Lucchin, *Cosmology: the origin and evolution of cosmic structure*, John Wiley and Sons, West Sussex, 1995.
- [18] A. A. Coley, Y. He, and W. C. Lim, “Isotropic singularity in inhomogeneous brane cosmological models”, 2004, *Class. Quant. Grav.*, **21**, 1311–1342.
- [19] C. B. Collins and G. F. R. Ellis, “Singularities in Bianchi cosmology”, 1979, *Phys. Rep.*, **56**, 67–105.
- [20] G. F. R. Ellis, “Dynamics of pressure-free matter in general relativity”, 1967, *J. Math. Phys.*, **8**, 1171–94.
- [21] G. F. R. Ellis, “Relativistic cosmology”, In R. K. Sachs, editor, *General Relativity and Cosmology, Proceedings of XLVII Enrico Fermi Summer School*, pages 104–182, London, 1971. Academic Press.
- [22] G. F. R. Ellis, “The Expanding Universe: A History of Cosmology from 1917 to 1960”, In D. Howard and J. Stachel, editors, *Einstein and the History of General Relativity*, pages 367–431, Boston, 1989. The Center for Einstein Studies.
- [23] G. F. R. Ellis and M. A. H. MacCallum, “A class of homogeneous cosmological models”, 1969, *Commun. Math. Phys.*, **12**, 108–141.

- [24] H. Friedrich and A. D. Rendall, “The Cauchy Problem for the Einstein Equations”, In B. G. Schmidt, editor, *Einstein’s Field Equations and Their Physical Implications: selected essays in honour of Jürgen Ehlers*, pages 127–223, Berlin, 2000. Springer.
- [25] D. Garfinkle and M. Weaver, “High velocity spikes in Gowdy space-times”, 2003, *Phys. Rev. D*, **67**, 124009.
- [26] S. W. Goode, “Analysis of spatially inhomogeneous perturbations of the FRW cosmologies”, 1989, *Phys. Rev. D*, **39**, 2882–92.
- [27] S. W. Goode and J. Wainwright, “Isotropic singularities in cosmological models”, 1985, *Class. Quant. Grav.*, **2**, 99–115.
- [28] B. Gustafsson, H-O. Kreiss, and J. Olinger, *Time dependent problems and difference methods*, Wiley, New York, 1995.
- [29] A. H. Guth, “Inflationary universe: A possible solution to the horizon and flatness problem”, 1981, *Phys. Rev. D*, **23**, 347–56.
- [30] D. Harnett, unpublished work, 1996.
- [31] D. Harnett, “Tilted Bianchi type V cosmologies with vorticity”, Master’s thesis, University of Waterloo, Canada, 1996.
- [32] S. Hervik, “The asymptotic behaviour of tilted Bianchi type VI₀ universes”, 2004, *Class. Quant. Grav.*, **21**, 2301–17.
- [33] S. Hervik and A. Coley, private communication, 2004.
- [34] C. G. Hewitt, *Asymptotic states of G₂ cosmologies*, PhD thesis, University of Waterloo, Canada, 1989.
- [35] C. G. Hewitt, R. Bridson, and J. Wainwright, “The asymptotic regimes of tilted Bianchi II cosmologies”, 2001, *Gen. Rel. Grav.*, **33**, 65–94.
- [36] C. G. Hewitt, J. T. Horwood, and J. Wainwright, “Asymptotic dynamics of the exceptional Bianchi cosmologies”, 2003, *Class. Quant. Grav.*, **20**, 1743–56.
- [37] C. G. Hewitt and J. Wainwright, “Dynamical systems approach to tilted Bianchi cosmologies: irrotational models of type V”, 1992, *Phys. Rev. D*, **46**, 4242–52.

- [38] J. T. Horwood, M. J. Hancock, D. The, and J. Wainwright, “Late-time asymptotic dynamics of Bianchi VIII cosmologies”, 2003, *Class. Quant. Grav.*, **20**, 1757–77.
- [39] F. Hoyle and R. J. Tayler, “The mystery of the cosmic helium abundance”, 1964, *Nature*, **203**, 1108–10.
- [40] W. Hu and M. White, “The Cosmic Symphony”, 2004, *Scientific American*, **290**, 44–53.
- [41] J. Isenberg and V. Moncrief, “Asymptotic behaviour of the gravitational field and the nature of singularities in Gowdy spacetimes”, 1990, *Ann. Phys. (N.Y.)*, **199**, 84–122.
- [42] S. Kichenassamy and A. D. Rendall, “Analytic description of singularities in Gowdy spacetimes”, 1998, *Class. Quant. Grav.*, **15**, 1339–55.
- [43] A. R. King and G. F. R. Ellis, “Tilted homogeneous cosmological models”, 1973, *Commun. Math. Phys.*, **31**, 209–242.
- [44] A. Krasinski, *Inhomogeneous Cosmological Models*, Cambridge University Press, Cambridge, 1997.
- [45] R. J. LeVeque, *Finite Volume Methods for Hyperbolic Problems*, Cambridge University Press, Cambridge, 2002.
- [46] E. M. Lifshitz and I. M. Khalatnikov, “Investigations in relativistic cosmology”, 1963, *Adv. Phys.*, **12**, 185–249.
- [47] W. C. Lim, unpublished calculations, 2000.
- [48] W. C. Lim, H. van Elst, C. Uggla, and J. Wainwright, “Asymptotic isotropization in inhomogeneous cosmology”, 2004, *Phys. Rev. D*, **69**, 103507.
- [49] H. Lin, R. P. Kirshner, S. A. Sackett, S. D. Landy, A. Oemler, D. L. Tucker, and P. L. Schechter, “The power spectrum of galaxy clustering in the Las Campanas redshift survey”, 1996, *Astrophys. J.*, **471**, 617–35.
- [50] L. Lindblom, M. A. Scheel, L. E. Kidder, H. P. Pfeiffer, D. Shoemaker, and S. A. Teukolsky, “Controlling the growth of constraints in hyperbolic evolution systems”, 2004, *Phys. Rev. D*, **69**, 124025.

- [51] P. K-H. Ma and J. Wainwright, “A dynamical systems approach to the oscillatory singularity in Bianchi cosmologies”, In Z. Perjés, editor, *Relativity Today*, pages 65–80, New York, 1992. Nova Science Publishers. Reprinted in *Deterministic Chaos in General Relativity*, edited by D. Hobill, A. Burd, A. Coley, Plenum Press, 1994.
- [52] M. A. H. MacCallum, “Cosmological models from a geometric point of view”, In E. Schatzman, editor, *Cargèse Lectures in Physics*, pages 61–174, New York, 1973. Gordon and Breach.
- [53] M. A. H. MacCallum, “Anisotropic and inhomogeneous relativistic cosmologies”, In S. W. Hawking and W. Israel, editors, *General relativity: An Einstein centenary survey*, pages 533–80, Cambridge, 1979. Cambridge University Press.
- [54] C. W. Misner, “Mixmaster universe”, 1969, *Phys. Rev. Lett.*, **22**, 1071–4.
- [55] V. F. Mukhanov, H. A. Feldman, and R. H. Brandenberger, “Theory of cosmological perturbations”, 1992, *Phys. Rep.*, **215**, 203–333.
- [56] U. S. Nilsson, M. J. Hancock, and J. Wainwright, “Non-tilted Bianchi VII₀ models – the radiation fluid”, 2000, *Class. Quant. Grav.*, **17**, 3119–34.
- [57] U. S. Nilsson, C. Ugglå, J. Wainwright, and W. C. Lim, “An almost isotropic cosmic microwave temperature does not imply an almost isotropic universe”, 1999, *Astrophys. J.*, **521**, L1–L3.
- [58] J. P. Ostriker and P. Steinhardt, “The quintessential universe”, 2001, *Scientific American*, **284**, 46–53.
- [59] J. A. Peacock, *Cosmological Physics*, Cambridge University Press, Cambridge, 1999.
- [60] P. J. E. Peebles, *Principles of Physical Cosmology*, Princeton University Press, Princeton, 1993.
- [61] A. D. Rendall, “Asymptotics of solutions of the Einstein equations with positive cosmological constant”, 2003, *arXiv.org: gr-qc/0312020*.
- [62] A. D. Rendall and M. Weaver, “Manufacture of Gowdy spacetimes with spikes”, 2001, *Class. Quant. Grav.*, **18**, 2959–76.

- [63] A. G. Riess and M. S. Turner, “From Slowdown to Speedup”, 2004, *Scientific American*, **290**, 62–7.
- [64] H. Ringström, “The Bianchi IX attractor”, 2001, *Annales Henri Poincaré*, **2**, 405–500.
- [65] Sloan Digital Sky Survey Collaboration, I. Zehavi, M. R. Blanton, J. A. Frieman, D. H. Weinberg, H. J. Mo, and M. A. Stauss, “Galaxy clustering in early SDSS redshift data”, 2002, *Astrophys. J.*, **571**, 172–190.
- [66] D. N. Spergel, L. Verde, H. V. Peiris, E. Komatsu, M. R.olta, C. L. Bennett, M. Halpern, G. Hinshaw, N. Jarosik, A. Kogut, M. Limon, S. S. Meyer, L. Page, G. S. Tucker, J. L. Weiland, E. Wollack, and E. L. Wright, “First-year Wilkinson Microwave Anisotropy Probe (WMAP) observations: Determination of cosmological parameters”, 2003, *Astrophys. J. Suppl. Ser.*, **148**, 175–94.
- [67] A. A. Starobinskii, “Isotropization of arbitrary cosmological expansion given as effective cosmological constant”, 1983, *Sov. Phys. JETP*, **37**, 66–9.
- [68] M. A. Strauss, “Reading the Blueprints of Creation”, 2004, *Scientific American*, **290**, 54–61.
- [69] M. Tegmark, M. R. Blanton, M. A. Strauss, F. Hoyle, D. Schlegel, R. Scoccamarro, M. S. Vogeley, D. H. Weinberg, I. Zehavi, A. Berlind, T. S. Budavari, A. Connolly, D. J. Eisenstein, D. Finkbeiner, J. A. Frieman, J. E. Gunn, A. J. S. Hamilton, L. Hui, B. Jain, D. Johnston, S. Kent, H. Lin, R. Nakajima, R. C. Nichol, J. P. Ostriker, A. Pope, R. Scranton, U. Seljak, R. K. Sheth, A. Stebbins, A. S. Szalay, I. Szapudi, L. Verde, Y. Z. Xu, J. Annis, N. A. Bahcall, J. Brinkmann, S. Burles, F. J. Castander, I. Csabai, J. Loveday, M. Doi, M. Fukugita, J. R. Gott, G. Hennessy, D. W. Hogg, Z. Ivezić, G. R. Knapp, D. Q. Lamb, B. C. Lee, R. H. Lupton, T. A. McKay, P. Kunszt, J. A. Munn, L. O’Connell, J. Peoples, J. R. Pier, M. Richmond, C. Rockosi, D. P. Schneider, C. Stoughton, D. L. Tucker, D. E. Vanden Berk, B. Yanny, and D. G. York, “The three-dimensional power spectrum of galaxies from the Sloan Digital Sky Survey”, 2004, *Astrophys. J.*, **606**, 702–40.
- [70] S. A. Teukolsky, “Stability of the iterated Crank-Nicholson method in numerical relativity”, 2000, *Phys. Rev. D*, **61**, 087501.

- [71] M. S. Turner and A. G. Riess, “Do type Ia supernovae provide direct evidence for past deceleration of the universe?”, 2002, *Astrophys. J.*, **569**, 18–22.
- [72] C. Uggla, H. van Elst, J. Wainwright, and G. F. R. Ellis, “Past attractor in inhomogeneous cosmology”, 2003, *Phys. Rev. D*, **68**, 103502.
- [73] H. van Elst and C. Uggla, “General relativistic 1+3 orthonormal frame approach”, 1997, *Class. Quant. Grav.*, **14**, 2673–95.
- [74] H. van Elst, C. Uggla, and J. Wainwright, “Dynamical systems approach to G_2 cosmology”, 2002, *Class. Quant. Grav.*, **19**, 51–82.
- [75] J. Wainwright, “A classification scheme for non-rotating inhomogeneous cosmologies”, 1979, *J. Phys. A.: Math. Gen.*, **12**, 2015–29.
- [76] J. Wainwright, “Relativistic Cosmology”, In G. S. Hall and J. R. Pulham, editors, *General Relativity, Proceedings of the Forty Sixth Scottish Universities Summer School in Physics*, pages 107–141, Bristol, 1996. Institute of Physics Publishing.
- [77] J. Wainwright and G. F. R. Ellis, *Dynamical systems in cosmology*, Cambridge University Press, Cambridge, 1997.
- [78] J. Wainwright, M. Hancock, and C. Uggla, “Asymptotic self-similarity breaking at late times in cosmology”, 1999, *Class. Quant. Grav.*, **16**, 2577–2598.
- [79] J. Wainwright and B. J. Marshman, “Some exact cosmological models with gravitational waves”, 1979, *Phys. Lett. A*, **72**, 275–6.
- [80] R. M. Wald, “Asymptotic behaviour of homogeneous cosmological models in the presence of a positive cosmological constant”, 1983, *Phys. Rev. D*, **28**, 2118–20.
- [81] M. Weaver, unpublished work, 2002.
- [82] S. Weinberg, *Gravitation and Cosmology*, John Wiley & Sons, New York, 1972.
- [83] S. Weinberg, *The first three minutes: A Modern View of the Origin of the Universe*, Basic Books, New York, 1977.

- [84] G. Whitham, *Linear and Nonlinear Waves*, Wiley-Interscience, New York, 1974.